**Federal Research Centre**
**«Kola Science Centre of the Russian Academy of Sciences»**

# XIX INTERNATIONAL MEETING ON CRYSTAL CHEMISTRY, X-RAY DIFFRACTION AND SPECTROSCOPY OF MINERALS

**Dedicated to the memory of Academician E.S. Fedorov (1853 – 1919)**

Apatity
2019

# Table of contents

# 1. General Aspects

## E.S.Fedorov promoting the Russian-German scientific interrelationship

Peter Paufler

Technische Universitaet Dresden, D-01062 Dresden, Germany

peter.paufler@t-online.de

The eminent Russian crystallographer Evgraf Stepanovič Fedorov (1853–1919) has received numerous tokens of appreciation for his pioneering contributions to the fundamentals of crystallography (e.g., [Shafranovskij et al., 1962]). His most important contributions, the derivation of 230 space group types and the methods of the experimental survey of crystal morphology, are named after him.

On the occasion of the 100th anniversary of his death, we will pay attention to an aspect of his oeuvre, relating the scientific communities in Russia and Germany. We refer to publications of E.S. Fedorov in the 'Zeitschrift fuer Krystallographie und Mineralogie' (founded in 1877) and restrict ourselves to their impact upon crystallography. The latter journal played a leading role in crystallography during the turn of the 19th century. So, his results became known worldwide with special influence upon science in German-speaking countries. As nowadays publications in German will not find duly reference as previously, the present contribution may help to improve this, too.

Importantly, the author E.S.Fedorow (applying previous German writing) started a very close exchange of ideas and news with the German mineralogist and editor Paul Heinrich von Groth in Munich. Having submitted his first paper in German to the 'Zeitschrift' on the comparison between Arthur Schoenflies' and his own findings of space groups [Fedorow, 1892], a mutual correspondence developed between Fedorow and Groth and remained during the entire period 1891–1914 before World War I. It was more than businesslike exchange of letters, well documented by 223 samples [Shafranovskij et al., 1991]. They showed quite nicely the response of both scientists to actual new developments and contributed a lot to the mutual understanding.

When browsing through about 30 articles of E.S. Fedorow written in German, the following features will be stressed: (i) A wide field of topics is covered, including both original theoretical and experimental investigations. (ii) Unlike numerous other workers in the field of crystallography and mineralogy, Fedorow preferred the application of efficient mathematical methods. (iii) With the aid of (ii), he became an effective reviewer and discerning reader of other publications in that journal, so that way advancing the growing field on the whole. (iv) He was devoted to clear concepts and exerted considerable influence on the crystallographic terminology. (v) His publications proved essential to pave the way for a quantitative determination of crystal structures utilizing X-ray diffraction by M.v.Laue in 1912 and W.L. & W.H.Bragg in 1913.

Fedorow E.S. Zusammenstellung der krystallographischen Resultate des Herrn Schoenflies und der meinigen. Zeitschrift für Krystallographie 1892, 20, 25–75.

Shafranovskii I.I., Belov N.V. In Memoriam: E. S. Fedorov 1853–1919. In P. P. Ewald, ed., Fifty Years of X-ray Diffraction. Utrecht, International Union of Crystallography, 1962, 341–350.

Shafranovskij I.I., Frank-Kamenetskij V.A., Dolivo-Dobrovol'skaja E.M. Evgraf Stepanovič Fedorov. Perepiska. Neizdannye i maloizvestnye raboty. Naučnoe Nasledstvo, t.16, Nauka Leningrad 1991.

**The Fedorov–Groth Law Revisited: Complexity Analysis Using Mineralogical Data**

Sergey V. Krivovichev[1,2,*], Vladimir G. Krivovichev[1]

[1] Institute of Earth Sciences, St. Petersburg State University, 199034 St. Petersburg, Russia
[2]Russian Academy of Science, Kola Science Centre, Apatity 184209, Russia

* s.krivovichev@spbu.ru

E.S. Fedorov noted that with the increasing chemical simplicity, their symmetry of mineral species is increasing. Similar observations were made by the German crystallographer P. Groth. In Russian literature, this tendency was called the Fedorov-Groth law (cf., [Yuskin et al., 1987]). This law is statistical in nature (there are exceptions), but, in general, it reflects the correlation of minerals' chemical composition and crystal structure.

The main purpose of our work is to revisit this law on the quantitative level using the data on chemical and structural complexities of minerals. For the study, a total of 4931 datasets on chemical compositions and 2989 datasets on crystal structures of minerals were considered. The ideal chemical formulas of minerals used for the calculations are those approved by the International Mineralogical Association (IMA) and contained in the continuously updated lists published by M. Pasero (the New IMA List of Minerals)at the website of Commission on New Minerals, Nomenclature and Classification IMA (CNMNC IMA). Only essential chemical elements were taken into account, without consideration of isomorphic substitutions [see also: Krivovichev et al., 2018b].

The amounts of structural Shannon information per atom (${}^{str}I_G$) and per unit cell (${}^{str}I_{G,total}$) were calculated using the approach developed by S.V.Krivovichev [2012; and etc.]. By analogy with structural complexity, chemical complexity was evaluated by the amount of chemical information per atom (${}^{chem}I_G$) and per formula unit, f.u. (${}^{chem}I_{G,total}$) [Krivovichev et al., 2018a].

Information-based chemical and structural complexity parameters for minerals calculated have been separated into ten groups according to the order of point-symmetry groups (*PGO*) which ranges from 1 (lowest symmetry) for triclinic minerals to 48 (highest symmetry) for cubic minerals. The best fitting for the ${}^{chem}I_G$–*PGO*, ${}^{str}I_G$–*PGO*, ${}^{chem}I_{G,total}$–*PGO* and ${}^{str}I_{G,total}$–*PGO* relations was obtained by means of exponential and allometric functions, respectively:

$${}^{chem}I_G = 1.265 + 0.510 \times \exp[-PGO/20.944] \text{ bits/atom} \quad (R^2 = 0.948)$$
$${}^{chem}I_{G,total} = 2.831 + 2.438 \times \exp[-PGO/24.494] \text{ bits/atom} \quad (R^2 = 0.896)$$
$${}^{str}I_G = 1.370 + 3.465 \times \exp[-PGO/11.655] \text{ bits/atom} \quad (R^2 = 0.968)$$
$${}^{str}I_{G,total} = 155.177 + 137.488 \times \exp[-PGO/9.366] \text{ bits/atom} \quad (R^2 = 0.962)$$

The relations obtained indicate that there are strong relationships (confidence level > 0.99) between the chemical and structural complexities (${}^{chem}I_G$, ${}^{str}I_G$, ${}^{chem}I_{G,total}$, ${}^{str}I_{G,total}$) and the order of point symmetry groups (*PGO*).

This research was supported by the Russian Science Foundation (grant 19-17-00038).

Krivovichev S.V. Structural complexity of minerals: information storage and processing in the mineral world. Mineral. Mag., 2013, 77, 275–326.

Krivovichev S.V., Krivovichev V.G., Hazen R.M. Structural and chemical complexity of minerals: relations and time evolution. Eur. J. Mineral., 2018a, 30, 231–236.

Krivovichev V.G., Charykova M.V., Krivovichev S.V. Mineral system based on the number of species-defining chemical elements in minerals, their types, distribution and mineral evolution of Earth's crust. Eur. J. Mineral., 2018b, 30, 219–230.

Yushkin N.P., Shafranovsky I.I., Yanulov K.P. Zakony symmetrii v mineralogii (Laws of symmetry in Mineralogy). Leningrad: Nauka, 1987 [in Russian].

**Crystal defects and flow in minerals from the Earth's mantle**

Patrick Cordier

University of Lille, CNRS, INRA, ENSCL, UMR 8207
UMET – Unité Matériaux et Transformations, F-59000 Lille, France

patrick.cordier@univ-lille.fr

The Earth is still a hot planet which dissipates its internal heat through large scale convection cells which stir the mantle and drive plate tectonics. At the surface, the resulting displacements occur very slowly, but they are measurable. Very early, in 1865, T.F. Jamieson recognized and reported evidence that the uplifted beaches of Fennoscandia were the result of the removal of the ice sheet from the last glaciation. Based on these observations and measurements, N.A. Haskell proposed in 1935 a very good estimate of the viscosity of the mantle, $10^{21}$Pa.s, which is still well accepted. The fact that, over very long timescales, the Earth's mantle flows as a Newtonian fluid raises fundamental questions. Especially considering that the mantle is made of solid rocks. How can we reconcile the ability of matter to flow with the crystal regularity promoted by crystallographers like E.S. Fedorov?

The answer is that all real crystals contain defects which can act as agent for the deformation. Their structures and mobilities are thus essential for understanding rheology of rocks and it is at the microscopic scale that one should look for the origin of the convection of the mantle.

In this presentation, we will show some recent progress in the modelling of defects in some major minerals of the Earth's mantle and how their microstructures and dynamics can be studied by transmission electron microscopy.

Haskell N.A. The motion of a fluid under the surface load. Physics,1935,6, 265–269.

Jamieson T.F. On the history of the last geological changes in Scotland. Geological Society of London Quarterly Journal, 1865, 21,161–203.

**Synchrotron Radiation in Geoscience: Current State and Future Perspectives**

Sergey V. Rashchenko

Sobolev Institute of Geology and Mineralogy SB RAS, 630090 Novosibirsk, Russia
Budker Institute of Nuclear Physics SB RAS, 630090 Novosibirsk, Russia

rashchenko@igm.nsc.ru

Advantages of bright and tunable synchrotron radiation have been successfully used by geoscientists starting from the emergence of the first user-dedicated synchrotron facilities. Currently, ~10% of available experimental time at such facilities is used to study composition and structure of various geomaterials down to atomic level by numerous synchrotron-based techniques:

- X-ray diffraction
- Small-angle X-ray scattering
- X-ray absorption spectroscopy (EXAFS, XANES)
- X-ray fluorescence
- Synchrotron Mössbauer spectroscopy
- Inelastic X-ray scattering
- X-ray topography
- X-ray tomography
- X-ray microscopy
- *etc.*

Until recently, the state-of-the-art synchrotron facilities were those based on the so-called 3$^{rd}$ generation storage rings – accelerators with horizontal *emittance*[1] of an electron beam of 1-5 nm·rad (ESRF, SPRING-8, APS *etc.*). At such facilities initial size of X-ray beam is ~0.5 mm at angular divergence of ~10 μrad. However, recent developments in accelerator physics opened the way to synchrotron facilities of a new – 4$^{th}$ – generation with emittance of ~0.1 nm·rad. The latter corresponds to X-ray beams with initial size of ~0.03 mm at angular divergence of ~3 μrad, which can be easily focused to micro- and nanosized spots, opening new horizons for nanomineralogy, high-pressure research *etc.* Another exceptional property of 4$^{th}$ generation synchrotron beams is high *coherence*, making such methods as ptychography and coherent diffraction imaging available for many innovative applications in geoscience.

The introduction of the concept of 4$^{th}$ generation storage rings forced the most of synchrotron facilities worldwide to plan a corresponding refurbishment in the next few years. In order to ensure access of the Russian users to such a powerful research infrastructure, the Russian government decided to establish two national 4$^{th}$ generation synchrotron facilities: a 3 GeV 'pilot' storage ring SKIF in Novosibirsk, and a 6 GeV 'flagship' storage ring SSRS-4 in Protvino. As the commissioning of the first six beamlines of SKIF is planned for 2024, a feedback from the Russian geoscience community would be beneficial for the most effective development of the facility for needs of Earth, planetary and environmental science.

[1]Horizontal emittance of an electron beam can be calculated as a product of its horizontal size and angular divergence, taken in a focal point.

**Still waters run deep**

Wulf Depmeier

Institute of Geosciences, Kiel University, Kiel, Germany

wulf.depmeier@ifg.uni-kiel.de

Standardization of methods, units, nomenclature and symbols represents an important part of the self-assigned mission of the International Union of Crystallography (https://www.iucr.org/). S.V. Krivovichev made an essential contribution to this task by suggesting quantitative measures for the widely-used, but often quite ambiguous term "complex" for the description of certain crystal structures [Krivovichev, 2012]. Among others, he applied the new concept to the mineral kingdom [Krivovichev, 2013a] as well as to zeolites and related inorganic microporous structures [Krivovichev 2013b]. It seems that the classification relies essentially on data obtained from diffraction methods and with the understanding that the studied objects are periodically ordered.

In his [2013b] paper, Krivovichev identified the topology of the sodalite framework as the most simple one of all the zeolite and zeolite-type topologies and the structural complexity of the mineral sodalite proper is classified as simple. Hence, at a first glance one could come to the conclusion that the structural family of sodalite were not worth further studies, at least as far as its structural aspects are concerned. This is somehow at variance with the presenting author's experience [Depmeier, 2005], and was in fact acknowledged and fully supported by Krivovichev in his [2013b] paper.

The present talk will deal mostly with a particular subgroup of the sodalite family, so-called aluminate sodalites, and their structural complexity, which is the result of the high flexibility of the framework and frustrated interactions of three partial structures resulting in dynamically disordered high-temperature cubic phases and cascades of phase transitions to commensurately or incommensurately modulated structures at lower temperatures - around room temperature for strontium chromate aluminate sodalite. In some cases, it proved necessary to complement the information obtained from diffraction methods by NMR spectroscopy in order to get a deeper understanding of the structures on a shorter time-scale [Többens and Depmeier, 1998, 2001a, 2001b]. Complexity measures $I_{G,\mathrm{total}}$ as high as 860 bits/u.c. were observed for at least one ordered member of the family and it was found for the disordered cubic phases that the calculated measures depend significantly on the model used. Especially in the latter case(s) the particularities of the system might be called emergent.

Depmeier W. The Sodalite Family – A Simple but Versatile Framework Structure. Reviews in Mineralogy & Geochemistry, 2005, 57, 203–240.

Krivovichev S. V. Structural and topological complexity of zeolites: An information-theoretic analysis. Microporous and Mesoporous Materials, 2013b, 171, 223–229.

Krivovichev S. V. Structural complexity of minerals: information storage and processing in the mineral world. Mineralogical Magazine, 2013a, 77, 275–326.

Krivovichev, S. V. Topological complexity of crystal structures: quantitative approach. Acta Cryst. 2012, A68, 393–398.

Többens D.M. and Depmeier W. Intermediate phases in the Ca-rich part of the system $(Ca_{1-x}Sr_x)_8[Al_{12}O_{24}](WO_4)_2$. Z. Kristallogr., 1998, 213, 522–531.

Többens D.M. and Depmeier W. Superstructure of strontium chromate aluminate sodalite at low temperatures. Z. Kristallogr., 2001a, 216, 586–590.

Többens D.M. and Depmeier W. The intermediate phase of strontium chromate aluminate sodalite. Z. Kristallogr., 2001b, 216, 611–615.

**On the crystal chemical identification and classification of minerals**

Ferdinando Bosi

Department of Earth Sciences, Sapienza University of Rome, 00185 Roma, Italy

ferdinando.bosi@uniroma1.it

In order to distinguish mineral species on the basis of the empirical formula, two approaches could be used: (1) the dominant-valency approach, which identifies mineral species by determining the dominant *root-charge arrangement*; (2) the dominant-end-member approach, which identifies species by determining the most abundant end-member component. These two approaches generally converge, but for some intermediate compositions, significant differences can be observed. The Commission on New Minerals Nomenclature and Classification (CNMNC) of the International Mineralogical Association (IMA) recommends the use of the dominant-valency approach/rule [Hatert, Burke, 2008], because it alone may lead to unambiguous mineral identification. Although the simple application of the dominant-valency rule is successful for the identification of many mineral compositions, sometime it leads to unbalanced end-member formulae, due to the occurrence of a coupled heterovalent substitution at two sites along with a heterovalent substitution at a single site. In these specific cases, it may be useful to use the site total charge approach to identify the dominant root-charge arrangement on which to apply the dominant-constituent rule [Bosi, 2018].

Mineral species characterized by coupled heterovalent-homovalent substitutions at two sites require the application of the dominant-valency rule. On the other hand, minerals with coupled heterovalent-homovalent substitutions *at a single site*such as two heterovalent substitutions ${}^{M}A^{2+} \leftrightarrow {}^{M}(B^{3+}_{0.5} + C^{1+}_{0.5})^{2+}$ and ${}^{M}D^{2+} \leftrightarrow {}^{M}(B^{3+}_{0.5} + C^{1+}_{0.5})^{2+}$ combined with the homovalent substitution ${}^{M}A^{2+} \leftrightarrow {}^{M}D^{2+}$, may be identified by using dominant-constituent (100%/*n*) rule as the site total charge (+2) is always preserved: *i.e.*, the 33.3 mol.% mark, derived from $n = 3$ constituents involved in the substitution process,$A^{2+}$, $D^{2+}$ and $(B^{3+}_{0.5} + C^{1+}_{0.5})^{2+}$, is applicable. The aforementioned concepts are best shown by the composition ternary diagrams.For coupled heterovalent-homovalent substitutions occurring at two sites, plotting some specific compositions in a triangular diagram with the three constituents placed at each corner, the typical boundaries crossing at the center of the diagram are displacedby 25% for one component, 37.5% for the other two components. Conversely, these boundaries are not displaced(33% of each component), if heterovalent-homovalent substitutions occur at a single site.

A mineral supergroup consists of four or more minerals with essentially the same structure and composedof chemically similar elements [Mills et al., 2009]. Based on the observation that most of the mineral supergroups approved by the IMA-CNMNCcontain species having different anions or anionic groups,we may conclude that usuallya supergroup contains species belonging to different mineral classes. This observation is in contrast to the current use of chemical composition as the distinguishing factor at the highest level of mineral classificationsystem.

Bosi F. On the mineral nomenclatures: the dominant-valency rule. Abstract to XXII meeting of the IMA, Melbourne, Australia, 2018, 354.

Hatert F., Burke E.A.J. The IMA–CNMNC dominant-constituent rule revisited and extended. Canadian Mineralogist, 2008, 46, 717–728.

Mills S.J., Hatert F., Nickel E.H., Ferraris G. The standardization of mineral group hierarchies: application to recent nomenclature proposals. European Journal of Mineralogy, 2009, 21, 1073–1080.

**Semi empirical atomistic modeling in inorganic crystal chemistry and structural mineralogy: limitations and possibilities**

Nikolai N. Eremin

Moscow State University Geological Faculty, 119991 Moscow, Russia

neremin@geol.msu.ru

In the 21st century, mathematical modeling has firmly taken its place as a method that complements or in some cases replaces physical experiment. The basis of such mathematical approaches in crystal chemistry is the principle of the structure energy minimum of the crystal. Energy minimum search is carried out both by quantum-chemical methods based on the so-called "first principles" (*ab-initio* calculations) and by using semi-empirical (or atomistic) structure modeling methods.

Quantum chemistry tries to solve this procedure by minimizing the interaction energy of all electrons and nuclei in the system under consideration; this requires an extremely precise definition of the basis wave functions set and very powerful and high-speed computing equipment. And even in this case the satisfactory accuracy of calculation can be achieved only for rather simple crystal systems. On the other hand, semi-empirical methods do not put intra-atomic interactions into consideration; inter-atomic interactions are described by empirical functions of a relatively simple analytical form, which immediately simplifies greatly the computational procedure of the system minimum energy search. Therefore, atomistic methods are widely used in a number of scientific groups for many crystal chemical problems studying: polymorphic transitions, isomorphic substitutions limits, prediction of the properties of virtual compounds, phase stability prediction, creating a realistic picture of deep Earth geospheres structure and many other problems of crystal chemistry, physics and chemistry of solids [Oganov, 2011; Urusov and Eremin, 2012].

This report illustrates the predictive ability of the atomistic semi-empirical modeling method (both in the static and in the molecular-dynamic aspect), its advantages and limitations are also described. To illustrate the effectiveness of the method, the following examples are considered:

- static and molecular dynamic study of variable composition oxide and phosphate systems in order to find the best solid solution composition, useful for high-level radioactive waste immobilization;
- atomistic potentials using for the mineral phases of the Earth lower mantle evolutionary search;
- isomorphic capacity estimation of some impurity elements in main Earth mantle phases;
- order-disorder simulation and the demonstration of ordering effect on various structural characteristics and physical properties of the objects under modeled.

Oganov A.R., Ed. Modern Methods of Crystal Structure Prediction. Wiley-VCH, 2011.

Urusov V.S., Eremin N.N.Atomistic Computer Modeling of the Structure and Properties of Inorganic Crystals and Minerals, Their Defects and Solid Solutions. GEOS, Moscow, 2012[in Russian].

# 200 years after discovery of the general phenomena of crystal chemistry by Eilhard Mitscherlich: iso- and polymorphism, highly anisotropic and negative thermal expansion

Stanislav K. Filatov[1,*], Rimma S. Bubnova[2]

[1]Saint-Petersburg State University, 199034 Saint-Petersburg, Russia
[2]Institute of Silicate Chemistry, 199034 Saint-Petersburg, Russia

* filatov.stanislav@gmail.com

The great German chemist EilhardMitscherlich was one of the first to be at the forefront of crystal chemistry about 200 years ago. He discovered and generalized the phenomena of isomorphism, polymorphism, anisotropy of thermal expansion and negative thermal expansion. Brief information on the discovery of these phenomena and its development to date is given below.

**Isomorphism** was first introduced by Mitscherlich in 1819 (Abhandl. Berlin. Akad.Wissensch.)as a term meant an equality of formsof a solid matter and he formulated a law [Mitscherlich, 1821]: *crystals composed of the same number of similar elements tend to demonstrate isomorphism*. Later it was determined as a substitution of some fragments of a crystal structure by other (atoms, ions, vacancies, molecules, atomicgroups) to form an isomorphic mixture (solid solution). A reverse process, i.e. discontinuation of an existence of the solid solution is reached by an ordering of the atoms by positions in the original crystal structure(*factor of structural diversity*[Filatov et al., 2018, p. 182]). If a number of such positions is insufficient, then the problem can be solved by the solid solution's decomposition, formation of superstructures, incommensurate modulations, splitting of atomic positions*etc*.[Filatov et al., 2018, p. 190].

**Polymorphism.**A doctrine of mineral's dimorphism created by Mitscherlich[1825] raised a doubt of*R. J. Haüy*and other chemists due to a presence of impurities in minerals. In response, Mitscherlich was the first scientist to conduct experiments on the synthesis of various crystals from pure synthetic compounds, in particular, fromthe sulfur, and provedthe phenomenon of dimorphism (polymorphism generally). In the mid-twentieth century, M.J. Buerger created a unified theory of polymorphism as transformations of I (coordination polyhedron, *c.p.*) and II (local environment of the *c.p.*) coordination spheres (*c.s.*) with and without a break of chemical bonds [Buerger, 1951]. S.K. Filatov and P. Paufler introduced zero *c.s.* (atom, ion) and an intermediate (local) break of bonds [Filatov, Paufler, in press].

**Anisotropy of thermal expansion and negative thermal expansion.**E. Mitscherlich made an optical tube for the Wollaston's reflective goniometer in order to fix a position of an eye when registering a luster of a crystal's face. This allowed him to find the difference of values of angles between the faces of calcite crystal at different time of a day as a function of temperature, i.e. to discover the anisotropy of the thermal expansion. Moreover,Mitscherlichdiscovered the negative thermal expansion of calcite crystals. Later, this led to the understanding of reasons causing a thermal cracking ofrocksand metensomatosisprocesses as well as of a deposition of ores in the Earth's crust[Filatov et al., 2018, p. 246].

The studies have been supported by Russian Foundation of Basic Researches, project №18-29-12106. X-Ray diffraction experiments were performed at the X-Ray Diffraction Center of Saint-Petersburg State University.

Buerger M. J. Crystallographic aspects of phase transformations. Phase transformations in solids / eds. R. Smoluchowski, J. E. Mayer, W. A. Weyl. New York: J. Wiley & Sons, 1951. P. 183–211.

Filatov S. K., Krivovichev S. V., Bubnova R.S. General crystal chemistry: Textbook. St. Petersburg: Publishing House of St. Petersburg University, 2018.

Filatov S.K. and Paufler P.C. Classification of polymorphic transformations in crystals. Proceed. Russ. Miner. Soc. (in press).

Mitscherlich E. Sur la relation qui existe entre les proportions et la forme crystalline. II. Mémoires sur les arséniates et les phosphates. Ann. Chim Phys. Paris 1821, 19, 350–419.

Mitscherlich E. Über die Körper, welche in zweiverschiedenen Formenkristallisieren. Abhandl. Berlin. Akad. Wissensch., aus d. Jahren 1822–1823, 1825. S. 43–48.

**Unusual polymorph transformations: in situ HTXRD data**

Maria Krzhizhanovskaya[1,*], Rimma Bubnova[2], Sergey Volkov[2], Liudmila Gorelova[1], Nadezhda Zhuk[3], Stanislav Filatov[1]

[1] Dept. Crystallography, St. Petersburg State University, 199034 St. Petersburg, Russia
[2]Institute of Silicate Chemistry RAS, 199034 St. Petersburg, Russia
[3]Syktyvkar State University, 167001 Syktyvkar, Komi Republic, Russia

* mariya.krzhizhanovskaya@spbu.ru

Within the last two decades, thermal behavior and polymorphismof agreat variety ofinorganic substances was examined by us by powder low- andhigh-temperature X-ray diffraction (HTXRD). According to the“rules of polymorphism”, the symmetry of a crystal structurerises with temperature[Filatov, 1973,2011; Hazen, Finger, 1982]. The number of exclusions islimited. Here, the most unusual thermal transformations are presented for the structuresbased on triangular, tetrahedral and octahedral oxygen polyhedra.The possible reasons are discussed.

The sequence of reversible phase transitions of $Sr_2B_2O_5$ structure based on $BO_3$ triangles was known for half a century [Witzmann,Beulich, 1964], although the symmetry of HT phases was unknown. Using HT single-crystal and powder XRD, we showedthat the sequence of transitions is associated with an unusual change of symmetry, with modulated triclinic intermediate β-phase and monoclinic LT γ-$Sr_2B_2O_5$ as well as HT α-$Sr_2B_2O_5$[Volkov et al., 2017].

According to powder HTXRD, $KBSi_2O_6$ and $Ca_2B_2SiO_7$ undergo reversible polymorph transformations with lowering symmetry [Krzhizhanovskaya et al. 2016, 2018]. Their tetrahedral motifsjust slightly change the symmetry, meanwhile the topology remains unchanged.

On heating, both orthorhombic (α) and triclinic (β) modifications of octahedral-based $BiNbO_4$ structure transform to HT (γ) phase, which symmetry was proposed by Sleight and Jones [1975] as monoclinic. We refined the HT phase at 1100 °C and showed that it is actually orthorhombic. Thus, in this case, there is no decreasing symmetry;the complex sequence of unusual polymorph transformations was studied in detail [Zhuk et al., 2019].

The work was supported by the Russian Foundation of Basic Research, 17-03-00887. XRD studies were performed in the Research Center of XRD studies of St. Petersburg StateUniversity.

Filatov S.K. General concept of increasing crystal symmetry with an increase in temperature. Crystallogr. Rep., 2011, 56, 953–961.

Filatov S.K. Some structure-geometric regularities of crystal deformations on heating, pressure and compositional changes. In: Crystallography and Crystal Chemistry. LGU Publising, Leningrad, 1973, 2, 5–12 [in Russian].

Hazen R.M., Finger L.W. Comparative crystal chemistry. London, 1982. 231 p.

Krzhizhanovskaya M.G., Bubnova R.S., Derkacheva E.S., Depmeier W., Filatov S.K. Thermally induced reversible phase transformations of boroleucite, $KBSi_2O_6$. Eur. J. Mineral., 2016, 28, 15–21.

Krzhizhanovskaya M.G., Gorelova L.A., Bubnova R.S., Pekov I.V., Krivovichev S.V. High-temperature crystal chemistry of layered calcium borosilicates: $CaBSiO_4(OH)$ (datolite), $Ca_4B_5Si_3O_{15}(OH)_5$ (‘bakerite’) and $Ca_2B_2SiO_7$ (synthetic analogue of okayamalite). Phys. Chem. Mineral., 2018, 45, 463–473.

Sleight A.W., Jones G.A. Ferroelastic transitions in β-$BiNbO_4$ and β-$BiTaO_4$. Acta Cryst., 1975, B31, 2748–2749.

Volkov S., Dušek M., Bubnova R., Krzhizhanovskaya M., Ugolkov V., Obozova E., Filatov S. Orientational order-disorder γ↔ β ↔ α′ ↔ α phase transitions in Sr $_2B_2O_5$ pyroborate and crystal structures of β and α phases. Acta Cryst., 2017, B73, 1056–1067.

Witzmann H., Beulich W.Z. Phys. Chem. (Leipzig). 1964. 225, 336–341.

Zhuk N.A., Krzhizhanovskaya M.G., Belyy V.A., Makeev B.A. High-temperature crystal chemistry of α-, β-, and γ-$BiNbO_4$ polymorphs. Inorg. Chem., 2019, 58, 1518–1526.

**Theoretically and experimentally investigation of deviation from the Vegard's law forsolid solutions: hybrid halide perovskite system**

Sergey A. Fateev*, Ekaterina I. Marchenko, Golib A. Mascharipov, Nikolay N. Eremin

Lomonosov Moscow State University, 119991 Moscow, Russia

*saf1al@yandex.ru

There is much evidence that X-ray measurements of sufficient accuracy reveal deviations from the linear dependence of unit-cell parameters on composition of solid solutions, i.e., departures from Vegard's rule. The dependence of such deviations on composition for a random solid solution with one substitutional position is usually of a parabolic form with a positive deviation [Urusov, 1992]. The study of deviations from the Vegard's law is an important crystal chemical problem.

Theoretical and experimental study of the deviation of parameters and volumes of unit cells using the example of hybrid halide perovskites $A\mathrm{PbI}_{3-x}\mathrm{Br}_x$ (where $A$ is Cs or organic cation) was considered.Theoretical calculations were carried out by a semi-empirical approach using disordered supercells. We firstly use new efficient algorithm for determining the most disordered atomic configuration of an arbitrary composition and pick improved set of interatomic potentials for modelling the large (7×7×7) $A\mathrm{PbI}_{3-x}\mathrm{Br}_x$ supercells. Such approach makes it possible to simulate more accurately the mixing properties of a crystal structure with an infinite size approximation.

The simulation shows that unit cell volumes deviate from their additive values (Retger's rule) by several $Å^3$, which affects their functional characteristics, such as band gap and light absorption. It is worth noting that the magnitude of the deviation significantly depends on the configuration and long-range ordering. Moreover, a positive correlation was found between positive deviations and positive differential enthalpy of formation of solid solutions, which is in good agreement with previously reported experimental results suggesting the tendency of solid solutions to decompose at room and low temperatures [Nandi et al., 2018].

The simulation data of cell volumes and the short- and long-range ordering were confirmed experimentally by refinement of the structure and anion composition of single crystals based on our experimental X-ray structural analysis data.

In addition, we determine the optimal growth parameters of large low-defect single crystals from solutions. The single crystals of $A\mathrm{PbI}_{3-x}\mathrm{Br}_x$ were synthesized from DMF and GBL solutions by temperature-induced crystallization. It was found that the stoichiometry of solid solutions differs significantly from the ratio of components in the crystallization solution, which can be explained by the significant difference in solubility of bromide and iodide perovskite.

The obtained results are also of high practical importance due to the increasing popularity of mixed halide hybrid perovskites for application in photovoltaics [Turkevych et al., 2019].

Nandi P. et al. Temperature Dependent Photoinduced Reversible Phase Separation in Mixed-Halide Perovskite. ACS Applied Energy Materials, 2018, doi: 10.1021/acsaem.8b00587

Turkevych I. et al. Strategic advantages of reactive polyiodide melts for scalable perovskite photovoltaics. Nature Nanotechnology, 2019, doi: 10.1038/s41565-018-0304-y

Urusov V.S. A geometric model of deviations from Vegard's rule. Journal of Solid State Chemistry, 1992, 98(2), 223–236.

**The Quantitative Estimation of the Degree of Similarityof Coordination Polyhedra**

Nikolay V. Somov*, Pavel V. Andreev, Evgeny V. Chuprunov

Lobachevsky StateUniversity of Nizhny Novgorod, 603950 Nizhny Novgorod, Russia

* somov@phys.unn.ru

The atomic structure of crystals is often conveniently described using coordination polyhedra (CPs). The geometrically regular CP form in real atomic structures of crystals occurs rather rarely. In the general case, real CPs have deviations from the ideal geometry, such CPs are usually called distorted. CP geometry is usually described by a set of bond lengths and angles, however, such a description is not always convenient, since contains a large number of parameters. To conduct a comparative analysis of several CPs, it is convenient to introduce some numerical characteristic, replacing a set of bond lengths and angles, with a single number.

We have proposed a new method for estimating the degree of similarity of two CPs with the same coordination number (CN). The proposed method takes into account the distortion of the lengths of chemical bonds and valence angles. The numerical criterion is a dimensionless limited quantity. The algorithm allows us to distinguish enantiomers and adapt the sensitivity of the method to the task[Somov and Andreev, 2018].

The method for estimating the degree of similarity of coordination polyhedra was implemented in the *Polyhedron* program, which is part of the Pseudo Symmetry software package [Somovetal., 2014]. The main features of the Polyhedron program are listed below:

- The quantitative estimation of the degree of similarity based on geometrical parameters of CPs.
- The quantitative estimation of the degree of similarity based on electron density functions.
- Calculate the degree of similarity of CP relative to the reference polyhedra from the database.
- The ability to create reference polyhedra based on the studied crystal structures.
- The automatic determination of a CP type.

The effectiveness of the proposed method and software is confirmed by the results of the study of coordinated compounds of bismuth and antimony complexes, as well as salts of polyphosphonic acids. In crystals of dicarboxylates of triarylantimony and triarylbismuth, it was shown that that an increase in the degree of similarity of the complex former CP of the tetragonal pyramid corresponds to a decrease in the frequency difference between the symmetric and asymmetric modes of vibration of the carbonyl fragment on the IR spectra.

Somov N.V., Andreev P.V. On Quantitative Estimation of the Degree of Similarity of Coordination Polyhedra. Crystallography Reports, 2018, 63(1), 38–42.

Somov N.V, Chuprunov E.V. Pseudosymmetry software for studying the pseudosymmetry of crystal atomic structures. Crystallography Reports, 2014, 59(1), 137–139.

**Fedorov's Group of Crystallographic Symmetry – Transformation Algorithms Space and Energy while Implementing a Stable Atomic Configurations**

Stanislav V. Borisov[1,*], Natalie V. Pervukhina[1,2], Svetlana A. Magarill[1]

[1]Nikolaev Institute of Inorganic Chemistry, SB RAS, Novosibirsk, Russia
[2]Novosibirsk State University, Novosibirsk, Russia

*borisov@niic.nsc.ru

*The 100th anniversary of the death of E. S. Fedorov*

Under terrestrial conditions, the crystal state is perceived as the most stable, corresponding to the minimum energy of atomic configurations (in thermodynamics, the ideal crystal structures are assigned zero entropy). In the mechanical-wave concept of the crystal state, the crystallization process means the loss of individual degrees of freedom (individual movements) by atoms in favor of more economical collective: plane standing elastic waves, where the masses are concentrated in the nodal planes of the waves. Standing waves of different orientations recreate pseudo-translational and then ideal translational ordering of material particles, reducing all the variety of configurations of atoms to their positions in the unit cell with volume $V_0$. In an elementary cell, the degrees of freedom of atoms are reduced by symmetry axes and mirror planes. The independent part of the volume is reduced to the fundamental volume $V^*=V_0/M$ ($M$– order (multiplicity) of the symmetry group). In this volume, the number of variable coordinates is $n_S$ atoms. The ratio $n_s/n_p=S$ ($n_p$ is the number of atoms in a primitive cell) represents the characteristic of the structure. Thus, crystallographic symmetry transforms the space filled with atoms, reducing its independent region to $V^*$ and the number of degrees of freedom of atoms to $n_s$. This achieves the minimum energy of the atomic system [Borisov et al., 2019]. The stability of such configurations (stencils) is confirmed by the popularity of highly symmetric structural types in nature and human practice. For example, in the structural type spinel $MgAl_2O_4$ with symmetry $Fd\bar{3}m$ ($a$=8.075 Å; $Z$=8; $V_0$=526.54 Å$^3$; $M$=192) the fundamental volume is only 2.75 Å$^3$. Both cations are fixed in particular positions at the intersections of the symmetry elements, and only oxygen anions located on the triple axes can move along these axes, having the coordinates of the basic atom a particular position with one degree of freedom*: x,x,x*. Therefore, 14 atoms in a primitive cell have only one degree of freedom: $S$=1/14=0.017. Four anions form the correct tetrahedral environment of the Mg cation, the parameter $x$=0.381 determines the length of the Mg–O bond, and the possibility of its variation provides to the popularity of the structural type of spinel for different sets of cations and anions. The situation is similar in other popular structural types (sphalerite, apatite, garnet, corundum...), and structural stencils are preserved with significant deviations from the ideal stoichiometry for the stencil. Thus, in the inanimate nature, in the continuum the space + energy, the transformation of material systems into stable States is carried out by symmetry, the forms of which were brilliantly predicted by E. S. Fedorov. Energy processes of crystallization became clear in the analysis of large arrays of structures [Borisov et al., 2015].

Borisov S.V., Magarill S.A., Pervukhina N.V. Fedorov's group of crystallographic symmetry – transformation algorithms space and energy while implementing a stable atomic configuration.J. Struct. Chem., 2019, 60(1), 81–86.

Borisov S.V., Magarill S.A., Pervukhina N.V. Crystallographic analysis of a series of inorganic compounds. Russ. Chem. Rev., 2015, 84(4), 393–421.

**Evolutional search of own mineral phases of aluminum in the lower mantle of the Earth**

Ekaterina I. Marchenko*, Nikolay N. Eremin

Lomonosov Moscow State University, 119991 Moscow, Russia

* marchenko-ekaterina@bk.ru

The question of the existence of aluminum own phases in the mantle of the Earth remains controversial up to date. The search of Ca-Al-O stable phases under high *P-T* was carried out by an evolutionary approach implemented in the USPEX software package [Oganov and Glass, 2006] by semi-empirical and quantum chemical methods of modeling.

In addition to the simplest $CaAl_2O_4$ composition in the Ca-Al-O system, the appearance of several potentially stable structures was predicted: $Ca_2Al_6O_{11}$ (space group *C*2/*m*), $Ca_2Al_2O_5$ (*Cmcm*), $Ca_3Al_4O_9$ (*C*2/*m*), $CaAl_6O_{10}$ (*P*1), $Ca_3Al_2O_6$ (*C*2/*c*) (Figure). All predicted structures have tunneled character. Calcium atoms are located in different channels formed by $AlO_6$ octahedra and $AlO_5$ bipyramids.

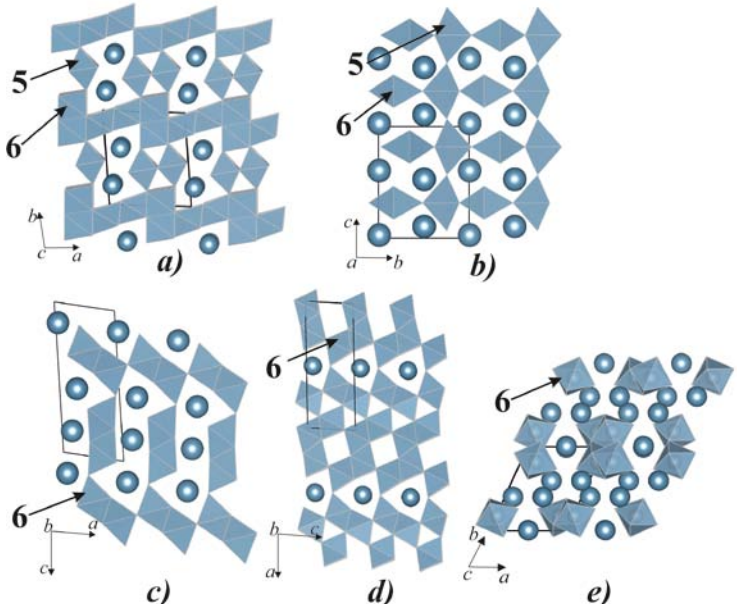


Figure. Predicted crystal structuresin Ca-Al-O system at 100 GPa. a) $Ca_2Al_6O_{11}$, b) $Ca_2Al_2O_5$, c) $Ca_3Al_4O_9$, d) $CaAl_6O_{10}$, e) $Ca_3Al_2O_6$. Calcium atoms are shown as balls. The numbers mean the aluminum coordination number.

Oganov A.R., Glass C.W.Crystal structure prediction using evolutionary algorithms: principles and applications. J. Chem. Phys., 2006, 124, 244704.

**An evolutionary system of mineralogy: Proposal for a classification of planetary materials based on natural kind clustering**

Robert M. Hazen, Shaunna M. Morrison

Geophysical Laboratory, Carnegie Institution for Science,Washington, DC 20015, U. S. A.

Minerals preserve a vivid narrative of the physical, chemical, and biological histories of their origins and subsequent alteration, and thus provide our clearest window to the evolution of Earth and other worlds through billions of years of Cosmic history. Mineral classification systems have the potential to elucidate this rich evolutionary story; however, the present mineral taxonomy, based as it is on idealized major element chemistry and crystal structure, lacks a temporal aspect and thus cannot reflect planetary evolution. A complementary evolutionary system of mineralogy based on the quantitative recognition of "natural kind clustering" for a wide range of condensed planetary materials with different paragenetic origins has the potential to amplify, though not supersede, the present classification system.

Mineral properties, including trace and minor elements, ratios of isotopes, structural defects, inclusions, external morphologies, and other idiosyncratic attributes, represent information that points to specific modes of formation and subsequent environmental histories–information essential to understanding the co-evolving geosphere and biosphere. We present the first in a series of contributions to explore an alternative and complementary evolutionary system of mineralogy. The earliest stage of mineral evolution, commencing with the appearance of the first crystals in the universe at >13 Ga and continuing today in the expanding, cooling atmospheres of countless energetic stars, saw the high-temperature ($T$> 1000 K), low-pressure ($P$< $10^{-2}$atm) condensation of refractory minerals and amorphous phases.

Varied types of carbon- and/or oxygen-rich mineral-forming stars, including red giant branch, asymptotic giant branch, and type 1A and type II supernovas, impart distinctive isotopic and trace element signatures to the micro- and nanoscale stardust grains that are collected from chondrite meteorites, atmospheric sampling, Antarctic ice, asteroids, and comets. Although our understanding of the diverse mineral-forming environments of stars is as yet incomplete, we present a preliminary catalog of 41 distinct natural kinds of stellar minerals, representing 17 official International Mineralogical Association (IMA) mineral species, as well as three kinds of non-crystalline condensed phases not codified by the IMA.

**Data-driven discovery in mineral systems: applications of advanced analytics and visualization**

Shaunna M. Morrison[1]*, Anirudh Prabhu[2], Ahmed Eleish[2], Feifei Pan[2], Hao Zhong[2], Fang Huang[2], Peter Fox[2], Xiaogang Ma[3], Jolyon Ralph[4], Joshua J. Golden[5], Robert T. Downs[5], Chao Liu[1], Simone E. Runyon[6],and Robert M. Hazen[1]

[1]Geophysical Laboratory, Carnegie Institution for Science, Washington, DC 20015;
[2]Rensselaer Polytechnic Institute;
[3]University of Idaho;
[4]Mindat.org;
[5]University of Arizona;
[6]University of Wyoming

*smorrison@ciw.edu

The key to answering many compelling and complex questions in Earth, planetary, and life science lies in breaking down the barriers between scientific fields and harnessing the integrated, multi-disciplinary power of their respective data resources. We have a unique opportunity to integratelarge and rapidly expanding “big data” resources, to enlist powerful analytical and visualizationmethods, and to answer multi-disciplinary questions that cannot be addressed by one field alone.

Recent years have seen a dramatic increase in the volume of mineralogical and geochemicaldata available for study. These large and expanding data resources have created an opportunity tocharacterize changes in near-surface mineralogy through deep time and to relate these findings to thegeologic and biologic evolution of our planet over the past 4.5 billion years [Hazen et al., 2008; Hummer et al., 2018; Liu et al., 2017]. Using databasessuch as the RRUFF Project, the Mineral Evolution Database (MED), mindat, and EarthChem, weexplore the spatial and temporal distribution of minerals on Earth’s surface while considering themultidimensional relationships between composition, oxidation state, structural complexity [Krivovichev et al., 2013], andparagenetic mode.

These studies, driven by advanced analytical and visualization techniques such as mineral ecology [Hazen et al., 2015; Hystad et al., 2018], network analysis [Morrison et al., 2017], and affinity analysis, allow us to begin tackling big questions inEarth, planetary, and biosciences. These questions relate to understanding the relationships of mineralformation and preservation with large-scale geologic processes, such as Wilson cycles, the oxidationof Earth’s atmosphere, and changes in ocean chemistry. We can also investigate the abundance andlikely species of as-yet undiscovered mineral, as well as estimate the probability of finding a mineralor mineral assemblage at any locality on Earth or another planetary body. Given the spatial andtemporal distribution of minerals on Earth, which was heavily influenced by life, we can explore thepossibility that Earth’s mineral diversity and distribution is a biosignature that can be used for futureplanetary evaluation and exploration. These geologic resources also facilitate integration acrossdisciplines and allow us to explore ideas that one field alone cannot fully characterize, such as howthe geochemical makeup of our planet affected the emergence and evolution of life, and, likewise,how life influenced chemical composition and geological processes throughout Earth history.

Hazen et al. Am. Mineral., 2008,93, 1693–1720

Hazen et al. Can. Min., 2015, 53(2), 295–324

Hummer et al. The oxidation of Earth’s crust: Evidence from the evolution of manganese minerals, Nat. Comm., 2018 (in Revision)

Hystad et al. Bayesian estimation of Earth’s undiscovered mineralogical diversity. Mathematical Geosciences, 2018 (in Press)

Krivovichev et al. Min. Mag., 2013, 77(3), 275–326.

Liu et al. Nat. Comm., 2017, 8, 1950

Morrison et al. Am. Mineral., 2017, 102, 1588–1596.

**Mineral phylogeny by means of secondary transformationof precursorspecies**

Taras L. Panikorovskii[1,2,]*, Gregory Yu. Ivanyuk[1] and Sergey V. Krivovichev[1,2]

[1] Kola Science Centre of RAS, 184209 Apatity, Murmansk Region, Russia
[2]Department of Crystallography, St. Petersburg State University, 199034 St. Petersburg Russia

* taras.panikorovsky@spbu.ru

In the process of evolution of geological matter, minerals “born, live and die” [Severgin, 1798]. The idea of mineral evolution developed by R.M. Hazen [Hazen et al., 2008] attracts considerable scientific and public attention [Rosing, 2008]. The phenomenon of genetic control upon the characteristic features of minerals underlies the concept of mineral typomorphism proposed by F. Bekke [1903] and developed by A. E. Fersman [1939].

The mineral evolution includes nucleation, crystal growth, structural transformations and exsolution under cooling, ion-exchange reactions and, finally, low-temperature alteration, which determine corresponding changes of its typomorphic properties and allows to estimate physico-chemical conditions and mechanisms of these processes. Sometimes, mineral alteration results in the formation of a novel mineral species inheriting structure topology of the precursor, which is frequently accompanied by the increase in structural complexity. The inheritance concept was applied by A.P. Khomyakov [1990] totitanosilicates from the massifs of the Kola alkaline province, in particular, to thelomonosovite–murmanite and vuonnemite–epiostolite series formed due to the exchange of $PO_4$ groups by $H_2O$ molecules in the interlayerspaces.

In this work, we shall report on the mineral phylogeny by means of structural-chemical transformations of primary (precursor) minerals with the formation of transformation series such asmurmanite–selivanovaite, kihlmanite-(Ce)–tundrite-(Ce), ivanyukite-Na-*T*–ivanyukite-Na-*C*–ivanyukite-*K*–ivanyukite-Cu–«ivanyukite-Th», parakeldyshite–M34–keldyshite, andradite–nikmelnikovite, vesuvianite–manaevite-(Ce) and pyrrhotite-4*C*–5*C*–6*C*[Yakovenchuk et al., 2009, 2014; Pakhomovsky et al., 2018; Ivanyuk et al., 2018]. We shall also demonstrate how these transformations can be applied to the topo-crystal-chemical mapping of mineral deposits.

This research is supported by the Russian Science Foundation (19-17-00038) and Russian Foundation for Basic Research (18-29-12039).

Becke F. Über Mineralbestand und Struktur der krystallinischen Schiefer. Gerold, 1903.

Fersman A.E. Geochemical and mineralogical methods of mineral exploration. M.-L., 1939.

Hazen, R.M. Papineau D., Bleeker W., Downs R.T., Ferry F., McCoy T., Sverjensky D., Yang H. Am. Mineral., 2008, 93, 1693–1720.

Ivanyuk G.Y.; Pakhomovsky Y.A.; Panikorovskii T.L.; Mikhailova J.A.; Kalashnikov A.O.; Bazai A.V.; Yakovenchuk V.N.; Konopleva N.G.; Goryainov P.M. Three-D Mineralogical mapping of the Kovdor phoscorite-carbonatite complex, NW Russia: II. Sulfides. Minerals, 2018, 8, 292.

Khomyakov A.P. Mineralogy of hyperagphaitic alkaline rocks. M. 1990.

Pakhomovsky Y.A., Panikorovskii T.L., Yakovenchuk V.N., Ivanyuk G.Y., Mikhailova J.A., Krivovichev S.V., Bocharov V.N. Kalashnikov A.O. Selivanovaite, $NaTi_3(Ti,Na,Fe,Mn)_4[(Si_2O_7)_2O_4(OH,H_2O)_4]\cdot nH_2O$, a new rock-forming mineral from the eudialyte-rich malignite of the Lovozero alkaline massif (Kola Peninsula, Russia). Eur. J. Min., 2018, 30(3), 515–523.

Rosing M. On the evolution of minerals. Nature, 2008, 456, 456–458.

Severgin V.M. The first bases of mineralogy or natural history of fossil bodies. SPb, 1798.

Yakovenchuk V.N., Krivovichev S.V., Ivanyuk G.Y., Pakhomovsky Ya.A., Selivanova E.A., Zhitova E.A., Kalashnikova G.O., Zolotarev A.A., Mikhailova J.A., Kadyrova G.I. Kihlmanite-(Ce), $Ce_2TiO_2[SiO_4](HCO_3)_2(H_2O)$, a new rare-earth mineral from the pegmatites of the Khibiny alkaline massif, Kola Peninsula, Russia. Mineral. Mag., 2014, 78, 483–496.

Yakovenchuk V.N., Nikolaev A. P., Selivanova E.A., Pakhomovsky Ya.A., Korchak Yu.A., Spiridonova D.V., Zalkind O.A., Krivovichev S.V. Ivanyukite-Na-T, ivanyukite-Na-C, ivanyukite-K, and ivanyukite-Cu: New microporous titanosilicates from the Khibiny massif (Kola Peninsula, Russia) and crystal structure of ivanyukite-Na-T. Amer. Mineral., 2009, 94, 1450–1458.

**Evolution and structure complexity of lithium minerals: applying of network analysis**

Alexandra Ostroverkhova[1,*], Anirudh Prabhu[2]

[1] Institute of Earth Sciences, St. Petersburg State University, 199034 St. Petersburg, Russia
[2]Tetherless World Constellation, Department of Earth and Environmental Sciences, Rensselaer Polytechnic Institute, Troy, NY 12180 US

* alex.ostroverkhova@gmail.com

Lithium is an incompatible element, mostly concentrated in pegmatites, which can count as a final stage of a magma's crystallization. This alkali metal has an uncommon occurrence, single oxidation state and a minor role for biological life. All of this enables to use for searching of correlation between such features like age, occurrences, number of localities and structure complexity [Krivovichev, 2012].

Analysis of the coexisting of the 114 IMA-approved lithium minerals (in 2017) by Network Analysis and particularly by clustering [Morrison et al., 2017] show three main and three small clusters. This method illustrates non-random connections, but an actual reason to group together. Each of the clusters has chemical features and indeed different sources of magma. Minerals of the first group such as spodumene, elbaite, amblygonite and etc., in the main case, belong to LCT pegmatites and subduction and orogeny zones as well. The second (neptunite, ephesite, etc.) and the third ones (sogdianite, polylithionite) relate to alkaline rocks (Lovozero, Khibiny and etc.) and rifting zones. A few minerals (ferri-leakeite, sugulite) from these two clusters were found in metamorphic rocks enriched in Mn. The ages of the first occurrence are closely connected to supercontinental cycles and show a strong connection with an intensity of pegmatite forming. Furthermore, most of the first occurrence of Li-minerals (63 to 51) younger than 600 Ma. [Grew et al., in preparation]

Grew E.S., Hystad G, Toapanta M., Eleish A., Ostroverkhova A., Golden J., Hazen R. M. Lithium mineral evolution and ecology: Comparison with boron and beryllium [in preparation].

Krivovichev S., Topological complexity of crystal structures: quantitative approach. Acta Crystallographica, 2012, A68(3), 393–398.

Morrison S.M., Liu, C., Eleish, A., Prabhu, A., Li, C., Ralph, J., Downs, R.T., Golden, J.J., Fox, P., Hummer, D.R. and Meyer, M.B., Networkanalysisofmineralogical systems. AmericanMineralogist, 2017, 102(8), 1588–1596.

# 2. Diffraction: Theory and Experiment

**Modern day mineralogy utilizing X-ray diffraction**

Stuart J. Mills

Geosciences, Museums Victoria, GPO Box 666, Melbourne 3001, Victoria, Australia

smills@museum.vic.gov.au

We live in challenging times. The Earth is warming and we face more extreme weather events. Mineralogy and Earth Sciences stand in a unique position to offer solutions and insight into some of the problems that the planet faces and that we are going to face into the future. And underpinning the science to these solutions is X-ray diffraction.

One of the most important materials that can help us are layered double hydroxides (LDH) or hydrotalcites. Here I present some of our work using LDHs for a number of diverse applications including: carbon sequestration, nitrate removal from contaminated water and removal of U and fission products for application to nuclear spills such as Fukushima Daiichi.

Today in a climate where getting grants is increasingly difficult, it is important for mineralogists and Earth scientists to show the real world impact of their work. One way to do this is to work at the interface between the bio- and geosphere. Here I present some of our work on one of the seven natural wonders of the world, the Great Barrier Reef.

**Quantitative nanostructure information from diffraction data: what can the diffraction pattern tell you?**

Matteo Leoni

DICAM University of Trento, via Mesiano, 77 38123 Trento, Italy
Saudi Aramco Research and Development Centre, PO box 12, 31311 Dhahran, Saudi Arabia

*matteo.leoni@unitn.it, matteo.leoni@aramco.com

Powder diffraction data are often employed for phase identification/quantification or for structural determination. In these cases, symmetrical and narrow peaks are necessary to obtain an accurate result, as the powder can be considered as made of well crystallized and similar grains free of defects.

In most practical cases, however, the powder diffraction pattern presents peaks that are broad or have peculiar shapes. This is a signature of the presence of defects (nano size, grain boundaries, dislocations, stacking faults, antiphase boundaries…).

The possibility of extracting some quantitative information about those defects will be shown, with some discussion about the limitation of traditional methods such as Scherrer formula, and about the actual information that the diffraction peaks can give us in practical cases.

**Evaluation of the best weighting schemefor the maximum entropy Patterson method**

Koichi Momma

National Museum of Nature and Science, Amakubo 4-1-1, Tsukuba, Ibaraki, 305-0005 Japan

k-momma@kahaku.go.jp

The maximum entropy method (MEM) is extensively used in crystallography to reconstruct electron densities, nuclear densities, and Patterson function from diffraction data. To obtain reasonable distribution of densities, it is reported that observed diffraction data need to be weighted with a proper function. Without weighting, residuals of observed and calculated structure factors, ($F_o - F_c$), of low-$Q$ (large $d$-spacing) region tend to be very large. While a weighting scheme based on $d^4$ was reported to be the best for X-ray diffraction data [de Vries et al., 1994], it sometimes tends to force too strict fitting of $F_c$to$F_o$atlow-$Q$ region, and the best weighting scheme depends on data types [Momma et al., 2013].

The necessity of weighting in MEM for crystallography comes from intrinsic nature of crystals that electron/nuclear densities are smooth.Such nature of crystals causes distribution of the information entropy $S$to be also smooth and amplitudes of$\partial S/\partial F_c$ to decrease with decreasing $d$-spacing. By evaluating distribution of$\partial S/\partial|F_c|^2$in the maximum entropy Patterson method, it was found that even more steep weighting function is necessary to obtain smooth distribution of Patterson function, and also a reasonable distribution of residuals.However, such steep weighing functions were found to suffer from very slow convergence of MEM iterations because residuals of high-$Q$ region are having too little contribution to the function maximized in the MEM iterations.

de Vries R. Y., Briels W. J., Feil D. Acta Cryst., 1994, 50, 383–391.
Momma K., Ikeda T., Belik A. A., Izumi F. Powder Diffraction, 2013, 28, 184–193.

**The direct derivation (DD) method: a new technique for quantitative phase analysis using observed intensities of individual phases and their chemical composition data**

Hideo Toraya

Rigaku Corporation, Matsubara, Akishima, Tokyo 196-8666, Japan

toraya@rigaku.co.jp

The direct derivation method, a new technique for quantitative phase analysis, is based on a simple principle. For instance, a solid cube, even if it is too big to be put on a balance, can be weighed by dividing its volume by the volume per unit weight of the same material. In the same manner, the weight proportion of the $k^{\text{th}}$component material ($W_k$) in a $K$-component mixture can be calculated by $W_k = S_k / a_k^{-1}$, where $S_k$ is the total scattered intensity from that material and $a_k^{-1}$ is the total scattered intensity per unit weight. As in the case of weighing the solid cube, we need to know two parameter values, $S_k$ and $a_k^{-1}$, for individual components in order to derive weight fractions ($w_k$) by $w_k = W_k / \sum W_k^{'} = a_k S_k / \sum a_k^{'} S_k^{'}$. The parameter $a_k^{-1}$ has been verified to be a function of the numbers of electrons belonging to the atoms in the chemical formula and the chemical formula weight [Toraya, 2016;Toraya, Omote, 2019]. Therefore, the $a_k^{-1}$ is calculable if we know the chemical compositions of phases present in the mixture. On the other hand, the $S_k$ can be obtained, for example, by summing up the integrated intensities of respective phases if we can decompose the observed powder pattern of a target mixture into individual Bragg components by using the pattern decomposition methods such as the Pawley or Le Bail method. Another way of obtaining the $S_k$ is to use the observed powder patterns of single-phases for modeling the individual powder patterns of the mixture just like multi-component Rietveld refinement using calculated patterns[Toraya, 2018]. In utilizing the observed patterns, it has been required to subtract the background intensities from observed patterns. The present procedure can use the observed patterns without subtracting their background intensities[Toraya, 2019].To utilize the background-included observed pattern is advantageous to the quantification, in particular, of samples containing low crystallinity materials like hydrates, amorphous component materials, low symmetry materials with many weak peaks in middle and high angle regions *etc*. Some examples of applications, including inorganic materials and some minerals, will be presented in this report.

Toraya, H. J. Appl. Cryst., 2016, 49, 1508–1516.
Toraya, H. & Omote, K. J. Appl. Cryst., 2019, 52, 13–22.
Toraya, H. J. Appl. Cryst., 2018, 51, 446–455.
Toraya, H. J. Appl. Cryst., 2019, 52 (in press).

**Quantitative X-ray analysis of natural and artificial supplementary cementitious materials originating from Industrial residues and natural pozzolanic rocks**

Herbert Pöllmann

University of Halle/Saale, Mineralogy/geochemistry, 06120 Halle, Germany

herbert.poellmann@geo.uni-halle.de

$CO_2$-reduction in the field of technical production of building and construction materials participates with about 5-7% of the total amounts of carbon dioxide. To replace the main source of $CO_2$ (decarbonation of limestone) different other natural and technical materials came into focus. These $CO_2$-free raw materials are used from basic raw material mining industry, processing industry and also from different primary industries. These inorganic-based materials are mainly composed of crystalline and amorphous components. As complex mixtures of these different materials occur their mineralogical characterization can be very difficult, but is highly necessary to understand the complex reaction behavior and the overall compositions of these different mixtures of pozzolans (mine tailings, leaching products, slags, ashes, flue gas products, heat treated clays, volcanic and sedimentary rocks, recycling products) and high temperature synthesized cement clinkers. All these differently and very complex mixtures must be characterized to ensure optimal quality of these new cementitious and $CO_2$-reduced mixtures. Other possibilities are in the field of producing different types of cement clinkers at elevated temperatures with new mineralogical compositions. To establish a precise but also fast quantification different determination methods were applied to quantify the different crystalline and amorphous phases. A difference in hydration behavior due to the chemical and mineralogical composition of the materials based on contents of crystalline and amorphous phases can be attributed and is therefore a must in the determinations. The different reaction behavior is based on a definition as is given in Figure 1.

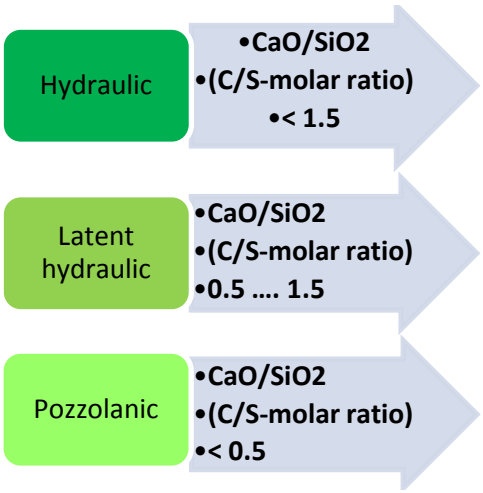


Figure 1. Definitions of hydraulic, latent hydraulic and pozzolanic behavior of cementitious materials.

For these complex cement-based mixtures, several different methods will be applied to show a fast and reliable quantification as base for later hydration. These are Rietveld analysis, Partial least squares regression (PLSR), cluster analysis and partial or not known crystal structures analysis (PONKCS). The results for different cements with a bunch of different added pozzolans using several examples will be demonstrated. As an example, a comparison of the results for amorphous contents obtained by Rietveld method and PLSR is given in Figure 2.

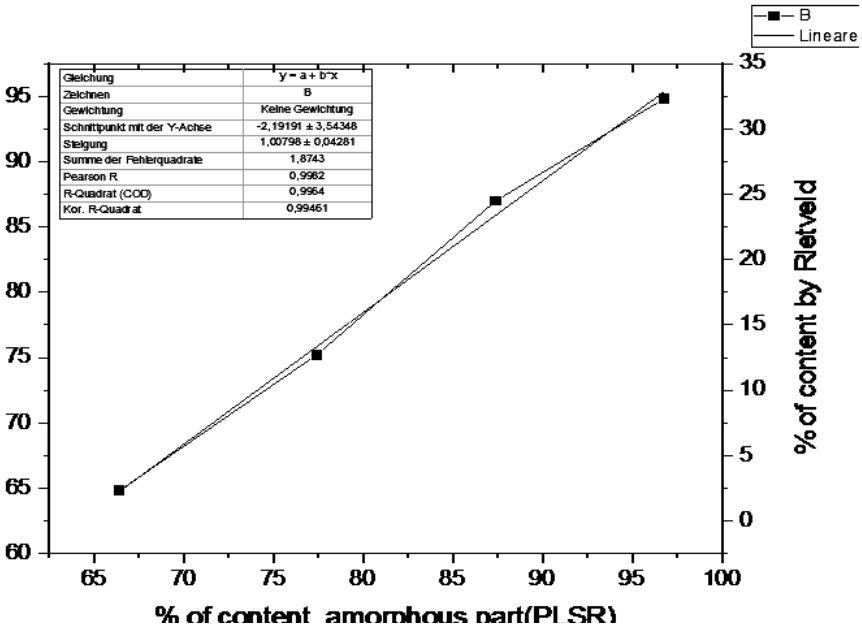


Figure 2. Comparison of results for determinations of amorphous contents in a composite mixture by PLSR and Rietveld analysis

Becckers D., Degen T. & König U. Analysis of hidden information – PLSR on XRD raw data. Acta Cryst. Section A, 2014, 70.

Degen T., Koenig U., Norberg N. PLSR as a new XRD method for downstream processing of ores: - Case study: $Fe^{2+}$determination in iron ore sinter. Powder Diffraction,2014, 29.

Galluccio S., BeiraU T., Pöllmann H. Maximization of the reuse of industrial residues for the production of eco-friendly CSA-belite clinker. Construction and Building Materials, 2019, 208, 250–257.

Galluccio S. & Pöllmann H. Quantifications of cements composed of OPC, Calcined Clay, Pozzolanes and Limestone, Proceedings LC3-meeting Delhi, India, October 2019.

König U., Norberg N. Partial Least Square Regression (PLSR) – A new alternative XRD method for process control in aluminium industries, Conference. paper, 2014.

Rietveld H. M. A Profile Refinement Method for Nuclear and Magnetic Structures. J. Appl. Crystallogr.,1969, 2, 65–71.

Scarlett N.V.Y., Madsen I.C. Quantification of phases with partial or no known crystal structure, Powder Diffraction, 21(4), 278–284.

Scrivener K., Vanderley M. J., Gartner E. M. Eco-efficient cements: Potential economically viable solutions for a low-$CO_2$, cement-based materials industry. UNEP, 2016.

Snellings R., Mertens G., Elsen J. Supplementary Cementitious Materials. – Broekmans, M.A.T.M. & Pöllmann, H. (Eds.): Applied Mineralogy in Cement & Concrete: 211-278, Chantilly (Mineralogical Society of America), 2012.

Stetsko Y.P., Shanahan N., Deford H., Zayed A. Quantification of supplementary cementitious content in blended Portland cement using an iterative Rietveld–PONKCS technique, J. Appl. Cryst.,2017, 50, 498–507.

Westphal T., Füllmann T., Pöllmann H. Rietveld quantification of amorphous portions with an internal standard – Mathematical consequences of the experimental approach. Powd. Diff. 24, 239–243.

**A multi-criteria genetic algorithm for a crystal structure determination from powder diffraction data**

Aleksandr N. Zaloga[1,*], Sergey V. Burakov[2], Igor S. Yakimov[1],
Konstantin A. Gusev[2] and Petr S. Dubinin[1]

[1]Siberian Federal University, Krasnoyarsk, 660025 Russia
[2]Institute of Computer Science of Reshtnev Siberian State University of Science and Technology, 660037 Krasnoyarsk, Russia

* zaloga@yandex.ru

Sometimes, the determination of the crystal structure of a mineral can be difficult due to the complexity of the atomic structure and the inability to obtain a good quality diffraction pattern. In such cases, global optimization methods are used, because they can even work with powder diffraction patterns of mediocre quality. The method of simulated annealing [David et al., 2006; Favre-Nicolin et al. 2002; Whitfield et al., 2010] and genetic algorithms [Feng et al., 2007; Lutterotti et al., 2003] are two methods of global optimization, which are used for the task of the crystal structure determination most often.

The report provides a general description of the crystal structure search method with use of a multi-criteria genetic algorithm from powder diffraction data. This work is a development of the previously presented single-criterion genetic algorithm [Zaloga et al., 2018], in which the profile P-factor of the Rietveld method and the penalty for too short interatomic distances were summed up into one common value of the fitness function. In the new method, these two values represent two separate criteria, and optimization occurs for each of them. This approach allows us to store during the optimization not just one the best solution, but a whole front of solutions (the so-called “Pareto front”), which are the best according to two criteria. This provides an extension of a search space and increases the efficiency of searching the right solution. The report shows the results of applying this algorithm to several test samples determination, as well as comparing the effectiveness of its work with the effectiveness of the previous version of the algorithm.

The reported study was funded by Russian Foundation for Basic Research, Government of Krasnoyarsk Territory, Krasnoyarsk Regional Fund of Science to the research project № 18-43-243009 «Coevolutionary modeling of an atomic-crystal structure of new substances by diffraction data on basis of parallel genetic algorithms and supercomputer computations».

DavidW. I. F., ShanklandK., Van de StreekJ., PidcockE., Motherwell W.D.S., Cole J.C. DASH: a program for Crystal Structure Determination from Powder Diffraction Data. J. Appl. Crystallogr., 2006, 39, 910–915.

Favre-Nicolin V., Cerny R. FOX, ‘free objects for crystallography’: a modular approach to ab initio structure determination from powder diffraction. J. Appl. Cryst., 2002, 35, 734–743.

Feng Z. J., Dong C. GEST: A program for structure determination from powder diffraction data using a genetic algorithm. J. Appl. Crystallogr., 2007, 40, 583–588.

LutterottiL., BortolottiM. Object oriented programming and fast computation techniques in Maud, a program for powder diffraction analysis written in java. IUCr: Compcomm Newsletter, 2003, 1, 43–50.

Whitfield P.S., Davidson I.J., Mitchell L.D., Wilson S.A., Mills S.J. Problem Solving with the TOPAS Macro Language: Corrections and Constraints in Simulated Annealing and Rietveld Refinement. Materials Science Forum, 2010, 651, 11–25.

Zaloga A.N., Yakimov I.S., Dubinin P.S. Multipopulation Genetic Algorithm for Determining Crystal Structures Using Powder Diffraction Data. Journal of Surface Investigation: X-ray, Synchrotron and Neutron Techniques, 2018, 12, 128–134.

# 3. Spectroscopy: Theory and Experiment

**Multilayered mineralogical information in spectroscopy of minerals**

Pavel Yu. Plechov[1]*, Sergey V. Trousov[1], Kirill A. Bychkov[1], Ksenia A. Konovalova[1]

[1] Fersman Mineralogical Museum of Russian Academy of Science, Moscow, Russia

* pplechov@gmail.com

Scientific information for mineralogical objects of study (mineral species, mineral deposits, mineral assemblages) is forming by many methods of study. These methods include various types of descriptions, photo and video documentation, data of chemical composition, X-ray diffraction data, IR and Raman spectra and other data from instrumental mineralogical studies. Each type of the data could be represented as separate layer of information whereas full mineralogical information for each object represents a time-varying complex system of associative connections of these layers of information. The talk is devoted to the methods of formalization of various types of mineralogical information (chemistry, physical properties, spectroscopic data) and the methods of organization for heterogeneous information in the information system.

The primary source of mineralogical information is a mineralogical specimen (sometimes the separate grain in a mount or even a small region of the grain) where mineralogical studies are performed. Grains and mount are often lost during or after the research, which leads to significant difficulties in trying to repeat the study of the object. The special collection of well-characterized samples, grains and mounts was founded (Dec. 2017) in Fersman Mineralogical Museum in addition to etalon mineral collection. At the moment it contains about 400 samples, grains, polished thin sections and mounts. Several thousand microprobe analyzes, LA-ICPMS data, $H_2O$ and $CO_2$ measurements, microphotos and BSE images, IR and Raman spectra as well as results of experimental studies of various physical properties of these minerals have been collected. The research results are partially published in scientific papers. The actual task is to systematization of the accumulated information without significant losses. The report is devoted to the methods of formalization of various types of mineralogical information (chemistry, physical properties, spectroscopic data) and the organization of heterogeneous information in the information system.

For the experiment on systematization of heterogeneous mineralogical information, we used elements of the semantic network that are embedded in non-formalized or partially formalized descriptions. The experience of widely used “mindat.org” and “rruf.info” databases has been taken into account. The main object of information is the specimen for which there is a mandatory and additional attributes. Also, the objects of the information system are mineral species, geographical objects, the results of scientific research, storage sites, personalities and many others. The novelty of the approach to the organization of information in the system is the organization of the information space on semantic relationships between objects in different layers of mineralogical information, which are set automatically by the system itself, but can be corrected in manual editing mode if necessary. Formalized data include chemical composition data, X-ray structural data, IR and CS spectra, as well as the results of other instrumental methods of mineralogical studies. The data is bounded to the specimen (or even to a specific grain in the specimen), but each data type forms a separate information layer, which includes a method for data storage of this type, methods for formalizing and grouping data, methods for matching and processing search queries. As a result, a multilayered information system of mineralogical knowledge is gradually being formed, which can be used as an independent tool in mineralogical studies, for the distribution of mineralogical knowledge, education and self-education.

**Cathodoluminescence (CL) microscopy and spectroscopy of magmatic and metamorphic minerals: New avenues for petrological applications**

Hans-Peter Schertl

Ruhr-University Bochum, Faculty of Geosciences, Institute of Geology, Mineralogy and Geophysics, 44780 Bochum, Germany

hans-peter.schertl@rub.de

During the last 60 years, the technique of cathodoluminescence (CL) microscopy has become a standard tool in mineralogy. While in the past routine application mainly focused on sedimentary rocks and on the characterization of zircon domains prior to ion probe dating, within the last two decades this technique has also been applied to various magmatic and metamorphic rocks.

The current study likes to demonstrate the impact of the "hot cathode" CL microscope, in particular in conjunction with EMP-studies on magmatic and metamorphic rocks, using conventional polished thin sections. Many of the specific features presented could easily have become overlooked without applying CL microscopy. With respect to magmatic rocks, the compilation of data presented includes examples of K-feldspar (blue luminescence), concentric zoning of plagioclase (blue to reddish) and nepheline (dark blue), oscillatory zoning patterns of leucite (blue), heterogeneous zoning of sodalite-group minerals (yellow to blue) and Li-bearing mica (red), datolite (brownish) veins in altered basalt. Selected studies on metamorphic rocks focus on UHP-rocks from the Dora-Maira Massif / Italy, the Kokchetav Massif / Kazakhstan, Sulu and Dabie / China, the Western Gneiss region / Norway, Pohorje / Slovenia, and Erzgebirge / Germany. Further examples include HT- and UHT-metamorphic rocks from Romania and South Africa, skarn deposits from Romania, and Jadeite-rich rocks from the Rio San Juan Complex / Dominican Republic that were formed due to fluid-rock interaction. Among other features, we introduce here: 1) oscillatory zoning patterns of garnet, kyanite, wollastonite, diopside and zircon; 2) regular and irregular – in some cases very complex – growth structures of garnet, jadeite, omphacite, metamorphic olivine, carbonates, and clinopyroxenes; 3) dolomite exsolution patterns in calcite and K-feldspar exsolutions in clinopyroxene; 4) breakdown features of metamorphic coesite (bluish-green luminescence), producing different silica phases as various quartz generations (dark red to violet) and chalcedony (yellow) as well as 5) different carbonate generations of calcite (yellow), Mg-calcite (orange), and dolomite (red) from UHP-rocks.

Note that using high-resolution spectroscopy of the CL-emission, it is possible to characterize and evaluate the colors of different minerals. Narrow bands attributed to the presence of e.g. $Cr^{3+}$, $Dy^{3+}$, $Sm^{3+}$ or $Tb^{3+}$ and broad bands caused by the incorporation of $Mn^{2+}$ and $Fe^{2+}$ can be easily distinguished, even in different zones of the same mineral, for instance in clinopyroxene, kyanite, carbonate sand in garnet. The introduced CL-investigations also contribute to the understanding of mineral reactions, particularly considering the formation of symplectites and pseudomorphs. Further studies focus on interstitial phases and different annealed crack systems of rock matrices; accessory luminescent minerals like diamond (greenish blue and partly zoned), zircon (blue), apatite (green), and bearthite (green) are easily identified in thin section, even when they occur in very small abundance.

In essence, CL enables colour images of important but otherwise invisible growth features and internal structures of minerals to be obtained easily and quickly within seconds. Knowledge of the detailed structural characteristics of magmatic and metamorphic minerals has an high impact on a better understanding of crystallization processes in melts and a more precise derivation of *PT*-paths, respectively, and thus on the evolution of geodynamic processes with any magmatic or metamorphic rocks involved. Thus, we propose the CL-technique to be used more intensively for routine investigations of thin sections as a pathfinder prior to chemical characterization by EMP.

**Luminescence of natural zircon at VUV- and soft X-ray excitation induced by laser and synchrotron**

Sergej L. Votyakov, Yuliya V. Shchapova

Zavaritsky Institute of Geology and Geochemistry, Ural Branch of RAS, Yekaterinburg, Russia

votyakov@igg.uran.ru

Zircon is a brightly luminescent mineral. Luminescence is widely used to study the zircon structural defects when analyzing the U-Pb-system of the mineral in petrochronological applications, predicting the safety of zircon ceramics for the disposal of radioactive elements, etc. [Krasnobaev et al., 1988; Hanchar, Rudnic, 1995; Gotze et al., 1999; Gaft, 2002; Ewing et al., 2003]. To justify models of the luminescence centers (LC) in zircon, it is necessary to study both intra- and interband electronic processes. Taking into account the high value of the band gap ($E_g$>6 eV), such studies can be carried out only using synchrotron radiation (SI) in the VUV- and soft X-ray energy region. In this work, photoluminescence (PL) of the structurally perfect zircons from Yakutia's kimberlites induced by SI at temperatures 10 and 300 K has been investigated at HASYLAB, DESY (Germany). Luminescence spectra (2.5-6 eV), luminescence excitation spectra (5-25, 50-200 and 500-620 eV) as well as the decay kinetics of luminescence has been analyzed. Luminescent peculiarities of initial and annealed at 1200 ºC crystals have been compared. Initial crystals are characterized by radiation damaged structure due to self-irradiation of U and Th impurities radioactive decay. The crystal structure mainly recovers after annealing. Zone structure of the natural zircon crystals has been studied; the value of $E_g$has been estimated as 7.1 eV. Two groups of luminescence bands (2.1, 2.7-2.8, 3.2-3.3 eV and 4.4-4.7, 5.4 eV) connected with impurities (radiation?) defects of crystalline structure and attributed to intrinsic emission have been analyzed due to the peculiarities of the luminescence excitation spectra under $E_{exc}<E_g$, $\sim E_g$ and $>>E_g$. The kinetics of luminescence 5.4 eV band has been estimated as 4 ns. PL of the structurally imperfect zircons from carbonatites of Australia and alluvial deposits of Sri Lanka induced by a xenon lamp and laser lines 473, 488, 514, 633 nm has been studied at 300 K, as well as PL induced by laser lines 263, 527, 1053 nm at 6.5–320 K. Imperfect zircons are characterized by autoirradiation doses 0.02–$5.07\cdot10^{18}$ $\alpha$/g. Mechanisms of luminescence in structurally imperfect zircons have been analyzed; some physical models have been proposed. The outlines of the zircon broadband PL spectrum have been found to have a number of gaps at 428.3, 477.3, 586.2–586.4, 616.0, 649.2, 686.0–687.5 nm, caused by the reabsorption of impurity $U^{4+}$-ions. The effect of U-reabsorption has been found to depend on its concentration, observation temperature and the mineral imperfectness. The U-impurity centre structure has been considered. The possibilities of an integrated approach, including the PL and Raman scattering spectra analysis, spectroscopic imaging of zircon grains for investigation of the local features of zircon structure have been demonstrated.

The work was carried out at the Common Use Center "Geoanalyst" with the financial support by the Russian Science Foundation (grant No. 16-17-10283).

Ewing R., Meldrum A., Wang L., Weber W., Corrales L. Zircon. Reviews in Mineralogy and Geochemistry, 2003, 53, 387–425.

Gaft M., Shinno, Panczer G., Reisfeld R. Laser-induced time-resolved spectroscopy of visible broad luminescence bands in zircon. Min. Petr., 2002, 76, 235–246.

Gotze J., Kempe U., Habermann D., Nasdala L., Neuser R., Richter D. Hight-resolution CL combined with SHRIMP measurments of detrital zircons. Min. Mag., 1999, 63, 179–187.

Hanchar J., Rudnic R. Revealing hidden structures: the application of CL and BSE imaging to dating zircons from lower crustal xenoliths. Lithos, 1995, 36, 289–303.

Krasnobaev A., Votyakov S., Krokhalev V. Spectroscopy of Zircon (Properties, Geological Applications). Nauka, Moscow, 1988 (in Russian).

**The Crystals of Ge, Ga-rich Topaz: Crystal Growth, Germanium and Gallium Distribution, Raman Spectroscopy**

Vladimir S. Balitsky[2], Pavel S. Kvas[1,2], Elena Yu. Borovikova[1,*], Dmitry Yu. Pushcharovsky[1], Tatiana V. Setkova[2] and Valentina A. Nesterova[1,2]

[1] Department of Geology, Lomonosov Moscow State University, 119991 Moscow, Russia
[2] D.S. Korzhinskii Institute of Experimental Mineralogy of Russian Academy of Sciences, 142432 Chernogolovka, Russia

* alena.amurr@gmail.com

We report the first successful growth of Ge,Ga-rich topaz single crystals on seed by hydrothermal method at 650 ºC and 100 MPa. Before now, the small crystals of Ge-analogue of high-pressure phase topaz-OH were synthesized at 650 ºC and 2 GPa [Wunder et al., 1997]. The crystal growth procedure of Ge,Ga-rich topaz was based on the method previously developed [Balitsky et al., 2006] and founded to results of study of silica/alumina transport phenomena in supercritical water solutions. The experiments were carried out in chromium–nickel alloy autoclaves. The nutrient consisted from mixture of both quartz and topaz places in the upper (colder) zone of autoclave. The topaz seeds and mixture of powdered oxide germanium and gallium was putted in lower (hotter) zone of autoclave. Duration of the crystal growth runs was from 1 to 2 months.

As a result, topaz single crystals of bluish-green color with a thickness of up to 4 mm on one side of the seed has been grown. The external morphology of the as grown crystals is determined by crystallographic orientation of seeds, their form and sizes. Grown layer characterized by a clear zoning and sectorial structure. The distribution of gallium and germanium in Ge,Ga-rich topaz is highly uneven. The maximum replacement of silicon and aluminum by the indicated elements occurs at the boundary of the seed crystal and the grown layer, reaching 25 wt.% $GeO_2$ and 6 wt.% $Ga_2O_3$, respectively.

Polarized Raman spectra in two back -scattering geometries $\overline{y}(zz)y$ and $\overline{y}(xx)y$ obtained in five points. The Raman spectra of the Ga- and Ge-rich boundary layer had a sharply different character, which is intermediate between topaz and kriselite spectra. All vibrational bands of this layer are much broader than those of the natural topaz and synthetic OH-Ge-topaz [Schlüter et al., 2010], which indicates a strong disordering of cations of different sizes both in the octahedral and tetrahedral structural sites. The vibrational modes corresponding to $(Si,Ge)O_4$ and (Al,Ga)–O vibrations are significantly shifted towards lower frequencies in comparison with natural topaz spectra due to Si/Ge and Al/Ga mass effects. Some bands in the region of lattice vibration at ~268, ~291 $cm^{-1}$ show the inversed trend of shifting to higher frequencies, which can also be observed in the kriselite spectrum. The Raman spectra taken in 3-5 points had the topaz-like character. The bands of $(Si,Ge)O_4$ and (Al,Ga)–O vibrations in these spectra show the gradually shift to higher frequencies, which indicates a decrease of Ge and Ga content in respective cation positions.

Balitsky V.S., Balitsky D.V., Balitsky S. D., Aurisicchio C. and Roma M.A. Silica and alumina transfer in supercritical aqueous fluids and growing of topaz monocrystals in them. Geochemistry International, 2006, 44, 2, 175–181.

Schlüter J., Geisler T, Pohl D, Stephan T. Krieselite, $Al_2GeO_4(F,OH)_2$: A new mineral from the Tsumeb mine, Namibia, representing the Ge analogue of topaz N. Jb. Miner. Abh., 2010, 187/1, 33–40.

Wunder B., Marler B. Ge-analogue of aluminum silicates: High-pressure synthesis and properties of orthorhombic $Al_2GeO_4(OH)_2$. Eur. J. Miner, 1997, 9, 1147–1158.

**VIS-spectroscopy Study of Co-blue spinel from Luc Yen, Vietnam.**

Marakhovskaya O.Y.[1,2,*], Kuksa K.A.[1,2], Sokolov P.B.[2]

[1] St. Petersburg State University, 199034 St. Petersburg, Russia
[2] Sokolov Co. Ltd, 197136 St. Petersburg, Russia

* o.y.marakhovskaya@gmail.com

Nowadays, “cobalt” blue spinel is considered as the most expensive and sought-after spinel on the gemstone market due to its unusual bright color. It is believed that this neon-like color is the result of the accumulation of $Co^{2+}$ and / or $Fe^{2+}$ impurities in the spinel structure. However, the precise position of $Co^{2+}$ in the structure of blue spinel is still open. Some argue that cobalt occupies octahedral position [Huong et al., 2018], others – tetrahedral [D’Ippolito et al., 2015; Chauvire et al., 2015].

Detailed investigation of 22 blue spinel crystals from Luc Yen, Vietnam with LA-ICP-MS allows us to outline its average chemical composition in regard with trace elements. In comparison with spinel of blue color from other deposits [D’Ippolito, 2013, D’Ippolito et al., 2015, Peretti, 2003, our unpublished data], studied samples are characterized by higher Li, Ga, Cr, Co and Ni contents, and lower Fe, Mn and Zn amounts. Co concentration varies from 77 to 297 ppm and Fe one ranges from 2590 to 10500 ppm.

In order to determine the position of Co in the crystal structure of “cobalt” spinel, the visible absorption spectra were measured for 4 samples. Figure 1 shows the adsorption peaks of $Co^{2+}$ ions in the spinel at 544, 551, 578, 623 nm, which is in a good agreement with data of previous researches [Chauvire et al., 2015]. In addition, there is a fan-like peak characteristic of $Co^{2+}$ ions in the range of 550–650 nm, which indirectly confirms that the blue color of spinel is due to cobalt but not iron [Platonov et al., 1984]. Also, the $Co^{2+}$ peak is positioned at 544 nm, which is typical for $Co^{2+}$ in the octahedral position [Cotton et al., 1999].

Since the peaks of $Co^{2+}$ ions are in the range of 550–650 nm, we may assume, that $Co^{2+}$ ions in the blue spinel of Luc Yen occupy both octahedral and tetrahedral positions in the structure of the mineral [Platonov et al., 1984]. Also, $Co^{2+}$ and $Fe^{2+}$ peaks are equally suited to wavelengths for blue spinel.

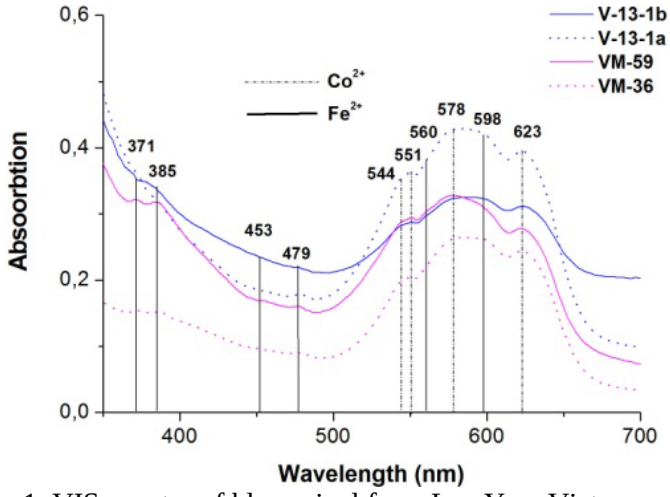


Figure 1. VIS-spectra of blue spinel from Luc Yen, Vietnam.

Chauviré et al. Blue spinel from the Luc Yen district of Vietnam. Gems & Gemology, 2015, 51, 2–17.

Cotton F.A., Wilkinson G., Murillo C.A., Bochmann M. Advanced inorganic chemistry. A Wiley-Interscience publication, 1999, part 3, 17.F. (Co).

D'Ippolito et al. Color mechanisms in spinel: cobalt and iron interplay for the blue color. Phys Chem Minerals, 2015.

D’Ippolito A. Linking crystal chemistry and physical properties of natural and synthetic spinels: an UV–VIS–NIR and Raman study. PhD Thesis, Sapienza Università di Roma, 2013.

Huong et al. Study of impurity in blue spinel from the Luc Yen mining area, Yen Bai province, Vietnam. Viet. J. Earth Sci., 2018, 40(1), 47–55.

Peretti, G.. Spinel from Namya. Contributions to Gemology, 2003, 2, 15–18.

Platonov et al. The nature of gems color. Nedra, Moscow, 1984 (in Russian).

**Optical spectroscopy for analyzing of the cation disordering in $MgAl_2O_4$ spinel**

Yuliya V. Shchapova[1]*, Elizaveta A. Pankrushina[1], Aleksander Yu. Kisin[1], Sergey L.Votyakov[1]

[1]Zavaritsky Institute of Geology and Geochemistry UB RAS, 620016 Ekaterinburg, Russia

*shchapova@igg.uran.ru

In spinel $^{IV}(A_{1-\delta}B_{\delta})^{VI}(A_{\delta}B_{2-\delta})O_4$, the disordered $A^{2+}$ and $B^{3+}$ cation distribution over tetrahedral and octahedral sites can be stabilized; the inversion parameter δ depends on the chemical composition, *P*,*T*-conditions of crystallization, the subsequent thermal and radiation history, etc. Evaluation of the disordering degree is necessary for solving the petrological and mineralogical problems as well as for synthesis of spinel structure ceramics with desired properties. Traditionally, the determining of δ values relies on single crystal X-ray or neutron diffraction techniques. The development of optical micro-spectroscopy based on Raman scattering (RS) and photoluminescence (PL) seems to be relevant for this purpose. In this study, we have analyzed the RS and PL spectroscopic properties of spinel with different structure disordering degree achieved by the variation of the $Cr^{3+}$ content, the heat treatment and the ion and electron irradiation. The natural spinel from the Kukhilal deposit (Pamir) and the Murzinsko-Aduysky and Kochkarsky anticlinoria (Urals), as well as the $MgAl_2O_4$ synthetic ceramics obtained by the high-temperature pressing method were investigated. The analysis of superimposed RS and PL spectra was performed. In the Raman spectrum of the pure, highly ordered spinel from Kukhilal, the vibrational modes $A_{1g}$, $E_g$, $3F_{2g}$ with narrow (5-6 $cm^{-1}$ for the $E_g$) and symmetric maxima are distinguished (Figure); the contribution of luminescence of typical impurity ions $Mn^{2+}$ and $Cr^{3+}$ is analyzed. It was shown that the zero-phonon $R_{1,2}$ lines (684.7 and 684.5 nm) and the phonon sideband dominate in the PL spectrum of $Cr^{3+}$ ($^2E_g \rightarrow {}^4A_{2g}$); a set of low-intensity zero-phonon N-lines associated with $Cr^{3+}$ emission in distorted octahedral sites and the $N_4$-line associated with Cr-Cr paired centers were detected. The effect of annealing at 700–760 °C on the RR and PL spectra was studied and a number of structurally sensitive RS and PL parameters were established: the $E_g$ 408 $cm^{-1}$ Raman mode width; the intensity ratio of $E_g$ 408 $cm^{-1}$ and $E_g$ 380 $cm^{-1}$ modes; the position of the $F_{2g}(1)$ mode near 313 $cm^{-1}$; the ratio of the PL line intensities $n_2/N_1$. The regular trends in RS and PL are analyzed depending on the Cr content, annealing temperature and sample irradiation dose (Figure).

The work was carried out at the Common Use Center “Geoanalyst” with the financial support by the Russian Science Foundation (grant No. 16-17-10283) and RFBR (№18-05-01153). The authors are grateful to A.N. Kiryakov and A.F. Zatsepin for providing samples of synthetic spinel.

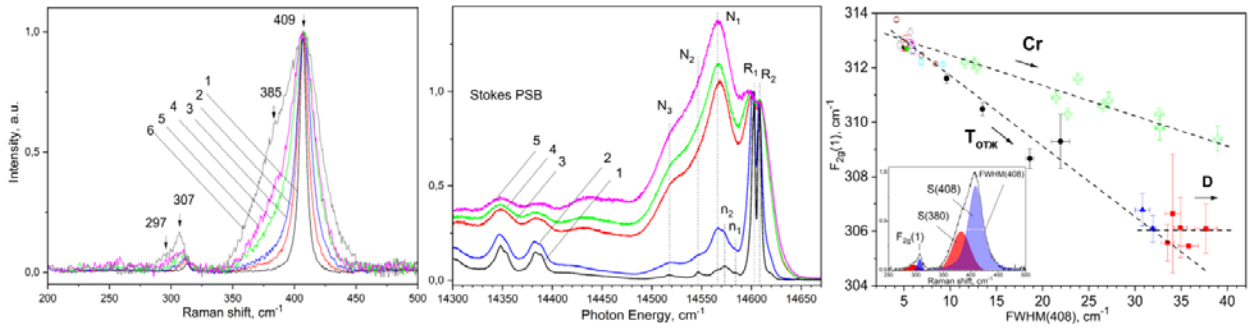


Figure. Raman (a, *T*=300K) and PL (b, 77 K) spectra of the Kukhilal’s spinel in the initial state (1) and after annealing at 700 (2), 720 (3), 740 (4), 760 °C (5) and of the synthetic $MgAl_2O_4$ ceramic (6); the variation in RS parameters with increasing Cr content, annealing temperature *T*, and irradiation dose D. Spectrometer LabRam HR800 Evolution, the excitation line 488 nm

**Raman study of hydroxide-perovskite [$MgSi(OH)_6$] at high pressure up to 7 GPa**

Ulyana O. Borodina*, Sergei V. Goryainov, Anton F. Shatskiy

Sobolev Institute of Geology and Mineralogy, Siberian Branch of Russian Academy of Sciences, 630090 Novosibirsk, Russia

* borodinauo@igm.nsc.ru

Dense hydrous magnesium silicates (DHMS) are important potential water carriers into deep parts of the Earth's mantle. OH-perovskite (or hydroxide-perovskite, 3.65 Å-phase) [$MgSi(OH)_6$] is the less studied phase of DHMS group and the DHMS phase with maximum water content (up to ~35 wt.% $H_2O$) and is one of the largest repositories of water among all the known hydrous phases [Mookherjee et al., 2015]. Besides, it presents great crystal chemistry interest as one of the six-coordinated silicon compounds.

Raman spectra of hydroxide-perovskite (grown at P = 12 GPa, T = 425 °C for 2 hours in DIA-type multianvil apparatus) were recorded in the region from 70 to 3800 $cm^{-1}$. High pressures up to ~7 GPa at room temperature ($T$= 22 °C) were obtained in an apparatus with lever-arm-driven diamond anvils. Methanol-ethanol mixture was used as a pressure transmitting medium.

OH-perovskite Raman spectrum at ambient pressure exhibits external and internal octahedral stretching/bending (Mg-O / O-Mg-O and Si-O / O-Si-O) modes, bending δ(OH) -vibrations at 681 and 1036 $cm^{-1}$ and OH-stretching vibrations at frequencies above 3000 $cm^{-1}$. In the region of octahedral vibrations, intense modes at 197, 271+290 $cm^{-1}$ (duplet) and less intense modes at 265, 300 и 404 $cm^{-1}$, OH-stretching vibrations at 3147, 3225, 3291, 3404 and 3463 $cm^{-1}$ are observed.

In order to interpret the Raman modes, three methods were used: the lattice dynamics method by means of the LADY program [Smirnov & Kazimirov, 2001]; empirical exponential function by Novak and Libowitzky [Libowitzky, 1999]; Morse-potential model of hydrogen bond [Goryainov, 2012]. The O-H…O bond lengths, calculated by the last model [Goryainov, 2012], are in a good agreement with structural data [Wunder et al., 2011].

Upon the pressure increase, octahedral and δ(OH) vibrations exhibit linear positive pressure shift, while frequencies of the OH-stretching modes have inverse pressure dependence. The ν/$P$ dependences have rather regular character. However, minor anomalies are observed in the OH-stretching vibrations region.

This work was supported by the Russian Federation state assignment (Project No. 0330-2016-0004) and the Russian Foundation for Basic Research (Grant No. 18-05-00966).

Goryainov S. A model of phase transitions in double-well Morse potential: Application to hydrogen bond. Physica B: Condensed Matter, 2012, 407, 4233–4237.

Libowitzky E. Correlation of O-H stretching frequencies and O-H… O hydrogen bond lengths in minerals. Monatshefte für Chemie/Chemical Monthly, 1999, 130, 1047–1059.

Mookherjee M., Speziale S., Marquardt H., Jahn S., Wunder B., Koch-Müller M., Liermann H.-P. Equation of state and elasticity of the 3.65 Å phase: Implications for the X-discontinuity. American Mineralogist, 2015, 100, 2199–2208.

Smirnov M. & Kazimirov V. LADY: software for lattice dynamics simulations. 2001.

Wunder B., Wirth R., Koch-Mu¨ller M The 3.65 A phase in the system MgO-$SiO_2$-$H_2O$: Synthesis, composition, and structure. American Mineralogist, 2011, 96, 1207–1214.

**EPR in single crystals of technogenic gypsum and powders of its dehydration products**

Ravil A. Khasanov[1,2,*], Nazim M. Nizamutdinov[1], Nailia M. Khasanova[1]

[1] Kazan Federal University, 420008 Kazan, Russia
[2]Central Research Institute for Geology of Industrial Minerals, 420097 Kazan, Russia

* ravil.khasanov.40@mail.ru

Technogenic gypsum irradiated with X-rays became a marker of arid, dry conditions with a set of paramagnetic centers analogous to that in the known natural crystals. The parameters of the spin Hamiltonian were found and models of centers were established that are suitable for reliable EPR dating and environmental reconstruction [Khasanova et al., 2015].

The powder EPR spectra of technogenic gypsum derivatives subjected to isothermal annealing with an exposure time of 30 minutes in the range of 100–375 °C and 600 °C, and subsequent X-ray irradiation at 25 °C were studied. Paramagnetic centers and main phase states of the gypsum annealing products were interpreted and compared with the results of the study in the plaster "Marino glass" [Khasanov et al., 2014].

Khasanova N.M. et. al. Morphology and radiation-induced centers of technogenic gypsum. Procedia Earth and Planetary Science, 2015, 15, 579–584.

Khasanov R.A. et. al. Phase States of the Gypsum Thermal-Annealing Derivatives According to Electron Spin Resonance Spectra. Crystallography Reports, 2014, 59(3), 399–406

**Investigation of ceramics $BiNbO_4$ doped by ions of Fe and Mn by ESR spectroscopy**

Vladimir P. Lyutoev[1]*, Nadezhda A. Zhuk[2]

[1] IG Komi SC UB RAS, 167982 Syktyvkar, Russia
[2] Syktyvkar State University, 167001 Syktyvkar, Russia

* vlutoev@geo.komisc.ru

The compound of bismuth orthoniobate $BiNbO_4$ (bismutocolumbite) is of scientific and practical interest due to their magnetic, microwave dielectric and catalytic properties, strongly dependent on doping elements of transition metal. Bismuth orthoniobate and its solid solutions are promising as a dielectric interface in monolithic capacitors and EMC filters for super-high frequency equipment. To optimize the electrophysical properties of ceramics, the composition of $BiNbO_4$ was modified by iso- and heterovalent substitution of niobium and bismuth atoms with transition elements, but the structural state of the doping elements was not determined experimentally.

The low-temperature orthorhombic ($\alpha$-$BiNbO_4$) and high-temperature triclinic ($\beta$-$BiNbO_4$) modification of bismuth orthoniobate doped with oxides of Mn and Fe in the proportions of substitution of Nb atoms were studied by us using the ESR [Lutoev et al., 2018; Zhuk et al., 2019a,b]. Solid solutions of $BiNb_{1-x}Mn(Fe)_xO_{4-\delta}$ with $0.003 \le x \le 0.06$ are synthesized by standard ceramic procedure using staged calcination at 650, 950 ($\alpha$-$BiNbO_4$) and 1100 °C ($\beta$-$BiNbO_4$). Monophase composition of the obtained compounds was confirmed by SEM and x-ray diffraction.

According to EPR data in $\alpha$-$BiNbO_4$, impurity ions $Fe^{3+}$, $Mn^{2+}$ are localized in isolated weakly distorted octahedral positions of Nb atoms, but most of them are clustered. A well-resolved ESR spectra of $Fe^{3+}$ and $Mn^{2+}$ were obtained for $\beta$-$BiNbO_{4-\delta}$ phase, which allowed to determine their spin-Hamiltonian parameters: $H = g\cdot\mu\cdot\boldsymbol{B}\cdot\boldsymbol{S} + A\cdot\boldsymbol{S}\cdot\boldsymbol{I} + D\cdot O_2^0/3 + E\cdot O_2^2$.

The triclinic phase of $BiNbO_4$ has two types of octahedral positions of $Nb^{5+}$, differ by average bond length Nb-O. However, EPR spectra reveal the distribution of isolated $Fe^{3+}$ ions in position of four types. Two positions $Fe^{3+}$ with the same zero-field splitting D = 0.72 $cm^{-1}$, but with different degree of rhombic distortion E/D = 0.24 and 0.17 were assigned, respectively, to two octahedral positions $Nb^{5+}$ with the nearest oxygen vacancy. Pair of additional positions of $Fe^{3+}$ with a lower value of D = 0.47 $cm^{-1}$ and low rhombic distortion E/D = 0.12 and 0.08, were be attributed to the same structural positions of $Nb^{5+}$, but with a remote oxygen vacancy. The positions $Nb^{5+}$ with longer average bond length Nb-O turn out to be two times more occupied by $Fe^{3+}$ ions with more high value of rhombic distortion E/D. A similar distribution of the lattice structure position $\beta$-$BiNbO_{4-\delta}$ was found for $Mn^{2+}$ ions. The EPR spectra of this ion are a superposition of the signals from the ions by large and small value of D in rhombic and, respectively, axially distorted octahedral positions (E/D = 0.31, D = 0.158 $cm^{-1}$, A($^{55}$Mn) = 8.4 mT and E/D ≈ 0, D ≈0.02 $cm^{-1}$, A($^{55}$Mn) = 8.6 mT).

The measured total integrated intensities of the EPR spectra of isolated $Fe^{3+}$ and $Mn^{2+}$ ions in the structure of $\beta$-$BiNbO_{4-\delta}$ in the studied range of their concentrations are in the saturation region, depending weakly on the concentration of the dopant. A significant part of the impurity ions in the structure of bismuth orthoniobate is in the cluster form.

Lutoev V. P., et al. Modeling EPR Powder Spectra of triclinic $BiNb_{1-x}Mn_xO_4$ // Journal of Siberian Federal University. Mathematics & Physics. 2018. V. 11(5). P. 615–621.

Zhuk N. A., et al. EPR and NEXAFS study of $BiNb_{1-x}Fe_xO_{4-\delta}$ceramics. Physica B: Condensed Matter., 2019a, 552, 142–146.

Zhuk N. A., et al. Mn doped $BiNbO_4$ ceramics: thermal stability, phase transitions, magnetic properties, NEXAFS and ESR spectroscopy. Journal of Alloys and Compounds, 2019b, 778, 418–426.

**Complex internal textures in kyanite: a CL, EBSD and Raman spectroscopic study**

Olga V. Rezvukhina[1,*], Andrey V. Korsakov[1], Dmitriy I. Rezvukhin[1], Dmitry A. Zamyatin[2], Evgeny D. Greshnyakov[3], and Vladimir Ya. Shur[3]

[1] Sobolev Institute of Geology and Mineralogy, Siberian Branch of the Russian Academy of Sciences, 630090 Novosibirsk, Russia
[2]ZavaritskyInstitute of Geology and Geochemistry UB RAS, 620016 Ekaterinburg, Russia
[3]School of Natural Sciences and Mathematics, Ural Federal University, 620000 Ekaterinburg, Russia

* olgashchepetova@igm.nsc.ru

The study of the ultrahigh-pressure metamorphic (UHPM) rocks is of great interest today because of their use for the reconstruction of the processes occurring in the subduction zones. A characteristic feature of the UHPM complexes is the absence of the prograde *PT*-path part, which is erased as a result of the dehydration reactions, as well as during high-temperature anatexis. Kyanite is widely distributed in HP rocks and has a simple chemical composition ($Al_2SiO_5$), which allows using it for the reconstruction of UHPM rock evolution [Kendrick, Indares, 2018]. Previous studies have shown that the study of the kyanite internal textures by means of electron backscatter diffraction (EBSD) provides important data for the study of deformation processes occurring in subduction zones [Beane, Field, 2007], whereas cathodoluminescence (CL) mapping of kyanite allows deciphering the metamorphic history of UHPM rocks [Kendrick, Indares, 2018]. This paper presents the results of a combined CL+EBSD+Raman investigation of the kyanite porphyroblasts from the diamond- (Kumdi-Kol block) and coesite-grade (Kulet block) kyanite-bearing rocks from the Kokchetav massif. Kyanite porphyroblasts from both localities have a zonal distribution of graphite, which is expressed in the presence of the graphite-rich cores and the clean overgrowth zones. In the kyanite porphyroblasts from coesite-grade rocks, the inclusions of quartz, coesite, xenotime, rutile, zircon, apatite and monazite were identified. Kyanite porphyroblasts from the diamond-grade rocks, in addition to the minerals listed above contain diamond, allanite, dumortierite and siderite.

The study revealed that the kyanite porphyroblasts from both types of rocks have complex internal textures which are related to its complicated metamorphic history. The radial fibrous pattern and irregular spotty zoning were distinguished by means of Raman imaging and CL, whereas the intergrowth of two kyanite crystals and twinning were identified only by EBSD and Raman spectroscopy methods. The study of the kyanite porphyroblasts by the CL method shows that it consists of domains with different CL intensity, and displays red CL which is commonly related to the high concentrations of $Cr^{3+}$ impurity [Müller et al., 2012]. However, the study of kyanite chemical composition revealed that there is no any correlation between the impurities (Cr, Ti, Ni, V) level and CL-intensity in kyanite. The study showed that the combined CL, EBSD and Raman spectroscopic study of the kyanite porphyroblasts provides better spatial resolution for the deciphering the internal textures in kyanite, rather than the selective approach employment.

This study was supported by the Russian Science Foundation (grant № 18-17-00186).

Beane R. J., Field C. K. Kyanite deformation in whiteschist of the ultra high pressure metamorphic Kokchetav Massif, Kazakhstan. Journal of Metamorphic Geology, 2007, 25 (2), 117–128.

Kendrick J., Indares A. The reaction history of kyanite in high-P aluminous granulites.Journal of Metamorphic Geology, 2018, 36(2), 125–146.

Müller A., van den Kerhof A. M., Broekmans M. A. T. M. Trace element content and optical cathodoluminescence of kyanite. Proceedings of the 10th International Congress for Applied Mineralogy (ICAM), 2012, 453–461.

**Crystal-chemistry, Raman spectroscopy and origin of some natural LILE-enriched exotic titanate minerals**

Dmitriy I. Rezvukhin[1,*], Taisia A. Alifirova[1], Andrey V. Korsakov[1] and Alexander V. Golovin[1]

[1] Sobolev Institute of Geology and Mineralogy, Siberian Branch of the Russian Academy of Sciences, 630090 Novosibirsk, Russia

* m.rezvukhin@igm.nsc.ru

Large-ion lithophile element (LILE)-enriched titanates of the magnetoplumbite, crichtonite and hollandite groups have been investigated in a mantle xenolith from the Udachnaya-East kimberlite mine, Russia. The studied titanate minerals occur within an orthopyroxenitic assemblage consisting of enstatite with subordinary Cr-bearing suite of minerals, i.e. pyrope, diopside and spinel. Magnetoplumbite-group minerals (yimengite-hawthorneite, YIHA) and crichtonite-group minerals (CGM) compose abundant inclusions (10–100 μm) in enstatite in association with other Ti- and/or Cr-rich oxide minerals (rutile, Mg-Cr-ilmenite, Cr-spinel) and pentlandite. CGM are also typical of intergranular space, where they form complex oxide aggregates together with rutile, picroilmenite and Cr-spinel. Hollandite-type titanates (priderite and redledgeite) are rare and have been identified only in the rock interstices.

The examined YIHA grains, $(K,Ba)(Ti,Cr,Al,Fe,Mg)_{12}O_{19}$, are compositionally interjacent between yimengite and hawthorneite end-members with an overall tendency towards K-dominant compositions. Ba- and K-specific in the *A* site CGM ($ABC_{18}T_2O_{38}$) inclusions in enstatite chemically resemble lindsleyite-mathiasite minerals (LIMA), though contain much lower Zr in the *B* site than typical LIMA titanates. CGM in interstitial oxide intergrowths show highly diverse compositions even within individual aggregates, where they are chemically dominated by Ba, Ca and Sr. Priderite and redledgeite, ideally $KFe^{3+}Ti_7O_{16}$ and $BaCr^{3+}{}_2Ti_6O_{16}$, respectively, can be easily distinguished in the sample by optical properties and composition, albeit both typically occur as a solid solution towards one another. The Raman spectra of the all examined titanates have major bands at ~680–710 $cm^{-1}$, reflecting the symmetric stretching vibrations of $Ti^{4+}O_6$, $Cr^{3+}O_6$ and other $CationO_6$ octahedra; other strong bands appear in the region of 130–680 $cm^{-1}$.

The orthopyroxenite is spectacular due to a remarkable variety of minerals presented in volumetrically small proportions, including titaniferous and Cr-bearing oxides, silicates (olivine, phlogopite, tetraferriphlogopite, amphiboles, serpentine, chlorite, talc), carbonates (calcite, dolomite, siderite), sulfides (pentlandite, djerfisherite, pyrrhotite), sulfate (barite), phosphates (apatite and $Na_2BaMg[PO_4]_2$), hydroxides and hydroxochlorides of Fe. Their occurrence is interpreted to result from at least three superimposed processes: 1) deep-seated mantle metasomatism, 2) infiltration of a kimberlite melt and 3) late hydrothermal alterations. The YIHA and CGM are considered to be epigenetic in respect to the host orthopyroxenite and were formed from a Ba-K-rich metasomatic agent responsible for the exotic titanate (YIHA, CGM) and pentlandite precipitation during the residence of the rock in the lithospheric mantle. Priderite and redledgeite chiefly replaced earlier-formed oxides and are suggested to have been crystallized much later; priderite is possibly related to the (post)kimberlitic stage, whereas redledgeite appears to be the latest, showing genetic affinity to late-stage hydrothermal fluids.

Additional information on the YIHA and CGM in the orthopyroxenite with implications for mantle processes is provided in [Rezvukhin et al. 2019].

This work was supported by the RFBR grant № 18-05-00643.

Rezvukhin D.I., Alifirova T.A., Korsakov A.V., Golovin A.V. A new occurrence of yimengite-hawthorneite and crichtonite-group minerals in an orthopyroxenite from kimberlite: Implications for mantle metasomatism. American Mineralogist, 2019, doi10.2138/am-2019-6741.

**Raman spectroscopy and imaging in mineralogical stomatology**

Daria V. Kiseleva[1]*, Sergei L. Votyakov[1], Elizaveta A. Pankrushina[1], Yulia V. Mandra[2]

[1] A.N. Zavaritsky Institute of Geology and Geochemistry, UB RAS, 620016 Ekaterinburg, Russia
[2] Ural State Medical University, 620028 Ekaterinburg, Russia

* Kiseleva@igg.uran.ru

Interdisciplinary research is the major trend in modern science, including dental medicine. Mineralogical stomatology is developed at the interface of dental medicine and biomineralogy [Votyakov et al., 2017]. This discipline is focused on studies of human hard dental tissues, restoration materials, dental prosthetics, zones of interaction (hybridization) using techniques and approaches developed in biomineralogy and based on the application of modern analytical techniques (scanning and transmission electron microscopy with EDX analysis, electron probe microanalysis, laser ablation ICP mass spectrometry, IR and Raman spectroscopy, etc.)

In the report the results of spectroscopic studies of tooth tissues (intact and with various pathologies) are considered. In order to investigate the local structural variations of tooth tissues, both intact and affected, we performed hyper-spectral Raman imaging and mapping of their properties, such as carbonate-ion contents, degree of crystallinity, and collagen content through the various structural zones of dental tissues (Figure). The issues of measuring the degree of conversion of light-cured composites by Raman spectroscopy were examined as well.

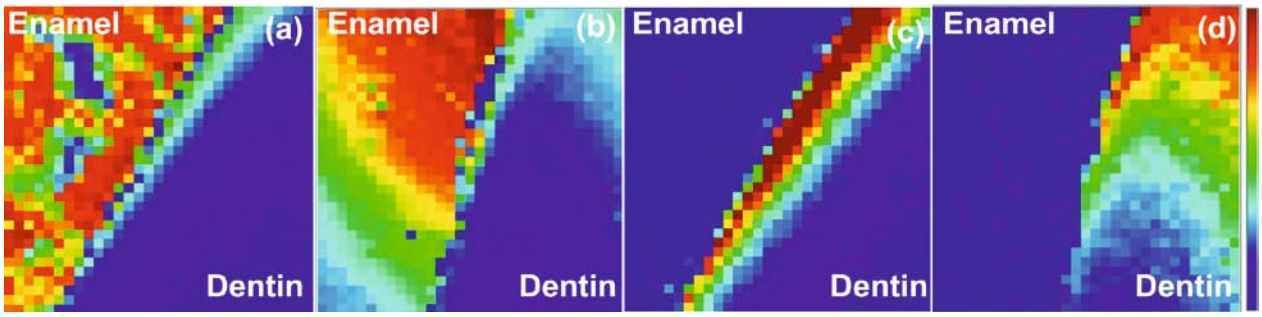


Figure. Raman mapping of the intact (a, c) and eroded (b, d) tooth using the integral intensity of the 960 $cm^{-1}$ P-O stretching mode (a, b) and C-H bond vibrations in lipids and proteins in the region of 2880–2700 $cm^{-1}$ (c, d) across the dentin–enamel junction. Image size is 450 μm by 450 μm with 15 μm step size.

The results obtained substantiate the structural variations in intact and affected teeth as the degree of bioapatite disorder [Wang et al., 2018]. The changes observed in the degree of mineralization and their manifestation through the linewidth and peak position of P-O stretching vibration at 960 $cm^{-1}$ and C-H stretching vibration at 2940 $cm^{-1}$ are the sensitive probes of the local structural environment.

The work is carried out in the UB RAS Geoanalytic Center for Collective Use and supported by AAAA-A18-118053090045-8 topic of IGG UB RAS State Assignment.

Votyakov S.L., Mandra Yu.V., Kiseleva D.V., Grigoriev S.S., Ron G.I., Panfilov P.E., Zaytsev D.V., Ivashov A.S., Saypeev K.A., Abdulina Yu.N. Mineralogical stomatology as an interdisciplinary research field: recent results and development prospects. Actual problems in dentistry, 2017, 13(1), 3–16.

Wang P., Anderson E.J.D., Muller E.A., Gao F., Zhong Y., Raschke M.B. Hyperspectral Raman imaging correlating chemical substitution and crystallinity in biogenic hydroxyapatite: dentin and enamel in normal and hypoplastic human teeth. Journal of Raman spectroscopy, 2018, 1–9.

**Application of Mössbauer, ESR, and FT-IR spectroscopy for mineralogical and technological studies of refractory Fe-Ti and Fe-Mn ores**

Vladimir P. Lyutoev[1]*, Alexander B. Makeev[2], Viktor A. Saldin[1],
Andrei Yu. Lysiuk[1], Oxana S. Golovataya[3]

[1] IG Komi SC UB RAS, 167982 Syktyvkar, Russia
[2] IGEM RAS, 119017 Moscow, Russia
[3] Syktyvkar State University, 167001 Syktyvkar, Russia

* vlutoev@geo.komisc.ru

Due to the significant content of X-ray amorphous phases in the composition of refractory titanium and manganese ores, the use of conventional chemical and XRD phase analyses does not allow to obtain complete information about their quantitative mineral composition, which is extremely necessary for the development of effective technology for their processing. Since these ores are usually ferrous, the necessary mineralogical and technological characteristics of the ores can be obtained using $^{57}$Fe Mössbauer spectroscopy and ESR, probing the local environment of Fe ions, and Fourier transform IR spectroscopy, which allows for phase analysis of even x-ray amorphous substances. In complex with chemical data, they make it possible to perform a quantitative phase analysis of iron-containing minerals to obtain objective information about their ratios in ores. We used these spectroscopic methods as the main methods for studying the concentrates of titanium ores from the sandstones ($D_2$mr) of the Pizhemskoye deposit on Middle Timan and siderite-rhodochrosite ores ($D_3$-$C_1$sl) of the Famennian volcanogenic-sedimentary manganese-bearing province on the Pai-Khoi peninsula.

The concentrates of titanium ores from the Pizhemskoye deposit, obtained in the process of crushing, grinding, desliming, gravity enrichment, classification and magnetic separation were studied [Makeev & Lyutoev, 2015]. The ratio of leucoxene and magnetic titanium minerals (≈ 5:3) in the collective concentrate, as well as the ratio of pseudorutile, ilmenite and Fe-rutile in the magnetic fraction (≈ 20:4:6, respectively) was obtained. It is established that pseudorutil as the main component of the magnetic fraction of Ti-concentrates, being the product of the decomposition of ilmenite, partially retains the $Fe^{2+}$ ions and has a mixed ferri-ferropseudorutile composition: $Fe^{3+}_{1.50}Fe^{2+}_{0.13}Mn^{2+}_{0.12}Ti_{3.22}O_9$. Before the finishing desiliconizations of concentrates it was recommended the operations of extraction of zircon and monazite and removal siderite and garnet.

Manganese ores, widespread in the Famennian Upper Devonian sediments on Pai-Khoi, generally do not correspond to industrial conditions. Recently, however, new manifestations with relatively rich rhodochrosite ores have been discovered in the region of the Kara Astrobleme. Technological probes (VSEGEI) of rich massive rhodochrosite ore and strongly ferruginous rhodochrosite-siderite ore, as well as the products of their laboratory modification after: i) ultrasonic scrubbing; ii) magnetization in reductive roasting (<650 °C) and iii) fluorination with $NH_4HF_2$ were investigated. According to Mössbauer spectroscopy, in rich rhodochrosite ores more than 80 at.% Fe is localized in the structure of rhodochrosite, and in rhodochrosite-siderite ores, this value is less than 30 at.%. In both types of ore, the remainder of Fe is mainly composed of superparamagnetic goethite and other hydroxide Fe-Mn phases. The tendencies of quantitative changes of the main natural mineral and newly formed Fe-containing spinel phases, including X-ray amorphous, occurring during the used laboratory modification of carbonate manganese ore samples are determined. The reaction of ores to the modification processes strongly depends on the content of iron oxyhydroxides in them, which should be considered when choosing an enrichment technology.

Makeev A. B., Lyutoev V. P. Spectroscopy in process mineralogy. the Pizhemskoye deposit titanium ores concentrates mineral composition. Obogashchenie Rud, 2015, No. 5, 33–41. DOI: http://dx.doi.org/10.17580/or.2015.05.06

**Statistical methods for processing large sets of spectroscopic digital data**

Elizaveta A. Pankrushina*, Aleksandr S. Kobuzov, Yuliya V. Shchapova, Sergey L. Votyakov

Zavaritsky Institute of Geology and Geochemistry of the Ural Branch of the Russian Academy of Sciences, 620028 Ekaterinburg, Russia

* lizaveta.94@list.ru

Large spectroscopic data sets are formed while mapping the properties of heterogeneous mineral grains based on Raman scattering (RS) and luminescence spectroscopic and microprobe data, and Raman (IR, luminescence, X-ray diffraction) spectral analysis obtained under various observation temperatures and magnitude (duration) of the external factor. The data recorded during these studies contain the information on the processes kinetics, dynamic changes of their crystal lattice, spatial structural (chemical) heterogeneity of minerals, etc. One of the objectives of large data analysis is determining the critical values of the external factor, at which the mineral properties are transformed. Conventionally, data processing methods ("peak fitting" and others) are based on the algorithms of determining the characteristics of individual bands in the spectrum, followed by the analysis of dynamic changes in their position, width and intensity.

At the same time, the problem of ambiguous spectral deconvolution remains, particularly for poorly resolved spectra obtained at high observation temperatures in structurally imperfect minerals. In this paper, we have analyzed the prospects of using statistical methods for processing large data sets of spectroscopic data through the example of RS data sets obtained at temperatures of 80–880 K with a step of 5 K in quartz, zircon, and titanite (Figure), as well as the spectroscopic mapping of heterogeneous grains of these minerals. A number of algorithms have been implemented, including "integral" ones, which transform a complex spectrum (its temperature dependence) into a simple function, such as the autocorrelation function (ACF) [Salje et al., 2000] and the Fourier transform. The "differential" algorithms that give numerical assessment of differences (similarities) of two spectra (their temperature dependencies), such as the covariance method and the Pearson coefficient [Press et al., 1992] have been considered as well.

The proposed methods for processing data sets of mineral spectra have been shown appropriate for in situ identification of thermally induced phenomena (phase transitions, recrystallization, defect healing, etc.), as well as "special" transition zones on spatial profiles in heterogeneous mineral grains.

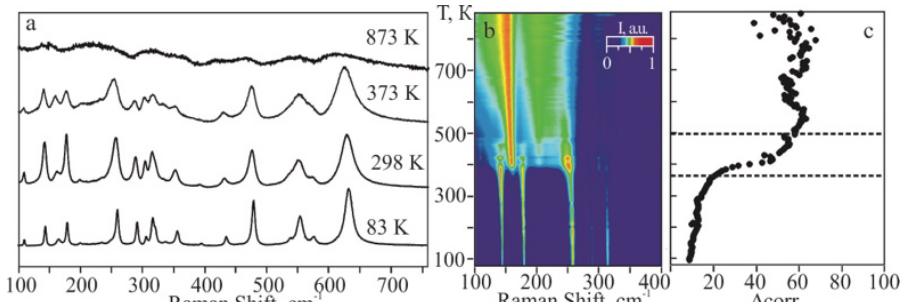


Figure. Raman spectra of titanite (a), a 2D map of the mode temperature change (b), and Δcorr vs T (c). Δcorr - ACF parameter (the band width characteristic) [Salje et al., 2000]; the dotted line is the α →β phase transition zone [Zhang et al., 2013]. LabRamHR800 Raman spectrometer, laser excitation line 633 nm, Linkam TSM 600 thermal cell.

The work was carried out at the Common Use Center "Geoanalyst" with the financial support by the Russian Science Foundation (grant No. 16-17-10283).

Press W.H, Teukolsky S.A., et al. Numerical Recipes in Fortran 77. Cambridge University Press, 1992.

Salje E. K. H., Carpenter M.A., Malcherek T., Boffa Ballaran. Autocorrelation analysis of infrared spectra from minerals. European Journal of Mineralogy, 2000, 12(3), 503–519.

Zhang M., Salje E.K.H., Redfern S.T., Bismayer U., Groat L.A. Intermediate structures in radiation damaged titanite (CaTiSiO5): a Raman spectroscopic study. Journal of Physics. Condensed Matter., 2013, 25(11), 115402.

**Europium as a spectroscopic probe to determination site symmetry**

Ivan V. Nikiforov*, Dina V. Deyneko and Bogdan I. Lazoryak

Lomonosov Moscow State University, 119991 Moscow, Russia

* niva.nli@yandex.ru

Trivalent europium ion can be used as antennas in inorganic solids solutions for estimating local crystal structure. Electro-dipole transitions are forbidden by selection rules, but can be released in non-centrosymmetric space group. A phosphate with type of nature mineral whitlockite crystallizes in different space groups. However, determination of local crystal environment is not simple task. So, the luminescence spectroscopy is the best site selective method for study local crystal environment of $Eu^{3+}$-doped whitlockite-type phosphates [Belik et al., 2017].

The whitlockite-type structure phosphates $Ca_{9-x}Mg_xEu(PO_4)_7$ $0 < x < 1$ were prepared by standard solid-state reaction from stoichiometric mixtures of $CaHPO_4 \cdot 2H_2O$ (99.9%), $CaCO_3$ (99.9%), MgO (99.99%) and $Eu_2O_3$ (99.9%). Synthesis was carried out in the air for 100 hours with an intermediate mixing.

With the substitution of $Mg^{2+}$ for $Ca^{2+}$ a phase transition from non-centrosymmetric group ($R3c$) to centrosymmetric group ($R\bar{3}c$) is observed. It is difficult to observe a limit concentration of $Mg^{2+}$, when this transition is detected, due to powder XRD patterns for these samples don't have much difference. In addition, for observed phosphates with very low the second harmonic generation signal, this method cannot give objective result too.

But this deference can be observed on PL spectra and $^5D_0 \rightarrow {}^7F_0$transition. The substitution of $Mg^{2+}$ for $Ca^{2+}$ is accompanied by the vanishing of two bands for $^5D_0 \rightarrow {}^7F_0$transition [Deyneko et al., 2019]. Cation $Eu^{3+}$ in centrosymmetric group has three possibility sites ($M1$-$M3$-$M2$);emitting of $Eu^{3+}$ in each of these contribute in $^5D_0 \rightarrow {}^7F_0$transition. In opposite, in non-centrosymmetric space group, there are only two possibility sites ($M1$ and $M3$), but the emitting of $Eu^{3+}$ ions in $M3$ do not contribute in $^5D_0 \rightarrow {}^7F_0$the transition, that is why is observed only one line (Figure).

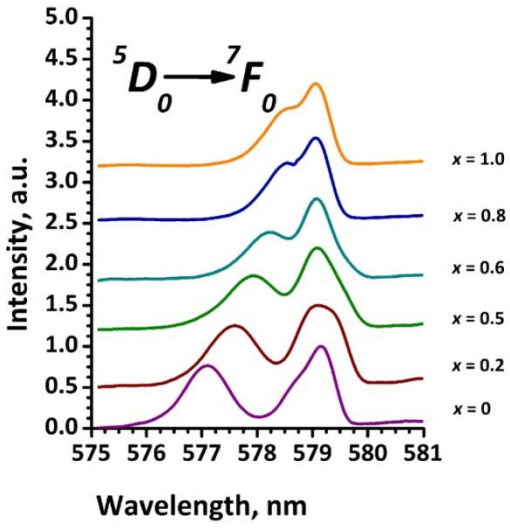


Figure. $^5D_0 \rightarrow {}^7F_0$transition for $Ca_{9-x}Mg_xEu(PO_4)_7$.

This work was supported by the Foundation of the President of the Russian Federation MK-3502.2018.5 and Russian Science Foundation (16-13-10340).

Belik A.A., Morozov V.A., Deyneko D.V., Savon A.E. Antiferroelectric properties and site occupations of $R^{3+}$ cations in $Ca_8MgR(PO_4)_7$ luminescent host materials. J. Alloys Compd., 2017, 699, 928–937.

Deyneko D. V., Nikiforov I. V., Lazoryak B. I., Spassky D. A. et. al. $Ca_8MgSm_{1-x}(PO_4)_7$:$xEu^{3+}$, promising red phosphors for WLED application. J. Alloys Compd., 2019, 776, 897–903.

**Crystal Chemical and Structural Characterization of Minerals by Vibrational Spectroscopy and X-Ray Diffraction Methods**

Tatyana N. Moroz[1]*, Nadezhda A. Palchik[1], Sergey M. Zhmodik[1]

[1]Sobolev Institute of Geology and Mineralogy SB RAS, 630090 Novosibirsk, Russia

moroz@igm.nsc.ru

A space group of the crystal structure belongs to one of the most important its characteristics of the materials. Determing the Fedorov' space group [Fedorov, 1981], one can "project, draw up the field of the further space group and many structures often with much different formulas and motives" (academician N.V. Belov) [Ocherki, 1995]. Of the total 230 space groups, only 61 ones including enantiomorphic pairs are determined unambiguously by X-ray diffraction method. In the other cases from two to five space groups only can be specified by the same rules of systematic absences. Using additional ways in analysis of intensities of X-ray diffraction reflections and physicochemical methods (measuring a refraction, piezo effect, and etc.) allows most of space groups to be determined uniquely [Bokij, Poraj-Koshits, 1964; Arkhipenko, Bokii, 1977]. In studied the order-disorder problem, shot-sensitive IR spectroscopy as well as mean – and long – range sensitive Raman spectroscopy supplement the long – range sensitive X-ray diffraction method. The combination of diffraction and non-diffraction methods allow the perfect information both as a structure as a whole and dynamics of its separate fragments to be obtained.

The problem of determination of the space group symmetry can be solved uniquely using the methods of vibrational spectroscopy – infrared (IR) and Raman spectroscopy [Bokij, Poraj-Koshits, 1964; Arkhipenko, Bokii, 1977; Arkhipenko, Moroz, 1996; Moroz, Palchik, 2009]. The method proposed for refinement of space groups based on selection rules for IR and Raman spectra and comparison them with experimental data allow eliminating the unique arising when structures of solids are assigned to the space groups with the same rules of systematic absences. It has been shown that 11 pair of enantiomorphic groups and one pairs from orthorhombic system are indistinguishable by methods of vibrational spectroscopy; the remaining 206 groups practically can be distinguished. The possibilities of the method have been demonstrated by the example of mineral such as rhodonite crystallizing in triclinic system; nontronite crystallizing in monoclinic system, and other. The universality of the approach was investigated on the minerals of the Tomtor Nb-*REE* deposit (Yakutia), where, using the micro-Raman spectroscopy, in addition to the vibrational spectrum, the luminescence spectra were obtained. For certain minerals the references in which the problem was discussed are given.

The work was conducted within the governmental task of IGM SB RAS and the partial support of the Russian Science Foundation, project No. 18-17-00120.

Arkhipenko D., Moroz T. On possible refinement of a space group of a mineral by analyzing the selection rules for vibrational spectra. Crystallography Reports, 1996, 41,925–928.

Arkhipenko D.K., Bokii G.B. Determination of symmetry space group by vibrational spectroscopy. Crystallography Reports, 1977, 22.1176–1181(in Russian).

Bokij G. B., Poraj-Koshits M.A. X-ray analysis. Moscow: MSU publ. 1964. V.1.

Fedorov E.S. The symmetry of real systems of configuration. Trans. Mineral. Soc, 1981, 28, 1–146.

Moroz T.N., Palchik N.A. The uniqueness of determination of the space group symmetry by the methods of vibrational spectroscopy. Crystallography Reports, 2009, 54, 734–737.

Ocherki po strukturnoi mineralogii akademika Belova N.V. Advances in science and technics. Crystal chemistry. E.N. Belova, E.A. Pobedimskaya. V.30. VINITI. Moscow, 1995.

**Spectral Characterization of the Ammonium Cation located in the structurally `Inappropriate` Positions**

Anastasia V. Sergeeva* and Elena S. Zhitova

Institute of Volcanology and Seismology FED RAS, 683006 Petropavlovsk-Kamchatsky, Russia

valraf2009@yandex.ru

The symmetry of an isolated ammonium cation is described by the $T_d$ tetrahedron group, which has the following elements: $E$, $8C_3$, $3C_2$, $6S_4$ and $6\sigma_d$. The subgroups of the group are $T$, $D_{2d}$, $C_{3v}$, $S_4$, $D_2$, $C_3$, $C_2$, $C_s$ and $C_1$. In the crystal structures of some ammonium minerals, the ammonium cation is located in crystallographic positions with symmetry that is not a subgroup of the $T_d$ group, i.e. symmetrically `inappropriate` position (the coordination polyhedron of $NH_4^+$ is different from site symmetry). Therefore, there is a disorder at ammonium site caused by the need to adjust the ammonium to the local symmetry of the position. Resulting in the fact that the averaged polyhedra of $NH_4^+$ cation is a superposition of disordered $NH_4^+$ tetrahedra. The disordering of ammonium cation can be either statistical or dynamical or even positional (shift from general position to special); the latter has been observed for tschermigite [Zhitova et al., 2019]. Ammonium minerals are reasonably common at geothermal fields related to Koshelev and Kambalny volcano (Southern Kamchatka, Russia). This association includes such minerals as ammonioalunite, ammoniojarosite, tschermigite, ammoniovoltaite [Zhitova et al., 2018].

Isolated $NH_4^+$ cation has four normal vibrations: $\nu_1$ ($A_1$), $\nu_2$ ($E$), $\nu_3$ and $\nu_4$ ($T_2$), two of which are active in the IR spectrum ($\nu_3$ and $\nu_4$), whereas all of them are active in the Raman spectrum [Zhitova et al., 2018]. The lowering of symmetry $NH_4^+$ cation results in an activation of $\nu_1$ and $\nu_2$ modes and a splitting of the of $\nu_3$ and $\nu_4$ modes. In the crystal structure of ammonioalunite and ammoniojarosite, the $NH_4^+$ cation is in the position with $D_{3d}$ symmetry, thus only $\nu_3$ (3300 $cm^{-1}$) and $\nu_4$ (1430 $cm^{-1}$) modes are active at the IR spectrum. The splitting of these modes for ammonioalunite and ammoniojarosite is not observed, although the $\nu_4$ band is asymmetric. In the structure of tschermigite the $NH_4^+$ cation is located in $S_6$ ($C_{3i}$). For tschermigite $\nu_1$ mode is active and $\nu_3$ and $\nu_4$ modes are split into several components. On the basis of that it has been concluded that $NH_4^+$ cation is shifted to the $C_3$ position from $S_6$ position. In ammoniovoltaite, $NH_4^+$ cation is located in the position $D_3$ [Zhitova et al., 2019]. The $\nu_4$ band on its IR spectrum is clearly asymmetric, which may be due to dynamic or static $NH_4^+$ disordering. Formally, figures of suitable symmetry ($D_{3d}$, $S_6$, $D_3$) are obtained by rotating $NH_4^+$ with respect to $C_2$ and $C_3$ directions.

The study has been supported by the President of Russian Federation Grant for Young Candidates of Sciences (to ESZ, grant MK-3246.2019.5).

Nakamoto, K. Infrared and Raman Spectra of Inorganic and. Handb. Vib. Spectrosc., 2006.

Zhitova, E. S. et al. Ammoniovoltaite, $(NH_4)_2Fe^{2+}{}_5Fe^{3+}{}_3Al(SO_4)_{12}(H_2O)_{18}$, a new mineral from the Severo-Kambalny geothermal field, Kamchatka, Russia. Mineral. Mag., 2018, 1–40.

Zhitova, E. S., et al. Tschermigite from thermal fields of Southern Kamchatka: high-temperature transformation and peculiarities of IR-spectrum. Proceedings of the Russian Mineralogical Society. Vol. 148. No. 1. 2019.

**Measurement of platinum group elements in catalysts processing products using SEM and energy dispersive spectrometer**

Nikolai S. Chebykin[1,*], Ivan P. Sandalov[2], Dmitry A. Zamyatin[1]

[1] Institute of Geology and Geochemistry UB RAS, Ekaterinburg, Russia
[2]Plaurum AO "Ekaterinburg non-ferrous metals processing plant", Verhnyaya Pyshma, Sverdlovsk Region, Russia

* tchebykinnikolai@yandex.ru

The high cost of platinum group elements (PGE) determines the economic feasibility of their processing from various catalysts used in the automotive, petroleum and chemical industries. In order to extract them, JSC EZOCM introduced a smelting technology to an iron collector [Maslenickij, 1987] using a Tetronics plasma furnace, with the subsequent processing of the collector in acids. The processed product is powdered platinum concentrate, the quantitative microanalysis of the composition of which is difficult due to the complex surface of the fragments and the significant overlaps of the PGE X-ray emission lines. To optimize the technology and assess the efficiency of metal extraction, the development of a method for microanalysis of the PGE content in the products of catalyst processing is relevant.

The current study reports on its development and testing on samples K176-177 of concentrates, obtained by melting catalysts with lime, quartz sand, magnetite and coke (samples differ in melting parameters and composition of the charge). According to SEM data, the surface the particles has a complex branched structure, with inclusions bright in BSE (K176), or a rounded shape with developed edges without inclusions bright in BSE (K177) (scanning electron microscope JEOL JSM-6390LV equipped with EDS Oxford INCA X- Max80; working distance 10 mm, accelerating voltage 30 kV, accumulation time 60 s). Semi-quantitative analysis was performed by the method of one standard by default calibrations. Analytical lines Fe$K_{\alpha 1}$, Si$K_{\alpha 1}$, Sn$L_{\alpha 1}$, Pt$L_{\alpha 1}$ and Re$L_{\alpha 1}$ were used to measure the contents. The last two are free from the overlaps of impurity elements. Testing methods performed on samples K176-177; for sample K176 average contents are Fe=81.69, Si=12.12, Pt=2.42, Sn=1.26 wt.% and for K177 are Fe=77.72, Si=16.22, Pt=1.48, Re=2.32 wt.%. Relative standard deviations are ΔFe=1.28, ΔSi=4.97, ΔPt=4.28 and ΔRe=4.88 %, within which the data of microanalysis and chemical analysis coincide.

This work was supported by the theme of state assignment of IGG UB RAS (theme No.0316-2019-0004).

Maslenickij I.N. Metallurgiya blagorodnyh metallov. Metallurgiya, Moscow, 1987.

# 4. Inorganic Crystal Chemistry

# 4.1. Silicates

## Bond Topology of Chain-, Ribbon- and Tube-Silicates

Maxwell C. Day and Frank C. Hawthorne*

Geological Sciences, University of Manitoba, Winnipeg, Manitoba R3T 2N2, Canada

*frank.hawthorne@umanitoba.ca

We consider the topology of all chains, ribbons and tubes formed by corner-linked tetrahedral. All chain, ribbon and tube arrangements of tetrahedral can be represented graphically by reducing ($TO_4$) tetrahedral to vertices and linkages between those tetrahedral to edges. In this representation of a chain, only the connectivity of tetrahedra are preserved and no geometrical properties. The topology of all chains may be described by the expression $G_t = n_t$:(a-b-c-d), where $G_t$ = the graphical representation of a given chain, $n_t$ = topological repeat unit and a, b, c and d are the number of 1-, 2-, 3- and 4-connected vertices in $n_t$. The topological repeat unit ($n_t$) contains the minimum number of vertices required to generate a given graph through *repetition operations*. By sequentially inserting different values of a, b, c and d, all topologically distinct graphs are generated. Figure shows examples of the tetrahedron and graphical representation of various chains observed and not observed in inosilicates and their corresponding $G_t$ expressions.

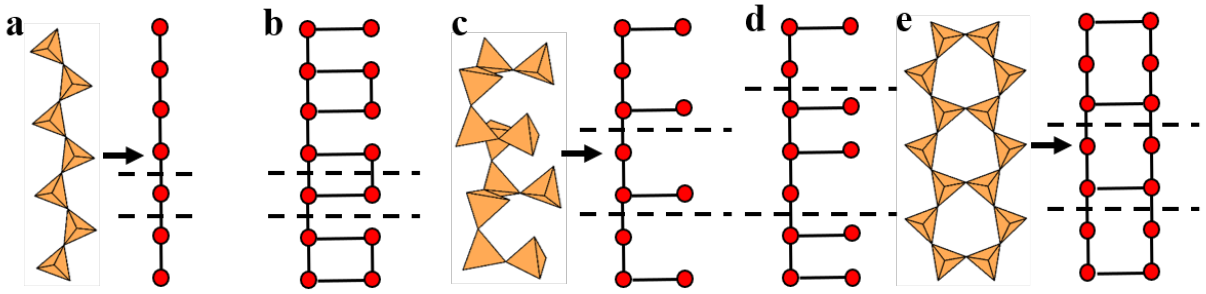


Each $G_t$ expression corresponds to a set of topologically unique (non-isomorphic) graphs. This set can be generated using *modified adjacency matrices*, where each row (or column) represents a vertex in $n_t$. The sums of all rows and columns can then be permuted, each permutation generating a topologically unique graph that corresponds to the $G_t$ expression. By comparing all possible non-isomorphic graphs that correspond to chains, we have begun to identify topological characteristics that correspond to more abundant inosilicates and/or more stable chain arrangements.

**Polytypes in charoite and denisovite structures**

Rozhdestvenskaya I.[1,*], Depmeier W.[2]

[1] Saint Petersburg State University, 199155 Saint Petersburg, Russia
[2] Christian-Albrechts-University, Kiel, D-24098 Germany

* ivrozhdestvenska@mail.ru

Charoite, ideally $(K,Sr,Ba,Mn)_{15\text{-}16}(Ca,Na)_{32}[(Si_{70}(O,OH)_{180})](OH,F)_{4.0}\bullet nH_2O$, and denisovite, $K_{14}Ca_{42}Na_6[Si_{60}(O,OH)_{162}]F_{16}(O,OH)_8\bullet 2H_2O$, are rare minerals occurring as aggregates of asbestos-like fibres. Both minerals belong to the family of Ca-bearing alkaline minerals.

The **structures** of these minerals are composed of three topologically distinct *dreier* silicate chains running along [001]: a dreier double xonotlite-like chain, $[Si_6O_{17}]^{10-}$ (DC), a tubular loop-branched dreier triple chain, $[Si_{12}O_{30}]^{12-}$(TC) and in the charoite structure also a tubular hybrid dreier quadruple chain, $[Si_{17}O_{43}]^{18-}$ (QC) [Rozhdestvenskaya et al., 2010, 2011, 2017] (Figure).

The silicate chains are separated from each other by ribbons of edge-sharing octahedra running along [001]. In the denisovite structure, the octahedra walls form a rigid framework with channels along [001] in which the various types of silicate anions are located. These channels are situated between zigzag sequences of walls and form strips along [010].

In chain silicates,**polytypism** is often connected with stacking faults or shifts of structure blocks. The lattice parameter $c \approx 7.2$ Å spans two octahedra edges and in principle permits the silicate chains to be connected to the octahedral fragment in two distinct positions, ≈ 3.6 Å apart.

In both structures, horizontal $Si_2O_7$ groups of chains are bonded to vertical octahedron edges and are therefore displaced with respect to each other by the length of one octahedron edge, i.e. $c/2$.

In charoite, three silicate chains DC, TC and QC stack along the *x* axis and form a fixed block. In charoite-90, adjacent blocks are stacked without shifts. In charoite-96, adjacent blocks are shifted by a translation of ½ *c*. The shifts take place between (QC) and (DC). Randomly distributed + or - shifts would lead to disorder along [100] (charoite-d), which actually have been observed.

In denisovite, within one strip along [010], all silicate anions are fixed with respect to the *z*- and to the *y*-direction. In two-octahedra-wide horizontal wall, neighboring octahedra columns are mutually displaced along [001] by $c/4$ with respect to each other. Two DC on opposite sides of this wall belong to two neighboring strips. Consequently, the silicate chains in both strips are displaced with respect to each other by $+c/4$ or $-c/4$, and this is true for the whole strip. This could lead to twinning, or to a new ordered structure, where shifts $+c/4$ and $-c/4$ alternate regularly, or to disorder when the directions of the shifts reverse randomly.

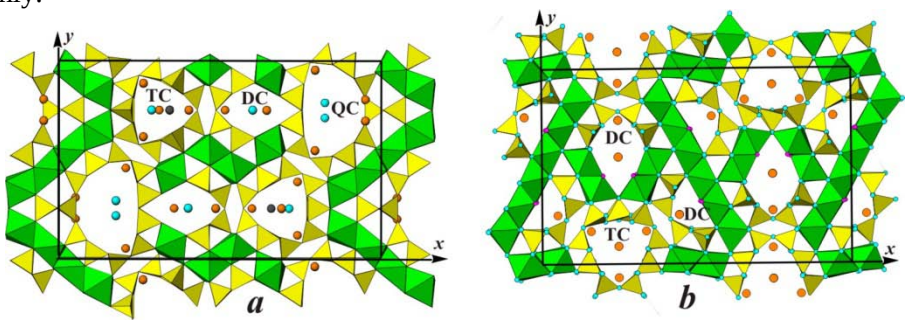


Figure. Structures of charoite (a) and denisovite (b) projected along the *z*-axis

Rozhdestvenskaya I., Mugnaioli E., Czank M., Depmeier W., Kolb U., Reinholdt A., Weirich T. The structure of charoite, solved by conventional and automated electron diffraction. Mineral. Mag., 2010, 74, 159–177.

Rozhdestvenskaya I., Mugnaioli E., Czank M., Depmeier W., Kolb U., Merlino S. Essential features of the polytypic charoite-96 structure compared to charoite-90. Mineral. Mag., 2011, 75, 2833–2846.

Rozhdestvenskaya I.V., Mugnaioli E., Schowalter M., Schmidt M., Czank M., Depmeier W., Rosenauer A. The structure of denisovite, a fibrous nanocrystalline. IUCr J., 2017, 4, 223–242.

**Complexity and stability of Group-I of the ABC-6 family of zeolites**

Fernando Cámara

Dipartimento di Scienze della Terra, Università degli Studi di Milano, 20133 Milano, Italy

*fernando.camara@unimi.it

The ABC-6 family of zeolites [Gies et al. 1998] have a common periodic building unit (PBU) consisting on a hexagonal array of non-connected planar rings of 6 tetrahedra (S6R) centered at (0, 0) in the ***ab*** layer, which is considered as **A**-position. There are two other possible location for the S6R: centered at (1/3, 2/3) and called **B**-position, and centered at (2/3, 1/3) and called **C**-position. PBU's are related along ***c*** direction by stacking resulting in periodic sequences. Three groups are defined upon the alternance of the PBU's. I will refer to the members of Group I. In this group, adjacent layers are always of different type and give rise to increasing complexity structures with even and odd number of layers sequences. The ***ab*** layer in this group has typically periodicity values of 12.57–12.96 Å. The known minerals belonging to this group have variable length for ***c*** periodicity depending on the stacking sequence, and it is found to be an approximate multiple of the layer thickness, i.e. ~ 2.51 Å. Connection of the S6R across shifted PBU's through tilted 4-tetrahedra rings (S4R) that constitute double *zigzag* chains of tetrahedra (*dzc* units), and lead to a 3D framework. The known structures are related to hexagonal or trigonal symmetries, but for sodalite and related solid solutions that show cubic symmetry, although ordering and relaxation of the framework can lead to lowering of symmetry and modulated structures. Frameworks form also open spaces or cages (in some cases channels) that host anions, oxoanionic groups, $H_2O$ groups or even more complex molecules. Charge of extra-frameworks anions or oxoanionic groups are balanced by cations (usually Na, K and Ca). The 3D topology of these structures can be also described through the association of a periodic array of a limited number of cages types, having in common the presence the so-called CAN cage (CAN = cancrinite; or ε-cage). Minerals derived from these arrays give rise to some of the most complex mineral structures in the sense of Krivovichev [2012], which were listed as belonging to the 20 most complex minerals by Krivovichev [2013]. This makes this group of minerals very interesting.

The relation between the different known mineral structures belonging to this group and some aspects related to extra-framework relaxation as a function of composition, temperature and pressure will be portrayed.

Gies H., Kirchner R., Van Konigsveld H., Treacey M.J. Faulted zeolite framework structures. In: M.J. Treacey, M.B.K. Marcus, M.E. Bisher, J.B. Higgins (eds) Proc. 12th International Zeolite Conference, Baltimore, Maryland, USA, Materials Research Society, Warrendale, Pennsylvanya, USA, 1998, 2999–3029.

Krivovichev S.V. Topological complexity of crystal structures: quantitative approach. Acta Cryst., 2012, A68, 393–398.

Krivovichev S.V. Structural complexity of minerals: information storage and processing in the mineral world. Miner. Mag., 2013, 77, 275–326.

**Renaissance of Alkali Lithosilicates with Surprising Luminescence Properties**

Daniel Dutzler and Hubert Huppertz*

Institute of General, Inorganic, and Theoretical Chemistry,
University of Innsbruck, A-6020 Innsbruck, Austria

*Hubert.Huppertz@uibk.ac.at

In the last years, the search for new alternative light sources to replace incandescent light bulbs has resulted in the syntheses and characterization of numerous phosphors for the use in phosphor converted light-emitting diodes (pc-LEDs). In these devices, a short wavelength emitting light source represented by an UV or blue LED is regularly combined with special converting phosphors, which emit light of longer wavelengths, to compose the desired color. A lot of examples concerning red phosphors exist, which show that especially ternary and multinary alkaline earth nitrides represent suitable host structures for doping with $Eu^{2+}$.For example, appropriate phosphors with surprising narrow band red emissions are represented by the compositions $Ca[LiAl_3N_4]:Eu^{2+}$, $Sr[Mg_3SiN_4]:Eu^{2+}$, $M[Mg_2Al_2N_4]:Eu^{2+}$ ($M$ = Ca, Sr, Ba, Eu), $Sr[LiAl_3N_4]:Eu^{2+}$[Pust et al., 2014], and $Sr_4[LiAl_{11}N_{14}]:Eu^{2+}$[Wilhelm et al., 2017].

From these examples, $Ca[LiAl_3N_4]$ and $Sr[Mg_3SiN_4]$ crystallize in the $Na[Li_3SiO_4]$ structure type and $Sr[LiAl_3N_4]$ in the $Cs[Na_3PbO_4]$ structure type. $K[Li_3GeO_4]$ and $K[Li_3SiO_4]$ also have the $Cs[Na_3PbO_4]$ structure. This finding is remarkable because pure nitrogen compounds normally do not possess oxide species as isotypic counterparts. So, $Ca[LiAl_3N_4]$–$Na[Li_3SiO_4]$ and $Sr[LiAl_3N_4]$–$K[Li_3SiO_4]$ are two typical examples. Only little is known about mixed phases in this synthetic area. Based on these considerations, the question arose if there are alkali metal silicates or lithosilicates, which could be suitable for modern phosphor materials.

We started to investigate alkali metal silicates like $Na[Li_3SiO_4]$ and $K[Li_3SiO_4]$, which were already realized by R. Hoppe in the 80s and 90s of the last century. Despite of the fact that this class only contains monovalent cations, we tried to dope these structures with $Eu^{2+}$. So in this talk, results from our doping activities of the three lithosilicate phosphors $Na[Li_3SiO_4]:Eu^{2+}$, $K[Li_3SiO_4]:Eu^{2+}$, and $NaK_7[Li_3SiO_4]_8:Eu^{2+}$ (possessing a new structure type) are given, which were the first examples of this substance class [Dutzler et al. 2018].

Dutzler D., Seibald M., Baumann D., Huppertz H. Alkali Lithosilicates: Renaissance of a Reputable Substance Class with Surprising Luminescence Properties. Angew. Chem. Int. Ed. Engl., 2018, 57, 13676–13680.

Pust P., Weiler V., Hecht C., et al. Narrow-band red-emitting $Sr[LiAl_3N_4]:Eu^{2+}$ as a next-generation LED-phosphor material. Nat. Mater. 2014, 13, 891–896.

Wilhelm D., Baumann D., Seibald M., et al. Narrow-Band Red Emission in the Nitridolithoaluminate $Sr_4[LiAl_{11}N_{14}]:Eu^{2+}$. Chem. Mater. 2017, 29, 1204–1209.

**The Astrophyllite Supergroup: Topological Constraints and New Chemical Compositions**

Elena Sokolova

Department of Geological Sciences, University of Manitoba, Winnipeg, R3T2N2 Canada

* Elena.sokolova@umanitoba.ca

The structure topology and crystal chemistry have been considered for the fourteen astrophyllite-supergroup minerals: astrophyllite, niobophyllite, zircophyllite, tarbagataite, nalivkinite, bulgakite, kupletskite, kupletskite-(Cs), niobokupletskite, laverovite, heyerdahlite, devitoite, sveinbergeite, lobanovite and related nafertisite. The HOH block is the main structural unit in all astrophyllite-supergroup structures; it consists of three H–O–H sheets: a central O (Octahedral) and two adjacent H (Heteropolyhedral) sheets of [5]- and [6]-coordinated D polyhedra and the astrophyllite $T_4O_{12}$ ribbons. In each structure, HOH blocks alternate with **I** (Intermediate) blocks along [001]. The **I** block comprises atoms between two HOH blocks. There are two types of structures based on the type of self-linkage of HOH blocks [Sokolova, 2012]: (a) HOH blocks link directly where they share common vertices of D octahedra, and (b) HOH blocks do not link directly via D polyhedra of the H sheets. The fourteen minerals of the astrophyllite supergroup are divided into three groups based on (1) the type of self-linkage of HOH blocks, *i.e.*, (a) HOH blocks link directly via D–$X^P_D$–D bridges, or (b) HOH blocks do not link directly; and (2) the dominant cation of the O sheet [the C group: $C_7$*apfu* (atoms per formula unit)] [Sokolova et al., 2017]. In the astrophyllite group, HOH blocks connect via D–$X^P_D$–D bridges, $Fe^{2+}$ is dominant at $C_7$; in the kupletskite group, HOH blocks connect via D–$X^P_D$–D bridges, $Mn^{2+}$ is dominant at $C_7$; in the devitoite group, HOH blocks do not connect via D–$X^P_D$–D bridges.

The general formula for the astrophyllite-supergroup minerals is of the form $A_{2p}B_rC_7D_2(T_4O_{12})_2I(X^O_D)_2(X^O_A)_4(X^P_D)_n(W_A)_2$, where C [cations at the *M*(1–4) sites in the O sheet] = $Fe^{2+}$, Mn, Na, Mg, Zn, $Fe^{3+}$, Ca, Zr, Li; D (cations in the H sheets) = $^{[6,5]}$Ti, Nb, Zr, $Sn^{4+}$, $^{[5]}Fe^{3+}$, Mg, Al; T = Si, minor Al; the **I** (Intermediate) block is composed of the peripheral layers of the form $A_{2p}B_rW_{A2}$ where p = 1,2; r = 1,2; A = K, Cs, Ba, $H_2O$, Li, Rb, $Pb^{2+}$, Na, □; B = Na, Ca, Ba, $H_2O$ (only in sveinbergeite), □; $W_A$ = $H_2O$, □ and I represents the composition of the central part of the **I** block, *e.g.*, $(PO_4)_2(CO_3)$ in devitoite; $X^O_D$ = O; $X^O_A$ = OH, F; $X^P_D$ = F, O, OH, $H_2O$, □, where n = 0, 1, 2 for $(X^P_D)_n$. The *A* site can split into *A*(1) and *A*(2) sites.

Here I consider

(1) linkage of M octahedra (O sheet) and polyhedra of the H sheets;
(2) order of Na in the O sheet which results in different topology of the HOH block;
(3) occurrence of F at the $X^P_D$ site of the D–$X^P_D$–D bridge;
(4) occurrence of Na and Li at the [6]-coordinated *A*(2) site and $H_2O$ at the $W_A$ site,

and predict new chemical compositions for the astrophyllite supergroup.

Sokolova E., Cámara F., Hawthorne F.C., Ciriotti M.E. The astrophyllite supergroup: nomenclature and classification. Mineralogical Magazine, 2017, 81, 143–153.

Sokolova E. Further developments in the structure topology of the astrophyllite-group minerals. Mineralogical Magazine, 2012, 76, 863–882.

**Crystal structure features of lamprophyllite-group minerals: Single crystal X-ray diffraction and Raman spectroscopy study**

Anastasiya D. Ryanskaya[1,*], Sergey M. Aksenov[2,**], Nikolay V. Vladykin[3], Yulia V. Shchapova[1],Sergey L. Votyakov[1],and Ramiza K. Rastsvetaeva[2]

[1]Zavaritsky Institute of Geology and Geochemistry UB RAS, 620016 Ekaterinburg, Russia
[2]FSRC "Crystallography and Photonics" RAS, 119333 Moscow, Russia
[3]Vinogradov Institute of Geochemistry SB RAS, 664033 Irkutsk, Russia

* tosenka2008@gmail.com; ** aks.crys@gmail.com

Lamprophyllite-group minerals (LGM) are widely distributed in agpaitic rocks and their pegmatites. According to the nomenclature approved by the IMA CNMNC, LGM are included in the seidozerite supergroup [Sokolova, Cámara, 2017]. The general formula of LGM ($Z$ = 2) can be written as follows [Rastsvetaeva et al., 2016]: $A_2[M1M2_2M3X_2][L_2(Si_2O_7)_2O_2]$, where $A$ = Ba, Sr, K, or Na; $M1$ = Na or $Mn^{2+}$; $M2$ = Na, $Mn^{2+}$, $Fe^{2+}$, or Ca; $M3$ = Ti, $Mn^{2+}$, Mg, $Fe^{3+}$, or $Fe^{2+}$; $L$ = Ti or $Fe^{3+}$; $X$ = OH, F, or O. The $M$1–3 and L cations have octahedral and 5-fold pyramidal coordinations, respectively. The following nine mineral species belong to the lamprophyllite group: lamprophyllite, fluorlamprophyllite, barytolamprophyllite, fluorbarytolamprophyllite, lileyite, emmerichite, ericssonite, ferroericssonite, and schüllerite. Many compositional varieties of these minerals were also described [Rastsvetaeva et al. 2016; Filina et al., 2019].

LGM from the alkaline rocks of Murunskii massif [lamprophyllite (**1**), *oxylamprophyllite* (**2**)] and pegmatites of Rocky Boy [lamprophyllite (**3**)] and Gordon Butte [barytolamprophyllite (**4**)] have been studied using single crystal X-ray analysis and Raman spectroscopy. Minerals are structurally related to the previously reported LGM, and the crystal chemical formulas are:

**1** – $(Sr_{0.725}K_{0.18}Na_{0.055}Ba_{0.04})_2[Na(Na_{0.83}Mn_{0.09}Ca_{0.08})_2(Ti_{0.52}Fe_{0.38}Mg_{0.10})((OH)_{1.16}F_{0.55}O_{0.26})][Ti_2O_2(Si_2O_7)_2]$;
**2** – $(Ba_{0.425}Sr_{0.25}K_{0.215}Na_{0.11})_2[Na(Na_{0.645}Fe_{0.15}Mn_{0.12}Ca_{0.085})_2(Ti_{0.86}Mg_{0.08}Fe_{0.06})(O_{0.84}(OH)_{0.66}F_{0.50})][Ti_2O_2(Si_2O_7)_2]$
**3**–
$(Sr_{0.7}Na_{0.125}K_{0.05}Ba_{0.025})_2[Na(Na_{0.705}Fe_{0.1}Mn_{0.08}Mg_{0.065}Ca_{0.05})_2(Ti_{0.65}Fe_{0.30}Mg_{0.05})((OH)_{1.08}F_{0.48}O_{0.44})][Ti_2O_2(Si_2O_7)_2]$;**4** – $(Ba_{0.56}K_{0.2}Sr_{0.135}Na_{0.05})_2[Na(Na_{0.765}Fe_{0.09}Ca_{0.085}Mn_{0.06})_2(Ti_{0.53}Fe_{0.35}Mg_{0.12})((OH)_{1.26}F_{0.58}O_{0.16})][Ti_2O_2(Si_2O_7)_2]$.

Raman spectra were collected using a LabRam HR800 Evolution spectrometer with 514 nm and 633 nm laser excitation. In the spectra, lattice (100–500 $cm^{-1}$) and oscillation modes of Si-$O_b$-Si bridge and Si-$O_{nb}$ non-bridge oxygen atoms of $Si_2O_7$dimers as well as the oscillations of $TiO_5$-groups of the titanium silicate sheet (500–1200 $cm^{-1}$) are identified. The energy variations of Si-$O_b$-Si and Si-$O_{nb}$ vibrational modes within 5–10 $cm^{-1}$ are established, which correlate with the cation composition of $A$ site of the structure. In the region 3400–3800$cm^{-1}$, the oscillations of OH-groups and $H_2O$ are observed; their spectrum varies significantly in energy, width and relative intensity of vibrational modes between samples.

The work was carried out at the Common Use Center "Geoanalyst" with the financial support by the Russian Science Foundation (grant No. 16-17-10283).

Filina M.I., Aksenov S.M., Sorokhtina N.V. et al. The new mineral fluorbarytolamprophyllite, $(Ba,Sr,K)_2[(Na,Fe^{2+})_3TiF_2][Ti_2(Si_2O_7)_2O_2]$ and chemical evolution of lamprophyllite-group minerals in agpaitic syenites of the Kola Peninsula. Mineral. Petrol. 2019, doi:10.1007/s00710-019-00664-0.

Rastsvetaeva R.K., Chukanov N.V., Aksenov S.M. The crystal chemistry of lamprophyllite-related minerals. Eur. J. Mineral. 2016, 28, 915–930.

Sokolova E., Camara F. The seidozerite supergroup of TS-block minerals: nomenclature and classification, with change of the following names: rinkite to rinkite-(Ce), mosandrite to mosandrite-(Ce), hainite to hainite-(Ce) and innelite 1T to innelite-1A. Can. Mineral. 2017, 81, 1457–1484.

**Crystal structure and topological features of manganonaujakasite, $Na_6(Mn,Fe)[Al_4Si_8O_{26}]$**

Sergey M. Aksenov,[1,2,*] Nikita V. Chukanov,[3] Igor V. Pekov,[4] Ramiza K. Rastsvetaeva,[2] and Amy E. Hixon[1]

[1] University of Notre Dame, Notre Dame, Indiana 46556, United States
[2]FSRC "Crystallography and Photonics", RAS, 119333 Moscow, Russia
[3]Institute of Problems of Chemical Physics, RAS, 142432 Chernogolovka, Moscow Region, Russia
[4]Moscow State University, 119991 Moscow, Russia

* aks.crys@gmail.com

Manganonaujakasite, $Na_6(Mn,Fe)[Al_4Si_8O_{26}]$, the Mn-dominant analogue of naujakasite $Na_6Fe[Al_4Si_8O_{26}]$, was discovered by A.P. Khomyakov and co-authors in lovozerite-lomonosovite lujavrites on the Lovozero alkaline massif (Kola Peninsula, Russia) [Khomyakov et al., 2000]. The mineral forms light blue grains that are irregular in shape and up to 5 mm across. The empirical formula of the sample is $(Na_{5.96}Ca_{0.01})(Mn_{0.53}Fe_{0.49})Al_{3.95}Si_{8.03}O_{26.00}$ [Khomyakov et al., 2000].

The crystal structure of manganonaujakasite [Aksenov et al., 2019] was studied by single crystal X-ray analysis and infrared spectroscopy using a holotype sample. The monoclinic unit cell parameters are: $a$ = 15.029(1) Å, $b$ = 7.999(1) Å, $c$ = 10.467(1) Å, $\beta$ = 113.551(1)°; $V$ = 1153.47(15) Å$^3$, space group $C2/m$, $Z$ = 2.The microporous crystal structure of manganonaujakasite is similar to that of naujakasite and is based on tetrahedral $[Al_4Si_8O_{26}]$-double layers which are linked *via* isolated $(Mn,Fe)O_6$-octahedra to form a heteropolyhedral framework containing two systems of parallel wide channels. The general crystal chemical formula of manganonaujakasite and related compounds (i.e., naujakasite and products of its hydration) can be written as follows ($Z$ = 4)

$$\left|{}^{[7]}A^{+}\right|\left[M^{[4+2]}T_{12}^{[4]}\mathrm{O}_{26}\right]_{h}\{3\}_{p}\left\{\begin{array}{l}1\left[3^{3}5^{1}6^{4/2}\right][010](6-\mathrm{ring})\\ 1\left[3^{3}5^{1}6^{3}8^{2/2}\right][010](8-\mathrm{ring})\end{array}\right\}(C2/m),$$

indicating that (1) the guests are monovalent $A^+$ cations (predominantly $Na^+$) and (2) the 3D host structure consists of two different unidimensional channels (both running along [010] direction) with the topology of $[3^35^16^{4/2}]$ [6-membered ring (6R) pore opening] and $[3^35^16^38^{2/2}]$ [8-membered ring (8R) pore opening], respectively.

The naujakasite-type framework topologically relates to the **ATV**-type of $AlPO_4$. Both are built from the same *t-kah* $[6^3]$ and *t-lov* $[4^2.6^2]$ tiles and are characterized by similar one-dimensional *composite building units* represented by the narsarsukite-type *nsc*-chain. The comparative data for the frameworks of naujakasite- and **ATV**-types are given.

The calculated structural complexity parameter for the naujakasite-type framework ($I_{G,\mathrm{total}}$= = 136.131 bits/unit cell) is similar to that of **ATV** ($I_{G,\mathrm{total}}$= 102.117 bits/unit cell) [Krivovichev, 2013]. The insertion of $MO_6$ octahedra into the tetrahedral framework between naujakasite-type double silicate layers leads to an increase of the framework density (FD); FDs are 22.54 ($M$+$T$)/1000 Å$^3$ and 19.9 $T$/1000 Å$^3$ for naujakasite and **ATV**, respectively.

This study was supported by the Russian Foundation for Basic Research (grant Nos. 18-29-12005 – topological analysis, and 18-29-12007 – mineralogical and IR spectroscopic study).

Aksenov S.M., Chukanov N.V., Pekov I.V., Rastsvetaeva R.K., Hixon A.E. Crystal structure and topological features of manganonaujakasite, a mineral with microporous heteropolyhedral framework related to AlPO-25 (ATV). Micropor. Mesopor. Mater. 2019, 279, 128–132.

Khomyakov A.P., Nechelyustov G.N., Ferraris G., Ivaldi G. Manganonaujakasite, $Na_6(Mn,Fe)Al_4Si_8O_{26}$, a new mineral from the Lovozero alkaline massif, Kola peninsula. Zap. Vseross. Mineral. Obshch. 2000, 129(4), 48–53.

Krivovichev S.V. Structural and topological complexity of zeolites: An information-theoretic approach. Micropor. Mesopor. Mater. 2013, 171, 223–229.

**Sodalite-type aluminosilicates $Na_8[(Al,Si)_{12}O_{24}]X \cdot nH_2O$ (X = $SO_4$, $MoO_4$, $WO_4$): synthesis, X-ray diffraction and thermal studies**

Nadezhda V. Shchipalkina[1,2*], Alexey R. Kotelnikov[3], Sergey N. Britvin[4], Lyubov' V. Mel'chakova[1], Natalia N. Koshlyakova[1] and Igor V. Pekov[1]

[1]Faculty of Geology, Moscow State University, 119991 Moscow, Russia
[2]FSRC «Crystallography and Photonics» RAS, 119333 Moscow, Russia
[3]Institute of Experimental Mineralogy RAS, 142432 Chernogolovka, Russia
[4]Department of Crystallography, St. Petersburg State University, 199034 St. Petersburg, Russia

*estel58@yandex.ru

Representatives of the sodalite structure type (SOD-type) are well-known microporous materials with the general formula$M_8X_{1-2}[T_{12}O_{24}]$, where *M* and *X* are extraframework and intracage (located in β-cages) cations and anions, respectively, and *T* are tetrahedrally coordinated framework-forming components. Among these compounds there are different aluminosilicates (e.g. sodalite, nosean, lazurite, haüyne), beryllosilicates (e.g. danalite, tugtupite), chlorides, sulfides (e.g. fahlerz), synthetic phosphates, aluminates, phosphides, nitrides, clathrate hydrates with aristotypic space group *Im*-3*m*. The detailed review of chemical variations and symmetry aspects of SOD-type materials was given by Fischer and Baur [2009].

Our recent find of Mo- and W-bearing haüyne in fumarolic sublimates of the Tolbachik volcano (Kamchatka, Russia) triggered the studies of similar synthetic systems. Thus, our hydrothermally synthesized ($t$ = 750 ºC, $p$ = 3 kbar) compounds belong to SOD-type hydrous aluminosilicates with *M* = Na and *X* = $SO_4^{2-}$, $MoO_4^{2-}$ and $WO_4^{2-}$. In the studied system $Na_8[(Al,Si)_{12}O_{24}]SO_4 \cdot nH_2O$–$Na_8[(Al,Si)_{12}O_{24}]MoO_4 \cdot nH_2O$ – $Na_8[(Al,Si)_{12}O_{24}]WO_4 \cdot nH_2O$ ($n$<2), continuous solid solution between $SO_4$- and $MoO_4$- phases and discontinuous solid solutions between $WO_4$- and both $SO_4$- and $MoO_4$-phases were observed. Unlike the Si-free SOD-type aluminates with intracage anions $MoO_4^{2-}$ and $WO_4^{2-}$ [Peters et al. 2009 and references therein], our phases possess the space group *P*-43*m*. This suggestion is based on the presence of strong reflections $h+k+l = 2n+1$ and *hhl*, where $l = 2n+1$, on powder X-ray diffraction patterns and results of Rietveld refinements. The unit-cell parameters for hydrous compounds are as follows: $a$ = 9.085(1) Å, $V$ = 749.9(2) Å$^3$ for $Na_8[(Al,Si)_{12}O_{24}]SO_4 \cdot nH_2O$; $a$=9.138(5) Å, $V$ = 763.06(8) Å$^3$ for $Na_8[(Al,Si)_{12}O_{24}]MoO_4 \cdot nH_2O$; $a$ = 9.146(1) Å, $V$ = 765.0(1) Å$^3$ for $Na_8[(Al,Si)_{12}O_{24}]WO_4 \cdot nH_2O$. The unit-cell parameters of members with $[(SO_4)_{0.6}(MoO_4)_{0.4}]$ and $[(SO_4)_{0.8}(WO_4)_{0.2}]$ are $a$ = 9.089(3) Å, $V$ = = 750.9(4) Å$^3$ and $a$ = 9.091(3) Å, $V$ = 751.3(5) Å$^3$, respectively.

The thermal studies of phases with $[(SO_4)_{0.6}(MoO_4)_{0.4}]$ and $[(SO_4)_{0.8}(WO_4)_{0.2}]$ show the gradual mass loss in the temperature range 100–1000 ºC. The single broad DTA signal with peak at 350 ºC was observed for both samples. This signal is due to the dehydration process. The corresponding mass loss is 3.5 wt.% that is equal to two $H_2O$ molecules per formula unit. The crystal structures of compounds heated to 700 ºC and 1000 ºC are slightly changed in comparison with their initial, hydrous analogues: the thermal expansion was fixed for these anhydrous phases.

This work is supported by the Russian Foundation for Basic Research, grant 18-05-00332 (X-ray diffraction studies) and Russian Science Foundation, grant 19-17-00050 (synthesis and study of chemical composition).

Fischer R.X., Baur W.H. Symmetry relationships of sodalite (SOD) – type crystal structures. Zeitschrift für Kristallographie, 2009, 224, 185–197.

Peters L., Vega-Flores G., Depmeier W. Some remarks on substitution effects in sodalites. Progress in Solid State Chemistry, 2009, 37, 243–249.

**Ion-exchanged forms of the microporous zirconosilicate $Na_6Zr_3[Si_9O_{27}]$, a product of catapleiite annealing**

D.A. Ksenofontov, A.A. Artamonova*, N.V. Zubkova, I.V. Pekov, A.Yu. Bychkov, V.O. Yapaskurt, D.Yu. Pushcharovsky

[1] Faculty of Geology, Moscow State University, 119991 Moscow, Russia

*art4anya@yandex.ru

One of the actual problems of modern crystallography and materials science is connected with the obtaining of new crystalline microporous materials with technologically important properties (ion-exchange, sorption, catalytic properties, *etc*.) In particular, there are minerals and their synthetic analogues and relatives with heteropolyhedral (usually octahedral-tetrahedral) frameworks. One of them is catapleiite, $Na_2ZrSi_3O_9 \cdot 2H_2O$. Its thermal behavior was studied by us before. A product of catapleiite high-temperature transformation obtained after annealing of the mineral at 1000 ºC was structurally investigated [Ksenofontov et al., 2018]. It turned out that, under high-temperature treatment, catapleiite transforms into the new microporous zirconosilicate with the idealized formula $Na_6Zr_3[Si_9O_{27}]$, a representative of a novel structure type. It is hexagonal, $P6_3/mcm$, $a$ = 11.5901(9), $c$ = 9.9546(9) Å, $V$ = 1158.05(16) $Å^3$, $Z$ = 2. The structure of this zirconosilicate is based on the heteropolyhedral framework which essentially differs from that of catapleiite and is built by nine-membered tetrahedral rings $Si_9O_{27}$ connected with isolated $ZrO_6$ octahedra. Extra-framework Na cations are located in wide channels of the framework and between the rings $Si_9O_{27}$. The topology of the heteropolyhedral Zr-Si-O framework of this zirconosilicate and dimensions of zeolite-like channels allowed to propose for this compound ion-exchange properties [Ksenofontov et al., 2018] that was confirmed in the frame of the present study.

Two series of ion-exchange experiments were carried out with the grains of $Na_6Zr_3[Si_9O_{27}]$: (1) in 1*M* aqueous solutions of KCl, $SrCl_2$ and RbF (temperature 300 ºC,two weeks; (2) in 10% aqueous solutions of Sr, Rb and Cs chlorides (temperature 350 ºC,three weeks). After the experiments, the grains were mounted into solidified epoxy resin samples, polished and further studied using scanning electron microscopy and electron-microprobe analysis (EMPA). $Na^+$ exchange for all above-mentioned large cations occurred and preliminary X-ray diffraction study of the cation-exchanged forms makes possible to assume that no change of the framework is observed. The results of the EMPA show an uneven, spotty distribution of exchanged cations and residual sodium in the grains of the zirconosilicate after the experiments. Sr content reaches 1.58 *apfu* after experiments of the 1st series and 0.56–0.85 *apfu* after the 2nd one. K content varies from 0.35 to 0.66 *apfu*. The widest variations were detected for the largest cations, Rb [0.21–0.71 *apfu* after 1st series and 0.35–0.58 *apfu* after 2nd series] and Cs (up to 1.10 *apfu*).

This work was financially supported by the RFBR, grant 18-29-12007-mk.

Ksenofontov D.A., Grebenev V.V., Zubkova N.V., Pekov I.V., Kabalov Yu.K., Chukanov N.V., Pushcharovsky D.Yu., Artamonova A.A. Catapleiite behavior under heating and crystal structure of the product of its high-temperature transformation, the new phase $Na_6Zr_3[Si_9O_{27}]$ with nine-membered rings of Si,O-tetrahedra. Zapiski RMO, 2018, 3, 94–108.

**Lead orthosilicate $\{Pb_4(O(OH)_2)\}[SiO_4]$ with a framework of anion centered Pb tetrahedra related to sodalite**

Tatiana A. Eremina, Elena L. Belokoneva, Olga V. Dimitrova, Anatoliy S. Volkov

Moscow State University Geological Faculty, 119991 Moscow, Russia

* t_eremina@list.ru

Silicate $\{Pb_4(O(OH)_2)\}[SiO_4]$ synthesized under hydrothermal conditions was structurally characterized, sp. gr. $P2_13$, $a$ = 8.9756(13) Å. The unit cell parameters were determined on an Xcalibur S diffractometer equipped with a CCD detector using a visually high-quality regular tetrahedral-shaped crystal. In agreement with the morphology, the crystal symmetry was cubic, the parameter $a$ = 8.97 Å being similar to that of sodalite.The three-dimensional X-ray diffraction intensity data set was collected at $T$ = 100 K within a full sphere of reciprocal space on a Bruker SMART APEX DUO diffractometer equipped with a CCD area detector and was processed using the APEX2 program. Structure was solved using direct methods in SHELX program package [Sheldrick, 1997], $R_{gt}$ = 0.0479, S = 1.03, final atomic coordinates and displacement parameters are given in Table.

According to the commonly used classification, the new compound belongs to orthosilicates, however numerous Pb atoms allow to analyze their coordination and to separate $\{OPb_4\}^{6+}$tetrahedron, composed of four Pb atoms and centered by O3 anion presented by $O^{2-}$ and hydroxyl groups in relation of 1:2. The $\{OPb_4\}^{6+}$ tetrahedra are linked via shared edges to form the triple clusters $\{O_3Pb_7\}^{8+}$. The Pb1 atom, being common to three tetrahedra, is located at the center. The symmetry of the cluster corresponds to a threefold axis, whereas the local symmetry is higher and corresponds to 3*m*.The clusters are linked through the apical Pb2 atoms to form an anion- centered positively charged framework $\{O(OH)_2Pb_4\}^{4+}$, and its cavities are occupied by negatively charged $[SiO_4]^{4-}$ tetrahedra. Framework may be described as sodalite-like with the lattice nodes presented by triple clusters with a one common vertex. When approximating the clusters by the centers of gravity and representing them as spheres, it can be seen that they are arranged as an Archimedean cuboctahedron. This consideration supports the initial assumption that the new compound is related to sodalite because these compounds have similar unit cell parameters and cubic symmetry: the sodalite unit in framework is also described by a cuboctahedron but with a different ratio of octahedra to cubes.

Table. Coordinates of the basis atoms and equivalent displacement parameters

| **Atom** | **position** | **x/a** | **y/b** | **z/c** | $U_{eq.}$ |
|---|---|---|---|---|---|
| Pb1 | 4 *a*, 3 | 0.79272(8) | 0. 29272 | 0. 20728 | 0.0179(3) |
| Pb2 | 12 *b*, 1 | 0.78730(8) | 0.94233(8) | 0.37957(8) | 0.0191(2) |
| Si | 4 *a*, 3 | 0.9422(5) | 0.5578(5) | 0.4422(5) | 0.0189(17) |
| O1 | 4 *a*, 3 | 0.56(3) | 0.027(7) | 0.000(18) | 0.002(18) |
| O2 | 12 *b*,1 | 0.982(2) | 0.2286(17) | 0.070(2) | 0.031(3) |
| O3* | 12 *b*,1 | 0.5905(17) | 0.3601(16) | 0.3217(15) | 0.019(3) |

*Position is occupied by O atoms and (OH) groups in ratio 1:2

Sheldrick G.M. SHELX-97. Program for Structure Refinement. University of Goettingen, Germany. 1997.

**Crystal structures of silicate-germanate family with a mixed microporous framework: $(K_{2.9}Cs_{0.1})(Sc_{0.7}In_{0.3})[(Si_{2.9}Ge_{0.1})O_9]\cdot H_2O$ and $(K_{2.22}Cs_{0.78})Bi[(Si_{0.5}Ge_{0.5})O_9]\cdot H_2O$**

Anastasiia P. Topnikova[1,*], Elena L. Belokoneva[1], Anatoly S. Volkov[1], Olga V. Dimitrova[1], and Sergey Yu. Stefanovich[2]

[1] Faculty of Geology, Lomonosov Moscow State University, 119991 Moscow, Russia
[2]Faculty of Chemistry, Lomonosov Moscow State University, 119991 Moscow, Russia

*nastya_zorina@rambler.ru

Crystals of new silicate-germanates $(K_{2.9}Cs_{0.1})(Sc_{0.7}In_{0.3})[(Si_{2.9}Ge_{0.1})O_9]\cdot H_2O$ (I) and $(K_{2.22}Cs_{0.78})Bi[(Si_{0.5}Ge_{0.5})O_9]\cdot H_2O$ (II), sp. gr. $Pmn2_1$, were obtained under hydrothermal conditions at temperature 280–290°C and pressure 70–100 atm. in a search of perspective compositions. New structures belong to the structure type determined first for $K_3Ho[Si_3O_9]$*in situ* at high temperature and then realized for $K_3Sc[Si_3O_9]\cdot H_2O$ (Sc– smaller analogue of rare earth elements) [Belokoneva et al., 2013]. Another member of the family, $K_{1.46}Pb_{1.54}Ca[(Ge_{0.23}Si_{0.77})_3O_9](OH)_{0.54}\cdot 0.46H_2O$, was synthesized and structurally investigated as well [Belokoneva et al., 2019]. All mentioned structures have mixed microporous framework combined from wollastonite chains of $Si(Ge)O_4$-tetrahedra and from (Sc,In)- (I) and Bi- (II) octahedra (Figure). The structural family is characterized by wide isomorphic substitution in octahedron position and in framework channels. The position of K3 in all structures is split into two, but one of the positions is occupied by Cs atoms in (II). The proposed ion-exchange properties for the compounds of this structure type is confirmed by isomorphic substitution compared to the pure $K_3Sc[Si_3O_9]\cdot H_2O$. For $(K_{2.9}Cs_{0.1})(Sc_{0.7}In_{0.3})[(Si_{2.9}Ge_{0.1})O_9]\cdot H_2O$, nonlinear optical properties were found.

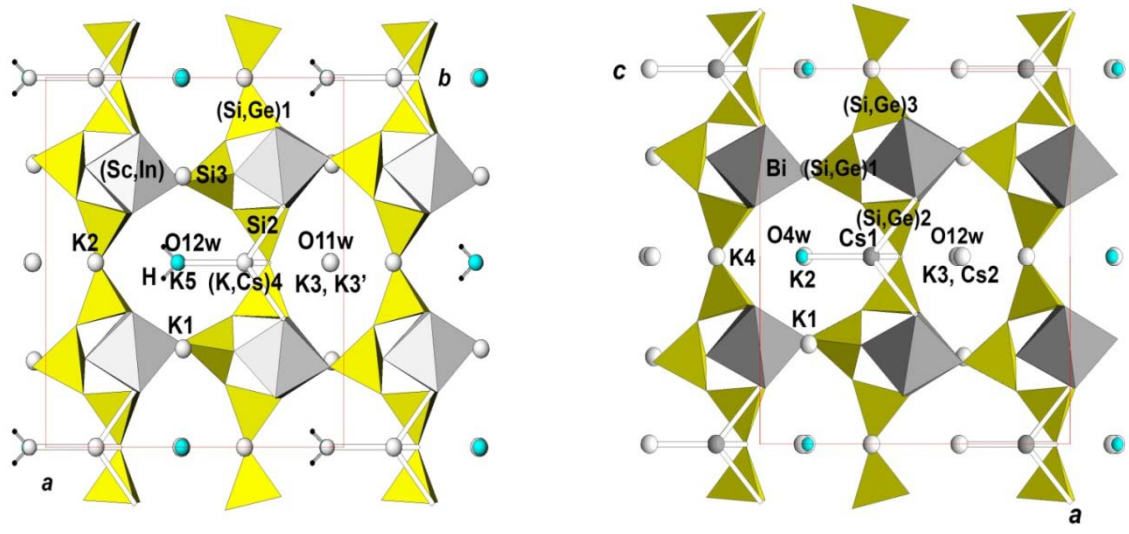


The reported study was funded by RFBR according to the research projects Nos 18-35-00645 and 17-03-00886.

Belokoneva E.L., Morozov I.A., Dimitrova O.V., Volkov A.S. Polar silicogermanate $K_{1.46}Pb_{1.54}Ca[(Ge_{0.23}Si_{0.77})_3O_9](OH)_{0.54}\cdot 0.46H_2O$ with a wollastonite chain and wide isomorphism. Cryst. Rep., 2019, 64(2), 247–251.

Belokoneva E.L., Zorina A.P., Dimitrova O.V. New framework hydrous silicate $K_3Sc[Si_3O_9]\cdot H_2O$ related to the hight temperature anhydrous silicate $K_3Ho[Si_3O_9]$ and symmetry analysis of phase transition with prediction of the structures. Cryst. Rep., 2013, 58(4), 586–593.

# $(Y,REE)_6(SiO_4)(Si_3O_{10})F_6$, a novel sorosilicate mineral based on a framework of fluorine-centered triangles and tetrahedra

Fabrice Dal Bo,* Tomas Husdal, and Henrik Friis

Natural History Museum, University of Oslo, 0318 Oslo, Norway

* f.d.bo@nhm.uio.no

$(Y,REE)_6(SiO_4)(Si_3O_{10})F_6$ is a new mineral discovered in the Stetind pegmatite, Tysfjord, Nordland, Norway. The Stetind pegmatite belongs to a series of quartz-microcline pegmatites of the NYF-family found in the Tysfjord granite, an 1800 Ma old granitic gneiss deformed during the Caledonian orogeny [Andresen, Tull, 1986]. Bodies of Y-rich fluorite are a characteristic feature of these pegmatites, and fluorite from the Stetind pegmatite is particularly rich in inclusions of various REE-bearing minerals [Husdal, 2008], including seven type locality minerals: alnaperbøeite-(Ce), atelisite-(Y), bastnäsite-(Nd), cayalsite-(Y), perbøeite-(Ce), schlüterite-(Y), and stetindite-(Ce). The new mineral occurs as pink and transparent fibers (up to ~1 mm long) forming aggregates in cavities in fluorite.

The crystal structure of this new mineral has been refined to $R$ = 0.037 ($wR$ = 0.076) using 3144 reflections. The unit-cell is monoclinic, space group $I2/c$, with $a$ = 9.2574(2), $b$ = 12.8362(3), $c$ = 13.1594(4) Å, $\beta$ = 107.572(3)°, $V$ = 1490.77(7) Å$^3$, $Z$ = 4. The structure is characterized by three symmetrically independent $A$-sites containing a mix of Y and other REE. These sites are eight-fold coordinated to oxygen and fluorine atoms to form the polyhedra $A(1)O_5F_3$, $A(2)O_5F_3$ and $A(3)O_4F_4$ (Fig. 1). The $A(1)$ polyhedron can be described as a regular square antiprism, while the $A(2)$ and $A(3)$ polyhedra can be described as distorted square antiprisms. The average bond distances are 2.465(4), 2.418(5) and 2.370(4) Å, for the $A(1)$-$A(3)$ sites, respectively. In addition, three sites containing Si in tetrahedral coordination are observed. The Si(1) and Si(2) are sharing one corner to form a 3-membered finite chain with the composition $[Si_3O_{10}]^{8-}$ along [101]. The <Si(1)-O6-Si(2)> angle is 133.5(3)° (Fig. 1). The Si(3) site occurs as an isolated $SiO_4$ tetrahedron. The average bond distances for the Si1, Si(2) and Si3 sites are 1.629(4), 1.627(5) and 1.646(4) Å, respectively. Finally, seven sites containing oxygen and three sites containing fluorine atoms are also occurring in the structure. The formula derived from the crystal structure refinement is $(Y,REE)_6(SiO_4)(Si_3O_{10})F_6$ ($Z$ = 4).

The structure of $(Y,REE)_6(SiO_4)(Si_3O_{10})F_6$ is described as a framework built by the corner-, edge- and face-sharing $A(1)$, $A(2)$ and $A(3)$ polyhedra (Fig. 2). The Si tetrahedra are occurring in the cavities of the framework, and therefore the structural formula can be expressed as $[(Y,REE)_6F_6][(SiO_4)(Si_3O_{10})]$ in order to distinguish the framework building units and the host units in the first and second bracket, respectively. In addition, the framework can be described using an anion-centered point of view [Krivovichev et al., 2013]. In that case it appears that the framework is built around corner- and edge-sharing fluorine-centered triangles, $F(1)A_3$ and $F(2)A_3$, and tetrahedra, $F(3)A_4$ (Fig. 2). These polyhedra have respectively mean bond-lengths of 2.364(5), 2.403(4) and 2.482(4) Å (Fig. 1). Unlike $FA_3$ triangles ($A$ = Y or REE), which are relatively common in minerals, $FA_4$ tetrahedra are not reported in any mineral species.

Calculation of structural complexity parameters was performed using information-based complexity measures and the *ToposPro* software [Krivovichev, 2012; Blatov et al., 2014], and gave the structural complexity parameters $v$ = 66 atoms, $I_G$ = 4.07 bits/atoms, and $I_{G,total}$ = 268.93 bits/unit cell. These values indicate that $(Y,REE)_6(SiO_4)(Si_3O_{10})F_6$ is one of the most complex minerals reported so far in comparison to other chemically related mineral species.

Andresen A., Tull J.F. Age and tectonic setting of the Tysfjord gneiss granite, Efjord, North Norway. Norsk Geologisk Tidsskrift, 1986, 66, 69-80.

Blatov V.A., Shevchenko A.P., Proserpio D.M. Applied topological analysis of crystal structures with the program package ToposPro. Cryst. Growth Des., 2014, *14*, 3576.

Husdal T.A. The minerals of the pegmatites within the Tysfjord granite, northern Norway. Kongsberg Mineral symposium, 2008, 5-28.

Krivovichev S.V. Topological complexity of crystal structures: quantitative approach. Acta Cryst. Sect. A: Found. Cryst., 2012, 68, 393.

Krivovichev S.V., Mentré O., Siidra O.I., Colmont M., Filatov S.K. Anion-Centered Tetrahedra in Inorganic Compounds. Chem. Rev., 2013, 113, 6459-6535.

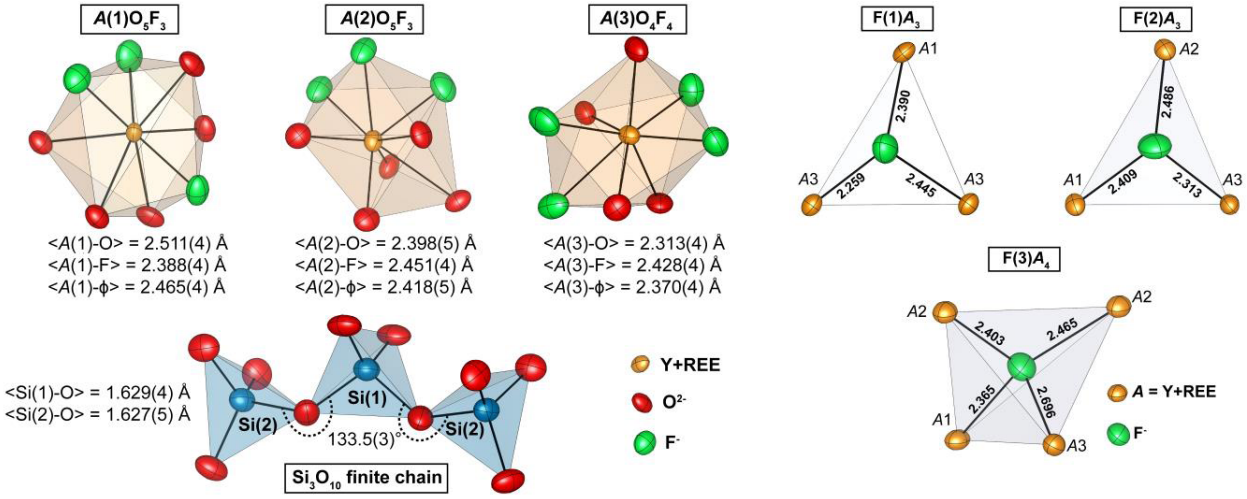


Figure 1. Representation of the $A\phi_8$ polyhedra containing Y+REE, $Si_3O_{10}$ chain, and fluorine-centered triangles and tetrahedra occurring in the structure of $(Y,REE)_6(SiO_4)(Si_3O_{10})F_6$.

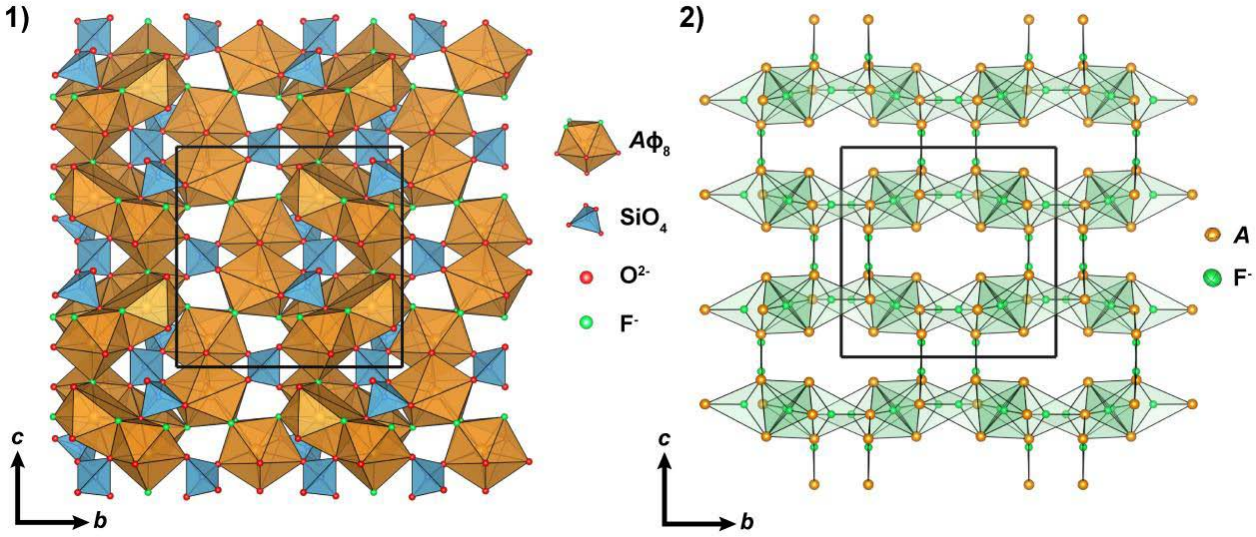


Figure 2. Cation-centered (1) and anion-centered (2) representation of the framework occurring in $(Y,REE)_6(SiO_4)(Si_3O_{10})F_6$ ($A$ = Y+REE; $\phi = O^{2-}$ or $F^-$).

# A New Mineral Khurayyimite, $Ca_{7.07}Zn_{3.89}Si_{4.02}O_{14}(OH)_{10}\cdot 4H_2O$, from Daba Siwaqa Pyrometamorphic Rock, Jordan

Irina O. Galuskina[1,*], Biljana Krüger[2], Evgeny V.Galuskin[1], Yevgeny Vapnik[3], Mikhail Murashko[4]

[1]University of Silesia, 41-200 Sosnowiec, Poland
[2]University of Innsbruck, 6020 Innsbruck, Austria
[3]Ben-Gurion University of the Negev, Beer-Sheva 84105, Israel
[4]Saint Petersburg State University, 199034 St Petersburg, Russia

* irina.galuskina@us.edu.pl

Khurayyimite (IMA2018-140), $Ca_7Zn_4(Si_2O_7)_2(OH)_{10}\cdot 4H_2O$, was found in small cavities and veins in altered spurrite marbles in Central Jordan within the largest area of the Hatrurim Complex rock – Daba-Siwaga, in the Dead Sea rift region. Khurayyimite occurs with other low-temperature minerals as calcite, Ca-hydrosilicates (e.g.jennite and foshagite), as well as minerals of the tobermorite group and ettringite-thaumasite series. Spurrite, calcite, fluorapatite and cuspidine are rock-forming minerals of unaltered dark spurrite marbles. Accessory minerals are presented by spinel-magnesioferrite, franklinite, fluormayenite-fluorkyuygenite, sphalerite, pyrite, chalcocite, hematite, clinohedrite. Khurayyimite forms spherulitic aggregates up to 200-300 μm in size. Individual elongated platy crystals in spherules are nearly 50 μm long and up to 10 μm thick. Mineral is colorless with vitreous lustre. The empirical formula of kurayyimiteis: $Ca_{7.07}Zn_{3.89}Si_{4.02}O_{14}(OH)_{10}\cdot 4H_2O$. Single-crystal X-ray studies were carried out with synchrotron radiation. The crystal structure was solved using direct methods to $R_1$= 0.0213. The new mineral is monoclinic, with $P2_1/c$ space group and parameters $a$ = 11.2450(8) Å, $b$ = 9.0963(5) Å, $c$ = 14.0679(10) Å, α = 90º, β = 113.237(8)º, γ = 90º, $V$ = 1322.25(17) Å$^3$, $Z$ = 2. The crystal structure of khurayyimite consists of sheets parallel to *b*-axis. Sheets are connected over oxygen atom, corner-shared by $CaO(OH)_4(OH_2)$ octahedra and $ZnO_2(OH)_2$ tetrahedra and additional hydrogen bonds between them. Each sheet is built by very unusual loop-branched *sechser* single chains {***lB***, $1\infty 1$}[$^6Zn_4Si_4O_{21}$]. Voids between chains are filled by blocks of five Ca-octahedra and two $CaO_7$ polyhedra with additional OH groups and $H_2O$ molecules. The main bands in the Raman spectrum of khurrayimiteare responded to Si-O vibrations in $(Si_2O_7)^{6-}$ groups: $\nu_1$ 907 cm$^{-1}$, $\nu_4$ 671 cm$^{-1}$, $\nu_2$ 346 cm$^{-1}$ and Zn-O tetrahedra $ZnO_2(OH)_2$: $\nu_1$ 461 cm$^{-1}$; $\nu_2+\nu_4$ 289 cm$^{-1}$, 312 cm$^{-1}$, 346 cm$^{-1}$. Band at 584 cm$^{-1}$ is rather connected with Si-O-Zn vibrations, and band at 522 cm$^{-1}$ is related to Si-O-Si vibrations. The main bands lower 200 cm$^{-1}$ are answered to vibrations of Ca-O in $CaO_4(OH)_3$ polyhedra and $CaO(OH)_4(OH_2)$, $CaO_4(OH)_2$, $CaO_3(OH)_2(OH_2)$ octahedra. Bands at 2855 and 3105 cm$^{-1}$ are related to O-H vibration in $H_2O$ with strong hydrogen bonds, whereas the main bands at 3506, 3582 and 3622 cm$^{-1}$ are corresponded to vibrations in OH groups. Name khurayyimite is given after of Khurayyim Mount (Jabal al Khurayyim), Siwaqa pyrometamorphic rock area, Um Al-Rasas Sub-district, central Jordan. Khurayyimite was found in the immediate vicinity of this mount. Khurayyimite does not have synthetic analogues. It is a new compound in the system CaO-ZnO-$SiO_2$-$H_2O$ with a new type of crystal structure.

The investigations were partially supported by the National Science Centre (NCN) of Poland, grant no. 2016/23/B/ST10/00869.

**A novel high-potassium manaksite analogue, $K(K_{0.72}Na_{0.28})Mn[Si_4O_{10}]$, in the row of isotypic compounds**

Galina V. Kiriukhina[1,2]*, Olga V. Yakubovich[1], Iurii Dovgaliuk[3]

[1] Lomonosov Moscow State University, 119991 Moscow, Russia
[2]The Institute of Experimental Mineralogy RAS, 142432 Chernogolovka, Moscow Region, Russia
[3]Swiss–Norwegian Beam Lines at ESRF, 38042 Grenoble, France

* g-biralo@yandex.ru

A rare mineral manaksite, $KNaMnSi_4O_{10}$, was discovered in 1992 in Lovozero alkaline massif, Kola Peninsula, Russia [Khomyakov et al., 1992]. At the moment, there are four litiodionite-group minerals $KNaM[Si_4O_{10}]$ distinguished by sort of the $M^{2+}$ cation: litiodionite, $KNaCuSi_4O_{10}$, manaksite, $KNaMnSi_4O_{10}$, fenaksite, $KNaFeSi_4O_{10}$, and calcinaksite, $KNaCa(H_2O)Si_4O_{10}$. Their crystal structures are based on the unique silicate tubes $[Si_8O_{20}]$ connected by $M_2O_9$ dimers of edge-sharing pyramids to a heteropolyhedral framework (Figure). The alkaline metal cations fill the framework cavities of the two types: between the silicate tubes and manganese dimers, and inside the 8-membered windows of these tubes. Synthetic analogues of the litiodionite-group minerals have been known to contain the sodium atoms in both types of the framework cavities, e.g. $Na_2MnSi_4O_{10}$ [Cadoni et al., 2011]. A new highly potassium analogue of manaksite, $K(K_{0.72}Na_{0.28})MnSi_4O_{10}$, was synthesized under hydrothermal conditions for the first time. Its triclinic $P\bar{1}$crystal structure was determined from single-crystal X-ray low-temperature synchrotron data and refined to $R$ = 0.0248 in an anisotropic approximation. It has been found that K atoms corresponding to Na in manaksite are split into two positions at the distance of 0.246 Å, populated by K and Na atoms in the K:Na ratio refined as 0.72:0.28. The new phase, $K(K_{0.72}Na_{0.28})MnSi_4O_{10}$, manaksite, $KNaMnSi_4O_{10}$, and its high-sodium analogue, $Na_2MnSi_4O_{10}$ [Cadoni et al., 2011], form the row of manaksite isotypic compounds *AA'*$Mn[Si_4O_{10}]$, *A*, *A'* = K, Na. The crystal chemical analysis showed that the *b* unit cell parameters and volumes of the series members change accordingly to the sort of the $A^+$ cation, owed to the structural movements of the 8-membered windows.

The reported study was funded by RFBR according to the research projects № 18-35-00623 to Galina Kiriukhina and № 18-29-12030 to Olga Yakubovich.

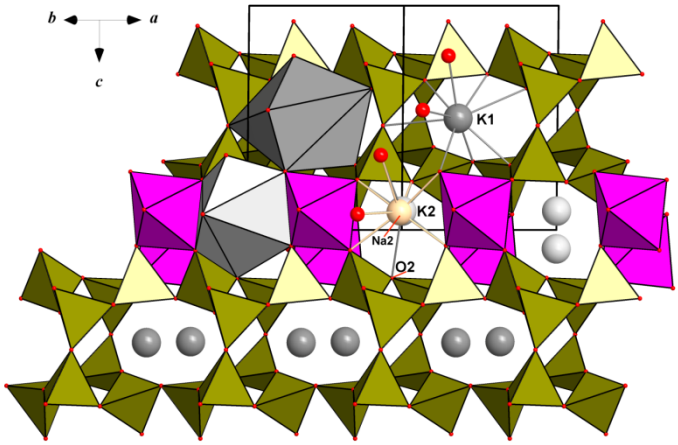


Figure. The crystal structure of $K(K_{0.72}Na_{0.28})Mn[Si_4O_{10}]$ in the [110] projection, showing main structural units – silicate tubes linked in a framework by dimmers of $MnO_5$ pyramids, and alkaline metal atoms in two positions in the open channels.

Cadoni M., Ferraris G. Synthesis and crystal structure of $Na_2MnSi_4O_{10}$: relationship with the manaksite group. Rend. Fis. Acc. Lincei, 2011, 22, 225–234.

Khomyakov A.P., Kurova T.A., Nechelyustov G.N. Manaksite, $KNaMnSi_4O_{10}$ – a new mineral. Zapiski VMO, 1992, 121, 112–115.

## Incommensurate modulation in flamite – natural analogue of $\alpha_H'$-$Ca_2SiO_4$

Sergey V. Rashchenko[1,2,*], Yurii V. Seryotkin[1,2], Ella V. Sokol[1], and Svetlana N. Kokh[1]

[1]Sobolev Institute of Geology and Mineralogy SB RAS, 630090 Novosibirsk, Russia
[2]Novosibirsk State University, 630090 Novosibirsk, Russia

*rashchenko@igm.nsc.ru

Crystal structures of unquenchable high-temperature polymorphs of $Ca_2SiO_4$, important for cement chemistry, have been remaining unavailable for single-crystal X-ray analysis. However, the problem may be addressed by studying chemically stabilized $Ca_2SiO_4$ polymorphs at ambient temperature. We solved an incommensurately modulated crystal structure of *flamite* [Sokol *et al.*, 2015] (*Pnma*(0β0)00*s*, **q** = 0.26677(13)**b***, *a* = 6.855 (5) Å, *b* = 5.4288 (10) Å, *c* = 9.3770 (8) Å) – a mineral analogue of orthorhombic $\alpha_H'$-$Ca_2SiO_4$ (stable between 1160 and 1425°C), naturally stabilized by admixture of phosphorus. The studied sample from Hatrurim Basin (Negev Desert, Israel) with composition $(Ca_{1.75}K_{0.12}Na_{0.12})_{\Sigma 1.99}(Si_{0.74}P_{0.26})_{\Sigma 1.00}O_4$ also demonstrates pseudomerohedral cyclic twinning around *a* axis, which results from pseudohexagonal topology of the crystal structure and complicates indexing of X-ray diffraction data (Figure).

Incommensurate modulation of flamite samples fits well the 'modulation vector vs. P / (Si + P) ratio' trends proposed by [Fukuda et al., 1994, 1997] for chemically stabilized $\alpha_H'$-$Ca_2SiO_4$, indicating a major influence of phosphorus on the crystal structure. It also suggests that truly commensurate modulation with **q** = 0.25**b*** should be typical for samples with P / (Si + P) ≈ 0.13.

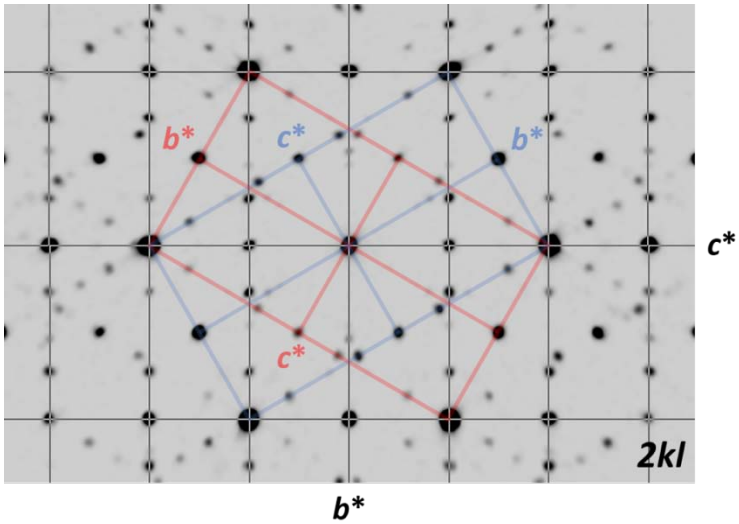


Figure.Reconstruction of 2*kl* slice of flamite reciprocal lattice.
Lattices of two other twin components are also shown.

Fukuda K., Maki I., Ito S., Miyake T. Structural change in phosphorus-bearing dicalcium silicates. J. Ceram. Soc. Jap., 1997, 105, 117–121.

Fukuda K., Maki I., Ito S., Yoshida H., Aoki, K. structure and microtexture changes in phosphorous-bearing $Ca_2SiO_4$solid solutions. J. Am. Ceram. Soc., 1994, 77, 2615–2619.

Sokol E.V., Seryotkin Yu.V., Kokh S.N., Vapnik Ye., Nigmatulina E.N., Goryainov S.V., Belogub E.V., Sharygin V.V. Flamite, $(Ca,Na,K)_2(Si,P)O_4$, a new mineral from ultrahigh-temperature combustion metamorphic rocks, Hatrurim Basin, Negev Desert, Israel. Min. Mag., 2015, 79, 583–596.

**Agrellite from Dara-i-Pioz (Tajikistan) and Murun (Russia) massifs: a comparative EPMA, SCXRD, FTIR, EPR and luminescence study**

Ekaterina V. Kaneva[1,2,*],Roman Y. Shendrik[1], Nikolay V. Vladykin[1], and Ernesto Mesto[3]

[1] Vinogradov Institute of Geochemistry SB RAS, 664033 Irkutsk, Russia
[2] National Research Technical University, 664074 Irkutsk, Russia
[3] University of Bari Aldo Moro, Dip. di Scienze della Terra e Geoambientali, 70125 Bari, Italy

* kev604@mail.ru

Agrellite is a rare inosilicate, having a crystal structure characterized by $SiO_4$-tetrahedral tubes located between continuous wall layers formed by edge-sharing $CaO_7$-polyhedra. The mineral has been found in alkaline rocks of Kipawa complex, Quebec (Canada), with simplified crystal chemical formula: $Na(Ca_{1.91}REE_{0.10})[Si_4O_{10}]F$ [Ghose, Wan, 1979], and in several geological sites on southeast periphery of the Murun alkaline massif(Siberia, Russia), with a reported chemical formula: $Na(Ca_{1.75}Sr_{0.16})[Si_4O_{10}](F,OH)$ [Rozhdestvenskaya, Nikishova, 1998]. Canadian and Russian agrellites crystallize in $2A_c$ and $2A_I$ polytypes, respectively, because of the different arrangement of silicate tubes in the crystal structure [Rozhdestvenskaya, Nikishova, 1998]. In the present work, for the first time, a detailed chemical, structural and physical study of agrellite specimen from the Dara-i-Pioz massif has been carried out by means of EPMA, IR, EPR, and SCXRD. The results are compared with new data obtained for agrellite from the Murun massif.

According to the EPMA, the simplified formula of agrellite from Dara-i-Pioz and Murun massifs is $NaCa_2[Si_4O_{10}]F$. Indeed, in both specimens Mn and Ce are present only in minor amounts (≤0.04 *apfu*). The region of the Si-O vibrational bands of the IR spectrum is very similar for both investigated agrellite, but the $H_2O$/OH vibration regions of the spectra (1500–4000 $cm^{-1}$) are different. In the sample from Murun massif, a strong absorption band of $H_2O$ molecules has been found, which is missing in Dara-i-Pioz IR spectrum.

The EPR analysis points out the Ca is replaced for Mn. The latter coordinates two fluorine ions. Luminescence due to 5*d*-4*f* transition in $Ce^{3+}$ ions has been observed in both investigated samples. Band gap of agrellite was estimated at about 8 eV. Using VRBE model [Dorenbos, 2013], position of trivalent and divalent lanthanide 4*f* states and $Ce^{4+}$ charge transfer energy have been estimated. Wide absorption band peaked at about 390 nm corresponds to the charge transfer transition of $Ce^{4+}$.

Dara-i-Pioz and Murun agrellite crystal structures, as determined by SCXRD data, confirm that the both crystals are triclinic and belong to 2-$A_c$ polytype. As the Si-tetrahedral tubes share vertexes with the Ca-polyhedra layers, the arrangement of the $SiO_4$ group is strongly affected by the polyhedron geometry. Dara-i-Pioz and Murun agrellites have volume, bond distances and edge lengths of the Ca-polyhedra smaller than corresponding Sr-polyhedra of agrellite-$2A_I$ [Rozhdestvenskaya, Nikishova, 1998], because of the difference of the ionic radius between $Sr^{2+}$ and $Ca^{2+}$ ions.

So, SCXRD data show that the structural and chemical features of the studied samples are similar, but different with respect to ones of the Murun agrellite of previously described in [Rozhdestvenskaya, Nikishova, 1998]

This work was supported by grant of the President of the Russian Federation MK-936.2019.5. FTIR experiments were supported by grant of Russian Science Foundation RSF 18-72-10085.

Dorenbos P. A review on how lanthanide impurity levels change with chemistry and structure of inorganic compounds. ECS J. Solid State Sci. Technol., 2013, 2(2), R3001–3011.

Ghose S., and Wan C. Agrellite, $Na(Ca,RE)_2Si_4O_{10}F$: a layer structure with silicate tubes. Am. Min., 1979, 64, 563–572.

Rozhdestvenskaya I.V., and Nikishova L.V. Crystal structure of $Na(Ca,Sr)_2Si_4O_{10}F$ strontium agrellite from Yakutian charoitites: agrellite polytypes. Cryst. Rep., 1998, 43(4), 589–597.

## $[X_{12}O_{36}]$ rings, X = Si, Ge, in crystal structures of silicates and germanates

Alexander V. Serdtsev[1,2], Irina D. Yushina[3], Sergey M. Aksenov[4] and Ivan I. Leonidov[1,*]

[1] Institute of Solid State Chemistry, UB RAS, 620990 Ekaterinburg, Russia
[2] Ural Federal University, 620002 Ekaterinburg, Russia
[3] South Ural State University, 454080 Chelyabinsk, Russia
[4] University of Notre Dame, Notre Dame, IN, 46556 United States

* ivanleonidov@ihim.uran.ru

The ring anions $[Si_{12}O_{36}]^{24-}$ are rare in crystal structures of natural silicates. In its turn, $[Si_{12}O_{36}]^{24-}$ belongs to the main structural units of traskite, $Ba_{21}Ca(Fe^{2+},Mn,Ti)_4(Ti,Fe,Mg)_{12}(Si_{12}O_{36})(Si_2O_7)_6(O,OH)_{30}Cl_6\cdot 14H_2O$. The mineral crystallizes in a hexagonal-type structure which is characterized by the space group *P*6/*mmm*, *P*6*mm*, *P*622, $P\bar{6}m2$ or $P\bar{6}2m$ [Malinovskii et al., 1976]. The unit cell is formed by a tubular set of barium polyhedra. The latter paired along a common edge form ditrigonal rings around the $\bar{6}$ axis in the center of the cell. The core of these rings being a trigonal Ca prism is connected to the Ba framework along the [0 0 1] direction by standing diorthogroups. The large polyhedra of the layer constructed from almost regular pentagonal prisms are coupled to one another along the vertical edges and form cavities (around $\bar{6}$ axis) in which $[Si_{12}O_{36}]$ rings are located. The tubular barium framework of traskite is bound by a discontinuous silicon–oxygen coupling: the larger spaces around the origin of coordinates by $[Si_{12}O_{36}]$ rings, the smaller ones around the 3-fold axes by $[Si_2O_7]$ pyrogroups.

Possible substitutions between monovalent Na-K and divalent Ca-Sr-Ba cations in ternary phases in the system $K_2O–CaO–SiO_2$ allow an extensive study on how the combination of different cations influences on the stability of certain structure types and physical/chemical properties of those compounds for further materials design. In fact, there are two main structure types among the alkali–alkaline earth silicates of the general composition $M^{I}_4M^{II}Si_3O_9$ (*M*I = Na, K; *M*II = Ca, Sr, Ba). $Na_4CaSi_3O_9$ (space group $Pa\bar{3}$) and the isotypic compounds $K_4M^{II}X_3O_9$ ($M^{II}$ = Ca, Sr; *X* = Si, Ge) belong to the group of ring silicates and germanates which are featured by distorted $[X_{12}O_{36}]^{24-}$anions, *X* = Si, Ge. The anionic sublattice of $Na_4SrSi_3O_9$ and the remaining barium silicates and germanates (space groups *B*2, *C*2 and *Ama*2) comprise spiral either *dreier*, or *sechser* single tetrahedral chains [Arroyabe et al., 2009].

The report represents an overview on structural chemistry, lattice dynamics and optical spectroscopy of the lanthanide-doped optical hosts $M^{I}_4M^{II}X_3O_9$ ($M^{I}$ = Na, K; $M^{II}$ = Ca, Sr; X = Si, Ge). Periodic *ab initio* calculations within DFT framework employing hybrid functionals (B3PW, B3LYP, HSEsol, etc.) have been performed in order to describe infrared and Raman spectra and band structure of the stoichiometric compounds on the basis of previous studies of cyclogermanates [Leonidov et al., 2014]. The results of photoluminescence spectroscopy study of $M^{I}_4M^{II}X_3O_9$-related compounds doped with $Sm^{3+}$, $Eu^{3+}$ and $Dy^{3+}$ ions demonstrate that these optical materials can find their application in solid-state lighting and laser engineering.

I.I.L. would like to acknowledge support from the Russian President Fellowship SP–931.2016.1. Periodic calculations were performed on the supercomputer «Tornado SUSU» at South Ural State University (Russia).

Arroyabe E., Kaindl R., Kahlenberg V. Structural and Raman spectroscopic investigations of $K_4BaSi_3O_9$ and $K_4CaSi_3O_9$. Z. Anorg. Allg. Chem., 2009, 635, 337–345.

Leonidov I.I., Petrov V.P., Chernyshev V.A., Nikiforov A.E., Vovkotrub E.G., Tyutyunnik A.P., Zubkov V.G. Structural and vibrational properties of the ordered $Y_2CaGe_4O_{12}$ germanate: a periodic ab initio study. J. Phys. Chem. C, 2014, 118, 8090–8101.

Malinovskii Yu.A., Pobedimskaya E.A., Belov, N.V. Crystal structure of traskite. Sov. Phys. Dokl., 1976, 21, 426–428.

**New data on crystal chemistry of eudialyte-group minerals**

Ramiza K. Rastsvetaeva[1,]*, Sergey M. Aksenov[1,2], and Nikita V. Chukanov[3]

[1] FSRC "Crystallography and Photonics", Russian Academy of Sciences, 119333 Moscow, Russia
[2] Nesmeyanov Institute of Organoelement Compounds, Russian Academy of Sciences, Moscow, Russia
[3] Institute of Problems of Chemical Physics, Russian Academy of Sciences, 142432 Chernogolovka, Moscow Region, Russia

* rast.crys@gmail.com

Members of the eudialyte group are represented by trigonal (space groups *R*-3*m*, *R*3*m*, or *R*3) microporous framework heteropolyhedral zircono- and titanosilicates which are wide spread in Kola Peninsula(Russia) and characterized by a unique structural and chemical complexity and variability [Johnsen et al., 2003; Rastsvetaeva, 2007; Rastsvetaeva and Chukanov, 2012; Rastsvetaeva et al., 2012]. At present,the eudialyte group includes 28 mineral species. Among them, recently, new minerals ilyuchinite [Rastsvetaeva, 2017] and siudaite [Chukanov, 2018] are proved by CNMNC. In accordance with the ordering of extra-framework cations, 12-layer and 24-layer species (with the *c* parameter of the unit-cell of ~30 and ~60 Å, respectively) are distinguished [Rastsvetaeva, Chukanov, 2012]. However, 24-layer minerals are very rare and are formed in minor amounts, under very specific conditions [Rastsvetaeva et al., 2012].

The simplified general formula of 12-layer eudialyte-group minerals is $[N1N2N3N4N5]_3M1_6M2_3M3M4Z_3(Si_9O_{27})_2(Si_3O_9)_2Ø_{4\text{-}6}X1X2$ [Johnsen et al., 2003]. Based on the recent data on the chemical variations of the eudialyte group minerals [Schilling et al., 2011; Rastsvetaeva et al., 2012; Borst et al., 2018], we can assume that *M*1 are cations (Ca, $Mn^{2+}$, *REE*, Na, Sr, $Fe^{2+}$) which form a six-membered ring of edge-sharing $M1O_6$-octahedra; *M*2 is a group of closely spaced sites which can be statistically occupied by $^{IV,V}Fe^{2+}$, $^{V,VI}Fe^{3+}$, $^{IV,V,VI}Mn^{2+}$, $^{V,VI}Na^{+}$, $^{IV,V}Zr^{4+}$, $^{VI}Ta^{5+}$, as well as subordinate $^{VII}K^{+}$; *M*3 and *M*4 are tetrahedrally (Si, S) and octahedrally (Nb, Ti, W, Na) coordinated atoms which occupy groups of closely spaced sites near the centers of two kinds of 9-membered rings of $SiO_4$ tetrahedra; the *Z* site has octahedral coordination and can contain Zr, Ti and Nb; Ø = O, OH, $H_2O$; *N*1–5 are extra-framework cations (Na, $H_3O^+$, K, Sr, *REE*, Y, Ba, $Mn^{2+}$, Ca); *X*(1) and *X*(2) are extra-framework water molecules, halide anions ($Cl^-$, $F^-$) and anionic groups ($OH^-$, $CO_3^{2-}$, $SO_4^{2-}$, $AlO_4^{5-}$, $MnO_4^{6-}$). The *M*1 cations can be disordered, or ordered and alternate in the octahedral ring. The sites *N*1–5, Ø, *X*1, *X*2, *M*2, *M*3 and *M*4 can be partly vacant. The *N*4 site concentrates selectively bi- and trivalent extra-framework cations ($Ca^{2+}$, $Mn^{2+}$, $Sr^{2+}$, $REE^{3+}$), whereas other *N* sites are usually Na-, $H_3O^+$-dominant.

Borst A.M., Friis H., Nielsen T.F.D. et al. Melt evolution in agpaitic intrusions: Insights from compositional zoning in eudialyte, Ilimaussaq complex, South Greenland. J. Petrol. 2018, 1–23

Chukanov N.V., Rastsvetaeva R.K. et al. Phys. Chem. Minerals., 2018, 45, 39–50.

Johnsen O., Ferraris G., Gault R.A., Grice J.D., Kampf A.R., Pekov I.V. Nomenclature of eudialyte-group minerals. Can. Mineral., 2003, 41, 785–794.

Rastsvetaeva R.K, Aksenov S.M., Rozenberg K.A. Crystal structure of the hydrated analogue of rastsvetaevite. Cryst. Rep., 2015, 60, 831–840.

Rastsvetaeva R.K. et al. Cryst. Rep., 2017, 62, 54–60.

Rastsvetaeva R.K. Structural mineralogy of eudialyte group: a review. Cryst. Rep., 2007, 52, 47–64.

Rastsvetaeva R.K., Chukanov N.V. Classification of eudialyte-group minerals. Geol. Ore Deposits, 2012, 54, 487–497.

Rastsvetaeva R.K., Chukanov N.V., Aksenov S.M. Eudialyte-Group Minerals: Crystal Chemistry, Properties, Genesis. University of Nizhny Novgorod, 2012 [in Russian]

Schilling J., Wu F.-Y., McCammon C., Wenzel T., Marks M.A.W., Plaff K., Jacob D.E., Markl G. The compositional variability of eudialyte-group minerals. Mineral. Mag., 2011, 75, 87–115.

**Crystal–Fluid Interaction: The Structural Evolution of Zeolites at High Pressure**

Yurii V. Seryotkin[1,*], Vladimir V. Bakakin[2]

[1] Institute of Geology and Mineralogy SB RAS, 630090 Novosibirsk, Russia
[2] Institute of Inorganic Chemistry SB RAS, 630090 Novosibirsk, Russia

* yuvs@igm.nsc.ru

The behavior of zeolites at high pressure depends on the nature of the pressure-transmitting medium, "penetrating" (mainly water-containing) or "non-penetrating". The usual effect of compression in non-penetrating medium is deformation of the tetrahedral framework. While compression in penetrating media usually leads to pressure-induced hydration (PIH). The PIH effect is controlled by a several parameters: (1) the configuration and size of the framework cavities; (2) the nature of their contents and (3) the partial pressure of the penetrating component in the pressure-transmitting medium. An important characteristic is also the diffusion mobility of $H_2O$ molecules in the channels, as well as the defectiveness of the extraframework subsystem (presence of vacancies).

Usually, the diffusion in solids as a typical activation process is suppressed under pressure. However, the compression of the hydrated fibrous zeolite natrolite $Na_2(H_2O)_2[Al_2Si_3O_{10}]$ in water was found to enhance the diffusive mobility of the encaged $H_2O$ molecules [Moroz et al., 2001]. An increase of self-diffusion in natrolite ultimately leads to a transition to a high-hydrated state [Lee et al., 2002]. The structural analog of natrolite, gonnardite, is characterized by a partly Si,Al-disordered framework and partly occupied $H_2O$ sites in the channels. In contrast to natrolite, the self-diffusion of $H_2O$ molecules in gonnardite is high initially. As a result, the transition of gonnardite to the high-hydration phase, paranatrolite, occurs on the increase of the air humidity. Note that in zeolites with high diffusion mobility of $H_2O$ molecules at ambient conditions (for example, heulandite), the compression in water-containing medium produces permanent additional hydration within a large pressure range [Seryotkin, 2015].

The structure of zeolites is usually characterized by the presence of vacancies in the water subsystem, which are populated during compression in a penetrating medium. Hydration, at a minimum, is accompanied by a compressibility decrease of the structure. However, there are exceptions. In those cases where the effect PIH is absent, the self-diffusion of $H_2O$ molecules is "frozen" or very low. So, bikitaite $Li_2(H_2O)_2[Al_2Si_4O_{12}]$ retains the initial $H_2O$ content up to 4 GPa [Seryotkin, 2016]. The absence of PIH effects could be attributed to insufficient diffusion mobility of extraframework species. Like bikitaite, analcime $Na_2(H_2O)_2[Al_2Si_4O_{12}]$ does not experience the pressure-induced hydration during the compression in penetrating medium [Gatta & Lee, 2014]. There is also a certain similarity in the configuration of the extraframework subsystems. Zeolite brewsterite $Sr_{1.30}Ba_{0.66}(H_2O)_{10}[Al_{4.00}Si_{12.00}O_{32}]$ doesn't undergo hydration under pressure [Seryotkin, 2019] due to lack of $H_2O$ vacancies. To compare, in natrolite there are $H_2O$ positions which are vacant at ambient conditions. At that, the $H_2O$ diffusion mobility in natrolite is low, but it increases upon the compression in penetrating medium, obviously through the partial filling of empty sites. In brewsterite structure the formation of such potential sites requires a certain rearrangement of $H_2O$ environment of the cations, which is not realized.

This study was supported by the RFBR (grant 19-05-00800).

Gatta G.D., Lee Y. Mineral. Magazine, 2014, 78, 267–291.

Lee Y., Vogt T., Hriljac J.A., et al. J. Amer. Chem. Soc., 2002, 124, 5466–5475.

Moroz N.K., Kholopov E.V., Belitsky I.A., Fursenko B.A. Micropor. Mesopor. Mater., 2001, 42, 113–119.

Seryotkin Yu.V. Micropor. Mesopor. Mater. 2015, 214, 127–135.

Seryotkin Yu.V. Micropor. Mesopor. Mater., 2016, 226, 415–423.

Seryotkin Yu.V. Micropor. Mesopor. Mater., 2019, 276, 167–172.

**Particular qualities of wollastonite from skarns of Kuparsaari occurrence**

V. Zhdanova[1,*], A. Berezin[1,2]

[1]St. Petersburg State University, 199034 St. Petersburg, Russia
[2]Institute of Precambrian Geology and Geochronology, 199034 St. Petersburg, Russia

*valeriia.zh.rock@gmail.com

An occurrence of wollastonite has been discovered in the Vyborgsky district of the Leningrad Region. This occurrence is associated with skarns of the Kuparsaari carbonate-bearing sequence [Eskola et al., 1919] of the Upper Proterozoic age. This is a unique locality on the territory of the Karelian Isthmus. The Kuparsaari sequence is a stratified unit of marbles and microgneisses, and skarns formed under effect of fluids. The skarns are zonal metasomatic rocks, encompassing layers and lenses with a wollastonite content up to 80%.

Wollastonite may occur in different polytypic modifications. Variations of the mineral structure depend on conditions of formation and chemical composition. Definition of wollastonite internal state is critical for choice of methods of production of its synthetic analogs [Lebedev et al., 2003]. Wollastonite of the Kuparsaari sequence has a triclinic crystal system (Wollastonite-1A). The orderly structure implies a low content of impurities in the mineral. Application of EPMA has showed that deviation from a theoretical composition of the wollastonite molecules is less than 1%. The complex data obtained indicates that the mineral formed in high-temperature zones of the calcareous skarns. This assumption has been confirmed by a detailed study of metasomatic zonality in field and laboratory experiments.

The wollastonite from skarns of the Kuparsaari sequence has a high quality, an ordered structure, and an elongated shape. Such properties make this type of wollastonite an optimal ingredient for protective coatings.

Eskola P., Hackman V., Laitakari A., Willkman W.W. Geotenillisiä Tiedonantoja. Helsinki, 1919.

Lebedev G.A., Inina I.S., Belashev B. Z. The composition and structure of the synthetic wollastonites on the basis of mineral raw materials of Karelia. In: Geological and technological research of industrial minerals Fennoscandia. Ed. Kabanova L. Karelian Research Center of Russian Academy of Sciences: Petrozavodsk, 2003, 69–74.

**Crystal-chemical features of glauconite from Karinskoe deposit (South Urals)**

Y.S. Simakova*, V.P. Lyutoev, A.Yu. Lysiuk

Institute of Geology Komi SC UB RAS, 167982 Syktyvkar, Russia

* yssimakova@geo.komisc.ru

Glauconite grains from the Karinskoe deposit were studied using complex of chemical and physical methods: X-ray diffraction, Mössbauer spectroscopy $^{57}Fe$, scanning electron microscopy and microprobe analyses, Fourier-transform infrared spectroscopy. Special attention is given to the crystal-chemical features of mineral and processes of glauconite formation.

Glauconite from the Karinskoe deposit is characterized by a relatively high content of K, Fe, Mg ($K_2O$ – 4.60–8.69; $Fe_2O_{3tot}$ – 14.67–21.74; MgO – 4.07–6.27, CaO –0.37–1.26; $Al_2O_3$ – 7.17–13.17; $SiO_2$ – 47.86–59.58 wt.%). Content of total iron and potassium display a direct correlation. According to Mössbauer and IR spectroscopy data, $Fe^{2+}$ occupies about 10% of the total iron content in glauconite. The most intensive absorption bands at the IR spectra are of $Fe^{3+}OHFe^{3+}$, AlOHAl, MgOHMg. According to the Mössbauer data, $Fe^{3+}/\Sigma Fe$ = 0.885 or $Fe^{2+}/Fe^{3+}$ = 0.13 values are corresponded to those calculated from the results of infrared spectroscopy OH-groups. Crystal-chemical composition of mineral show the correlation with the “mature” glauconite, which was formed during the slow “maturing” of glauconite grains with increasing of the mica layers in its structure. X-ray investigation showed that glauconite grains consist of two phases – glauconite and interstratified glauconite/smectite with 10–15% of swelling layers. It can be proposed that smectite was a “precursor” for glauconite formation. XRD pattern corresponds to 1Md mica polytype. Reflection with $d$ = 1.511 Å ($b$ = 9.066 Å) at the 060 region give an evidence of dioctahedral type of mineral structure.

An interesting feature of the glauconite globules of the Karinskoye deposit one can observe at the SEM micrographs – spherical grains (1-3) disseminated on glauconite surface (Figure), differing by a brighter SEM contrast, consisting of randomly oriented lamellas but having a slightly different chemical composition. The content of $SiO_2$ in spherical formations according to microprobe analysis varies from 73.07 to 82.21 wt. %, $Al_2O_3$ – from 6.30 to 7.05 wt. %, $Fe_2O_{3tot}$ – from 4.61 to 8.31 wt. %, $K_2O$ – from 1.27 to 1.91 wt. %, MgO – from 2.11 to 2.46 wt. %. In comparison with glauconite globules, the contents of Fe, Mg, K in spherical grains are significantly lower,whileamount of Si is higher. This mineral presumably corresponds to the illite / smectite phase with a predominance of smectite and a low layer charge.

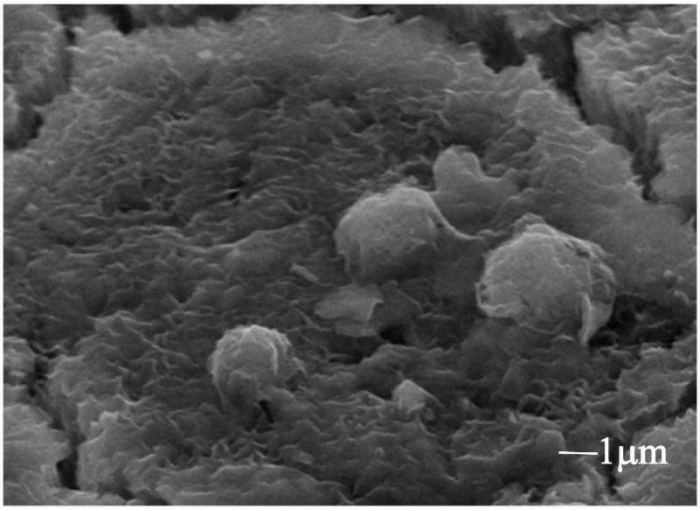

**Thermodynamic conditions of clay minerals formation in the deep horizons of the Earth crust**

L.M. Sitdikova

Kazan Federal University, Institute of Geology and Petroleum Technologies, 420008 Kazan, Russia

sitdikova8432@mail.ru

The problem of the deep structure of the Earth's crust is one of the most current in geology. A comprehensive study of materials of deep and ultra-deep wells allows to identify structural features of deep horizons. Destruction zones were established in the rocks of the crystalline basement (Tatar arch) of the East of the Russian plate [Sitdikova, 2014a,b].The substance of these zones of compound composition is dominated by a complex of clay minerals, which are not characteristic of regional metamorphic rocks (depths above 3500 m). The formation of the substance of the destruction zones is associated with the peculiarities of the geodynamic situation and the post-magmatic evolution of the territory. The elucidation of the formation conditions of clay minerals, their phase composition, typomorphic features, and patterns of distribution in the destruction zones of metamorphic rocks is of great interest.

In the development of destruction zones, staging has been established: compression and decompression types. The composition of newly-formed clay minerals depends on the type of rocks of crystalline basement and is confined to specific material formations. The main minerals of the destruction zones are chlorite, illite, kaolinite, mixed-layer phases such as illite-smectite, smectite-vermiculite, biotite-vermiculite, chlorite-montmorillonite. The variety of clay minerals indicates the complexity of low temperature mineral formation. According to the results, it has been established that clay minerals formed at great depths are characterized by a complex of typomorphic features. Clay minerals are sensitive indicators of the compression and decompression stages of the postmetamorphic processes of rocks of crystalline basement. The leading factor is oriented pressure – stress, which is reflected in the crystal-chemical features of clay minerals.

Chlorites are of polytypical modification IIb, the most stable in the destruction zones. However, according to the results of Mössbauer spectroscopy, three types of chlorites are distinguished: in the compression zones, chlorites are developed with partial colonization of the positions of the brucite layer by the $Fe^{2+}$ ions, along with its occurrence in the position of talc layers. Chlorites with the “standard” distribution of $Fe^{3+}$ ions in octahedral positions, chlorites with the predominant occurrence of $Fe^{3+}$ ions in the cis-position of talc layers and its practical absence in trans positions are typical for zones of rock stress relief (decompression stage) [Sitdikova, 2014b]. In intervals with stress pressure, illites of the $2M_1$ polytype are formed, and in stress relief zones, 1M and 1Md polytypes are spread(depths above 5300 m). The illites of the $2M_1$ polytype are stressful, and illite-1M is anti-stress. With the advent of polytypes 1M and 1Md, the ability to swell the crystal lattice appears. Kaolinite (1TC) in the compression zones has low degree of crystallinity, and in zones of stress relief, the degree of its perfection changes to medium-high. Disordered mixed-layer clay minerals are developed in decompression zones, and ordered types (illite-smectite, chlorite-montmorillonite) are characteristic for compression zones. Clay minerals of the destruction zones have complex of typomorphic features with morphometric and structural-crystal-chemical character. During the geodynamic evolution of the crystalline basement of the Tatar arch, there was a periodic change in the stages of compression and decompression, with the activation of hydrothermal activity and the processes of regressive metamorphism.

Sitdikova L.M. Mechanism of formation of pores and voids in unconventional reservoirs at great depths in the crystalline basement of the East Russian Plate. International Multidisciplinary Scientific GeoConference SGEM, 2014a, 1, 199–206.

Sitdikova L.M. Crystallochemical features of chlorites of the Earth crust deep horizons. International Multidisciplinary Scientific GeoConference SGEM, 2014b, 1, 43–50.

**Crystal chemistry of lintisite, AM-4 and their protonated form, SL3**

Galina O. Kalashnikova[1], Taras L. Panikorovsky[1], Elena S. Zhitova[2], Ekaterina A. Selivanova[1], Yakov A. Pakhomovsky[1], Sergey V. Krivovichev[1,2]

[1]Kola Science Centre of the Russian Academy of Sciences, 184209 Apatity, Russia
[2]Institute of Earth Sciences, St. Petersburg State University, 199034 St. Petersburg, Russia

* galka27_89@mail.ru

Over few recent years, more and more studies have appeared on the synthesis of new inorganic microporous and mesoporous cation-exchangers that perform well in a corrosive media. Our research interests have been concentrated on the study of unusual single-crystal-to-single-crystal transformation of natural framework titanosilicates of the lintisite family [Yakovenchuk et al., 2012] and their synthetic counterpartAM-4 [Dadachov et al., 1997]. The transformation occurs in any acidic solution. Protonation of the above-mentioned compounds results in the formation of layered titanosilicates K3 (after kukisvumite), L3 (after lintisite) and SL3 (after AM-4). All these compounds have the same composition, $Ti_2Si_4O_{10}(OH)_4$, and the similar structure motifs. The structural differences between K3 and L3 (SL3) are similar to those observed between kukisvumite and lintisite (Figure).

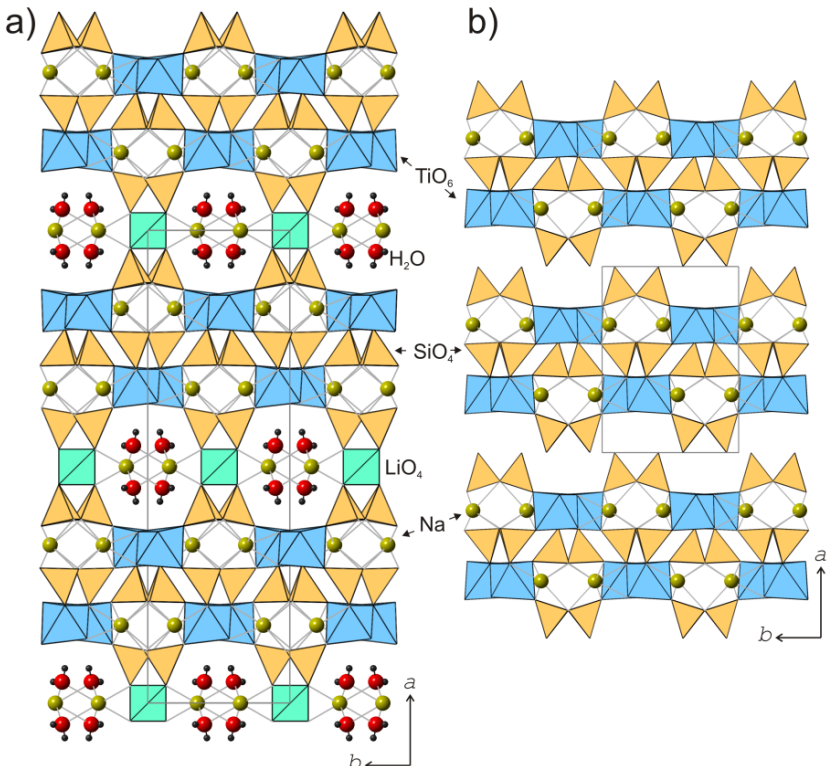


Figure. The crystal structures of lintisite (a) and L3 (b).

The perspectives of practical use of SL3 include (photo)catalysis, selective sorption of 1-2-valent cations, purification of radioactive wastes and energy storage. In particular, this material can be used for the catalytic synthesis of 1,5-benzodiazepine from 1,2-phenylenediamine and acetone [Timofeeva et al., 2019], selective removal of iodine from water solutions [Kalashnikova et al., 2015], cleaning of industrial electrolytes from noble metals, and production of self-cleaning building materials [Tyukavkina et al., 2019].

The research was funded by KSC RAS (0226-2019-0009) and the Russian Foundation for Fundamental Researches (18-29-12039).

Dadachov M. S., Rocha J., Ferreira A., et al. *Ab initio* structure determination of layered sodium titanium silicate containing edge-sharing titanate chains (AM-4) $Na_3(Na,H)Ti_2O_2[Si_2O_6]_2 \cdot 2H_2O$. Chem. Commun, 1997, 2371–2372.

Patent 2567314 RUC01G 23/00, C01B 33/20 (2006.01). Method for producing crystalline titanosilicate / Kalashnikova G.O., Nikolaev A.I., Gerasimova L.G., et al.; Institute of Chemistry and Technology of Rare Elements and Mineral Raw Materials of Kola Science Centre of the Russian Academy of Sciences, Kola Science Centre of the Russian Academy of Sciences. – 2014114241/05; application 10.04.2014; date of publication 10.11.2015, Bull. № 31.

Timofeeva M.N., KurchenkoYu.V., KalashnikovaG.O., et al. AM-4 a layered sodium titanium silicate containing edge-sharing titanatechains as novel material with tunable properties for catalysis. Journal of Catalysis, 2019 (in press).

Tyukavkina V.V., Gerasimova L.G., Tsyryatyeva A.V. Synthetic titanosilicate additives for special cement composites. Perspective materials, 2019, 4, 40–48.

Yakovenchuk V.N., Krivovichev S.V., Pakhomovsky Ya.A., et al. Microporous titanosilicates of the lintisite-kukisvumite group and their transformation in acidic solutions. Minerals as Advanced Materials II (Ed. S.V.Krivovichev). Springer-Verlag, Berlin-Heidelberg, 2012, 229–238.

**Structural and morphological features of kaolinite of the weathering crust according to X-ray diffraction and electron paramagnetic resonance**

Elena U. Sidorova, Lyalya M. Sitdikova, Nailia M. Khasanova, Victor G. Izotov

Kazan Federal University, Institute of Geology and Petroleum Technologies, 420008 Kazan, Russia

lena353@list.ru

The weathering crust develops on to the rocks of the crystalline basement within the North-Tatar and South-Tatar arch (Volga-Ural region) and lies at great depths under sedimentary cover deposits. They are characterized by the development of several types of weathering profiles and a variety of mineralogical and geochemical composition [Sidorova et al., 2015]. Areal type of weathering crust with zonal structure of the profile is most developed within the region. The rocks of the crystalline basement are represented by metamorphic (gneisses, amphibolites, crystalline schists, etc.) and magmatic (gabbro-diabase, gabbro-norite, etc.) species. Features of the mineral composition of the rocks largely determine the formation of various associations of hypergene minerals, and first of all, clay minerals.

According to X-ray analysis, the clay component of the weathering crust is presented in various combinations and ratios by chlorite, illite, illite-smectite and kaolinite. In the majority of studied weathering profiles, kaolinite predominates in the composition of clay mineral associations. Kaolinite is the final product of the evolution of the clay component in the process of weathering and composes the most modified upper zones of the profile. The degree of perfection of the crystal structure of kaolinite varies greatly and depends on the level of change of the initial rocks by weathering processes. This indicator was estimated by several parameters – indices: HI [Hinckley, 1963], IK [Stoch, 1974], AGFI [Aparicio, Galan, 1999] and others, which are calculated according to X-ray data. The "crystallinity" of kaolinite increases from the lower to the upper zones of the weathering profile. All studied kaolinites formed an ordered complex after the process of saturation with dimethyl sulfoxide. This is evidenced by the presence of integer basal reflexes of the initial kaolinite and its complex with dimethyl sulfoxide, the kinetics of complex formation varies for different kaolinites.

The features of kaolinites were studied by electron paramagnetic resonance (EPR) spectra, which, as expected, were different for kaolinites from different zones of the weathering profile. The kaolinites are characterized by the presence of two groups of signals – narrow lines with $g \approx 2.0$ (signal A) and a triplet of wide lines in the region $g \approx 4.3$ (signal B). For kaolinite with a high degree of crystalline perfection, the central signal of the triple B must be weaker relative to the sidelines, with increasing intensity of signal A [Bortnikov et al., 2010]. In general, the data on the EPR spectra confirm that kaolinite with the best structural and morphological parameters is characteristic for rocks of the highest degree of weathering.

Aparicio P., Galan E. Mineralogical interference on kaolinite crystallinity index measurements. Clays and Clay Minerals, 1999, 47, 1227.

Bortnikov N.S., Mineeva R.M., Savko A.D., Novikov V.M., Kraynov A.V., Berketta A.G., Speransky A.V. The history of kaolinite in the weathering crust and related clay deposits according to EPR data. Dokl. Akad. Sci., 2010, 433(2), 227–230.

Hinckley D. Variability in "crystallinity" values among the kaolin deposits of the Coastal Plain of Georgia and South Carolina. Proceedings of the 11th International Conference on Clays and Clay Minerals, 1963, 229–235.

Sidorova E., Sitdikova L., Izotov V. The major types of the weathering crust of the Eastern Russian plate and its mineralogical and geochemical features. Procedia Earth and Planetary Science, 2015, 15, 573–578.

Stoch L. Mineraly Ilaste (“Clay Minerals”). Geological Publishers, 1974, 186–193.

**Al-rich K-dioctahedral 2$M_1$ micas: structural factors affecting the crystal-chemical variability**

Bella B. Zviagina[1,*], Victor A. Drits[1], Olga V. Dorzhieva[1,2]

[1]Geological Institute RAS, 119017 Moscow, Russia
[2] Institute of Ore Deposits, Petrography, Mineralogy, and Geochemistry RAS, 119017 Moscow, Russia

*zbella2001@yahoo.com

To reveal factors that determine the different ranges of compositional variations in high- and low-temperature Al-rich K-dioctahedral micas, relationships between structural parameters and cation composition were analyzed for two sets of data: (1) structure models of synthetic 2$M_1$micas in the series muscovite-phengite-aluminoceladonite and (2) Al-rich, K-dioctahedral 2$M_1$ micas with refined structures. The dependences of the unit-cell parameters on cation composition and the variations in tetrahedral and octahedral lateral dimensions and sheet thicknesses, interlayer distances, and tetrahedral rotation angles were analyzed and compared with those found previously for the series 1*M*illite – 1*M* aluminoceladonite.

The similarities in the variations of unit-cell parameters with cation composition observed in 2$M_1$ and 1*M* natural and synthetic K-dioctahedral micas imply that these variations should be controlled by similar, albeit not identical, structural factors. These factors, which are related to the ability of tetrahedral and octahedral sheets having different lateral dimensions to form a layer with uniform two-dimensional periodicity, are realized in a different manner in micas formed under different *P* and *T* conditions.

Extremely high temperatures and pressures in a closed system under laboratory conditions allow structural readjustment of the differently sized tetrahedral and octahedral sheets for a wide range of cation compositions (from muscovite to aluminoceladonite through phengite). In nature, under the conditions of metamorphism, the temperatures and pressures are not high enough to enable this readjustment for the formation of micas having aluminoceladonite-like compositions, which, in particular, would require reduction of the *a* and *b* parameters to ensure higher tetrahedral rotation.

Unlike muscovites and phengites, micas in the illite-aluminoceladonites series are formed under low-temperature and low-pressure non-equilibrium conditions in systems with highly heterogeneous compositions. This suggests that along with the structure, other factors would have a significant effect on the occurrence of 1*M* aluminoceladonite. At the same time, the readjustment of the lateral dimensions of tetrahedral and octahedral sheets in 1*M* K-dioctahedral micas may be facilitated by the more heterogeneous composition of the environment leading to a wide range of cation compositions. Additional factors that could favor the occurrence of the 1*M* aluminoceladonite structure as compared to the 2$M_1$ polytype could be the relatively longer O-O distances across the interlayer and the relatively higher interlayer distance values.

**The X-ray determination of natural phlogopite monocrystals thermostability**

G.A. Kuznetsova, V.M. Kalikhman

Irkutsk State University, 664003 Irkutsk, Russia

kuznetsova46@mail.ru; decanat@phesdep.isu.ru

The X-ray investigation thermal changes of natural phlogopite monocrystals with micro admixtures are produced. It is established that the presence of micro admixtures exerts the essential influence on half-wide basal diffraction reflections character of changes under the heating to the temperature of high- temperature phase transition.

The thermal changes in the structure of single crystals of natural phlogopites of several Russian fields were conducted by method of high-temperature X-ray diffraction (DRON-2.0, UVD-2000 chamber). It is observed, that phlogopites contain admixtures of various layered silicates, where concentration of additions is individual for each sample [Kuznetsova et al., 2013].

The experimental results $\left|\ln\sin\theta\right| = f\left(T\right)$ and reflection of half-widths $B = f\left(T\right)$ for several phlogopites are presented in Figure (line *a*).

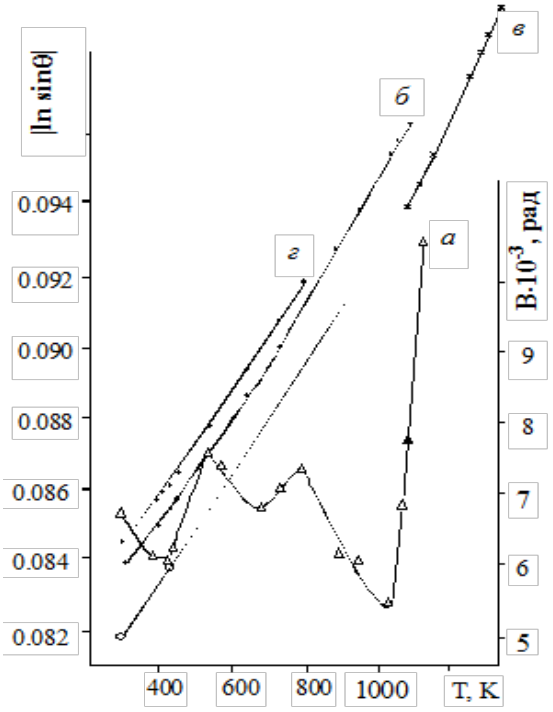


It has been established that in the temperature range preceding the restructuring of the mica packet of phlogopite crystals, the basal interplanar distances (function $\left|\ln\sin\theta\right|$) changed almost linearly with increasing of temperature. A non-monotonic changes of half-width reflections $B = f\left(T\right)$ occurred in the temperature range of the existence of an admixture (Figure, line *a*). Observed, that above the temperature of destruction of the structure of the admixture phase (Fig. 1*г*), the dependence is almost linear.

For most phlogopites one or two effects of increasing of B at temperatures of 350-450 K, 600-650 K, 750-850 K is observed. For all studied phlogopites, the temperature ranges of changing B corresponded to the above-mentioned ones. We can make the conclusion that the nature of the processes occurring during heating only in limited range of temperatures.

Kuznetsova G.A., Liopo V.A., Struk A.V., Feoktistova L.P. Mineral inclusions of varied thermostable phlogopites. Vesnik Hrodneskaha Dziarzhaunaha Universiteta Imia Ianki Kupaly. Seryia 6. Tekhnica. 2013, 2(154), 24–30.x

**Silica minerals from the Arsenatnaya fumarole, Tolbachik volcano (Kamchatka, Russia)**

Fedor D. Sandalov[1,*], Nadezhda V. Shchipalkina[1], Igor V. Pekov[1], Natalya N. Koshlyakova[1], Evgeny G. Sidorov[2]

[1]Faculty of Geology, Lomonosov Moscow State University, 119991 Moscow, Russia
[2]Institute of Volcanology and Seismology, Far Eastern Branch of the Russian Academy of Sciences, 683006 Petropavlovsk-Kamchatsky, Russia

* fyodor.sandalov@yandex.ru

The crystalline silica ($SiO_2$) polymorphs and X-ray amorphous opal are common in products of basaltic, andesitic and rhyolitic volcanism. In particular, these minerals occur in fumaroles of many active volcanoes [Balić-Žunić et al., 2016]. Three minerals of silica – tridymite, cristobalite and opal were identified by us in the Arsenatnaya fumarole located at the summit of the Second scoria cone of the Northern Breakthrough of the Great Tolbachik Fissure Eruption, Tolbachik volcano (Kamchatka, Russia). This fumarole is described in [Pekov et al., 2018]. Opal forms abundant crusts at the surface part of the Arsenatnaya fumarolic system being a product of basalt alteration under the influence of both fumarolic gas and atmospheric agents. Tridymiteis found in the polymineralic zone of Arsenatnaya with sanidine, pseudobrookite, cassiterite, and litidionite. Tridymite forms pseudo-hexagonal interpenetration twins, lamellar or acicular crystals and its intergrowths up to 0.1 mm. Cristobalite is associated in the same zone with hematite, johillerite, sylvite, tilasite, badalovite, and fluorophologopite and forms spherulites, botryoidal crusts, cavernous aggregates and, rarely, platy crystals. In polished section, its aggregates show characteristic 'fish-scale' cracks, which results from a 5% decrease in volume from the displacive transition from β- to α-cristobalite during cooling through *ca*. 240 °C [Carpenter et al., 1998]. Presumably, tridymite was formed as a result of gas-rock interaction. Cristobalite was presumably formed by direct deposition from hot gas, as volcanic sublimate, that is in accordance with the literature data [Baxter, 1999; Getahun et al., 1996]. Parameters of tetragonal unit cell of cristobalite from Arsenatnaya are: $a$ = 4.980(1), $c$ = 6.9526(1) Å, $V$ = 172.4(1) Å$^3$. Parameters of monoclinic unit cell of tridymite are: $a$ = 18.553(5), $b$ = 5.030(3), $c$ = 23.889(5)Å, β = 105.64(3)$^o$, $V$ = 2146.7(14) Å$^3$.

This work was supported by the Russian Science Foundation, grant no. 19-17-00050.

Balić-Žunić T., Garavelli A., Jakobsson S.P., Jonasson K., Katerinopoulos A., Kyriakopoulos K., Acquafredda P. Fumarolic minerals: an overview of active European volcanoes. In K. Nemeth (Ed.), Updates in Volcanology - From Volcano Modelling to Volcano Geology, 2016, 267–322.

Baxter P.J., Bonadonna C., Dupree R., Hards V.L., Kohn S.C., Murphy M.D., Nichols A., Nicholson R.A., Norton G., Searl A., Sparks R.S.J., Vickers B.P. Cristobalite in volcanic ash of the Soufriere Hills volcano, Montserrat, British West Indies. Science, 1999, 283, 1142–1145.

Carpenter M.A., Salje E.K.H., Graeme-Barber A. Spontaneous strain as a determinant of thermodynamic properties for phase transitions in minerals. Eur. J. Mineral, 1998, 10, 621–691.

Getahun A., Reed M.H., Symonds R. Mount St. Augustine volcano fumarole wall rock alteration: Mineralogy, zoning, composition and numerical models of its formation process. J. Volcanology and Geothermal Research, 1996, 7371(2-4),–107.

Pekov I.V., Koshlyakova N.N., Zubkova N.V., Lykova I.S., Britvin S.N., Yapaskurt V.O., Agakhanov A.A., Shchipalkina N.V., Turchkova A.G., Sidorov E.G. Fumarolic arsenates – a special type of arsenic mineralization. Eur. J. Mineral., 2018, 30(2), 305–322.

# 4.2. Tourmalines

## Relationships within the tourmaline supergroup and proposed *PT* conditions for a B-rich tourmaline endmember as well as for Li-rich tourmalines

Andreas Ertl *

Institut für Mineralogie und Kristallographie, Geozentrum, University of Vienna, 1090 Wien, Austria

* andreas.ertl@a1.net

The tourmaline supergroup is one of the mineral groups in which almost every element can occupy one or more crystallographic sites, because the tourmaline structure is very flexible. It would be very interesting to synthesize a B-rich tourmaline endmember with the formula $NaAl_3Al_6(BO_3)_3[Si_3B_3O_{18}](OH)_4$ and with lattice parameters of $a$ = 15.5, $c$ = 7.0 Å [Ertl et al., 2018]. But at which pressure-temperature (*PT*) conditions could such a tourmaline crystallize? By using a compiled data set from synthetic samples produced in the past and some more recent data from single-crystal structure refinements of B-rich tourmalines the *PT* conditions can be extrapolated [Ertl et al., 2008, 2012].Even with 100 % excess $B_2O_3$ in the starting material, the estimated $^{[4]}$B content in the synthetic tourmalines does not exceed certain values at given *PT* conditions. By using all these datasets, the exact *PT* conditions for synthesizing the B-rich tourmaline end member can be proposed for the first time with 1000 MPa/300 °C and also with 2000 MPa/350 °C.

Tourmaline samples of different compositions, which crystallized at similar *PT* conditions, show a strong positive linear correlation between the *X*-site charge and the fluorine content. This could be proven on tourmalines from different localities [e.g., Ertl et al., 2010]. Tourmalines, which contain mainly Al and Li at the *Y* site and which crystallized at similar *PT* conditions, show also a strong positive linear correlation between the *X*-site charge and the <*Y*-O> distance. Because the effective ionic radius of $Li^{1+}$ is significantly greater than $Al^{3+}$, the <*Y*-O> distances increases with an increasing Li content (elbaitic component). To the contrary, tourmalines with an increasing $^{[4]}$B content always show an increasing olenitic component ($^{Y}$Al content) and a decreasing <*Y*-O> distance. Therefore, a tourmaline cannot be Li- and $^{[4]}$B-rich simultaneously. Either it is $^{[4]}$B-rich or it is Li-rich. To synthesize Li-rich tourmaline the amount of $^{[4]}$B should hence be≤0.2 apfu, similar to natural elbaites [Ertl et al., 2010]. By using the correlations mentioned in the above section elbaites could therefore theoretically be synthesized either at *PT* conditions of 150 MPa/300 °C, 200 MPa/400 °C, or 250 MPa/500–700 °C. Because of the positive correlation between the *X*-site charge, the F content and the <*Y*-O> distance, it can be proposed, that the F content, the *X*-site occupancy and the Li content are strongly related to each other. It could also be helpful to add some Ca to the tourmaline starting material, to increase the *X*-site charge further, because Ca has the charge 2+ compared to $Na^{1+}$. I strongly invite scientific groups, which are interested in elbaitic tourmaline, to do syntheses at the proposed *PT* conditions, and to add also F (and maybe some Ca) to the starting material.

Ertl A., Giester G., Ludwig T., Meyer H.-P., Rossman G.R. Synthetic B-rich olenite: Correlations of single-crystal structural data. Am. Mineral., 2012, 97, 1591–1597.

Ertl A., Henry D., Tillmanns, E. Tetrahedral substitutions in tourmaline: A review. Eur. J. Mineral., 2018, 30, 465–470.

Ertl A., Rossman G.R., Hughes J.M., London D., Wang Y., O'Leary J.A., Dyar M.D., Prowatke S., Ludwig T., Tillmanns E. Tourmaline of the elbaite-schorl series from the Himalaya Mine, Mesa Grande, California, U.S.A.: A detailed investigation. Am. Mineral., 2010, 95, 24–40.

Ertl A., Tillmanns E., Ntaflos T., Francis C., Giester G., Körner W., Hughes J.M., Lengauer C., Prem M. Tetrahedrally coordinated boron in Al-rich tourmaline and its relationship to the pressure–temperature conditions of formation. Eur. J. Mineral., 2008, 20, 881–888

**Raman Spectra of Synthetic Ga-rich, Ge-bearing Tourmaline Crystals**

Elena Yu. Borovikova[1,*], Valentina A. Nesterova[1,2], Tatiana V. Setkova[2], Dmitry Yu. Pushcharovsky[1], Vladimir S. Balitsky[2], Pavel S. Kvas[1,2] and Sofia A. Tetroeva[1]

[1] Department of Geology, Lomonosov Moscow State University, 19234, Russia
[2] D.S. Korzhinskii Institute of Experimental Mineralogy of Russian Academy of Sciences, 142432 Chernogolovka, Russia

* alena.amurr@gmail.com

The synthesis of Ga- and Ge-substituted tourmaline is of particular interest both from the point of view of modeling changes of the mineral structure at high pressure, and with the aim of improving the pyro- and piezoelectric properties. The crystalline growth of Ga-rich, Ge-bearing tourmaline on natural elbaite seed was obtained in boric hydrothermal solutions at temperature of 600-650° C and pressure of 100 MPa using chromium–nickel alloy autoclaves. Single crystals of quartz and corundum with addition of gallium and germanium oxide were used as charge material. The autoclave was filled with solution in accordance to autoclave-filling factor, then sealed, and placed into electric furnace with two-section heaters. The duration of the runs was 14 days. The thickness of newly formed tourmaline layer was up to 100 μm in pinacoid direction.

Synthesized Ga-rich, Ge-bearing tourmaline was characterized by electron microprobe analysis (EMPA) and Raman spectroscopy. EMPA revealed the presence and uniform distribution of Ga (20.7 wt% $Ga_2O_3$), Ge (1.6 wt% $GeO_2$), Fe (9.5 wt% FeO), Na (1.6 wt% $Na_2O$), lowered Si (27.7 wt% $SiO_2$) and Al (21.6 wt% $Al_2O_3$) content. Previous investigation of Ga-rich tourmaline revealed the significant content of $Ga^{3+}$, $Fe^{3+}$, $Fe^{2+}$ ions in both Y and Z sites [Vereshchagin et al, 2016].

Polarized Raman spectra were obtained using a JY Horiba XPloRA microscope (Department of Petrology, Moscow State University) in two back-scattering geometries $\overline{y}(zz)y$ ($A_1$(TO)) and $\overline{y}(xx)y$ ($A_1$(TO), $E$(LO)). In the spectra of Ga-rich, Ge-bearing tourmalines, a shift of most bands to lower frequencies from 6 to 27 $cm^{-1}$ was observed compared with the spectra of elbaite seed. It can be explained by the mass effect at the substitution of Al ions by heavier and larger Ga and Fe in the octahedral Y and Z sites, and the replacement of part of Si by Al and Ge in the T sites.

Raman spectra in OH stretching region contain three bands. In high frequency region of spectra corresponding to $^{W}$OH stretching vibrations there is only one band at 3628 $cm^{-1}$. Low intensity of this band indicates a minor content of OH groups in this structural position. The absence of band splitting and the great width reveal the strong disordering of different cations in neighboring Y and X sites. We assigned this band to $^{W}$OH stretching vibration with $^{3Y}$(Ga, Fe, Al) + $^{X}$(□,Na) cations in neighboring positions. The $^{V}$OH ions are surrounded of three YZZ octahedral triplets. The wide intensive band at 3511 $cm^{-1}$ results from overlapping peaks related to a large set of different local arrangements around the $^{V}$OH group, caused by complex cation content ($Ga^{3+}$, $Fe^{3+}$, $Al^{3+}$) both in Y and Z sites. The appearance of additional band at 3565 $cm^{-1}$ probably related to partly occupation of Z site by $Fe^{2+}$ ions according to inverse correlation of the mode wavenumber with the sum of the charges of octahedral cations, which coordinate the OH group [Watenphul et al, 2016].

Vereshchagin O., Setkova T. Rozhdestvenskaya I., Frank-Kamenetskaya O., Deyneko D., Pokholok K. Synthesis and crystal structure of Ga-rich, Fe-bearing tourmaline. European Journal of Mineralogy, 2016, 28(3), 593–599.

Watenphul A., Burgdorf M., Schlüter J., Horn J., Malcherek T., Mihailova B. Exploring the potential of Raman spectroscopy for crystallochemical analyses of complex hydrous silicates: II. Tourmalines. American Mineralogist, 2016, 101, 970–985.

**Short-range order in Li-Al-tourmalines: a bond-valence theory, IR-spectroscopy and X-Ray single crystal diffraction analysis approach**

Yuliya M. Bronzova[1,*], Olga V. Frank-Kamenetskaya[1], Miriam S. Babushkina[2], Oleg S. Vereshchagin[1], Ira V. Rozhdestvenskaya[1], Anatoly A. Zolotarev[1]

[1]Saint Petersburg State University, 199034 St. Petersburg, Russia
[2]Institute of Precambrian Geology and Geochronology of Russian Academy of Sciences, St. 199034 St. Petersburg, Russia

* y.bronzova@spbu.ru

The tourmaline-super-group minerals are complex borosilicates, which occur in a wide variety of rocks. The general formula of tourmaline may be given as follows: $X^{IX}Y_3{}^{VI}Z_6{}^{VI}[T_6{}^{IV}O_{18}][B^{III}O_3]_3V_3W$,*X*– $Na^+$, $Ca^{2+}$; *Y*– $Li^+$, $Al^{3+}$ etc.; *Z* – $Al^{3+}$ etc.; *T* –$Si^{4+}$, $Al^{3+}$; B – $B^{3+}$; *V*– $OH^-$, $O^{2-}$; *W* – $OH^-$, $F^-$, $O^{2-}$. The information about short-range order in tourmaline structure can improve understanding of the effect of elemental composition on stability of these minerals. The short-range order in Li-Al – ($OH^-$, $F^-$) tourmalines with $[Li/Al]^Y \approx 1$ and different $Na^+/Ca^{2+}$ ratio was investigated by means of both bond-valence theory arguments [Hawthorne, 2002] and experimental IR spectroscopic data combined with the results of X-ray single diffraction analysis [Rozhdestvenskaya et.al., 2005; Shtukenberg et al., 2007]. The stability of the arrangements coordinating *W* and *V* crystallographic sites occupied by $OH^-$, $F^-$ and $O^{2-}$ ions was refined. A unified model of assignment of absorption bands in the IR spectra to the local arrangements (clusters) was suggested taking into the account the first and the second coordination spheres. Types of local cation arrangements around the *W* and *V* anion sites, alongside with clusters' ratio and distribution, were brought out.

As follows from the estimated stability of the coordinated arrangements and IR- spectral analysis results the *W* site surrounding in the studied Li-Al- tourmalines is presented with 3*Y* - *W* clusters: $(LiAlAl)^Y$ - $(OH^-)^W$, $(LiLiAl)^Y$ - $(OH^-)^W$, $(LiAlAl)^Y$ - $(F^-)^W$, $(LiLiAl)^Y$ - $(F^-)^W$. Since the *W* site in tourmaline is splitted due to the tendency of $F^-$ and $OH^-$ anions to be in order, the 3*Y*- $(OH^-)^W$ clusters are distributed in order relative to 3*Y* - $(F^-)^W$ clusters. Therefore, it is possible to state the presence of two coordination arrangements in the structure of tourmaline distributed by order, in each of which the ratio between $(LiLiAl)^Y$ – *W* and $(LiAlAl)^Y$ - *W* clusters is statistically constant. The *V*- site surrounding is represented in Li-Al-tourmalines by clusters (*Y* + 2*Z*) – $(OH^-)^V$: $Li^YAl^ZAl^Z$- $(OH^-)^V$and $Al^YAl^ZAl^Z$ - $(OH^-)^V$. Considering the second coordination sphere is composed of ($Na^+$, $Ca^{2+}$) ions and vacancies occupying the *X* – site, we can confirm the presence of larger clusters in the studied Li-Al – tourmalines: $(LiLiAl)^Y$ – $(OH^-)^W$ - □, ($Li^YAl^ZAl^Z$) – $(OH^-)^V$ – $Na^+$, ($Li^YAl^ZAl^Z$) – $(OH^-)^V$ – $Ca^{2+}$.The complex of the acquired experimental and calculated data confirms the idea expressed by Skogby [Skogby et.al., 2012] that arrangements of various sizes around the *W* (O1) and *V* (O3) sites in the tourmaline structure are not randomly distributed. The short-range order observed in the studied Li-Al tourmaline is controlled not only by the theory of valence bonds, but also by the long-range order (occupations of crystallographic sites).

Hawthorne F. Bond-valence constraints on the chemical composition of tourmaline. Can. Mineral., 2002, 40, 789–797.

Rozhdestvenskaya I., Frank-Kamenetskaya O., Zolotarev A., Bronzova Yu., Bannova I. Refinement of the crystal structures of three fluorine-bearing elbaites. Crystall. Rep., 2005, 50, 907–913.

Shtukenberg A., Rozhdestvenskaya I., Frank-Kamenetskaya O., Bronzova J., Euler H., Kirfel A., Bannova I., and Zolotarev A. Symmetry and crystal structure of biaxial elbaite-liddicoatite tourmaline from the Transbaikalia region, Russia. Am. Mineral., 2007, 92, 675–686.

Skogby H., Bosi F., and Lazor P. Short-range order in tourmaline: a vibrational spectroscopic approach to elbaite. P. C. Min., 2012, 39, 811–816.

**Thermal behavior and properties of synthetic Ni-bearing tourmaline**

Irina A. Chernyshova[1,*], Oleg S. Vereshchagin[1], Olga V. Frank-Kamenetskaya[1], Andrey A. Zolotarev[1], Maria G. Krzhizhanovskaya[1], Olga V. Malyshkina[2]

[1]Saint-Petersburg State University, 199034 St. Petersburg, Russia,
[2]Tver State University, 170100 Tver, Russia

*i.a.chernyshova@yandex.ru

Tourmaline is the most widespread boratosilicate with the general formula $XY_3Z_6T_6O_{18}(BO_3)_3V_3W$, where $X$ = $Na^+$,$Ca^{2+}$, □ (= vacancy), etc.; $Y$ = $Al^{3+}$, $Mg^{2+}$, etc.; $Z$= $Al^{3+}$, $Fe^{3+}$, etc.; $T$ = $Si^{4+}$, $Al^{3+}$, $B^{3+}$; $V$ =$OH^1$, $O^{2-}$; $W$ = $OH^{1-}$, $F^{1-}$, $O^{2-}$. Due to their unique electric properties, tourmalines are used in various scientific areas and technology.

The impact of the chemical composition on the pyroelectric properties [Hawkins et al., 1995; Zhou et al., 2018] and thermal expansion [Filatov et al., 1987] of tourmalines has not been fully explored. Besides, the results of pyroelectric measurements performed by different techniques bear little relevance with each other. The present research has a methodological focus and devote to the study of thermal behavior and properties of Ni-bearing synthetic tourmaline (ratio Ni/Al=0.38), synthesized by hydrothermal method [Lebedev et al., 1998]. This tourmaline was chosen due to the simple composition and homogeneity. The tourmaline crystal structure was refined by single-crystal X-ray diffraction at 100, 290 and 390 K. The intrinsic electric dipole moments ($P_c$) and the pyroelectric coefficients ($\gamma_{st.}$) were calculated using single crystal X-ray data. Pyroelectric coefficient was also obtained by dynamic method ($\gamma_{dyn.}$) at room temperature [Golovnin et al., 2013]. The thermal expansion of the sample (30–930°C) was measured using single crystal and powder X-ray diffraction data.

As the temperature increases, the unit cell parameters grow: from 100 to 290 °K slower than from 290 to 390 °K (Table). The most significant bond lengths vary in $XO_9$-polyhedra. The contribution of a single polyhedra to the electric dipole moment ranked as follows: $X>T>Y>Z\sim B$, but the main contribution to electric dipole moment of the unit cell belongs to $TO_4$-tetraedra, consisted well with the previous studies [Zhou et al. 2018].

Table. Crystal chemical characteristics and properties of Ni-bearing tourmaline

| $T$,°K | $a$, Å | $c$, Å | $X$-$O_{av}$ | $P_c$,$10^{-30}$Cm | $\gamma_{st.}$,$10^{-6}$C/m$^2$K | $\gamma_{dyn.}$,$10^{-6}$C/m$^2$K | $\alpha_a*10^{-6}$ | $\alpha_c*10^{-6}$ |
|---|---|---|---|---|---|---|---|---|
| 100 | 15.868(1) | 7.159(1) | 2.683 | 4.82 | $3.06_{100\text{-}290}$ $2.72_{290\text{-}390}$ | 2.9-3.0 | $1.0_{100\text{-}290}$ $5.5_{290\text{-}900}$ | $7.5_{100\text{-}290}$ $10.4_{290\text{-}900}$ |
| 290 | 15.872(1) | 7.169(1) | 2.685 | 3.94 | | | | |
| 390 | 15.880(1) | 7.176(1) | 2.691 | 3.53 | | | | |

The value of pyroelectric coefficients, received using X-ray data is in agreement with pyroelectric coefficient, obtained by the dynamic method and is close to the values of γ tourmalines with similar amount of $Me^{2+}$(γ=2.5-2.8) [Hawkins et al. 1995]. Thermal expansion coefficients along $c$ axis are higher than along $a$ axis and are in a good agreement with the previous investigations [Filatov et al., 1987]. From 100 to 290 °K thermal expansion is smaller than from 290 to 900°K.

The next goal of the research is to compare the thermal behavior of physical properties in tourmalines with various chemical composition and distribution of cations on crystallographic positions.

The research was supported by President of Russian Federation grant for leading scientfic schools №3.10.75.2018 and performed using the equipment of the SPbU Resource center «X-ray Diffraction Methods».

Filatov S.K et al. Inorg. Mater., 1987, 23(4), 594599.
Golovnin V.A. et al. Principal physics, research methods... Technosphera, 2013, 271.
Hawkins K. et al. Amer. Miner., 1995, 80, 491–501.
Lebedev A.S. et al. Synth. and prop. of tourm… Mat. on Gen. and Exp. Min., Cryst. Growth and Properties, 1998, 58–75.
Zhou et al. J. Alloys Compds., 2018, 744, 328–336.

**High-pressure structure evolution of maruyamaite (K-tourmaline) from diamondiferous gneisses of the Kokchetav massif: the role of K**

Anna Yu. Likhacheva[1,*], Sergey V. Rashchenko[1,2], Kira A. Musiyachenko[1], Andrey V. Korsakov[1], Ines E. Collings[3], and Michael Hanfland[3]

[1] V.S. Sobolev Institute of Geology and Mineralogy SibB RAS, 630090 Novosibirsk, Russia
[2] Novosibirsk State University, 630090 Novosibirsk, Russia
[3] European Synchrotron Radiation Facility, 38000 Grenoble, France

* alih@igm.nsc.ru

Maruyamaite, the K-oxydravite containing K > Na+Ca, has been found in ultrahigh-pressure (UHP) diamondiferous gneisses of the Kokchetav Massif (northern Kazakhstan) [Shimizu, Ogasawara, 2005]. This mineral is likely to form at UHP conditions in the stability field of diamond [Ota et al., 2008] and thereby stimulates the studies of its structural behavior under pressure. The large *X*-site, hosting alkali and alkali-earth cations, is the most compressible unit in tourmaline structure [O'Bannon et al., 2018]. Though it is found to have a secondary influence on tourmaline elasticity [Berryman et al., 2018], the role of different cations remains not well understood. The aim of the present study is to examine how the replacement Na→K in dravitic tourmaline influences its structural behavior at high pressure, with a particular attention to stabilizing function of a large $K^+$ cation. We report the results of single-crystal diffraction study of maruyamaite at high pressure up to 20 GPa.

No sharp distinction with the structural behavior of dravite is revealed, regarding the compression anisotropy and the evolution of the main structure parameters. A slightly higher bulk modulus of maruyamaite (115.6(9) GPa) is mainly caused by the presence of Al in octahedral site *Y*. However, a minor change in the rigidity of local contacts of the *X* site with $T_6O_{18}$ ring, due to the presence of K, is apparently critical for the stabilization of maruyamaite structure. This is evinced by the absence of the phase transition $R3m \rightarrow R3$ observed in dravite near 15.4 GPa [O'Bannon et al., 2018]. The stabilizing function of K becomes apparent at $P > 15$ GPa, in accordance with the recent findings of Berryman et al [Berryman et al., 2018]. A mixed occupation of the large *X* site by such different cations as Na and K apparently restricts specific distortions in tourmaline structure, which could fulfill the bond valence requirements of an individual cation. This seems to be the reason for the "invariance" of the pressure-induced changes in the structure polyhedra, surrounding the *X* site, in maruyamaite and dravite.

This study is supported by the Russian Scientific Foundation (project 18-17-00186). Diffraction experiments were carried at ID015B beamline at ESRF and supported by approval of Proposal ES-810.

Berryman E.J., Zhang D., Wunder B., Duffy T.S. High-pressure compressibility of synthetic tourmaline of near end-member compositions. AGU 2018 Abstracts.

O'Bannon E., Beavers C.M., Kunz M., Williams Q. High-pressure study of dravite tourmaline: Insights into the accommodating nature of the tourmaline structure. Am. Mineral. 2018, 101, 1622–1633.

Ota T., Kobayashi K., Kunihiro T., Nakamura E. Boron cycling by subducted lithosphere; insights from diamondiferous tourmaline from the Kokchetav ultrahigh-pressure metamorphic belt. Geochim Cosmochim Acta, 2008, 72, 3531–3541.

Shimizu R., Ogasawara Y. Discovery of K-tourmaline in diamond- bearing quartz-rich rock from the Kokchetav Massif, Kazakhstan. Mitteilungen der Österreichischen Mineralogischen Gesellschaft, 2005, 141–150.

**New synthetic tourmalines: crystal chemistry, functional properties and possible implication for geological reconstructions**

Oleg S. Vereshchagin[1,*], Olga V. Frank-Kamenetskaya[1], Bernd Wunder[2],
Sergey N. Britvin[1], Ira V. Rozhdestvenskaya[1]

[1]Institute of Earth Sciences,St. Petersburg State University, St. Petersburg, Russia
[2]GeoForschungsZentrum Potsdam, Potsdam, Germany

*o.vereshchagin@spbu.ru

Tourmaline is one of the commonest natural borosilicates. The generalized chemical formula of tourmaline supergroup minerals is $^{IX}X_{0\text{-}1}{}^{VI}Y_3{}^{VI}Z_6(^{IV}T_6O_{18})(BO_3)_3V_3W$ [Henry et al., 2011]. 22 chemical elements have been found in sufficient amount (> 1 wt.%) in natural tourmalines: $X$ = $Ca^{2+}$, $Na^{+}$, $K^{+}$; $Y$, $Z$ = $Li^{+}$, $Mg^{2+}$, $Al^{3+}$, $Ti^{4+}$, $V^{3+}$, $Cr^{3+}$,$Mn^{2+}$,$Mn^{3+}$,$Fe^{3+}$,$Fe^{2+}$,$Co^{2+}$,$Ni^{2+}$,$Cu^{2+}$,$Zn^{2+}$,$Sn^{4+}$,$Pb^{2+}$; $T$ = $Si^{4+}$, $Al^{3+}$, $B^{3+}$; $V$ = $OH^{-}$,$O^{2-}$; $W$ = $OH^{-}$, $F^{-}$, $O^{2-}$. Tourmalines can be formed under a wide range of thermodynamic conditions (up to ~6.5 GPa / 1000 °C). Tourmaline provides insight into the geologic environment of formation as its composition is sensitive to its geologic history [Dutrow and Henry, 2018].

Preparation of synthetic analogues of tourmaline makes it possible to study samples with simple composition and high concentrations of cations; detect crystal chemical patterns and structure-property correlations. Besides compositions, which occur in nature several new synthetic end-members, have been obtained since first tourmaline synthesis [Smith, 1948]. $^{VI}$Cu, $^{VI}$Ni [Lebedev et al., 1988], as well as $^{VI}$Co- and $^{VI}$Ga- end-members [Setkova et al., 2009, 2017], $^{IV}$B-rich [Kutzschbach et al., 2016], and $^{IX}$Ag-bearing [London et al., 2006] tourmaline have been obtained. However, no *REE*, $Ti^{4+}$, $V^{3+}$, $Zn^{2+}$, $Sn^{4+}$or $Pb^{2+}$-enriched tourmalines have been synthesized.

*REE* (*REE* = La, Nd, Eu, Yb), Sr, Pb, Ti and Sn-bearing tourmalines were synthesized at GFZ, Potsdam from an oxide mixture at 700 °C and 0.2–4.0 GPa. X-ray diffraction patterns reveal high content (up to 80 vol.%) of tourmaline in all synthesis. Content of *REE*, Ti, Sn and size of the synthetic tourmalines crystals depends on pressure. In all cases low-pressure tourmalines contain more dopant. Crystal size varies from 5 μm (4GPa) up to 300 μm (0.2 GPa). Pb-rich tourmaline contain up to 0.7 *apfu* Pb (4-12 wt.% PbO), Ti-bearing tourmaline – up to 0.3 *apfu* Ti (~2 wt.% $TiO_2$), Sr-bearing tourmaline – up to 0.2 *apfu* Sr (~2 wt.% SrO), Sn-bearing tourmaline – up to 0.1 *apfu* Sn (~1 wt.% $SnO_2$). Low-pressure *REE*-tourmalines contain up to 0.6 *apfu* Eu (4–10 wt.% $Eu_2O_3$), 0.4*apfu* La (2–6 wt.% $La_2O_3$), 0.3 *apfu* Nd (1–7 wt.% $Nd_2O_3$) and 0.1 *apfu* Yb (<1 wt.% $Yb_2O_3$). For the first time, luminescence properties have been obtained for synthetic Eu-rich tourmaline.

The authors thank the Resource Center of X-ray diffraction studies and Geomodel Resource Centre of Saint-Petersburg State University for providing instrumental and computational resources. This work was supported by the Russian Science Foundation Grant № 17-17-01171.

Dutrow B.L., Henry D. J. Tourmaline compositions and textures: reflections of the fluid phase. J. of Geosc., 2018, 63, 99–110.

Henry D.J., Novak M., Hawthorne F.C., Ertl A., Dutrow B., Uher P., Pezzotta F. Nomenclature of the tourmaline supergroup minerals. Am. Mineral., 2011, 96, 895–913.

Lebedev A.S., Kargalcev S.V., Pavlychenko V.S. Synthesis and properties of tourmaline series Al-Mg-(Na) and Al-Fe-(Na). In Proceedings of Genetic and Experimental Mineralogy. Growth and properties of crystals. Novosibirsk, Nauka, 1988, 58–75 [in Russian].

Smith F.G. Transport and deposition of the non-sulfide vein minerals. Econ. Geol., 1948, 186–192.

# 4.3. Boron Compounds

## Towards structural mineralogy and genetic crystal chemistry of boron: novel crystal structures of borate and borosilicate minerals from different geological formations

Igor V. Pekov[1,*], Natalia V. Zubkova[1], Vasiliy O. Yapaskurt[1], Dmitry A. Ksenofontov[1], Ilya I. Chaikovskiy[2], Oksana V. Korotchenkova[2], Elena P. Chirkova[2] and Dmitry Yu. Pushcharovsky[1]

[1]Faculty of Geology, Moscow State University, 119991 Moscow, Russia
[2]Mining Institute, Ural Branch of RAS, 614007 Perm, Russia

* igorpekov@mail.ru

Boron minerals occur in different geological environments and their crystal chemical features strongly depend on conditions of formation. Here we report our recent data on seven boron minerals belonging to novel, unique structure types. They are four new mineral species [krasnoshteinite, chubarovite, rhabdoborite-(V) and rhabdoborite-(W)] and three "old" minerals for which we first solved crystal structures and refined the idealized formulae (halurgite, satimolite and oyelite).

Borates formed in sedimentary rocks have the most complex and diverse B–O motifs in structures. **Halurgite**,$Mg_4[B_8O_{13}(OH)_2]_2\cdot 7H_2O$ (*P*2/*c*), from evaporites of Chelkar and Satimola salt domes (W. Kazakhstan) has a structure, which can be characterized using an approach based on three-layer *HOH* modules. In this mineral, considered by us as a microporous heterophylloborate, the *HOH* module consists of two heteropolyhedral (*H*) borate ($BO_3$ triangles + $BO_4$tetrahedra) layers $[B_8O_{13}(OH)_2]_\infty$ with sandwiched between them octahedral (*O*) layer composed of compact $MgO_6$ octahedra, while more voluminous $Mg(OH)_2(H_2O)_4$ complexes are between the *HOH* modules. In the structure of **satimolite**,$KNa_2(Al_5Mg_2)[B_{12}O_{18}(OH)_{12}](OH)_6Cl_4\cdot 4H_2O$ (*R*-3*m*), a mineral from the same localities and rocks, borate rings $[B_{12}O_{18}(OH)_{12}]$, consisting of $BO_3$ triangles and $BO_2(OH)_2$ tetrahedra, and octahedral clusters $[(Al_5Mg_2)O_6(OH)_{18}]$ form a 3D heteropolyhedral framework. Large ellipsoidal cages in this microporous framework host $Na^+$ and $K^+$ cations, $Cl^-$ anions and $H_2O$ molecules. **Krasnoshteinite** $Al_8[B_2O_4(OH)_2](OH)_{16}Cl_4\cdot 7H_2O$ (*P*2$_1$), discovered in evaporites of the Verkhnekamskoe potassium deposit (NWUrals, Russia), also has a microporous structure. It is based upon corrugated layers of Al-centered octahedra connected *via* common vertices. $BO_3$ triangle and $BO_2(OH)_2$ tetrahedron share common vertex to form insular $[B_2O_4(OH)_2]^{4-}$ group. These borate groups are connected with clusters of Al-octahedra *via* common vertices to form the aluminoborate pseudo-framework containing three-membered [2B + Al] rings. The 3D system of wide channels within this zeolite-like pseudo-framework hosts $Cl^-$ anions and weakly bonded $H_2O$ molecules.

Interesting borate mineralization was discovered by us in active fumaroles of the Tolbachik volcano (Kamchatka, Russia). All borates found here have compact structures with only $BO_3$ triangles isolated from each other. The structure of **chubarovite** $KZn_2(BO_3)Cl_2$ (*R*32) consists of the anionic $\{Zn_2(BO_3)Cl_2\}^-$ layers (formed by $BO_3$ groups sharing all O vertices with $ZnO_3Cl$ tetrahedra) alternating with the layers formed by $K^+$ cations centering $KCl_6$ octahedra. Isostructural **rhabdoborite-(V)**$Mg_{12}(V^{5+},Mo^{6+},W^{6+})_{1⅓}O_6\{[BO_3]_{6-x}[(P,As)O_4]_xF_{2-x}\}$ and **rhabdoborite-(W)** $Mg_{12}(W^{6+},V^{5+})_{1⅓}O_6\{[BO_3]_{6-x}[(P,As)O_4]_xF_{2-x}\}$ (both: $x< 1$; *P*6$_3$) form a continuous solid solution. In their structure six Mg-centered octahedra share edges forming triangular in shape clusters $Mg_6O_{21}F$. They are connected with each other *via* $BO_3$ triangles [partly substituted by $(P,As)O_4$ tetrahedra] to form a layer. Octahedrally coordinated *M* sites (*M* = V, W, Mo) are located in gaps of these layers.

The structure of **oyelite** $Ca_5[BSi_2O_7(OH)_2][Si_2O_6(OH)]\cdot 4H_2O$ (*P*-1) was studied on the sample from rodingite related to the Bazhenovskoe chrysotile asbestos deposit (Central Urals, Russia). It contains two kinds of linear tetrahedral units with different topology: (I) the chain $[BSi_2O_7(OH)_2]^\infty$ consisting of $Si_2O_7$ groups connected *via* single $BO_2(OH)_2$ tetrahedra and (II) the interrupted chain formed by $Si_2O_6(OH)$groups bonded with each other by very strong H-bonds. The units I and II are linked to the layers of Ca-centered polyhedra of three types: $CaO_6(H_2O)$, $CaO_3(H_2O)_4$ and $CaO_6OH$.

This work was supported by the RFBR, grants 18-29-12007 (crystal chemical analysis of microporous minerals) and 18-05-00332 (structural studies of minerals with complex B-O anions).

**Crystal structures of two novel borates in the SrO–BaO–$B_2O_3$ system**

S.N. Volkov[1], R.S. Bubnova[1,2], N.A. Morozov[2]

[1]Grebenshchikov Institute of Silicate Chemistry, 199053 Saint Petersburg, Russia
[2]Department of Crystallography, Saint Petersburg State University, 199034 Saint Petersburg, Russia

s.n.volkov@inbox.ru

Sr and Ba borates are of considerable interest for nonlinear optics, as well as for creating new luminescent materials on their basis. In the SrO–BaO–$B_2O_3$ system, previously, structural studies were almost not conducted, and here we present data on the crystal structure of two new borates from this system.

The borates $Sr_3Ba_2B_4O_{11}$ and $Sr_3Ba_3B_4O_{12}$ were obtained by the method of solid-state reactions synthesis, as well as by crystallization from the melt. Their crystal structure was determined from single crystal X-ray diffraction data on a Bruker Smart Apex II diffractometer and refined to $R_{obs}$ = 5.95 % ($Sr_3Ba_2B_4O_{11}$) and 4.32 % ($Sr_3Ba_3B_4O_{12}$).

The crystal structure of $Sr_3Ba_2B_4O_{11}$ is monoclinic, sp. gr. *C*2/*c*, composed by isolated $B_2O_5$ groups and $BO_3$ triangles in a 1: 2 ratio. Between them, cations of Sr (3 positions) and Ba (2 positions) are ordered. The relationship with chemically and structurally close borates of $Sr_2B_2O_5$ and $Ba_5B_4O_{11}$ is discussed. The crystal structure of $Sr_3Ba_3B_4O_{12}$ is tetragonal, sp. gr. *I*4/*mcm*, composed by isolated $BO_3$ triangles, some of which are orientationally disordered. Between these triangles, the Ba and Sr cations are partially disordered. The structure is an aristotype for the $Ba_3(BO_3)_{2-x}F_{3-x}$ family [Rashchenko et al., 2012] and relationship with this family is discussed**.**

The study was supported by the Russian Foundation for Basic Researches (project No. 18-29-12106).

Rashchenko S.V., Bekker T.B., Bakakin V.V., Seryotkin Y.V., Shevchenko V.S., Kokh A.E., Stonoga, S.Y. New Fluoride Borate Solid–Solution Series $Ba_{4-x}Sr_{3+x}(BO_3)_{4-y}F_{2+3y}$. Crystal Growth and Design, 2012, 12, 2955–2960.

**Investigation of thermal behavior of synthetic ($FeBO_3$, $Fe_3BO_6$) and natural (vonsenite, hulsite) iron-containing borates by high-temperature X-ray powder diffraction and Mössbauer spectroscopy over a wide temperature range**

Yaroslav P. Biryukov[1], Stanislav K. Filatov[2], Farit G. Vagizov[3], Almaz L. Zinnatullin[3], Rimma S. Bubnova[1,2,]*, Igor V. Pekov[4]

[1]Institute of Silicate Chemistry of the Russian Academy of Sciences, 199034 Saint Petersburg, Russia
[2]Institute of Earth Sciences, Saint Petersburg State University, 199034 Saint Petersburg, Russia
[3]Kazan Federal University, 420008 Kazan, Russia
[4]Department of Mineralogy, Faculty of Geology, Moscow State University, 119991 Moscow, Russia

* rimma_bubnova@mail.ru

In the $Fe_2O_3$–$B_2O_3$ system, two $Fe^{3+}$ borates are known: $FeBO_3$ (#34474-ICSD, trigonal, *R*-3*c*, calcite structure type) [Diehl, 1975] and $Fe_3BO_6$(#1910-ICSD, orthorh. sym., sp.gr. *Pnma*, norbergite-like structure) [White et al., 1965].$FeBO_3$ and $Fe_3BO_6$ are antiferromagnets with the Neel temperatures $T_N$ 348 and 508 K. Nowadays, antiferromagnets are extensively exploring due to their application in spintronics, as MRAM elements and other fields [Jungwirth et al., 2016]. Vonsenite [Swinnea, Steinfink, 1983] and hulsite [Konnert et al., 1976] are natural ($Fe^{2+}$, $Fe^{3+}$)-oxyborates.

The special points were revealed on the temperature dependencies of the unit cell parameters of $FeBO_3$ and $Fe_3BO_6$ near the magnetic phase transition temperatures. It was found that near the phase transition temperature thermal expansion coefficients of the borates abruptly change, which is consistent with the theoretical aspects of thermodynamics [Biryukov et al., 2018].

Single- and polycrystals of the natural mixed-valenced iron oxyborates (vonsenite and hulsite) were selected and investigated. Chemical composition of the borates was determined and calculated by data of electron-probe analysis. The crystal structures were refined from single-crystal X-ray diffraction data. Thermal behavior of vonsenite was investigated by Mössbauer spectroscopy (in a wide temperature range), thermal analysis (TG, DSC) and HTXRD. By Mössbauer spectroscopy data it was revealed that a partial $Fe^{2+} \rightarrow Fe^{3+}$ oxidation process starts approximately at 230–250 °C. This effect can also be seen in the DSC curve and in the plot of the temperature dependencies of the unit cell parameters. The data of the methods are consistent with each other. The structural mechanism of the thermal expansion is described in terms of crystal chemistry of inorganic compounds with cation- and anion-centered polyhedra.

Biryukov Y.P., Filatov S.K.,Vagizov F.G., Zinnatullin A.L., Bubnova R.S. Thermal expansion of $FeBO_3$ and $Fe_3BO_6$ antiferromagnets near the Neel temperature. J. Struct. Chem., 2018, 59, 1980–1988.

Diehl R. Crystal structure refinement of ferric borate, $FeBO_3$. Solid State Commun. 1975, 17, 743–745.

Jungwirth T., Marti X., Wadley P., Wunderlich J. Antiferromagnetic spintronics. Nature Nanotechn., 2016, 11, 231–241.

Konnert J.A., Appleman D.E., Clark J.R., Finger L.W., Kato T., Miura Y. Crystal structure and cation distribution of hulsite, a tin-iron borate. American Mineralogist, 1976, 61, 116–122.

Swinnea J.S., Steinfink H. Crystal structure and Mossbauer spectrum of vonsenite, $2FeO \cdot FeBO_3$. American Mineralogist, 1983, 68, 827–832.

White J.G., Miller A., Nielsen R.E. $Fe_3BO_6$, a borate isostructural with the mineral norbergite. Acta Crystallogr., 1965, 19(1), 1060–1061.

**Synthesis and thermal behavior of borate $CaBi_2B_4O_{10}$:Eu**

A.A.Yuriev[1]*, A.P.Shablinsky[1], R.S.Bubnova[1.2], S.K.Filatov[2]

[1]I.V. Grebenshchikov Institute of Silicate Chemistry RAS, St. Petersburg, Russia
[2] St. Petersburg State University, St. Petersburg, Russia

*viktorreyh@icloud.com

For the first time, this borate was obtained and studied by the DSC method in the $CaO$-$Bi_2O_3$-$B_2O_3$ system [Egorysheva et al., 2008]. A homogeneous samples of $CaBi_2B_4O_{10}$:*x*Eu (*x* = 0-30 at.%) were obtained by solid-phase synthesis at 630 °C / 20-26 hours. The initial reagents were $CaCO_3$ (e.c.), $H_3BO_3$ (e.c.), $Bi_2O_3$ (e.c.), taken in a stoichiometric ratio.

The compound is isostructural to the borate of $SrBi_2B_4O_{10}$ [Krzhizhanovskaya et al., 2009]. $CaBi_2B_4O_{10}$ crystallizes in the triclinic system, *P*-1 space group ($a$ = 6.6704(1), $b$ = 6.8317(1), $c$ = 9.5775(1) Å, $\alpha$ = 94.33, $\beta$ = 108.48, $\gamma$ = 101.34°, $V$ = 401.37 Å$^3$, $Z$ = 2). $CaBi_2B_4O_{10}$ is a borate whose polyanion is represented by isolated tetraborate group [$B_4O_9$]. Two triangles $BO_3$ and tetrahedron $BO_4$ form a triborate ring to which another single triangle $BO_3$ is attached.

$CaBi_2B_4O_{10}$ was studied *in situ* on a Rigaku "Ultima IV" powder diffractometer (CoKα radiation, $2\theta$ = 10–70°, temperature range 25–700 °C, pitch 25 °C) and the DSC method. Above 650 ° C, the texture of the diffraction pattern increases, which apparently indicates the effects of premelting. Melting occurs at a temperature of 729 °C according to DSC. Thermal expansion is sharply anisotropic. The coefficients and parameters of the thermal expansion tensor at 25 °C: $\alpha_{11} = 3\times10^{-6}$, $\alpha_{22} = 15\times10^{-6}$, $\alpha_{33} = 7\times10^{-6}$, $a_\alpha = -3\times10^{-6}$, $a_\beta = 5\times10^{-6}$, $a_\gamma = 3\times10^{-6}$,$\alpha_V = 25\times0^{-6}$ °C$^{-1}$, at 600 °C: $\alpha_{11} = 0.5\times10^{-6}$, $\alpha_{22} = 22\times10^{-6}$, $\alpha_{33} = 13.5\times10^{-6}$, $a_\alpha = -3\times10^{-6}$, $a_\beta = 10\times10^{-6}$, $a_\gamma = 2\times10^{-6}$, $\alpha_V = 36\times10^{-6}$°C$^{-1}$.

The parameters *a*, *b*, *c* increase by 0.45, 0.8 Å, 0.6 Å, and the angles $\alpha$, $\beta$, $\gamma$ change by -0.25°, 0.6°, 0.2° in the temperature range 25–700 °C. A sharp change in the angle $\beta$ indicates the presence of shear deformation in the plane of *ac*. The sharp increase in the parameter *b* with increasing temperature may be due to the position of the tetraborate groups ([$B_4O_9$]), which are perpendicular to the axis *b*.

X-ray studies were performed at the St. Petersburg State University Resource Center "X-ray diffraction methods of research". Luminescent properties of samples $CaBi_2B_4O_{10}$:*x*Eu (x = 0-30 at.%) are studied. The study was supported by RFBR (Project No. 18-03-00679).

Egorysheva A.V., Volodin V.D., Skorikov V.M. Calcium-bismuth borates in the $CaO$-$Bi_2O_3$-$B_2O_3$ system. Inorg. Materials, 2008, 44, 76–81.

Krzhizhanovskaya M.G., Bubnova R.S., Egorysheva A.V., Kozin M.S., Volodin V.D., Filatov S.K. Synthesis, crystal structure and thermal behavior of a novel oxoborate $SrBi_2B_4O_{10}$. J. Solid State Chem., 2009, 182, 1260–1264.

**Structure features of rare-earth iron borates ($R_{1-x}$,$Bi_x$)$Fe_3(BO_3)_4$, $R$ = Nd, Gd, Ho, Y in the temperature range 30 – 500 K**

Ekaterina S. Smirnova[1,*], Olga A. Alekseeva[1], Alexander P. Dudka[1], Igor A. Verin[1], Vladimir V. Artemov[1], Dmitry N. Khmelenin[1], Irina A. Gudim[2], Kirill V. Frolov[1], Igor S. Lyubutin[1]

[1] FSRC «Crystallography and Photonics» RAS, 119333 Moscow, Russia
[2]Kirensky Institute of Physics of the Siberian Branch of the RAS, 660036 Krasnoyarsk, Russia

* esmi@ns.crys.ras.ru

Rare-earth iron borates $R Fe_3(BO_3)_4$ with huntite structure type at high temperatures belong to multiferroic family. The variety of their physical properties is attributed to the presence of two magnetic sublattices formed by rare-earth and iron atoms, and to helicoidal type of the whole lattice. The rare-earth ion type influences strongly physical properties of these compounds, which currently are being studied vastly [Kadomtseva et al., 2010].

The present work is devoted to studying the crystal structure of $R Fe_3(BO_3)_4$ with $R$ = Nd, Gd, Ho, Y in a wide temperature range 30–500 K. The single crystals were grown from a solution in melt with $Bi_2Mo_3O_{12}$ in the system. The chemical composition was verified by X-ray energy-dispersive elemental analysis. It was shown that Bi atoms entered the composition of all the crystals during the growth process. On the basis of X-ray diffraction data, Bi atoms party occupy mixed 3a position along with $R$ atoms, and final composition is ($R_{1-x}$,$Bi_x$)$Fe_3(BO_3)_4$, $x$=4-6%.

Temperature dependence of unit cell parameters was measured in 30–500 K temperature range. Parameters $a,b$ for the crystals with $R$ = Gd, Ho, Y are descending with lowering temperature, whereas $a,b$ parameters of Nd-crystal do not change strongly over all the studied range. The sharp jump of $a,b$ parameters was registered for crystals with $R$ = Gd, Ho, Y demonstrating the presence of structural phase transition. At the same time, $c$ ($T$) dependence is similar for crystals with $R$ = Nd, Gd, Ho, Y – $c$ parameter decreases with lowering temperature to 80–100 K and then begins to grow smoothly down to 30 K.

Structure of all the crystals was determined at several temperatures in 90–500 K range to study temperature-dependent structure peculiarities, in particular, changes during the structural phase transition for $R$ = Gd, Y, Ho. On the base of systematic absences analysis and temperature dependence of $a,b$ parameters, the temperatures of the phase transition are $T_s$ = 155 K for $R$ = Gd,370 K for $R$=Y and 365 K for $R$ = Ho. It was shown that for yttrium compound the phase transition has the most diffuse character. The structure of the compounds with $R$ = Gd, Ho, Y was refined in trigonal sp. gr. $R32$ above the temperature of the phase transition and in trigonal sp. gr. $P3_121$ below it. Structure of Nd-crystal belongs to sp. gr. $R32$ at all studied temperatures. There is a slight steady decrease of specific distanced in ($R$,Bi)$O_6$ trigonal prisms, $FeO_6$ octahedra, $BO_3$ triangles and Fe–Fe helicoidal chains with lowering temperature in sp. gr. $R32$. When going to lower-symmetry sp. gr. $P3_121$ and with further temperature decreasing non-uniform changes in the bond lengths in the ($R$,Bi)$O_6$ prisms, $B2O_3$ and $B3O_3$ triangles, and $FeO_6$octahedra are observed. Equivalent atomic displacement parameters $U_{eq}$ decrease with temperature decreasing. However, $U_{eq}$ of oxygen atoms O1 and O2 as well as ones of boron atoms B2 and B3 (sp. gr. $P3_121$ labels) are highly sensitive to a structural phase transition, demonstrating fluctuations around $T_s$. Using multitemperature X-ray diffraction datasets for $R$ = Nd, Ho, Y crystals we calculated Debye and Einstein characteristic temperatures from atomic displacement parameters. On the base of these values, it was shown, that $R$ atoms have the weakest bonds with their neighbors and B atoms have the strongest ones.

The study was partly supported by the RFBR (pr. no. 17-02-00766 A).

Kadomtseva A.M., Popov Yu. F., Vorob'ev G.P., et al. Magnetoelectric and magnetoelastic properties of rare-earth ferroborates. Low Temperature Physics, 2010, 36, 511–521.

**Comparative crystal chemistry of borates Na*A*[$B_{10}O_{14}(OH)_4$] (*A* = K, $NH_4$, Rb, Cs)**

Pankova Yu.A.*, Krivovichev S.V.

Department of Crystallography, Institute of Earth Sciences, St. Petersburg State University
Kola Science Center of the Russian Academy of Sciences

*y.pankova.spbu@gmail.com

Colorless crystals of NaK[$B_{10}O_{14}(OH)_4$], Na($NH_4$)[$B_{10}O_{14}(OH)_4$] and NaRb[$B_{10}O_{14}(OH)_4$] were obtained using boric acid as a flux in autoclaves at autogenous pressure and temperature range 200–225 °C for 7 days, followed by cooling to room temperature. Three-dimensional sets of diffraction maxima were obtained on a Bruker SMART APEX single-crystal diffractometer (MoKα radiation, CCD detector) (X-Ray Diffraction Research Centre of St. Petersburg State University). The crystal structure was solved and refined using the SHELXL-97 software package. The shooting conditions and structural data are shown in Table. The cesium analogue of the compounds under study, the decaborate NaCs[$B_{10}O_{14}(OH)_4$], was first obtained in (Lian-Qing et al., 2014).

Table. Structural data, parameters of the X-ray experiment and refinement of crystal structures of Na *A*[$B_{10}O_{14}(OH)_4$] (*A* = K, $NH_4$, Rb, Cs)

| Compound | | *A* = $NH_4$ (our data) | *A* = K (our data) | *A* = Rb (our data) | *A* = Cs (Lian-Qing et al., 2014) |
|---|---|---|---|---|---|
| Unit cell parameters | *a* | 7.639(1) | 7.798(2) | 7.645(5) | 7.6588(3) |
| | *b* | 9.006(1) | 8.890(3) | 9.012(5) | 9.0074(3) |
| | *c* | 11.644(2) | 11.510(3) | 11.652(6) | 11.8708(6) |
| | *β* | 115.78(1) | 116.44(1) | 115.60(3) | 115.682(3) |
| V, Å$^3$ | | 721.3(2) | 714.5(4) | 724.0(8) | 738.02(5) |
| $\theta_{min}$ - $\theta_{max}$ | | 2.26° - 29.12° | 2.917° - 38.985° | 2.260 - 31.652 | 3.55° - 24.54° |
| $I>2\sigma_I$ / $F^{un}_{obs}>4.0\sigma_F$ | | 1941/1348 | 4043/3169 | 2377/1503 | 2124/971 |
| R/ wR | | 0.045/0.102 | 0.056/0.158 | 0.065/0.206 | 0.019/0.048 |
| GOF | | 1.030 | 1.070 | 1.048 | 1.004 |

The crystal structure of Na*A*[$B_{10}O_{14}(OH)_4$] has monoclinic symmetry, the space group is *P*2/*c* (*Z* = 2). The structure is based on the $[B_5O_7(OH)_2]^{2-}$ pentaborate complexes (one $BO_4$ tetrahedron and four $BO_3$ triangles), connected to each other by bridging oxygen atoms, forming corrugated chains linked by O-H ... O hydrogen bonds. $Na^+$ and $A^+$ cations are located between the chains. The B-O distances in $BO_3$ triangles range from 1.334 to 1.396 Å with an average value of 1.368 Å, and in $BO_4$ tetrahedra from 1.465 to 1.483 Å with the average value of 1.474 Å. The Na atom is coordinated by five O atoms with Na-O distances in the range 2.249 - 2.973 Å, while the A cation is coordinated by 12 O atoms with *A*-O distances in the range 2.816–3.665 Å.

The largest contribution to the unit-cell parameters change is made by changing *A*-O and Na-O distances in the range 2.816–3.665 and 2.249–2.973 Å, respectively, while the B-O distances remain almost unchanged in all three compounds. The change of the angle β is connected with the distortion of the crystal structure of Na*A*[$B_{10}O_{14}(OH)_4$] by a hinge mechanism, carried out by rotating $[B_5O_7(OH)_2]^{2-}$ rigid complexes relative to each other.

This work was supported by RFBR (Grant No. 17-05-01027). The studies were conducted using the equipment of the resource center of the Scientific Park of St. Petersburg State University "X-ray diffraction methods of research."

**Synthesis, crystal structure and thermal expansion of gaudefroyite-type borates: $Sr_3Bi(YO)_3(BO_3)_4$, $Sr_2CaBi(YO)_3(BO_3)_4$ and $Sr_2BaBi(YO)_3(BO_3)_4$**

Andrey P. Shablinskii[1,*], Lidiya G. Galafutnic[1], Rimma S. Bubnova[1,2], Stanislav K. Filatov[2]

[1]Institute of Silicate Chemistry, 199034 Saint-Petersburg, Russia
[2]Saint-Petersburg State University, 199034 Saint-Petersburg, Russia

* shablinskii.andrey@mail.ru

Borates are perspective materials for luminescent matrix due to the wide bandgap, relatively easy synthesis and high thermal stability.

The $Sr_3Bi(YO)_3(BO_3)_4$, $Sr_2CaBi(YO)_3(BO_3)_4$ and $Sr_2BaBi(YO)_3(BO_3)_4$ compounds were synthesized via solid state reactions. Reagents, $SrCO_3$ (99.99%), $CaCO_3$ (99.99%), $Y_2O_3$ (99.99%), $BaCO_3$ (99.99%), $Bi_2O_3$ (99.99%) and $H_3BO_3$ (99.99%), in stoichiometric ratios, were mixed in an agate mortar and pestle. This mixture was ground for 45 min and placed in platinum crucibles. The powder was heated at 600 °C for 3 h in air to decompose the metal carbonate and boric acid. Then, the mixture was pressed into a pellet and heated at 300 °C for 5 h, 500 °C for another 5 h, then ground carefully, and finally fired at 950 °C for 24 h.

Crystal structure of $Sr_3Bi(YO)_3(BO_3)_4$ was first investigated in [Gao, Li, 2012]. Unit cell parameters of $Sr_3Bi(YO)_3(BO_3)_4$ are: $a$ = 10.697(2), $c$ = 6.7222(1) Å, $V$ = 666.2(2) Å$^3$, space group $P6_3$. There are 10 crystallographically independent atoms in the asymmetric unit. Among them, the Bi and B1 atoms locate on the special sites, and Y and O atoms occupy the general sites. The Y atom is coordinated by seven O atoms to form a pentagonal bipyramid. These $YO_7$ polyhedra share edges to form a one-dimensional (1D) chain along the $c$ direction. The chains are bridged by $B_2O_3$ groups through sharing vertex oxygen atoms to construct a three-dimensional (3D) framework, which affords two kinds of channels along the [001] direction. Sr atoms and isolated $B(1)O_3$ triangles are located in the larger channel. The $B(1)O_3$ triangles are surrounded by Sr atoms.

The thermal behavior of $Sr_3Bi(YO)_3(BO_3)_4$, $Sr_2CaBi(YO)_3(BO_3)_4$ and $Sr_2BaBi(YO)_3(BO_3)_4$ compounds was studied using in situ high-temperature XRD in the range 25-800 °C by means of Rigaku Ultima IV powder X-Ray diffractometer (CuKα) with a high-temperature camera. According to the principles of high temperature crystal chemistry [Bubnova, Filatov, 2013] for borates with isolated triangle groups, thermal expansion of these borates is practically isotropic.

The studies have been supported by the Russian Foundation for Basic Researches, project №18-29-12106. X-Ray diffraction experiments were performed at the X-Ray Diffraction Center of Saint-Petersburg State University.

Bubnova R., Filatov S. High-temperature borate crystal chemistry. Z. Kristallogr, 2013, 228, 395–428.

Gao J., Li S. $BiSr_3(YO)_3(BO_3)_4$: a new gaudefroyite-type rare earth borate with moderate SHG response. Inorg. Chem., 2012, 51, 420-424.

**Some crystallographic parameters of $HoB_{12}$ single crystals in the temperature range 86-500 K**

Olga N. Khrykina*, Nadezhda B. Bolotina, Alexander P. Dudka

FSRC “Crystallography and Photonics” RAS, 119333 Moscow, Russia

* kvarkpower@gmail.com

Dodecaborides of rare earth elements $RB_{12}$ ($R$ = Y, Zr, Gd ÷ Lu) show a variety of physical properties due to both the metal ion nature and the external conditions. On the one hand, the rare earth dodecaborides at room temperature may be considered as the simplest, model objects with face-centered cubic lattice (*fcc*, sp. gr. *Fm*-3*m*) formed by $B_{12}$cuboctahedra with *R*-atoms accommodated in the octahedral cavities. On the other hand, many of these compounds exhibit unusual galvanomagnetic properties, anisotropic magnetoresistance, negative thermal expansion and other anomalies at temperatures below 150 K, what indicates possible distortions of the crystal lattice.

The $HoB_{12}$ crystals belong to the compounds with metal-type conductivity and strongly correlated electronic systems. The purpose of present research is to detect possible structure features in $HoB_{12}$ single crystals in the wide temperature range using advanced X-ray diffraction analysis techniques.The results of the analysis are important for the interpretation of the physical properties of these crystals.

Reproducible and accurate [Dudka, 2018] X-ray data were collected using an Xcalibur EOS S2 diffractometer at 29 temperatures in the temperature range 86–500 K. Crystal structure of $HoB_{12}$ has been refined in the *Fm*-3*m* symmetry group. Atomic displacement parameters (ADPs) were under special interest since they may help in detecting, for example, phase transitions. In the conventional approach, the structure analysis describes summary displacements of the atoms from crystallographic positions making no distinction between the temperature-induced and temperature-independent displacements. The new technique allows to separate the dynamic and static components of equivalent ADPs using two different models for atoms, which are weakly bonded to their neighbors (expanded Einstein model) and atoms with correlated displacements (Debye model). The method can give also the characteristic Debye and Einstein temperatures serving to describe the lattice dynamic.

Using this technique for $HoB_{12}$, an anomaly has been discovered at 180–210 K. Such behavior of the $HoB_{12}$ structure has been observed for the first time and requires further investigation.

The study was supported by RFBR (grant No. 18-29-12005).

Dudka A.P. ASTRA 4.0 program: data reduction for obtaining structure results of extreme accuracy. Crystallography Reports, 2018, 63, 1051.

**Distribution of the $Eu^{3+}$dopant ions over cation positions and luminescent properties in novel $M_3Bi_2(BO_3)_4$:$Eu^{3+}$ ($M$ = Sr, Ba) red phosphors**

Bubnova R.S.[1,]*, Shablinskii A.P.[1], Filatov S.K.[2], Kolesnikov I.E.[2], A.V. Povolotskiy[2]

[1]Grebenshchikov Institute of Silicate Chemistry RAS, 199034 St. Petersburg, Russia
[2] St. Petersburg State University, 199034 St. Petersburg, Russia

* rimma_bubnova@mail.ru

Here, we represent the results of investigation of structural and optical properties of novel $M_3Bi_2(BO_3)_4$:$Eu^{3+}$($M$ = Sr, Ba)red-emitting phosphors. These borates crystallize in *Pnma* space group and are related to $A_3REE_2(BO_3)_4$ family, $A$ = Ca, Sr, Ba [Khamaganova, 2017]. Crystal structure is consisted of the isolated $BO_3$ triangles and three independent $M$1, $M$2 and $M$3 sites. The $M$O-polyhedra are connected by corners and edges forming the framework.

Series of the $M_3Bi_2(BO_3)_4$:$Eu^{3+}$ ($M$ = Sr, Ba)were prepared using crystallization from a melt. X-ray powder diffraction data confirmed that samples were single-phased. There is an expectable decrease of the unit cell parameters and volume in these series along with the substitution of the larger $Bi^{3+}$ ion ($R_{CN\,8}$ = 1.31 Å) by the smaller $Eu^{3+}$ ion ($R_{CN\,8}$ = 1.206 Å). $M_3Bi_2(BO_3)_4$ ($M$ = Sr, Ba) solutions have positionally-disordered structures; in $Ba_3Bi_2(BO_3)_4$ end-member the $M$1–$M$3 sites are additionally splitted [Volkovet al., 2013].Itcan be assumed that as the amount of the europium increases, the $Eu^{3+}$ ions can replace the $Bi^{3+}$ ions in different $M$ sites. A few small single crystals were obtained and distribution of the $Eu^{3+}$ ions over three cation sites was refined for $Sr_3(Bi_{1-x}Eu_x)_2(BO_3)_4$ ($x_{Eu}$ = 0, 0.17) [Shablinskii et al., 2017], $Ba_3(Bi_{1-x}Eu_x)_2(BO_3)_4$[Volkov et al., 2013] and $Ba_3(Bi_{1-x}Eu_x)_2(BO_3)_4$solid solutions ($x_{Eu}$ = 0.05, 0.35 and 0.8) from single-crystal XRD data. The Ba, Bi and Eu atoms are disordered over these sites with thepreferential occupation but with no complete ordering. Therefore, we refined the Ba/Bi/Eu occupations over the sites: the $Eu^{3+}$ ions occupied the $M$2 site in $Ba_3Bi_{1.9}Eu_{0.1}(BO_3)_4$ and $Ba_3Bi_{1.3}Eu_{0.7}(BO_3)_4$, whilst the $Eu^{3+}$ ions were distributed over all the cation sites in the $Ba_3Bi_{0.4}Eu_{1.6}(BO_3)_4$ crystal structure.

Luminescent properties of the $M_3Bi_2(BO_3)_4$:$Eu^{3+}$ phosphors were investigated: the optimum concentration was found to be at 50 at. % for$Ba_3Bi_2(BO_3)_4$:$Eu^{3+}$ ($\lambda_{ex}$ = 393 nm),while for the structurally similar $Sr_3Y_2(BO_3)_4$ [Zhang, Li, 2004] and $Sr_3Bi_2(BO_3)_4$ [Shablinskii *et al*., 2017] borates, it was determined as 10 and 15 at.% ($\lambda_{ex}$ = 393 nm). Hence, a feature of the $Ba_3Bi_2(BO_3)_4$: $Eu^{3+}$ crystal structure is the high optimumconcentration of the $Eu^{3+}$ dopant in this phosphor matrix in comparison to the other borates of this family. The integral luminescence intensity of $^5D_0$–$^7F_2$transition increases when the largest amount of the $Eu^{3+}$ ions occupies the $M$2 site. The concentration quenching occurs when the $Eu^{3+}$ ions start to distribute over all three cation sites in the $Ba_3Bi_2(BO_3)_4$:$Eu^{3+}$ phosphor. The influence of the $Eu^{3+}$ ions distribution and splitting positions in the crystal structures of the $M_3Bi_2(BO_3)_4$: $Eu^{3+}$ is discussed. The results show that the $Ba_3Bi_2(BO_3)_4$:$Eu^{3+}$ phosphors are promising candidates for solid state lighting application.

The study was supported by the Russian Foundation of Basic Research No. 18-03-00679. X-ray measurements and photoluminescence were performed in the Research Centers of XRD Studies and Optical and Laser Materials Research of St. Petersburg State University.

Khamaganova T.N. Structural specific features and properties of alkaline-earth and rare-earth metal borates. Rus. Chem. Bull., 2017, 66, 187−200.

Shablinskii A.P., Bubnova R.S., Kolesnikov I.E., Krzhizhanovskaya M.G., Povolotskiy A.V., Ugolkov V.L., Filatov S.K.Novel $Sr_3Bi_2(BO_3)_4$:$Eu^{3+}$ red phosphor: synthesis, crystal structure, luminescent and thermal properties. Solid State Sci., 2017, 70, 93−100.

Volkov S.N., Bubnova R.S., Filatov S.K., Krivovichev S.V. Synthesis, crystal structure and thermal expansion of a novel borate, $Ba_3Bi_2(BO_3)_4$. Z. Kristallogr., 2013, 228, 436−443.

Zhang Y., Li Y. Red photoluminescence and crystal structure of $Sr_3Y_2(BO_3)_4$. J. Alloys Compd., 2004, 384, 88−92.

**Dynamical crystal chemistry of danburite-group minerals $MB_2Si_2O_8$ ($M$ = Ca, Sr, Ba)**

Liudmila A. Gorelova[1,*], Anna S. Pakhomova[2], Maria G. Krzhizhanovskaya[1], Leonid S. Dubrovinsky[3], Sergey V. Krivovichev[1,4]

[1]St. Petersburg State University, 199034 St. Petersburg, Russia
[2]DeutschesElektronen-Synchrotron (DESY), Petra III, 22607 Hamburg, Germany
[3]BayerischesGeoinstitut, University of Bayreuth, 95447 Bayreuth, Germany
[4]Kola Science Centre, Russian Academy of Sciences, 184209 Apatity, Russia

* l.gorelova@spbu.ru

Danburite-group minerals with the general formula $MB_2Si_2O_8$ ($M$ = Ca, Sr, Ba) include three minerals: danburite (Ca) [Bakakin et al., 1959], pekovite (Sr) and maleevite (Ba) [Pautov et al., 2004]. Their orthorhombic crystal structure is based upon a three-dimensional tetrahedral borosilicate framework, with an ordered distribution of the B and Si atoms. For all three isotypic minerals there are data about their high-temperature and compositional deformations [Sugiyama, Takeuchi, 1985; Gorelova et al., 2015]. Pakhomova et al. [2017] demonstrated that, upon compression up to 32 GPa, danburite undergoes two phase transitions with a stepwise transformations of Si coordination from $SiO_4$ via $SiO_5$ to $SiO_6$.

The behavior of pekovite and maleevite under high-pressure conditions was studied using *in situ* single-crystal X-ray diffraction in diamond anvil cells at the Extreme Conditions Beamline P02.2 of PETRA III (DESY, Hamburg, Germany) and at the beamline ID15B at the European Synchrotron Radiation Facility (ESRF, Grenoble, France). For the study, we have used crystals of natural maleevite and pekovite from the Dara-i-Pioz massive, Tajikistan [Pautov et al., 2004] (from the collection of Fersman Mineralogical Museum RAS, Moscow, Russia) with the size of 0.010×0.010×0.005 $mm^3$. Experiments were performed at ambient temperature in the pressure range from 0.0001 to 33-38GPa with the pressure step no more than 4 GPa (10-12 pressure points).

It has been found that maleevite undergoes one reconstructive phase transition between 36 and 38 GPa with the formation of a triclinic phase, maleevite-II, featuring octahedrally coordinated silicon. In contrast, pekovite undergoes two phase transitions: first isosymmetric order-disorder phase transition to pekovite-II (between 18 and 23 GPa), and then reconstructive phase transition with the formation of triclinic pekovite-III (between 29 and 33 GPa). The structure of pekovite-II is characterized by splitting of the Si site into two sites.

The comparison of the high-pressure behavior of danburite-group minerals reveals that the increasing size of extraframewok cation (Ca→Sr→Ba) governs the stability of the danburite structure type and prevents formation of pentacoordinate silicon species.

This study was supported by the Russian Foundation for Basic Research (17-05-01027).

Bakakin V.V., Kravchenko V.B., Belov N.V. The crystal structure of danburite $CaB_2Si_2O_8$ and hurlbutite $CaBe_2P_2O_8$. Doklady Akademii Nauk SSSR, 1959, 129, 420–423.

Gorelova L.A., Filatov S.K., Krzhizhanovskaya M.G., Bubnova R.S. High-temperature behavior of danburite-like-borosilicates$MB_2Si_2O_8$ ($M$ = Ca, Sr, Ba). Physics and Chemistry of Glasses, 2015, 56, 189–196.

Pakhomova A.S., Bykova E., Bykov M., Glazyrin K., Gasharova B., Liermann H.P., Mezouar M., Gorelova L.A., Krivovichev S.V., Dubrovinsky L. Closer look into close packing: pentacoordinated silicon in the high-pressure polymorph of danburite. IUCrJ, 2017, 4, 671–677.

Pautov L.A., Agakhanov A.A., Sokolova E.V., Hawthorne F.C. Maleevite, $BaB_2Si_2O_8$, and pekovite, $SrB_2Si_2O_8$, new mineral species from the, Dara-i-Pioz alkaline massif, Northern Tajikistan: Description and crystal structure. Canadian Mineralogist, 2004, 42, 107–119.

Sugiyama K., Takeuchi Y. Unusual thermal expansion of a B–O bond in the structure of danburite $CaB_2Si_2O_8$. Zeitschrift fuer Kristallographie, 1985, 173, 293–304.

## $Sr_{3-1.5y}Eu_yB_{2+x}Si_{1-x}O_{8-x/2}$ solid solutions: synthesis, crystal structure, thermal expansion and luminescence

S.N. Volkov[1,*], M.G. Krzhizhanovskaya [2], R.S. Bubnova[1,2], O.L. Belousova [1], A.V. Povolotskiy[3], I.E. Kolesnikov [3]

[1]Grebenshchikov Institute of Silicate Chemistry, 199053 Saint Petersburg, Russia
[2]Department of Crystallography, Saint Petersburg State University, 199034 Saint Petersburg, Russia
[3]Institute of Chemistry, Saint Petersburg State University, 198504 Saint Petersburg, Russia

*s.n.volkov@inbox.ru

Strontium borosilicates are of considerable interest for creating luminescent materials based on them due to their optical properties and high thermal and mechanical stability. Previously we discovered and structurally characterized the $Sr_3B_{2+x}Si_{1-x}O_{8-x/2}$ solid solutions [Volkov et al., 2015] – the first borosilicates with incommensurately modulated structure. Its crystal structure was described as periodic in (3 + 2)-dimensional superspace. In this work, in order to study the modulation parameters depending on the content of the dopant ion, we synthesized $Sr_{3-1.5y}Eu_yB_{2+x}Si_{1-x}O_{8-x/2}$ solid solutions and studied their structural, optical and thermal properties at $0 \le x \le 1$, $0 \le y \le 0.4$. The crystal structures were studied by single-crystal X-ray diffraction while its thermal expansion was studied by high-temperature X-ray powder diffraction. It is shown that two main schemes of isomorphic substitutions are realized in these solid solutions: $3Sr^{2+} \leftrightarrow 2Eu^{3+} + \square$, where □ denotes vacancies and $2B_2SiO_8^{6-} \leftrightarrow 3B_2O_5^{4-}$. With increasing Eu content, the volume of the unit cell increases to the formation of vacancies. With increasing in the content of silicon, the volume of the unit cell decreases due to an increase in the number of oxygen atoms per unit cell. Data on the luminescent properties and thermal expansion of solid solutions are also presented.

The study was supported by the Russian Foundation for Basic Researches (project No. 17-03-00887).

Volkov S., Bubnova R., Bolotina N., Krzhizhanovskaya M., Belousova O., Filatov S. Incommensurate modulation and thermal expansion of $Sr_3B_{2+x}Si_{1-x}O_{8-x/2}$ solid solutions. Acta Cryst., 2015, B71, 489–497.

## Thermal expansion of $Li_2B_4O_7$ revised

S.N. Volkov [1,*], R.S. Bubnova[1,2], M.G. Krzhizhanovskaya [2], S.A. Petrova[3]

[1]Grebenshchikov Institute of Silicate Chemistry, 199053 Saint Petersburg, Russia
[2]Department of Crystallography, Saint Petersburg State University, 199034 Saint Petersburg, Russia
[3]Institute of Metallurgy UD RAS, 620016 Ekaterinburg, Russia

*s.n.volkov@inbox.ru

The thermal expansion of $Li_2B_4O_7$ has been the subject of controversy over the past 20 years. Precision measurements of the thermal expansion of single crystals of lithium tetraborate, carried out in [Zub, 1997] by dilatometry and X-ray diffraction, demonstrated the strange "step-wise" character of the temperature dependence of the unit cell parameters. Such behavior contradicts classical thermodynamics, according to which the temperature dependence of the unit cell parameters should have a smoothed character in the absence of phase transitions. Subsequent work did not confirm such strange thermal expansion [Senyshyn et al., 2012].

In this work, we repeated the aforementioned studies and studied thermal expansion of $Li_2B_4O_7$ by high-temperature X-ray powder diffraction and single-crystal X-ray powder diffraction in the temperature range –173 – +20 °C with a step of 1 °C. The anomalies observed with a lithium tetraborate crystal may have a macroscopic nature cause. The crystal demonstrates good piezoelectric properties and at the same time it has a sharply anisotropic thermal expansion. The presence of a large number of antiphase domains in a single crystal can lead to the presence of additional electrostatic interactions, which is reflected in the “strange” temperature dependence of the linear dimensions of the single crystal.

This work was financially supported by the Russian Science Foundation through the grant 18-73-00176.

Senyshyn A., Boysen H., Niewa R., Banys J., Kinka M., Burak Ya., Adamiv V., Izumi F., Chumak I., Fuess H. High-temperature properties of lithium tetraborate $Li_2B_4O_7$. J. Phys. D.: Appl. Phys., 2012, 45, 175305.

Zub E.M. Existence of an incommensurate phase in a $Li_2B_4O_7$ crystal. Phys. Solid State, 1997, 39, 1297–1298.

## Study of $K_2O$-$B_2O_3$-$GeO_2$ Glasses at Pressures up to 9GPa

Anastasia S.Brazhnikova[1,3,*], Olga N. Koroleva[2], Sergey V. Rashchenko[1,3], Alexandr V. Romanenko[1,3], Boris A. Zakharov[1,4]

[1]Novosibirsk State University, Department of Geology and Geophysics, 630090 Novosibirsk, Russia
[2]Institute of Mineralogy, UB of RAS, Ilmensky Reserve, 456317 Miass, Russia
[3]Sobolev Institute of Geology and Mineralogy SB RAS, 630090 Novosibirsk, Russia
[4]Boreskov Institute of Catalysis SB RAS, 630090 Novosibirsk, Russia

* a.brazhnikova@g.nsu.ru

Glass can be considered as a model of melt, and is an important object in material science. In particular, borogermanate glasses models high-pressure silicate-carbonate melts, so that their behavior under pressure is relevant for the Earth sciences.

Previously by X-ray diffraction Ohtaka et al. [2004] investigated the behavior of $Li_2O$-$4GeO_2$ glass and $GeO_2$ melt at temperature of 1273 K. Transition of Ge from four-coordinated into six-coordinated was observed at pressures of 7-8 GPa and 4-5 GPa, respectively. Phase transition of B from three-coordinated to four-coordinated position was observed in the analysis of glass with composition $La_2O_3 \cdot B_2O_3 \cdot GeO_2$ by X-ray absorption spectroscopy at a pressure of 4-7 GPa [Coussa-Simon et al., 2010].

We used Raman spectroscopy to study the glasses of $30K_2O \cdot 70GeO_2$ and $30K_2O \cdot 35B_2O_3 \cdot 35GeO_2$ compositions at pressures up to 9 GPa. The spectra of samples are shown in Figure. The results obtained suggest that the structure of $30K_2O \cdot 70GeO_2$ glass changes at 4-5 and 8 GPa, and $30K_2O \cdot 35B_2O_3 \cdot 35GeO_2$ glass – at 3-4 GPa.

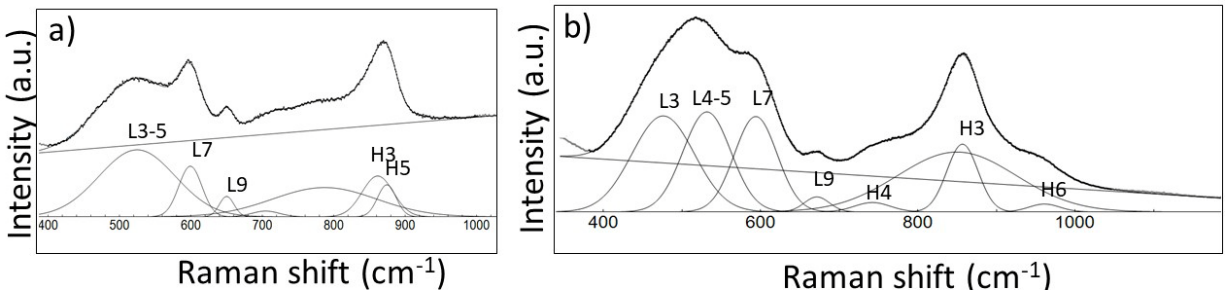


Figure. Decomposition of samples spectra a) $30K_2O \cdot 70GeO_2$ b) $30K_2O \cdot 35B_2O_3 \cdot 35GeO_2$ under ambient pressure

Coussa-Simon C. et al. Permanent Ge coordination change induced by pressure in $La_2O_3 \cdot B_2O_3 \cdot GeO_2$ glass. The American Ceramic Society, 2010, 93, 2726–2730.

Ohtaka O. et al. Pressure-induced sharp coordination change in liquid germanate. Physical Review Letters, 2004, 92, 155506.

# 4.4. Phosphates

## The crystal chemistry of natural and synthetic beryllophosphates

Frédéric Hatert[1,] *, Fabrice Dal Bo[1, 2] and Yannick Bruni[1]

[1] Laboratory of Mineralogy, University of Liège B18, B-4000 Liège, Belgium
[2] University of Oslo, National History Museum, Blindern, 0318 Oslo, Norway

* fhatert@uliege.be

Only 30 natural beryllophosphates are reported in the literature, occurring mainly in granitic pegmatites and resulting from the reaction of beryl with P-bearing hydrothermal solutions. The formation of these minerals is highly dependent upon the pH, temperature, availability of specific alkali cations, and Be:P ratio of the solution. Despite their low abundance, beryllophosphate minerals crystallize in many structure types, characterized by different polymerization degrees of the $BeO_4$-$PO_4$tetrahedra; these compounds form chain structures (fransoletite, väyrynenite), sheet structures (herderite, uralolite), framework structures (hurlbutite, babefphite, beryllonite), structures containing clusters of tetrahedra (gainesite), and even zeolite-type structures (pahasapaite). The crystal chemistry of the beryllophosphates is exciting, as their structures are similar to those of aluminosilicates and borosilicates; these analogies can be explained by the Pauling bond-valance rule. Indeed, the O atoms shared by Be and P in beryllosphosphates, by Al and Si in aluminosilicates, and by B and Si in borosilicates, receive exactly the same Pauling bond-valence sum of 1.75.

Dal Bo et al. [2014] performed extensive hydrothermal experiments starting from the $M^{2+}Be_2P_2O_8$ compositions ($M^{2+}$ = Ca, Sr, Pb, Ba), in order to better understand the crystal chemistry and the stability of beryllophosphates. Between 200 and 600°C, and under acidic or basic conditions, the synthesized compounds show the same structure types, without any phase transition. $CaBe_2P_2O_8$, $SrBe_2P_2O_8$, and $PbBe_2P_2O_8$ crystallize in space group $P2_1/c$ ($a$ = 7.81-8.09, $b$ = 8.80-9.02, and $c$ = 8.31-8.42 Å, β = 90.12-90.51°), and show a paracelsian-type structure composed of a framework of corner-sharing $BeO_4$and $PO_4$tetrahedra. These tetrahedra are assembled in four- and eight-membered rings showing the typical UUDD and DDUDUUDU patterns, respectively (U = tetrahedron pointing up, and D = tetrahedron pointing down). The $M^{2+}$ cations occur in distorted 7+3-coordinated polyhedra located in the eight-membered ring. $BaBe_2P_2O_8$ crystallizes in space group $P6/mmm$ ($a$ = 5.028(1) and $b$ = 7.466(1) Å), and its crystal structure consists of double layers of tetrahedra, which contain both Be and P in a 1:1 ratio. Inside the layers, the $(Be,P)O_4$tetrahedra form six-membered rings by sharing corners. The Ba atoms are located in very regular 12-coordinated polyhedra and connect two successive double layers. $CaBe_2P_2O_8$and $SrBe_2P_2O_8$are isostructural with the minerals hurlbutite and strontiohurlbutite, respectively [Rao et al., 2014], whereas $BaBe_2P_2O_8$ is the synthetic analogue of minjiangite [Rao et al., 2015].

These last years, three new Ba-bearing beryllophosphates were described in pegmatitic environments, showing exciting crystal structures. Minjiangite is a phyllophosphate, discovered in the Nanping No. 31 pegmatite, Fujian Province, China; it is the first example of a mineral showing a mixed occupancy of 0.5 P + 0.5 Be on the same tetrahedral site [Rao et al., 2015; Dal Bo et al., 2014]. Wilancookite, $(Ba,K,Na)_8(Ba,Li,\square)_6Be_{24}P_{24}O_{96}\cdot 32H_2O$, forms tiny rhombododecahedral crystals deposited on moraesite fibers from the Lavra Ponte do Piauí pegmatite, Minas Gerais, Brazil; its crystal structure ($I23$, $a$ = 13.5398(2) Å) is identical to those of pahasapaite and of synthetic zeolite RHO [Hatert et al., 2017]. More recently, a new species was submitted to the IMA-CNMNC under number 2019-011; it was discovered in the Vilatte-Haute pegmatite, Limousin, France, and shows the ideal formula $BaCa[Be_4P_4O_{16}]\cdot 6H_2O$. This beryllophosphate, which crystallizes in space group $P2_1/c$ ($a$ = 9.4958(4), $b$ = 13.6758(4), $c$ = 13.4696(4) Å, $\beta$ = 90.398(3)°), shows a zeolite framework identical to that of phillipsite; it is the third known zeolite-type phosphate.

The structural similarities between aluminosilicates and beryllophosphates would necessitate a classification of these mineral species into subclasses; such a classification scheme is elaborated herein.

Dal Bo F., Hatert F., Baijot M. Crystal chemistry of synthetic $M^{2+}Be_2P_2O_8$ ($M^{2+}$ = Ca, Sr, Pb, Ba) beryllophosphates. Canadian Mineralogist, 2014, 52, 337–350.

Hatert F., Philippo S., Ottolini L., Dal Bo F., Scholz R., Chaves M.L.S.C., Yang H., Downs R.T., Menezes Filho L.A.D. Wilancookite, $(Ba,K,Na)_8(Ba,Li,[])_6Be_{24}P_{24}O_{96}.32H_2O$, a new beryllophosphate with a zeolite framework. European Journal of Mineralogy, 2017, 29, 923–930.

Rao C., Hatert F., Wang R.C., Gu X.P., Dal Bo F., Dong C.W. Minjiangite, $BaBe_2(PO_4)_2$, a new mineral from Nanping No. 31 pegmatite, Fujian Province, southeastern China. Mineralogical Magazine, 2015, 79, 1195–1202.

Rao C., Wang R., Hatert F., Gu X., Ottolini L., Hu H., Dong C., Dal Bo F., Baijot M. Strontiohurlbutite, $SrBe_2(PO_4)_2$, a new mineral from Nanping No. 31 pegmatite, Fujian Province, Southeastern China. American Mineralogist, 2014, 99, 494–499.

**Polyfunctional materials based on β-$Ca_3(PO_4)_2$ structure type**

B.I. Lazoryak*, D.V. Deyneko, S.Y. Stefanovich, V.A. Morozov

Lomonosov Moscow State University, 119991 Moscow, Russia

* bilazoryak@gmail.com

The structural features of β-$Ca_3(PO_4)_2$ (five crystallographic sites of calcium cations, the absence of central symmetry) allow various hetero- and isomorphic measurements in a wide range of compositions without noticeable changes in structures. Such materials provide the preparation of laser crystals, ferroelectric and antiferroelectric materials with high nonlinear optical activity, solid electrolytes, phosphors, thermoluminescent dosimeters. In some cases, these properties are combined in the same compound, for example, ferroelectric, luminescent and nonlinear optical properties, ionic conductivity of two divalent cations, which allows obtaining polyfunctional materials. Doping into the system of rare earth cations $Ce^{3+}$, $Eu^{3+}$, $Dy^{3+}$, $Tb^{3+}$, $Tm^{3+}$, $Eu^{2+}$, $Eu^{2+}/Tb^{3+}$, $Tm^{3+}/Dy^{3+}$, $Eu^{2+}/Ce^{3+}$, $Tb^{3+}/Eu^{3+}$, $Eu^{2+}/Mn^{2+}$ allows you to obtain materials with luminescence in different regions of the visible spectrum. In addition, the combination of the cations allows to obtain more efficient single-phase phosphors with ideal optical properties. For tuning the luminescence spectra in the β-$Ca_3(PO_4)_2$ matrix, additional cations are also introduced, such as $Mg^{2+}$, $Zn^{2+}$, $Sr^{2+}$, which isovalent replace calcium cations in the structure. In some cases, such substitution can radically change the properties to the opposite. So, we have shown, that the substitution of calcium cations in the small octahedral *M*5 site for in $Ca_9R(PO_4)_7$ with the formation of $Ca_8MeR(PO_4)_7$ (Me = Mg, Zn; R = *REE*, Y) is accompanied by properties changing.

The report substantiates the criteria for the contribution of various physicochemical factors to the formation of dipole moments (ferroelectricity) of the β-$Ca_3(PO_4)_2$ structural type. It is shown that the increase in nonlinear optical activity is due to the following factors: a) the presence of cations with the presence of cations with a lone pair of electrons ($Pb^{2+}$, $Bi^{3+}$); b) the placement of different cations in sites *M*1 and *M*2, which are connected by a pseudo-center of symmetry and / or a different distribution of two or more cations in sites *M*1 and *M*2; c) a large difference in the distances between *M*1 - *M*3 and *M*2 - *M*3 sites (M3 is in the pseudo-center of symmetry); d) splitting the *M*4 into two / three subsites $M4_1$, $M4_2$ and $M4_3$; e) the splitting of the *M*3 into $M3_1$ and $M3_2$. All these factors increase the nonlinear optical activity when a radius of introduced cations is more than 0.8 Å are. It is shown that the nonlinear optical properties of β-$Ca_3(PO_4)_2$ structure type compounds can be changed by an order by means of isovalent replacement of $Ca^{2+}$ cations with $Pb^{2+}$ or larger $Ba^{2+}$ ions. A record value of nonlinear activity ($I_2\omega/I_2\omega(SiO_2)$ = 620, 50±5 μm) was obtained for $Ca_{5.6}Pb_{4.9}(VO_4)_7$. An increasing of $Pb^{2+}$ in the $Ca_{10.5-x}Pb_x(VO_4)_7$ system leads to an increase in the oxygen-oxygen distances in the polyhedra and thereby increases the conduction windows and, as a result, the ionic conductivity. The lead cations in the structure increases the ionic conductivity by an order (800 K) for $Ca_{5.6}Pb_{4.9}(VO_4)_7$. This value is a record for compounds with the β-$Ca_3(PO_4)_2$ structure. It was found that the introduction of divalent and trivalent ions into the structure is accompanied by a decreasing in the ferroelectric-paraelectric phase transition temperature. Such changes in the temperature of the phase transition are associated with an increasing in the unit cell volume and, easier rotation of the tetrahedra and mobility of cations in the structure. The phase transition temperature of an antiferroelectric-paraelectric is always lower than the transition temperature of the ferroelectric-paraelectric. Replacing the $Ca^{2+}$ by $Pb^{2+}$ in $Ca_3(VO_4)_2$ results in a 30-fold increasing in the intensity of second-harmonic generation (SHG) and a significant ($\Delta T$ = 608 deg.) decreasing in the ferroelectric-paraelectric phase transition temperature. This fact is due to an increasing in the *M*3 – O11 and *M*1 – O12 distances in the structure and, as a result, with a lighter rotation of the $V1O_4$ tetrahedron and splitting of the *M*4 site into three ($M4_1$, $M4_2$ and $M4_3$) and *M*3 into two ($M3_1$ and $M3_2$) subsites.

This research was supported by the Russian Science Foundation (Grant 16-13-10340).

**Cacoxenite and natrophosphate: crystal chemistry of very complex phosphates**

Margarita S. Avdontceva[1*], Maria G. Krzhizhanovskaya[1], Sergey V. Krivovichev[2]

[1]Institute of Earth Sciences, St. Petersburg State University, 199034 St.Petersburg, Russia
[2]Kola Science Center, Russian Academy of Sciences, 184209 Apatity, Russia

* m.avdontceva@spbu.ru

Information-based measures are important characteristics that provide useful information about structural complexity of minerals. According to the current classification, among 3949 minerals only about 100 could be attributed to the group of very complex structures [Krivovichev, 2013].

In our study, the sample of cacoxenite, $Fe^{3+}_{24}AlO_6(PO_4)_{17}(OH)_{12}\cdot nH_2O$, originated from the Těškov quarry, Bohemia, Czech Republic. It was studied by single-crystal X-ray diffraction analysis and high-temperature X-ray diffraction (25–200 °C). Synthetic natrophosphate, $Na_7(PO_4)_2F\cdot 19H_2O$, was prepared by evaporation from aqueous solutions of sodium phosphate and sodium fluoride at 25°C, whereas natural natrophosphate was taken from the microcline-pectolite-sodalite-aegirine vein from the Mt. Koashva, Khibiny alkaline massif [Yakovenchuk et al., 2005]. Natrophosphate and its synthetic analogue were studied by single-crystal X-ray diffraction at room temperature and at -173 °C for the refinement of hydrogen atoms positions.

The crystal structure of cacoxenite was refined to $R_1$ = 0.061 ($wR_2$= 0.154). The mineral is hexagonal, $P6_3/m$, $a$ = 27.4904(5), $b$ = 10.5307(2) Å, $V$ = 6892.1(2) Å$^3$. The crystal structure is based upon a three-dimensional framework with wide channels running parallel to the $c$ axis. The channels are occupied by $H_2O$ molecules. Their diameter exceeds 14 Å. The framework consists of corner-sharing $AlO_6$, $(Fe_{0.76}Al_{0.24})O_6$ octahedra, $AlO_5$ trigonal bipyramids and $PO_4$ tetrahedra. The crystal structure of cacoxenite is stable up to 190 °C. The thermal expansion is anisotropic and anisotropy increases with temperature. The direction of strongest thermal expansion is parallel to the $c$ axis.

Natural and synthetic natrophosphates are cubic, $Fd$-3$c$, $a$ = 27.9777(7) Å (synthetic), $a$ = 27.6241(1) Å (natural). The structure is based upon isolated polycationic complexes consisting of six corner-sharing $NaF(OH_2)_5$ octahedra sharing common fluorine vertex. The complexes could also be regarded as based upon F-centered octahedra $Na_6F$. The complexes form hydrogen bonds to $PO_4$ and $AO_4$ tetrahedra, where A site is statistically occupied by Na and $H_2O$.

The information-based structural complexity parameters were calculated for natrophosphate and cacoxenite according to the procedure outlined in [Krivovichev, 2013]. Both structures are very complex with $I_{G,total}$ more than 2000 bits per unit cell (2495.481 for cacoxenite, 2600.990 for natrophosphate and 2352.383 for synthetic analogue).

This work was supported by Russian Science Foundation (grant № 19-17-00038).

Krivovichev S.V. Structural complexity of minerals: information storage and processing in the mineral world. Mineral. Mag., 2013, 77, 275–326.

Yakovenchuk V.N., Ivanyuk G.Yu., Pakhomovsky Ya.A. & Men'shikov Yu.P. (2005): Khibiny. Laplandia Minerals, 2005, Apatity, Russia.

**Anapaite from the Kerch Oolitic Iron Ores: Geochemical Signals and Environment Marker**

Anna V. Nekipelova[1*], Ella V. Sokol[1], Dmitriy Artemyev[2], Olga A. Kozmenko[1], Svetlana N. Kokh[1]

[1]Sobolev Institute of Geology and Mineralogy SB RAS, 630090 Novosibirsk, Russia
[2]Institute of Mineralogy UrB RAS, 456317 Miass, Russia

[*]nekipelova@igm.nsc.ru

Lacustrine and estuary sediments are excellent archives of past environments but their primary geochemical signals are frequently changed by diagenetic and post-depositional alteration. Rare Fe and Ca-Fe phosphates (vivianite, anapaite, and mitridatite) are useful mineralogical traces of these secondary processes [Stamatakis, Koukouzas, 2001]. During the Cimmerian (5.5–3.2 Ma) brackish-marine and lacustrine environments prevailed in the Eastern Paratethys. Specific Fe-rich Cimmerian sediments known as the Kerch oolitic iron ores include abundant Fe and Ca-Fe phosphates [Chukanov, 2005]. Precise ICP-MS, LAICP-MS, SEM, microprobe and Rietveld XRD analyses of the Kerch iron ores (the basal member of the Kamysh-Burun deposit) provided constraints on the composition specificity of individual lithologies and minerals. The oolites are mainly composed of $Fe^{3+}$ (oxy)hydroxides (goethite-hydrogoethite and amorphous matter) and contain P, V, Mn, Co, Ni, Zn, As, Sb, Ba, and Pb (average concentrations from 2 to 12 times as high as the upper crustal average). Excepting P, they do not form separate phases and are hosted by $Fe^{3+}$ (oxy)hydroxides. Sulfur and Ba are mainly stored in barite (Ba-S $R^2 \geq 0.95$), and Mn and V in Fe-Mn-Ca carbonate cementation (V-Mn $R^2 \geq 0.87$). Similar REE patterns and strong positive goethite-Σ(REE+Y) correlation ($R^2 = 0.85$) reveal their predominant sorption on the hydrogenic $Fe^{3+}$ (oxy)hydroxides. The lack of Y minimum is due to the predominance of Fe-Mn-Ca authigenic carbonates instead of biogenic $CaCO_3$. All samples are enriched in MREE and have low Y/Ho (~ 17) and La/Yb (13-32) ratios typical for fine-grained sediments. The lack of negative Ce and Dy anomalies indicate that primary REE accumulation in $Fe^{3+}$ ores is not controlled by P-rich matter (proteins, teeth and bone fragments).

At the deep levels of the Kerch oolitic iron ore strata clots and leaf replacements of mollusks are mainly composed of vivianite. Anapaite ($Ca_2Fe^{2+}(PO_4)_2 \cdot 8H_2O$) was found in the current near surface level (shallower burial depth) as dull green veins 1-0.5 cm thick, oriented sub-parallel to the oolitic ore bedding. In spite of the potential possibility of anapaite structure to incorporate wide ranges of impurities, its perfect crystals (n =85) have stoichiometric composition with low content of uniformly distributed impurities (in ppm): Mg – 3230; Mn – 1480; Si – 1250; S – 464; Sr – 400; Na – 232; Y – 17.0; Se – 3.5; As – 0.61; U – 0.13. Anapaite is also REE-depleted relative to the upper crustal average values. The REE patterns are gently sloped with HREE enrichment, negative Y and positive Ce anomalies. Its geochemical fingerprints allow one to conclude that anapaite crystallized in reducing (Eh 0.3-2.5) environment from diluted solutions with high $Fe^{2+}/Fe^{3+}$ and $Ca^{2+}/Fe^{2+}$ ratios, which are rather ground than basinal water [Stamatakis, Koukouzas, 2001]. Thus, it is not plausible to assume direct precipitation of anapaite in the lacustrine basin. Anapaite growth marks episode of Fe-rich sedimentary strata uplifting and percolation of Ca-rich ground water into its upper fractured part. At the same time this sedimentary sequence was not totally outcropped, because of anapaite was not converted into mitridatite [$(Ca_2Fe_2(PO_4)_2(OH)_2 \cdot 8H_2O)$] or $Fe^{3+}$ (oxi)hydroxides.

The study was supported by grant 17-17-01056 from the Russian Science Foundation.

Chukanov N.V. Kerch iron-ore basin. Mineralogical Almanac, 2005, 8.

Stamatakis M.G., Koukouzas N.K. The occurrence of phosphate minerals in lacustrine clayey diatomite deposits, Thessaly, Central Greece. Sedimentary Geology, 2001, 139, 33–47.

**Transformation of the spectroscopy properties during the phase transition in phosphates $Ca_{9-x}Zn_xDy(PO_4)_7$ related to mineral whitlockite family**

Dina V. Deyneko*, Ivan V. Nikiforov, Insaaf Duskaev and Bogdan I. Lazoryak

Lomonosov Moscow State University, 119991 Moscow, Russia

* deynekomsu@gmail.com

Lanthanide luminescence is at the heart of applications as diverse as lighting [Bünzli, 2017], lasers [Goldner at al., 2015], sensors [Brites at al., 2016]. The corresponding emitting transitions occur either as allowed d–f transitions or as electronic rearrangements within the 4f shell (f–f transitions). Inter-configurational d–f transitions are more energetic and more intense than f–f transitions but are observed only for several ions. Electric-dipole (ed) f–f transitions are forbidden by selection rule, while magnetic-dipole f–f transitions are allowed but faint. The f–f transitions are sharp, and the corresponding excited states have long lifetimes, two decisive advantages that make Ln-containing compounds unique materials and probes.

The calcium phosphate with whitlockite-type structure (space group *R*-3*c*) was used as a host matrix. There are several advantages of β-$Ca_3(PO_4)_2$ lanthanide substitution such as no luminescence quenching, good stability, high intensity of emission.

$Dy^{3+}$dopedphosphates are a kind of full-color phosphors that can be excited by an UV LED chips. $Dy^{3+}$ is of great importance among the rare earth ions because of its 4f–4f transitions which lead to blue, yellow and red emission. The luminescence lines are located in the regions of 470–500, 570–600, and 650–680 nm due to the optical transitions $^4F_{9/2} \rightarrow {}^6H_{15/2}$, $^4F_{9/2} \rightarrow {}^6H_{13/2}$ and $^4F_{9/2} \rightarrow {}^6H_{11/2}$ of $Dy^{3+}$, respectively. Besides, it is well known that the emission light is different in color. This depends on whether the $Dy^{3+}$ ions are located at the high-symmetry sites with inversion centers or the low-symmetry without inversion centers [Yu at al. 2002].

The whitlockite-type structure phosphates $Ca_{9-x}Zn_xDy(PO_4)_7$ $0 < x < 1$ were prepared by standard solid-state reaction from stoichiometric mixtures of $CaHPO_4 \cdot 2H_2O$ (99.9%), $CaCO_3$ (99.9%), ZnO (99.99%) and $Dy_2O_3$ (99.9%). Synthesis was carried out in the air for 50 hours with an intermediate mixing.

The degradation of polar structure and ferroelectric properties is observed during substitution in $Ca_{9-x}Zn_xDy(PO_4)_7$ solid solution. The limit of $Zn^{2+}$ incorporation was found at $x = 1$. The typical emission of $Dy^{3+}$ ions was observed only for $Ca_9Dy(PO_4)_7$. The host matrix emission was admitted during $Ca^{2+} \rightarrow Zn^{2+}$ substitution, and its magnitude was rising up to existence limit of solid solution. Also, the intensity distribution of optical transitions was detected. Such behavior, apparently, is related with changes of coordination environment of emitting centers. The influence of crystal symmetry on the optical properties is discussed.

The work is supported by the Russian Science Foundation (Grant 16-13-10340). D. V. D. is grateful for Foundation of the President of the Russian Federation (MK-3502.2018.5).

Brites C.D.S., Millan A., Carlos L.D. Lanthanides in Luminescent Thermometry. Handbook on the Physics and Chemistry of Rare Earths, 2016, 49, 339–409.

Bünzli J-C. G. Rising Stars in Science and Technology: Luminescent Lanthanide Materials. Eur. J. Inorg. Chem., 2017, 5058–5063.

Goldner P., Ferrier A., Guillot-Noël O. Rare-Earth Doped Crystal for Quantum Information Processing, Handbook on the Physics and Chemistry of Rare Earths., 2015, 46 (267), 1–78.

Yu M., Lin J., Wang Z., Fu J., Wang S., Zhang H.J., Han Y.C., Chem. Mater., 2002, 14, 2224–2231.

**Crystal chemistry and structural complexity of transition metal diphosphates with alkaline cations**

Anastasia P. Chernyatieva[1], Sergey V. Krivovichev[1,2], Vadim M. Kovrugin[1,3]

[1]Saint-Petersburg State University, 199034 St. Petersburg Russia
[2]Kola Science Centre of Russian Academy of Sciences, 184209 Apatity, Russia
[3]ICMCB-CNRS, UMR5026, Université de Bordeaux, 33600 Pessac Cedex, France

chernyatieva@mail.ru

The chemistry of diphosphate (or pyrophosphate) compounds is developing over a long period of time. This class of materials attracts considerable scientific interest due to its fascinating structural and physical-chemical properties. The diphosphates are known to adopt various structural types depending on the ionic radii of the cations.

The research studies on minerals with mixed anion radicals have a significant fundamental aspect in revealing the principles of substance structural organization in chemically complicated natural systems and in broadening our knowledge about structural chemical variety of the Kingdom of Minerals. Besides, such research works are of great importance and serious practical interest since phosphates are considered to be one of the most insoluble and stable materials. Investigation of minerals and compounds with caged mixed anion radicals, thus, is of interest in terms of elaboration of matrices for immobilization of radionuclides, radioactive cesium in particular. Phosphates of transition metals are of great research interest both related to their multiple applications, and their wide structural chemical diversity [Durif, 1995; Mannasova et al., 2016].

In the present work, we show rich crystal chemistry and provide estimated data of informational complexity of known diphosphates with alkaline cations. In the crystal structures of these compounds, mixed anion radicals contain bivalent or trivalent cations of transition metals [Kovrugin et al., 2019]. The generalized data is provided, where we emphasize main crystallographic characteristics and structural features of $A_2B^{II}(P_2O_7)$ и $AB^{III}(P_2O_7)$ compounds as well as their structural complexity evaluation. All the compounds are described and considered according to the dimensionality of their basic structural complexes (1D: chain, 2D: layer and 3D: open framework). The revealed diversity of the examined crystal structures of diphosphates is determined by different coordination of bi-and trivalent cations of transition metals (square, tetrahedron, and octahedron) on the one hand, and by the size of alkaline cations on the other.

Durif A. Crystal chemistry of condensed phosphates. Plenum Press: New York. 1995.

Kovrugin V.M., Chernyatieva A.P, Krivovichev S.V. Crystal chemistry and structural complexity of alkaline-based diphosphates with $A_xM^{2+/3+}P_2O_7$ formula. Z. Kristallogr., 2019 (submitted).

Mannasova A.A., Chernyatieva A.P., Krivovichev S.V. $Cs_2CuP_2O_7$, a novel low-density open-framework structure based upon an augmented diamond net. Z. Kristallogr., 2016, 231, 65–70.

**Products of hydrothermal synthesis in phosphate systems with alkaline and transition metals and the $K_2Mn_3(H_2O)_2[P_2O_7]_2$ crystal structure**

Ekaterina M. Kochetkova*, Galina V. Kiriukhina, Olga V. Yakubovich

Moscow State University, 119991 Moscow, Russia

*kochetkova.katharine@yandex.ru

Hydrothermal and pegmatite deposits are well known for a variety of mineral species that are owed to the wide chemical composition of gases and solutions necessary for the formation of primary minerals and their recrystallization. The iron and manganese orthophosphates are the most common among the primary pegmatite phosphates. These minerals are closely related to each other: the process of separation of Mn from Fe takes place at the pegmatite stages of the magmatic differentiation. A large variety of phosphates of iron and manganese are related to the possibility of $Fe^{2+}$ to $Fe^{3+}$ and $Mn^{2+}$ to $Mn^{3+}$ oxidation.This process begins with the oxidation of iron, and follows by the oxidation of manganese.

We present here results of crystallization in complex multicomponent systems as close as possible to natural low-temperature hydrotherms ($T$ = 270–280 °C and $P$ = 90–100 atm.): $M_2O$ – $MeO/(Me_2O_3)$ – $P_2O_5/V_2O_5$ – $Z$ – $H_2O$, where $M^+$ are the alkali metal ions $Li^+$, $Na^+$, $K^+$, $Rb^+$, $Cs^+$ and ammonium $NH_4^+$; *Me* represents transition metal atoms Mn, Zn, Ni, Co, Fe, Cu and aluminum Al; and Z identifies anions $Cl^-$, $F^-$, $CO_3^{2-}$, $NO_3^-$, boric anhydride $B_2O_3$, or silicic acid $nSiO_2 \cdot mH_2O$, which work as mineralizers and regulate the pH value of the medium.

The crystallization products were examined under a binocular microscope and separated into phases according to morphological features. To determine the chemical composition of the synthesized phases, a semi-quantitative X-ray spectral analysis was performed on a scanning electron microscope. X-ray diffraction of powder and single-crystal samples was used to determine the symmetry and the unit cell parameters of the compounds. Based on the achieved data, the phases were identified using the ICSD crystal structure database.

As a result of 30 experiments, structural analogues of minerals boracite, leucite, milarite, triphylite-lithiophilite series, triploidite, alluaudite, lithiophosphate and berlinite were identified. We also "cooked": vanadyl-vanadate $(NH_4)_2(VO)(V_2O_7)$, two vanadyl-phosphates $Na(VO)PO_4$ and $(K,NH_4)(VO)PO_4$, borophosphate $Cs_2(Ni,Fe)_3(H_2O)_2[B_4P_6O_{24}(OH)_2]$, several transition and alkali metal orthophosphates $LiZnPO_4$, $NaZnPO_4$, $KCoPO_4$ and two pyrophosphate $Mn_2P_2O_7$ and $(Mn,Co)_2P_2O_7(H_2O)_2$. In some experiments, the mineralizers reacted with the main components of the mixture and became part of the crystals, namely CuBr, LiF, $Pb_2B_5O_9Br$. It is important to note that three compounds were obtained for the first time, namely, a synthetic potassium variety of the mineral manaksite, $K_2Mn[Si_4O_{10}]$, and two aqueous manganese and potassium phosphates $KMnAl_2(PO_4)_3(H_2O)_2$ and $K_2Mn_3(H_2O)_2[P_2O_7]$.

The last of the mentioned phases, $K_2Mn_3(H_2O)_2[P_2O_7]_2$ ($a$ = 9.1944(1), $b$ = 8.3134(1), $c$ = 9.3798(2) Å, $\beta$ = 98.924(1)°, space group $P2_1/c$, $Z$ = 2, $D_x$ = 2.94 g/cm$^3$) has been investigated using single-crystal X-ray diffraction (Xcalibur-S-CCD diffractometer, $R_{hkl}$ = 0.0233) in order to solve and refine its crystal structure, including positions of hydrogen atoms.

Funding for this research was provided by the Russian Foundation for Basic Research (grants No. 18-35-00623 and No. 18-03-00908).

**Ti-bearing hydroxyapatites: synthesis, crystal chemistry, properties**

Anatoliy V. Korneev[1,*], Olga V. Frank-Kamenetskaya[1], Maria A. Kuzmina[1], Vladimir K. Ryabchuk[1], Elena V. Sturm[2]

[1] Saint-Petersburg State University, 199034 St Petersburg, Russia
[2]University of Konstanz, 78464 Konstanz, Germany

* a_v_korneev@list.ru

According to [Wakamura et al., 2003; Tsukada et al., 2011], Ti-containing hydroxyapatites have photocatalytic activity comparable to activity of anatase. However, there are doubts if this activity is related to hydroxyapatite or to small concentrations of $TiO_2$ in precipitate, which can be not detected by X-ray diffraction. Also, it is needed refine the forms of interaction of Ti ions with hydroxyapatite.

Two series of hydroxyapatites were synthesized from solutions containing Ti. The 1st series was precipitated from $CaNO_3$, $(NH_4)_2HPO_4$ and $TiCl_3$ solutions, the 2nd series was precipitated from $Ca(OH)_2$, $H_3PO_4$ and $C_{12}H_{28}O_4Ti$ solutions and was annealed at 400°C for 2 hours. Synthesized precipitates were studied with a set of methods (X-ray powder diffraction, Raman spectroscopy, SEM, EDX, TEM, diffuse reflection spectroscopy) in order to confirm that precipitates are monophasic, make sure that titanium ions entered into apatite and estimate its photocatalytic properties.

X-ray phase analysis confirmed that hydroxyapatite was formed in both series of precipitates. Any other phases weren't detected. We obtained significant changes in lattice parameters relatively stoichiometric hydroxyapatite: in 1st series parameter a gets lower with growth of Ti/Ca ratio from 0 to 0.12 and then increases, which can mean that titanium ions enter at both calcium and phosphorous positions; in 2nd series parameter a is dramatically lower than in stoichiometric hydroxyapatite. Clarifying the nature of these changes is now in progress.

Raman spectroscopy did not detect $TiO_2$ in all samples of 1st and 2nd series. EDX analysis detected another phase (presumably anatase or amorphous $TiO_2$) in several samples of both series. In the 1st series the formation of anatase starts at Ti/Ca in solution = 0.12. According to TEM data samples with high Ti/Ca ratio contain crystalline anatase at the surface of hydroxyapatite crystals. In the 2nd series the formation of anatase starts at Ti/Ca in solution = 0,05. Maximum Ti/Ca ratio in apatite is reached at Ti/Ca in the solution = 0.56 and equals 0.13 in 1st series and 0.25 in 2nd. Moreover, in 2nd series titanium in precipitate is spread regularly, while in the 1nd it is spread irregularly and there are zones don't contain titanium at all. Therefore, second method of synthesis is preferable to the first.

Diffuse reflection spectra of the samples change their shape and become more similar to anatase spectra (KRONOClean 7050) with increase of Ti/Ca in apatite. Band gap energy estimated by Tauc method using Kubelka-Munk transformation of experimental diffuse reflectance spectra $R(\lambda)$ ranges from 4.34 to 3.25 eV and is less than band gap energy of pure hydroapatite (Eg = 6 eV).

The obtained data confirm that Ti-containing hydroxyapatites can show photocatalytic activity which depends on the entrance of titanium into apatite. The next step of our work is estimating their photocatalytic properties through decomposition of organics.

The research was supported by RFBR grant №19-55-45019 ind_a and following resource centers of SPBU: Geo-Environmental Research and Modelling (GEOMODEL), X-ray Diffraction Studies, Nanophotonics, Optical and Laser Materials Research, Microscopy and Microanalysis

Tsukada M., Wakamura M., Yoshida N., and Watanabe T. Band gap and photocatalytic properties of Ti-substituted hydroxyapatite: Comparison with anatase-$TiO_2$, J. Mol. Catal. A: Chem., 2011, 338, 18–23.

Wakamura M., Hashimoto K., Watanabe T. Photocatalysis by Calcium Hydroxyapatite Modified with Ti(IV): Albumin Decomposition and Bactericidal Effect. Langmuir, 2003, 19, 3428–3431.

**Crystal structure of a novel $CsBP_2O_6(OH)_2$ borophosphate and its relationship to the structures of minerals: fransoletite and parafransoletite**

Polina V. Krikunova*, Larisa V. Shvanskaya

M.V. Lomonosov Moscow State University, 119991 Moscow, Russia

*polinka3158@gmail.com

The colorless columnar crystals of a novel cesium borophosphate, $CsBP_2O_6(OH)_2$, has been synthesized under mild hydrothermal condition in $CsH_2PO_4$-$MnCl_2$-$H_3BO_3$-$H_2O$ system and structurally characterized by single-crystal X-ray diffraction. The compound crystallizes in the monoclinic system, space group *I*2/*a* with the unit cell parameters: $a$ = 14.5329(3) Å, $b$ = 7.4869(2) Å, $c$ = 13.4002(3) Å, $V$ = 1458.03(6) Å3, Z = 8. The crystal structure was solved by direct methods and refined by full-matrix least-squares method using the program SHELX [Sheldrick, 2015] to an $R1$ = 0.034 and $S$ = 1.13 for 1860 observed reflections with $I>2\sigma(I)$. Semi-quantitative X-ray spectral analysis (Jeol JSM-6480LV, energy-dispersive diffraction spectrometer Oxford X-MaxN) confirmed the presence of oxygen, phosphorous and cesium atoms.

The main structural features of the title borophosphate are four-ring chains composed of vertex sharing [$PO_4$] and [$BO_4$] tetrahedra. These chains are aligned along [010] direction and are connected by hydrogen bond interactions into three-dimensional framework. The $Cs^+$ cations occupy the space between the chains. Similar borophosphate chains were observed previously in the structure of $(NH_3CH_2CH_2NH_3)_2B_2P_4O_{14}(OH)_2$ compound obtained by solvothermal method [Shi et al., 2003]. It is interesting also that topologically identical 1*D* berillophosphate fragments are the basis of the crystal structures of fransoletite and parafransoletite [Kampf, 1992]. They are dimorphs with the chemical formula $Ca_3Be_2(PO_4)_2(PO_3OH)_2 \cdot 4H_2O$. The revealed topological similarity of boro- and berillophosphate chains is one more example demonstrating the tendency on the existence of phosphate archetypes for borophosphate compounds [Yakubovich et al., 2011].

The work was supported by the RFBR (grant №18-03-00908).

Kampf A.R. Beryllophosphate chains in the structures of fransoletite, parafransoletite, and ehrleite and some general comments on beryllophosphate linkages. American Mineralogist, 1992, 77, 848–856.

Sheldrick G.M. Crystal structure refinement with SHELXL. Acta Crystallographica Section C, 2015, 71, 3–8.

Sheldrick G.M. SHELXT – Integrated space-group and crystal structure determination. Acta Crystallographica Section A, 2015, 71, 3–8.

Shi H., Shan Y., He M., Liu Y. Impetus for solvothermal synthesis technique: synthesis and structure of a novel 1-D borophopshate using ionic liquid as medium. Journal of Solid State Chemistry, 2003, 176, 33–36.

Yakubovich O., Massa W., Steel I., Dimitrova O. Genetic aspects of borophosphate crystal chemistry. Acta Crystallographica A, 2011, 67, C127.

# 4.5. Sulfates

## Fumarolic Sulfate Minerals: New Data and Possible Applications

Oleg I. Siidra[1,2]

[1]Department of Crystallography, St. Petersburg State University, 199034 St. Petersburg, Russia
[2] Kola Science Center, Russian Academy of Sciences, 184200 Apatity, Murmansk Region, Russia

o.siidra@spbu.ru

Minerals with sulfate anions are one of the most diverse classes. More than 400 minerals containing sulfate anion are known to date. Most of known anhydrous sulfates have relatively simple chemical composition and structural architecture. In contrast, hydrated sulfate minerals have more complex compositions and structures. Most of the anhydrous sulfates are highly soluble compounds and unstable in humid atmosphere, namely, sulfates of alkali and alkaline earth metals. Under terrestrial conditions, hydrated sulfate minerals are common in various geological environments. Whereas the anhydrous sulfate minerals of alkali, alkaline earth and transition metals form almost exclusively in active fumaroles.

The fumaroles of Tolbachik volcano are a unique mineralogical locality with a large number of endemic mineral species. The variety of sulfate minerals observed in Tolbachik fumaroles is impressive. Since 2014, we have discovered 11 new mineral species with sulfate anions of fumarolic origin. Many of the fumarolic minerals demonstrate unique structure types with unprecedented and complex architectures and have no synthetic analogues. Several examples of the recently obtained synthetic sulfate materials inspired by Nature will be discussed.

This work was financially supported by the Russian Science Foundation through the grant 16-17-10085.

## Thermal behavior of new mineral belomarinaite ($KNaSO_4$)

Olga U. Saprykina[1,2], Stanislav K. Filatov[1,2,*], and Rimma S. Bubnova[2]

[1] Institute of Earth Sciences, Saint Petersburg State University, 199034 Saint Petersburg, Russia
[2] Institute of Silicate Chemistry of the Russian Academy of Sciences, 199034 Saint Petersburg, Russia

* filatov.stanislav@gmail.com

Belomarinaite, ideally $KNaSO_4$, is a new sulphate mineral. Belomarinaite was discovered on the Toludskoe lava field which was formed during Tolbachik Fissure eruption in 2012–2013. For the first time, the thermal behavior of a new mineral belomarinaite $KNaSO_4$ [Filatov et al., 2017] was studied on a natural sample and its synthetic analogue in the range of 30–800 °C. High-temperature X-ray diffraction studies were conducted using a Rigaku Ultima IV diffractometer equipped with a high-temperature accessory, $Cu_{k\alpha}$, radiation, the temperature was varied from 25 °C to 800 °C, the temperature step was 10 °C.

The mineral is stable up to a temperature of 475±10 °C, at which it has a polymorphic transformation into a high-temperature polymorphic modification ($P6_3/mmc$), stable up to 800 °C (Figure). The thermal expansion of both modifications is sharply anisotropic, and in the case of the high-temperature phase it is also variable as a function of temperature - the dependence of the parameter *a* has a U-shape with a minimum at $t$ = 660 °C. The volumetric expansion of modifications varies in the intervals of their existence for the low-temperature phase from 80 to 200 ($10^{-6}$ °C$^{-1}$), for the high-temperature phase, from 350 to 300 ($10^{-6}$ °C$^{-1}$). That is, on average, the expansion of the high-temperature modification increases by a factor of 2-3 relative to the expansion of the low-temperature phase, the main increase is in the parameter *c* and is determined, apparently, by restructuring the structure along this direction.

The investigations were performed using the equipment of the Saint-Petersburg State University Resource Center «X-ray diffraction studies». The authors express their gratitude to M. G. Krzhizhanovskaya, who made our experimental work in this Center easier. The authors also appreciate the financial support provided by the Russian Fund for Basic Research (project 18-29-12106).

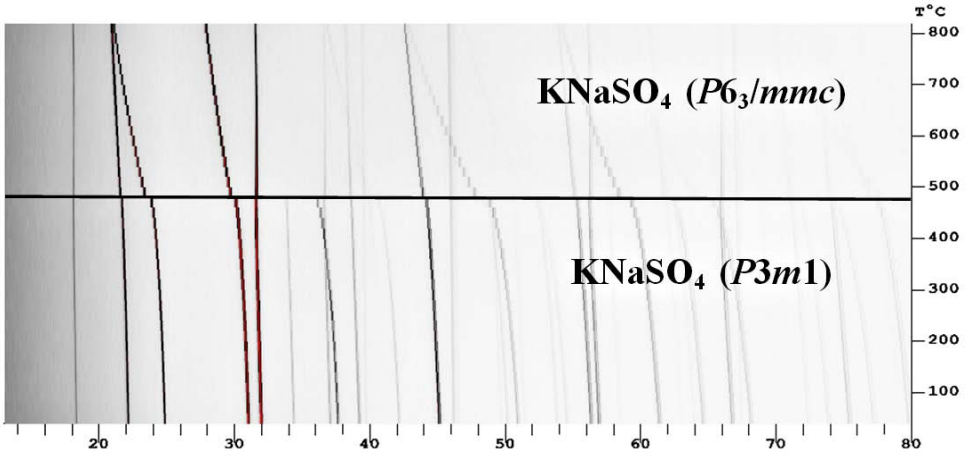


Figure. Thermal phase transformation upon cooling in a belomarinaite. The horizontal line indicates the phase transition temperature.

Filatov S.K., Shablinskii A.P., Vergasova L. P., Saprikina O.Y., Bubnova R.S., Moskaleva S.V. and Belonsov A.B. Belomarinaite. European Journal of Mineralogy, 2017, 43, 653.

**The crystal structure of a new microporous mineral kruijenite, $Ca_4Al_4(SO_4)F_2(OH)_{16}\cdot 2H_2O$**

Natalia V. Zubkova[1,*], Nikita V. Chukanov[2], Günter Blass[3], Igor V. Pekov[1], Dmitry A. Varlamov[4], Dmitry A. Ksenofontov[1] and Dmitry Yu. Pushcharovsky[1]

[1] Faculty of Geology, Moscow State University, 119991 Moscow, Russia
[2]Institute of Chemical Physics Problems, RAS, 142432 Chernogolovka, Moscow Region, Russia
[3]Merzbachstrasse 6, D-52249, Eschweiler, Germany
[4]Institute of Experimental Mineralogy RAS, 142432 Chernogolovka, Moscow Region, Russia

* n.v.zubkova@gmail.com

The crystal structure of the new mineral kruijenite, ideally $Ca_4Al_4(SO_4)F_2(OH)_{16}\cdot 2H_2O$, found in a metasomatically altered calcic xenolith from tephra of the Feuerberg paleovolcano (Eifel paleovolcanic region, Rhineland-Palatinate, Germany) [Chukanov et al., 2019] is presented. Kruijenite is tetragonal, sp. gr. *P*4/*ncc*, $a$ = 12.9299(4), $c$ = 5.2791(3) Å, $V$ = 882.57(6) Å$^3$, $Z$ = 2. The structure of kruijenite (Figure) is unique: the mineral represents a novel structure type. The structure is based on a microporous pseudo-framework built by $Al(OH)_6$ octahedra and $CaF_2(OH)_6$ eight-fold polyhedra. The Al-centered octahedra share edges to form zig-zag chains running along the *c* axis. The Ca-centered polyhedra share the F–F edge to form dimers; adjacent dimers are also connected *via* common edges thus building columns along [001]. Each column is connected with four octahedral chains of Al-centered octahedra. There are two crystallographically non-equivalent O sites and one F site which participate in the formation of the pseudo-framework. Both O atoms belong to OH-groups. All H sites of OH groups are located inside the wide channels (with approximate width of 7.4 Å) running along the *c* axis. These channels contain $H_2O$ molecules and significantly distorted $SO_4$ tetrahedra. The $SO_4$ tetrahedra and $H_2O$ molecules located in the channels are connected with the pseudo-framework *via* the system of H-bonds. The most interesting structural feature of kruijenite is a positively charged pseudo-framework hosting sulfate anions and $H_2O$ molecules, which is an indication of possible anion-exchange properties (in particular, the ability to accumulate sulfate anions) of compounds belonging to this structure type. This assumption is confirmed by the absence in association with kruijenite of ettringite-group members which are in general very typical for hydrothermally altered calcic xenoliths in Eifel volcanic rocks.

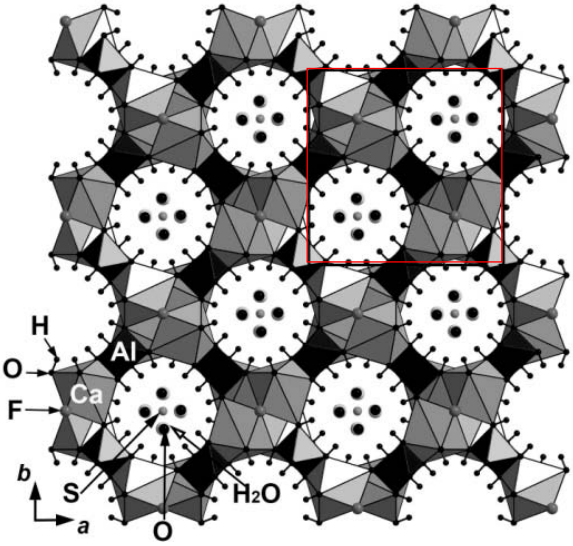


Figure. The crystal structure of kruijenite projected along the *c* axis. The unit cell is outlined.

This work was financially supported by the RFBR, grant 18-29-12007-mk.

Chukanov N.V., Zubkova N.V., Blass G., Pekov I.V., Varlamov D.A., Belakovskiy D.I., Ksenofontov D.A., Britvin S.N., Pushcharovsky D.Yu. Kruijenite, $Ca_4Al_4(SO_4)F_2(OH)_{16}\cdot 2H_2O$, a new mineral with microporous structure from the Eifel paleovolcanic region, Germany. Mineralogy and Petrology, 2019, 113, 229–236.

## Thermal behavior of kainite, ideally $KMg(SO_4)Cl \cdot 2.75H_2O$

Eugenia A. Lukina[1*], Anastasiia A. Meshcheriakova[1], Oleg I. Siidra[1,2], Igor V. Pekov[3]

[1]Department of Crystallography, St. Petersburg State University, 199034 St. Petersburg, Russia
[2] Kola Science Center, Russian Academy of Sciences, 184200 Apatity, Murmansk Region, Russia
[3]Faculty of Geology, Moscow State University, 119991 Moscow, Russia

*eugenialukina@mail.ru

Kainite, $KMg(SO_4)Cl \cdot 2.75H_2O$, is a sulfate mineral common in salt-bearing rocks enriched with soluble sulfates. Colorless transparent grains of kainite from Wilhelmshall deposit, Saxony-Anhalt, Germany were used in this study. Crystal structure of kainite was refined using Bruker Smart Apex II single crystal X-ray diffractometer: *C*2/*m*, $a$ = 19.763(5), $b$ = 16.250(5), $c$ = 9.537(3), $\beta$ = 94.977(7), $R_1$ = 0.03.

Low- and high-temperature powder X-ray diffraction studies of kainite were performed in the temperature range -150 – + 200 °C with a 5 °C step using Rigaku Ultima IV diffractometer.

Upon heating, the unit cell is expanding along all crystallographic axes. Temperature dependence of cell parameters of kainite can be described by the following linear functions ($T$ is a temperature):

$$a_t = 19.7379(9) + 0.414(1) \times 10^{-3}T$$
$$b_t = 16.2297(9) + 0.382(1) \times 10^{-3}T$$
$$c_t = 9.5322(5) + 0.268(6) \times 10^{-3}T$$
$$\beta_t = 94.928(4) + 0.44(5) \times 10^{-3}T$$
$$V_t = 3042.2(2) + 217(3) \times 10^{-3}T.$$

Thermal expansion of kainite is anisotropic. Thermal expansion of the crystal structure of kainite along $a$ and $b$ axes is greater than that along the $c$ axis. Kainite is stable up to 55 °C. At 55–65°C the possible phase transition occurs. At 70°C kainite almost completely transforms into the mixture of langbeinite, $K_2Mg_2(SO_4)_3$, carnallite, $KMgCl_3 \cdot 6H_2O$, hexahydrite, $MgSO_4 \cdot 6H_2O$, sylvine, KCl. The mixture of all compounds decays at 130°C.

This work was financially supported by the Russian Science Foundation through the grant 16-17-10085. Technical support by the SPbSU X-ray Diffraction Resource Center is gratefully acknowledged.

**Typomorphism of halotrichite-group minerals from volcanic exhalation (Kamchatka, Russia)**

M.A. Nazarova

Institute of Volcanology and Seismology FEB RAS, 683006 Petropavlovsk-Kamchatsky, Russia

nazarovamar@mail.ru

The typomorphism of halotrichite from different volcanic-related environments was investigated in this study. Samples were collected at: Dachnie geothermal field (Mutnovsky volcano); steaming ground of the First cone, Large Tolbachik fissure eruption (Tolbachik volcano); North-Kambalny geothermal field (the Kambalny volcanic ridge) and East-Pauzhetka geothermal fields (Pauzhetka village) and landslide area, which formed on the Zhupanovsky volcano after the eruption in 2015. The samples were represented by efflorescence originated at temperature around 100 ºC.

The samples were investigated using electron microscopy, X-ray powder diffraction and infrared spectroscopy. The powder X-ray diffraction demonstrated that the minerals of halotrichite group are the main phase in the studied samples. Based on the electron-microprobe analyses, the specie-defining elements are Al, Fe, S and O, while Mg is found as an admixture component; Na, Cl, F и Ca found in the analyses correspond to other closely associated minerals. Infrared spectroscopy revealed the presence of water and sulfate groups in the composition of the studied material. Based on this, we can conclude that the mineral forming low-temperature efflorescence found at different volcanic-related environments is halotrichite. Gypsum, native sulfur and pyrite associate with halotrichite.

The halotrichite formation at localities mentioned above occurred as a result of interaction of the sulphate solutions with the host rock at low temperatures (about 100 °C). Our investigations allowed us to conclude that geochemical characteristics of the processes of sulfate mineralization are similar at various volcanic environments and that halotrichite may be considered as an important indicator of low-temperature volcanic-related activity.

**High-temperature X-ray study and dehydration of coquimbite, ideally $Fe^{3+}_2(SO_4)_3 \cdot 9H_2O$**

Veronika R. Abdulina[1,*], Oleg I. Siidra[1, 2], Evgeny V. Nazarchuk[1], Artem S. Borisov[1]

[1] Department of Crystallography, St. Petersburg State University, St. Petersburg, 199034Russia
[2] Nanomaterials Research Center, Kola Science Center, Russian Academy of Sciences, Apatity, Murmansk Region, 184200 Russia

*abdnik@yandex.ru

Hydrated iron sulphate minerals, as coquimbite $Fe^{3+}_2(SO_4)_3 \cdot 9H_2O$, are found as secondary minerals in the oxidized zones of iron sulphide deposits in arid regions of Earth. Noteworthy, the experimental mineralogy of sulphates has intensified in the last decade due to the new data obtained via satellites and rovers on the Mars surface. The sulphate content reaches up to 30% at some sampling points on the Mars surface. Many of the sulfate minerals are hydrated, which indicates the existence of water on Mars in the past [Vaniman et al., 2004].

Physico-chemical study of coquimbite is also environmentally important. Dissolving in groundwater, coquimbite acidifies the environment [Majzlan et al., 2006].

Thermal behavior of coquimbite was studied in air by means of a Rigaku Ultima X-ray diffractometer (Cu$K\alpha$ radiation) with a high-temperature camera Rigaku HTA 1600. The sample was prepared from heptane's suspension on a Pt-Rh plate. Unit-cell parameters at different temperatures were refined by least-square methods. Main coefficients of the thermal expansion tensor were determined using linear approximation of temperature dependences by the *ThetaToTensor* program.

The diffraction maxima of coquimbite gradually disappear at approximately 175ºC. At this temperature, the probe becomes amorphous. At 275ºC the diffraction peaks corresponding to anhydrous iron sulfate mikasaite start to appear. Mikasaite-type phase is stable up to 525 ºC when it starts to decompose into hematite.

Temperature dependence of cell parameters of coquimbite can be described by the following linear functions:

$$a_t = 10.920 + 1.76\times10^{-4}t + 9.58\times10^{-6}t^2$$
$$c_t = 17.084\text{-}4.12\times10^{-5}t$$
$$V_t = 1765+0.01t+4.73\times10^{-4}t^2,$$

where $t$ is a temperature. Upon heating, the unit cell of coquimbite is expanding along $a$ axis and slightly shrinks along $c$ axis.

The thermal expansion of mikasaite was studied in the range 425–575ºC. The crystal structure of mikasaite is expanding in all directions:

$$a_t = 8.185+6.16\times10^{-6}t + 2.55\times10^{-7}t^2$$
$$c_t = 21.810+2.46\times10^{-5}t$$
$$V_t = 1255+0.06t\text{-}7.95\times10^{-6}t^2.$$

The anisotropy of thermal expansion for both minerals will be discussed in the presentation.

In addition, hydration experiments of mikasaite were carried out and revealed formation of akaganeite-type phases.

This work was financially supported by the Russian Science Foundation through the grant 16-17-10085. Technical support by the SPbSU X-ray Diffraction and Geomodel Resource Centers is gratefully acknowledged.

Vaniman D.T., Bish D.L., Chipera S.J., Fialips C.I., Carey J.W., Feldman W.G. Magnesium sulphate salts and the history of water on Mars. Nature, 2004, 431, 663–665.

Majzlan J., Navrotsky A., McCleskey R. B., Alpers C. N. Thermodynamic properties and crystal structure refinement of ferricopiapite, coquimbite, rhomboclase, and $Fe_2(SO_4)_3(H_2O)_5$. European Journal of Mineralogy, 2006, 18, 175–186.

**Belousovite - a sulfate mineral from the Tolbachik volcano, and its synthetic analogues $KZn(SO_4)X$, $X$ = Cl, Br**

Ruiqi Chen[1], Oleg I. Siidra[1,2], Evgeny V. Nazarchuk[1], Evgeniya A. Lukina[1], Karim A. Zagidullin[3] and Dmitri O. Charkin[3]

[1] Department of Crystallography, St. Petersburg State University, 199034 St. Petersburg, Russia
[2] Kola Science Center, Russian Academy of Sciences, 184200 Apatity, Murmansk Region, Russia
[3] Inorganic Chemistry Division, Department of Chemistry, Moscow State University, 119991 Moscow, Russia

Belousovite was found in July, 2015 in the Yadovitaya fumarole, Second scoria cone, Northern Breakthrough, Great Fissure eruption, Tolbachik volcano, Kamchatka, Russia [Siidra et al., 2018]. Belousovite occurs as a fumarolic mineral, associated with minerals like kamchatkite, langbeinite, euchlorine, anglesite and zincite. The chemical composition of the belousovite was determined: K, Zn, O and Cl are the major elements, and little amounts of Rb also occur in the mineral. That chemical composition makes belousovite very unique, because it is the first sulfate compound and mineral containing K, Zn and Cl in one mineral. The ideal formula is $KZn(SO_4)Cl$. Belousovite has an interesting structural feature – mixed-ligand polyhedra $ZnO_3Cl$. Each $SO_4$ tetrahedron connects with three $ZnO_3Cl$ tetrahedra via three vertices thus forming $[Zn(SO_4)Cl]^-$ layers. These layers have similar topology with the $[Si_4O_{10}]^{4-}$ layers in silicate minerals. Synthetic analogues of belousovite were unknown.

In this work, we successfullysynthesized the analogue of belousovite $KZn(SO_4)Cl$, and its bromineanalogue$KZn(SO_4)Br$. The analogues were grown in evacuated quartz ampoules from the equimolar quantities of anhydrous $ZnSO_4$ and KCl or KBr. $ZnSO_4$ was pre-dried at 400°C, while KCl and KBr were pre-dried at 200°C for 4 h, and further rapidly mixed and grounded in an agate mortar in air for 5 min. The reaction mixtures of precursors were placed into quartz ampoules, which were subsequently evacuated and sealed. The ampoules were heated up to 650 °C at a rate of 62°C/hour and further held at this temperature for 24 hours. Then the ampoules were slowly cooled down at a rate of 24°C/hour to 410°C and further held for 24 hours more. Finally, the furnace was turned off, and cooled to room temperature.

Synthetic analogue of Cl-belousovite was studied by the means of high temperature X-ray diffraction.

The reported study was funded by RFBR according to the research project № 18-35-00704. Technical support by the SPbSU X-ray Diffraction Resource Center is gratefully acknowledged.

Siidra O.I., Nazarchuk E.V., Lukina E.A., Zaitsev A.N., Shilovskikh V.V. Belousovite, $KZn(SO_4)Cl$, a new sulfate mineral from the Tolbachik volcano with apophyllite sheet-topology. Mineralogical Magazine, 2018, 82, 1079–1088.

# 4.6. Uranium Minerals and Compounds

## New Landscapes of Uranium Mineralogy

Peter C. Burns

University of Notre Dame, 301 Stinson-Remick Hall, Notre Dame, IN, 46556USA

pburns@nd.edu

The mineralogy of uranium, the heaviest natural element, is highly complex and unusual owing to its multiple oxidation states, the dominance of the uranyl ion for hexavalent uranium, and linkages between uranyl and many different oxyanions. The number of known uranium species and crystal structures has rapidly grown over the past decade, in part due to the emergence of a new locality in Utah, USA that has produced many new species. This presentation will focus on the compositions and structures of uranyl minerals discovered over the past decade.

**Crystal chemistry and structural complexity of the secondary uranium minerals and its synthetic analogs**

Vladislav V. Gurzhiy[1,*], Jakub Plášil[2], and Sergey V. Krivovichev[1,3]

[1] Department of Crystallography, St. Petersburg State University, 199034 St. Petersburg, Russia
[2]Institute of Physics ASCR, v.v.i., 18221 Praha 8, Czech Republic
[3]Kola Science Centre, 184209 Apatity, Murmansk Region, Russia

* vladgeo17@mail.ru

Within last few years, uranium mineralogy and crystal chemistry has witnessed a true Renaissance, due to the discoveries of exceptional suites of new uranium minerals in Jáchymov, Czech Republic and San Juan County, Utah, U.S. The diversity of new natural species is of particular interest since most of them do not have direct synthetic analogues and therefore are new to the synthetic inorganic chemistry as well. Most of the new uranium minerals are the products of secondary low-temperature hydrothermal processes, which are often associated with crystallization of very complex mineral species such as ewingite, $Mg_8Ca_8(UO_2)_{24}(CO_3)_{30}O_4(OH)_{12}(H_2O)_{138}$, the most structurally complex mineral known today. The structural architectures of novel natural phases, for instance, uranyl sulfates, show many similarities to synthetic uranyl sulfates, chromates, molybdates and selenates. In most of them, uranyl ions are interlinked via tetrahedral $TO_4$ groups ($T$ = S, Cr, Se, Mo) into finite clusters, chains or layers, in which interaction between adjacent uranyl groups is mediated by the hexavalent $T^{6+}$ cations.

In order to evaluate an influence of various crystal-chemical factors (such as dimensionality of the U-bearing units and its hydration state) on the structure and symmetry of uranyl complexes and on the structural architecture of minerals in general, the structural and topological complexity was studied in terms of the information-based approach developed in [Krivovichev, 2012, 2013, 2014] and recently developed in [Gurzhiy, Plášil, 2019]. The structural complexity is quantitatively estimated as a Shannon information content per atom ($I_G$) and per unit cell ($I_{G,total}$). The amount of Shannon information reflects diversity and relative proportion of different objects, *e.g.*, the number and relative proportion of different sites in an elementary unit cell of a crystal structure.

This work was supported by St. Petersburg State University and Russian Science Foundation (grant № 18-17-00018).

Gurzhiy V.V., Plášil J. Structural complexity of natural uranyl sulfates. Acta Cryst. 2019, B75, 39–48.

Krivovichev S.V. Structural complexity of minerals: information storage and processing in the mineral world. Mineral. Mag. 2013, 77, 275–326.

Krivovichev S.V. Topological complexity of crystal structures: quantitative approach. Acta Cryst. 2012, A68, 393–398.

Krivovichev S.V. Which inorganic structures are the most complex? Angew. Chem. Int. Ed. 2014, 53, 654–661.

**Synthesis and Crystal Structure of the Two New Uranyl Hydrogencarbonate Compounds**

S.A. Kalashnikova[1,*], I.V. Kornyakov[1,2], V.V. Gurzhiy[1]

[1]Saint Petersburg branch. Saint Petersburg State University, Saint Petersburg, Russia
[2]Kola Science Centre, 184209 Apatity, Murmansk Region, Russia

*st055416@student.spbu.ru

Single crystals of $Cs[(UO_2)(HCO_3)_3](H_2O)_{0.5}$ (**I**) and $K[(UO_2)(HCO_3)_3](H_2O)_{0.5}$ (**II**) have been prepared by evaporation from 3 ml aqueous solution of uranyl acetate dihydrate, ammonium carbonate, and cesium chloride or potassium chloride for **I** and **II**, respectively. Single crystal XRD data had been collected at 100(2) K using Bruker Kappa Apex II Duo diffractometer.

The unit cell parameters of compound **I** were determined and refined by least squares method from 9935 reflections. Compound **I** has a monoclinic symmetry [s.g. *P*-1, *a*=8.353(4) Å, *b*=11.008(5) Å, *c*=15.354(7) Å, $\alpha$=108.409(11)°, $\beta$=100.140(9)°, $\gamma$=96.370(9)°, *V*=1297.5(10) Å$^3$, *Z*=4]. The crystal structure has been solved by the direct methods from X-ray diffraction data and refined by the least-squares techniques to $R_1$ = 0.0378 ($wR_2$ = 0.0856) for 5897 unique reflections with $|F_o| \geq 4\sigma_F$.

The unit cell parameters of compound **II** were determined and refined by least squares method from 32884 reflections. Compound **II** has a tetragonal symmetry [s.g. $I4_1/a$, *a*=14.222(5) Å, *c*=25.715(8) Å, *V* = 5201(4) Å$^3$, *Z* = 16]. The crystal structure has been solved by the direct methods from X-ray diffraction data and refined by the least-squares techniques to $R_1$ = 0.0391 ($wR_2$ = 0.0796) for 2366 unique reflections with $|F_o| \geq 4\sigma_F$.

The structure of **I** contains two symmetrically distinct uranyl cations. A basic unit of the structure is hexagonal uranyl bipyramid sharing three edges with three $(HCO_3)^-$ groups. The uranyl hydrogencarbonate clusters are connected by $Cs^+$ cations in (010) plane to form infinite layer. In addition, the Cs2 cation is coordinated by a single symmetrically distinct water molecule. The connection of the layers is reached by the hydrogen-bonding network formed by hydrogencarbonate groups and water molecules. The equatorial planes of uranyl bipyramids are arranged approximately parallel to (-201) plane.

The structure of **II** contains one symmetrically non-equivalent uranyl cation. As in the case of **I**, the hexagonal uranyl bipyramid plays the main role in the structure formation and shares three edges with three $(HCO_3)^-$ groups. Each uranyl hydrogencarbonate cluster is surrounded by three $K^+$ cations placed approximately in the equatorial plane of uranyl bipyramid to form an infinite three-dimensional framework. The structure stabilization is reached by the presence of hydrogen-bonding network of $(HCO_3)^-$ and $H_2O$ groups.

The research was supported by SPBU and Russian Scientific Foundation grant № 18-17-00018. XRD studies have been performed at the X-ray Diffraction Resource Centre of St Petersburg State University.

**Structural and topological complexity of the uranyl selenates and selenites**

Ivan V. Kuporev*, and Vladislav V. Gurzhiy

Saint-Petersburg State University, 199155 St.Petersburg, Russia

* st054910@student.spbu.ru

In this study, more than a hundred uranyl selenate and selenite compounds were analyzed from the topological point of view. For the most common topologies of uranyl-selenate and selenite structural units, various isomers were found and complexity parameters were calculated. For each U-Se unit a dichromatic graph (where black vertices correspond to uranium polyhedra, and white to selenium tetrahedra) or an anion topology scheme was constructed and designated according to the accepted classification [Krivovichev, 2009]. To determine the structural isomers within the same topology, the orientation matrices were additionally used.

To summarize the impact of various crystal-chemical factors (such as dimensionality of the uranium-bearing units and their hydration state) on the structure and symmetry of uranyl selenate/selenite complexes and on the structural architecture of crystals in general, the structural and topological complexity was studied in terms of the information-based approach developed by Krivovichev [2014]. The structural complexity is quantitatively estimated as a Shannon information content per atom ($I_G$) and per unit cell ($I_{G;\text{total}}$) and reflects the number and relative proportion of different sites in an elementary unit cell of a crystal structure. This approach is convenient to consider the compounds having very close chemical composition (e.g. polymorphs, U-Se units), so we can exclude additional cations and water molecules occupying interlayer space from the thorough consideration.

All calculations were made on the basis of the original CIF files from the structural databases (ICSD, CCDC) and respective publications. The structural complexity of the U-Se units has been analyzed, taking into account their real layer (RL) or rod group (RG) symmetries. The topological complexity has been calculated according to the maximal symmetry group corresponding to a particular isomer.

The complexity of the U-Se structures turned out to be strongly dependent on the relative density of the layer, which in turn depends on the connectivity of the U and Se polyhedra. The two connected arrangement of selenium polyhedra allows rotation of these groups, which makes such structures less complex on average. Structures with more connected arrangement of Se polyhedra, on the contrary, usually show higher complexity. The effect of water molecules and cations in the interlayer space leads to the realization of a higher complexity with respect to the least for this topology.

This work was supported by St. Petersburg State University and Russian Science Foundation (grant 18-17-00018).

Krivovichev S.V. Structural Crystallography of Inorganic Oxysalts. Oxford University Press, 2009.

Krivovichev S.V. Topological complexity of crystal structures: quantitative approach. Acta Crystallographica, 2012, A68, 393–398.

## $UO_n$ Coordination Polyhedra, U-Substructures and the Concept of Antiliquid

Denis V. Pushkin*, Anton V. Savchenkov, Larisa B. Serezhkina, and Viktor N. Serezhkin

Samara National Research University, 443086 Samara, Russia

* pushkin@samsu.ru

Using the Voronoi-Dirichlet polyhedra (VDP), an analysis of the coordination of 3664 crystallographically nonequivalent U atoms (III, IV, V, or VI) in the structures of crystals of oxygen-containing compounds characterized with an R-factor <0.05 was performed. It was found that with a fixed degree of oxidation of uranium atoms, the volume of their VDP practically does not depend on the coordination number *n* in the $UO_n$ complexes, which varies from 3 to 12. It was shown that a number of VDP parameters that are absent in the arsenal of classical crystal chemistry can serve as descriptors that make it possible to detect errors that for various reasons appear in crystal-structural databases.

It was discovered that U substructures with greater than or equal to 20 crystallographically independent U atoms in the unit cell feature 15-faceted VDP as the most common type. Analogous unimodal distributions of VDP with maxima at 15 faces are observed for F and H substructures and the model system ‘ideal gas’, which has no order in the arrangement of atoms. This similarity allows one to assume that substructures of crystal structures with greater than or equal to 20 crystallographically independent atoms in the unit cell do not possess short-range (local) order in the mutual arrangement of atoms, but feature long range order (translational symmetry). Thus, crystalline compounds with such substructures can formally be regarded as ‘antiliquid’, that is the antipode of a liquid, whose structure possesses short-range order but lacks translational symmetry.

# The First Example of a 2D Uranyl Oxalatosuccinate Complex

Ekaterina F. Rogaleva[1,*], Larisa B. Serezhkina[1], and Mikhail S. Grigoriev[2]

[1] Samara National Research University, 443086 Samara, Russia
[2]Frumkin Institute of Physical Chemistry and Electrochemistry, Russian Academy of Sciences, 119071 Moscow, Russia

* e.f.rogaleva@gmail.com

Interest in uranyl oxalate-containing complexes is related to using of oxalate for purification and production of uranium ores, and to solving problems of processing and recycling of nuclear fuel [Matyukha et al., 2004]. The active synthesis of oxalate complexes is associated with this. Further, works devoted to synthesis and investigation of the structures of mixed-ligand complexes have appeared in literature. In this case, the uranium atom coordinates ligands of other nature, besides oxalate-ion, that results in obtaining of compounds with new useful properties.

Presently, the data about one compound of uranium with dianions of oxalic and succinic acids are represented in literature. This complex includes tetramethylammonium cations and forms 3D framework, which contains layers interconnecting with succinate-ions [Xie et al., 2017].

The aim of the present work is investigation of structure of $(CH_6N_3)_2[(UO_2)_2(C_4H_4O_4)_2(C_2O_4)]\times\times 4H_2O$ (**I**), where $CH_6N_3^+$ – guanidine cation, $C_4H_4O_4^{2-}$ – succinate-anion, $C_2O_4^{2-}$ – oxalate-anion. Synthesis was conducted in the hydrothermal conditions. Coordination numbers of all atoms in the structure are defined with the method of intersecting spheres [Serezhkin et al., 1997]. It is determined that three crystallographically nonequivalent uranium atoms are contained in the framework. Coordination polyhedra (**CP**) of these atoms are hexagonal bipyramids $UO_8$. Six atoms of oxygen take positions in the equatorial plane of uranium atom CP. Four of them belong to two succinate-anions, those are coordinated bridge-cyclically to uranium atoms with the formation of four-membered cycles. Remaining two oxygen atoms belong to oxalate-ion that is also coordinated bridge-cyclically to uranyl cations with the formation of five-membered cycles. The main structural units of crystals are anionic layered complexes $[(UO_2)_2(C_4H_4O_4)_2(C_2O_4)]^{2-}$, which belong to $A_2(Q^{02})_2Q^{02}$ crystallochemical group of uranyl complexes, where $A = UO_2^{2+}$, $Q^{02} = C_4H_4O_4^{2-}$ or $C_2O_4^{2-}$. Coordination types and crystallochemical formulas are written according to [Serezhkin et al., 2009]. The layers are linked into the framework due to the system of hydrogen bonds with the participation of outer-sphere water molecules and $-NH_2$ groups.

Results of FTIR spectroscopic study are well conformed with XRD analysis data.

Matyukha V.A., Matyukha S.V. Oxalates of rare-earth elements and actinoids, 2004.

Serezhkin V.N., Mikhailov Y.N., Buslaev Y.A. The Method of Intersecting Spheres for Determination of Coordination Numbers of Atoms in Crystal Structures. Rus. J. Inorg. Chem., 1997, 42, 2036–2077.

Serezhkin V.N., Vologzhanina A.V., Serezhkina L.B. et al. Crystallochemical formula as a tool for describing metal–ligand complexes – a pyridine-2,6- dicarboxylate example. Acta Crystallogr., 2009, B65, 45–53.

Xie J., Wang Y., Liu W. et al. Highly Sensitive Detection of Ionizing Radiations by a Photoluminescent Uranyl Organic Framework. Angewandte Chemie, 2017, 129, 7608–7612.

**Advanced crystal-chemical role of secondary metals in a series of uranyl crotonates**

Anton V. Savchenkov[1,*], Pavel A. Pirozhkov[1], Anna V. Vologzhanina[2], Yan V. Zubavichus[3,4], Pavel V. Dorovatovskii[3], Denis V. Pushkin[1], and Larisa B. Serezhkina[1]

[1] Samara National Research University, 443086 Samara, Russia
[2]Nesmeyanov Institute of Organoelement Compounds of Russian Academy of Sciences, 119991 Moscow, Russia
[3] National Research Center «Kurchatov Institute», 123182 Moscow, Russia
[4] Boreskov Institute of Catalysis, 630090 Novosibirsk, Russia

* anton.savchenkov@gmail.com

Crystal structures of three new uranyl compounds were solved using single crystal X-ray diffraction and studied using FTIR spectroscopy. Together with the previously characterized compound it resulted in a series of Mg, Ca, Sr and Ba uranyl crotonates with the following chemical formulae: $[Mg(H_2O)_6][UO_2(crt)_3]_2\cdot H_2O$ (**I**), $\{Ca(H_2O)_3[UO_2(crt)_3]_2\}\cdot 1.5H_2O$ (**II**), $\{Sr_2(H_2O)_4(crtH)_2[UO_2(crt)_3]_4\}\times\times 3.5H_2O$ (**III**) and $\{Ba_2(H_2O)_4(crtH)_2[UO_2(crt)_3]_4\}\cdot 3H_2O$ (**IV**), where crt = $C_3H_5COO^-$. The crystal structures of I–IV are different, containingmono-, tri- and hexanuclear metal building units.

The enhanced crystal chemical role of secondary metal cations in the title compounds is evident from the fact that crystals with different structures have crystallized from solutions containing similar chemical species. Being the only distinguishing feature in the syntheses of compounds I–IV the secondary metal cations serve as the driving force of formation of certain building units (mono-, tri- or hexanuclear) as opposed to simply responding to a space filling opportunity in crystal structures. Using the parameter $G_3$ of Voronoi-Dirichlet polyhedra it is possible to distinguish the type of atomic bonding between ionic and covalent. According to our calculations, Mg and Ca in the mentioned compounds form rather covalent bonding with their neighboring oxygen atoms, while Sr and Ba form non-directional ionic bonds. This is consistent with the increased size, increased coordination numbers and more profound metallic character of Sr and Ba in comparison with Mg and Ca atoms.

As expected based on different crystal structures, absolute values of parameters of molecular Voronoi-Dirichlet polyhedra showing supramolecular structure are different for compounds I–IV. On the other hand, the partial contributions of different types of *inter*- as well as *intra*molecular noncovalent interactions are almost equal for all the four compounds. That means that their ‘resources’ for forming noncovalent interactions are almost equal irrespective of their crystal structures. The packing of heteronuclear clusters and aqua cations in all the four compounds is topologically equal to the bcc lattice and is consistent with the stereoatomic model of crystal structures [Serezhkin et al., 2019]: the species pack in such a manner that the overlap of outer electron shells is minimal.

Serezhkin V.N., Rogaleva E.F., Savchenkov A.V., Pushkin D.V., Serezhkina L.B. Aspects of the topology of actinide atom substructures in crystal structures and the concept of antiliquid. Acta Crystallogr., 2019, A75, 370–378.

**Noncovalent interactions in the new methacrylate uranyl complexes with organic monovalent cations**

Nikita A. Shimin[1,*], Larisa B. Serezhkina[1], and Mikhail S. Grigoriev[2]

[1] Samara National Research University, 443086 Samara, Russia
[2]FrumkinInstitute of Physical Chemistry and Electrochemistry Russian Academy of Sciences, 119071 Moscow, Russia

* shiminikita.su@gmail.com

Synthesis of new methacrylate-containing uranyl complexes is hampered by the predisposition of methacrylic acid to rapid and irreversible polymerization, manifested in the turbidity of an aqueous solution and the subsequent formation of a gel-like product. Therefore, the synthesis was carried out in the black painted vessels. A portion of uranium oxide (VI) was dissolved in an aqueous or aqueous-alcoholic solution of methacrylic acid (**Hmacr**). After the transfer of uranium atoms into the uranyl forms completed, a portion of an organic compounds was added to the solution: $(NH_2)_2C=NH_2$(**Gu**), $(NHPh)_2C=NH_2$ (**DPhGu**), $[PhCH_2N(CH_3)_3]Cl$ (**TMBACl**) or $[PhCH_2N(C_2H_5)_3]Cl$ (**TEBACl**). By isothermal evaporation of the solutions the systems such as$R : UO_3 : Hmacr = 2 : 1 : 10$, where R = Gu, DPhGu, TMBACl or TEBACl, the new U(VI) complexes were crystallized with the compositions $(NH_2)_2CNH_2[UO_2(macr)_3]$ (**I**), $(NHPh)_2CNH_2[UO_2(macr)_3]\cdot 0.5C_2H_5OH$ (**II**), $PhCH_2N(CH_3)_3[UO_2(macr)_3]$ (**III**) and $PhCH_2N(C_2H_5)_3[UO_2(macr)_3]$ (**IV**).

The crystallographic parameters of I, II, III and IV were obtained by X-Ray analysis. The definitions of coordination numbers were carried out by the method of intersecting spheres [Serezhkin et al., 1997]. In all cases, the uranium atoms coordination polyhedra is hexagonal bipyramid $UO_8$, where six atoms of oxygen in equatorial plane belong to three bidentate cyclic (type of coordination $B^{01}$) methacrylate ions. The type of coordination is indicated according to [Serezhkin et al., 2009]. In structures I, II, III and IV, uranium containing units are 0D complexes with composition $[UO_2(macr)_3]^-$ and crystal chemical formula $AB^{01}{}_3$, where $A = UO_2^{2+}$, $B^{01}$ = macr. The 0D complexes form framework by noncovalent interactions with different organic cations.

The nonvalent interactions' evaluation was carried out by the method of molecular Voronoi-Dirichlet polyhedra.

The FTIR spectroscopy investigation is fully consistent with X-Ray analysis data.

Serezhkin V.N., Mikhailov Yu.N., Buslaev Yu.A. The method of intersecting spheres for determination of coordination numbers of atoms in crystal structures. Rus. J. Inorg. Chem., 1997, 42, 1871–1910.

Serezhkin V.N., Vologzhanina A.V, Serezhkina L.B. et al. Crystallochemical formula as a tool for describing metal-ligand complexes – a pyridine-2,6-dicarboxylate example. Acta Cryst., 2009, B65, 45–53.

# 4.7. Copper Minerals and Compounds

## Crystal Chemical Classification of Divalent Copper Oxysalt Minerals

Ilya V. Kornyakov* and Sergey V. Krivovichev

[1]Department of Crystallography, St. Petersburg State University, 199034 St. Petersburg, Russia
[2]Kola Science Centre, 184209 Apatity, Murmansk Region, Russia

*i.kornyakov@spbu.ru

Copper is one of the most important industrial metals, which has been mined for more than 10000 years. According to Rudnick and Gao (1995), the abundance of copper in the upper continental crust is 28 ppm, and it has been pointed out many times that, despite its relatively low abundance, copper is characterized by an anomalous mineralogical diversity. Its two main oxidation states, $Cu^{+}$ and $Cu^{2+}$, have different electronic and chemical properties. In terms of the chemical hardness, $Cu^{+}$ is soft and chalcophile, and occurs in Nature in the form of sulfides and sulfosalts. In contrast, $Cu^{2+}$ is hard and lithophile, i.e. tends to form oxygen-bearing mineral species. Indeed, from ca. 700 Cu mineral species recognized as valid by the International Mineralogical Association (IMA), about 60% are oxides, hydroxides, oxysalts and oxyhalogenides, whereas about 40% are sulfides and sulfosalts. The prevalence of oxygen-bearing species containing mostly $Cu^{2+}$ cations is due to the diversity of its coordination environments arising from the unique distortion of its octahedral geometry due to the Jahn-Teller effect [Jahn and Teller, 1937; Hathaway, 1984; Burns and Hawthorne, 1995a,b, 1996].

Crystal chemistry of Cu oxysalt minerals have been extensively investigated by Hawthorne and co-workers. In particular, Burns and Hawthorne (1995a) analyzed coordination geometries of $Cu^{2+}$ in inorganic oxysalts with theoretical examinations of existing (or non-existing) energy barriers between different configurations. Mixed-ligand coordination geometries in $Cu^{2+}$ minerals have been considered by Burns and Hawthorne (1995b), whereas Burns and Hawthorne (1996) discussed in details static and dynamic Jahn-Teller effects in $Cu^{2+}$oxysalt minerals. The structural relations in copper oxysalt minerals were reviewed by Eby and Hawthorne (1993), who considered a structural hierarchy for ninety-four minerals. More than 330 Cu minerals have been discovered since then, and the aim of the present review is to provide a new classification scheme for all natural Cu oxysalt minerals with reported crystal-structure determinations.

Herein, we consider chemical diversity of $Cu^{2+}$oxysalt minerals, analyze coordination geometry of $Cu^{2+}$ in oxysalt minerals with particular emphasis on description of fivefold coordinations and provide bond-length distribution statistics on each coordination geometry. After discussion of general principles of structural classification, we suggest a new scheme for crystal chemical systematics of $Cu^{2+}$oxysalt minerals, which is based upon the principle of leading structural organization.

Burns P.C., Hawthorne F.C. Coordination-geometry structural pathways in $Cu^{2+}$ oxysalt minerals. Can. Mineral., 1995, 33, 889–905.

Burns P.C., Hawthorne F.C. Mixed-ligand $Cu^{2+}\varphi_6$ octahedra in minerals: observed stereochemistry and Hartree-Fock calculations. Can. Mineral., 1995, 33, 1177–1188.

Burns P.C., Hawthorne F.C. Static and dynamic Jahn-Teller effect in $Cu^{2+}$ oxysalt minerals. Can. Mineral., 1996, 34, 1089–1105.

Eby R.K., Hawthorne F.C. Structural Relations in Oxysalt Minerals. I. Structural Hierarchy. Acta Cryst., 1993, B49, 28–56.

Hathaway B.J. A new look at the stereochemistry and electronic properties of complexes of the copper(II) ion. Structure and Bonding, 1984, 57, 55–118.

Jahn H.A., Teller E. Stability of polyatomic molecules in degenerate electronic states. I. Orbital degeneracy. Proc. Roy. Soc. 1937, 161, 220–236.

Rudnick R.L., Gao S. Composition of the Continental Crust. Treatise Geochem. 3, 1–64.

**Complex Cu-Pb selenite bromides: a new large family of layered compounds**

Michael S. Kozin[1,*], Oleg I. Siidra[1,2], Wulf Depmeier[3], Roman A. Kayukov[1], Vadim M. Kovrugin[1]

[1]Dept. Crystallography, St. Petersburg State University, 199034 St. Petersburg, Russia
[2]Kola Science Center, Russian Academy of Sciences, 184209 Apatity, Murmansk Region, Russia
[3] Institut für Geowissenschaften, Universität Kiel, D-24098 Kiel, Germany

*mikhail.s.kozin@gmail.com

Extensive experiments in the Pb–Cu–Se–O–Br system at 400°C yielded single crystals of nine new compounds [Siidra et al., 2018].The new compounds described herein illustrate the complexity of the system and new pathways for the synthesis of copper-lead selenite halides. They can be distributed in two groups and their formulae and designations used hereafter are all but one exhibiting new complex layered or open-framework architectures, organized via the host-guest principle. Five of these structures contain only bivalent copper: three with well-ordered 2D structures and completely filled atomic positions, two structures have 3D frameworks:

| | |
|---|---|
| $Cu^{2+}Pb_6(SeO_3)_4Br_6$ | (**CuPb 1:6**) |
| $Cu^{2+}Pb_2(SeO_3)_2Br_2$ | (**CuPb 1:2**) |
| $Cu^{2+}_3Pb_{2.4}(SeO_3)_5Br_{0.8}$ | (**CuPb 3:2.4**) |
| $Cu^{2+}_2Pb(SeO_3)_2Br_2$ | (**CuPb 2:1**) |
| $Cu^{2+}_4Pb(SeO_3)_4Br_2$ | (**CuPb 4:1**) |

The four remaining compounds contain both $Cu^{2+}$ and $Cu^{+}$ and are comprised of layers formed by edge- and vertex-sharing of oxocentered $OCu^{2+}_{4-n}Pb_n$ tetrahedra decorated with $SeO_3^{2-}$ and $Br^{-}$ anions. The interlayer spaces are filled by partially disordered $Cu^{+}$ - Br and Pb - Br associations.

| | |
|---|---|
| $[Cu^{2+}_9Pb_2O_4](Cu^{+}Br_2)(SeO_3)_4Br_5$ | (**CuPbOXO-1**) |
| $[Cu^{2+}_7PbO_3](Cu^{+}Br)_{0.35}(SeO_3)_3Br_4$ | (**CuPbOXO-2**) |
| $[Cu^{2+}_8Pb_2O_4](Cu^{+}Br)_{1.5}(SeO_3)_4Br_4$ | (**CuPbOXO-3**) |
| $[Cu^{2+}_6Pb_3O_4](Cu^{+}Pb_{1.27}Br_{3.54})(SeO_3)_4Br_2$ | (**CuPbOXO-4**) |

One remarkable feature of the latter group of compounds is the presence of tetrahedral $(Cu^{2+})_4$ complexes with arrangements derivable from a kagome network.

The diversity of structures and compositions among copper-lead selenite halides makes an overall comparison rather difficult; however, three trends can already be identified even upon a cursory survey. First, there are only very few structural analogues between the copper-lead selenite bromides and the corresponding chlorides, e.g. **CuPbOXO-1**.The second observation is that in the structures of copper-lead selenite bromides, oxocentered $OCu^{2+}_nPb_{4-n}$ tetrahedra have been found only in structures containing also $Cu^{+}$. Whenever $Cu^{2+}$ is the sole copper species, only $SeO_3^{2-}$ and bromide are involved as anions, but "additional oxygens" are absent. The third tendency reveals that $Cu^{2+}$ has pure oxide coordination with no bonds to Br at all in **CuPb1:6**, **CuPb1:2**, **CuPb3:2.4**, **CuPb2:1**, **CuPb4:1** and **CuPbOXO-4.** By way of contrast**,** in **CuPbOXO-1, CuPbOXO-2** and **CuPbOXO-3** some of the$Cu^{2+}$ cations demonstrate mixed-ligand coordination.

This work was financially supported by the Russian Foundation for Basic Research, grant no. 19-05-00413. Technical support by the SPbSU X-ray Diffraction Resource Centre is gratefully acknowledged.

Siidra O.I., Kozin M.S., Depmeier W., Kayukov R.A., Kovrugin V.M. Copper-lead selenite bromides: A new large family of compounds partly having $Cu^{2+}$ substructures derivable from Kagome-nets. Acta Crystallographica, 2018, B74, 712–724.

**Modification of spin-triplet state in novel copper synthetic sulfates**

Diana O. Nekrasova[1,3]*, Marie Colmont[3], Olivier Mentré[3], Alexander A. Tsirlin[4], Oleg I. Siidra[1,2]

[1]St. Petersburg State University, Department of Crystallography, 199034 St.Petersburg, Russia
[2]Kola Science Center, Russian Academy of Sciences, 184209 Apatity, Murmansk Region, Russia
[3]Université de Lille, ENSCL, CNRS, Unité de Catalyse et Chimie du Solide (UCCS), UMR 8181, Villeneuve d'ASCQ, 59650 France
[4] University of Augsburg, Experimental Physics VI, Center for Electronic Correlations and Magnetism, 86159 Augsburg, Germany

* diana.nekrasova@univ-lille.fr

Sulfates with transition metal cations show excellent redox potential for $Li^+$ or $Na^+$ (de)intercalation responsible for their renewed interest in the last decade. The synthetic terms often correspond to mineral analogues but their non-homogeneity imposed to synthesize them in the laboratory for further studies. Additionally, it is well known that mineral develop several complex phenomenologies, see for instance the quantum magnetism has often been observed on naturally occurring minerals [Inosov, 2018], which by itself deserve a systematic synthetic and characterization task on specific series.

Synthetic minerals euchlorine-based $A_2Cu_3O(SO_4)_3$ ($A$ = Na, K, Na/K) have been prepared while novel members, $Rb_2Cu_{3.07}O_{0.07}(SO_4)_3$and $Cs_2Cu_{3.5}O_{1.5}(SO_4)_3$ were also obtained by solid-state reaction in gold crucibles and crystals have been grown in evacuated quartz ampules. The obtained materials were investigated using single-crystal and powder X-ray diffraction analysis, IR spectroscopy and DSC-TGA analyzes. All these structures are built up of oxo-centered $OCu_4$ bricks, forming edge-sharing clusters consisting of six $Cu^{2+}$ ions with S = 1/2 spins. It was shown on the Na and K phases that due to strong exchanges within the clusters, the system started to behave as spin-triplet state (S = 1) around 100 K while no magnetic ordering between the hexamers have been reported [Fujihala et al., 2018; Furrer et al. 2018]. Here we investigate the full series using DFT calculations, magnetic susceptibility, magnetization and heat capacity measurements. In particular we pay attention to the occurrence or not of spin gap behavior versus magnetic ordering. Our results show a clear correlation between the size of the alkali spacers and the couplings/ordering between the units. Concerning $Cs_2Cu_{3.5}O_{1.5}(SO_4)_3$, the large $Cs^+$ ionic radius is responsible for the presence of additional $Cu^{2+}$ cations linking the hexamers.

This work was supported by the Russian Science Foundation through the grant 16-17-10085. D.O.N. Ph.D. is carried out within the framework of the ambassade de France co-tutorial Ph.D. program. Technical support by the SPbSU X-ray Diffraction Resource Centre is gratefully acknowledged.

Fujihala M., et al. Cluster-Based Haldane State in an Edge-Shared Tetrahedral Spin-Cluster Chain: Fedotovite $K_2Cu_3O(SO_4)_3$. Phys. Rev. Lett., 2018, 120, 7, 077201.

Furrer A. et al. Spin Triplet Ground-State in the Copper Hexamer Compounds $A_2Cu_3O(SO_4)_3$ (A=Na, K). Phys. Rev. B, 2018, 98, 180410(R).

Inosov D.S. Quantum magnetism in minerals. Advances in Physics, 2018, 67(3), 149–252.

**Physical properties and structural features of synthetic analogs of averievite, $[Cu^{2+}_5O_2](VO_4)_2 \cdot 2Cu^{+}Cl$, and yaroshevskite, $[Cu_9O_2](VO_4)_4Cl_2$**

Viktoriia A. Vladimirova[1], Oleg I. Siidra[1,2]

[1]Department of Crystallography, St. Petersburg State University, 199034 St. Petersburg, Russia
[2] Kola Science Center, Russian Academy of Sciences, 184200 Apatity, Murmansk Region, Russia

Vladimirovav.sbk.1998@yandex.ru

Known to date copper vanadate-chloride minerals include: leningradite, $PbCu_3(VO_4)_2Cl_2$ [Siidra et al., 2007], averievite $Cu_5O_2(VO_4)\cdot nMCl_x$ (M = Cu, Cs, Rb, K) [Krivovichev et al., 2015] and yaroshevskite, $Cu_9O_2(VO_4)_4Cl_2$ [Pekov et al., 2013]. Notably, all of these minerals originate from the fumarolic environments of the Second Scoria Cone, GFTE. Only recently synthetic analogues were reported for averievite [Botana et al., 2018].

Crystals of a synthetic structural analogue of averievite without alkaline metals and analogue of yaroshevskite were synthesized as a result of chemical vapor transport reactions in $CuO$-$V_2O_5$-$CuCl_2$ system.

The crystal structure of an analog of the averievite is based on $[Cu^{2+}_5O_2]^{6+}$ layers. There are wide channels extending along the *c* axis. In the structure of a mineral, chloride complexes with alkali metals and divalent copper are located within the channels, whereas in the structure of synthetic analog the $Cu^{+}Cl$ complexes fill in the space. $Cu^{2+}$ copper cations in crystal structure of a synthetic analog of averievite form the kagome lattice.

The crystal structure of the synthetic yaroshevskiteis based on chains formed by $[OCu_4]^{6+}$ oxocentered tetrahedra. Crystal structure of yaroshevskite demonstrates remarkable diversity of $Cu^{2+}$ coordination environments. Very complex copper-oxide substructure in synthetic analogue of yaroshevskite reflects in unusual magnetic properties which will be reported.

This work was financially supported by the Russian Foundation for Basic Research, grant no. 19-05-00413. Technical support by the SPbSU X-ray Diffraction and Geomodel Resource Centres is gratefully acknowledged.

Botana A.S., Zheng H., Lapidus S.H., Mitchell J.F., Norman M.R. Averievite: A copper oxide kagome antiferromagnet. Physical Review, 2018, B98, 054421.

Krivovichev S.V., Filatov S.K. and Vergasova L.P. Refinement of the crystal structure of averievite $Cu_5O_2(VO_4)\cdot nMCl_x$ (M = Cu, Cs, Rb, K). Proceedings of the Russian Mineralogical Society, 2015, 144, 101-109.

Pekov I.V., Zubkova N.V., Zelenski M.E., Yapaskurt V.O., Polekhovsky Yu.S., Fadeeva O.A., Pushcharovsky D.Yu. Yaroshevskite, $Cu_9O_2(VO_4)_4Cl_2$, a new mineral from the Tolbachik volcano, Kamchatka, Russia. Mineralogical Magazine, 2013, 77, 107-116.

Siidra O.I., Krivovichev S.V., Armbruster T., Filatov S.K. and Pekov I.V. The crystal structure of leningradite, $PbCu_3(VO_4)_2Cl_2$. Canadian Mineralogist, 2007, 45, 445-449.

## Crystal chemistry of the compound $Cu(Rb,NH_4)(NO_3)(SO_4)$

Rezeda M. Ismagilova[1]*, Andrey A. Zolotarev[1], Elena S. Zhitova[1,2], Sergey V. Krivovichev[1,3]

[1] Saint-Petersburg State University, 199034 Saint-Petersburg, Russia
[2]Institute of Volcanology and Seismology, Russian Academy of Sciences, 683006 Petropavlovsk-Kamchatsky, Russia
[3]Kola Science Center, Russian Academy of Sciences, 184209 Apatity, Russia

* rezeda.m.ismagilova@gmail.com

The compound $Cu(Rb,NH_4)(NO_3)(SO_4)$ was obtained by heating a mixture of reagents $CuSO_4 \cdot H_2O$, $RbSO_4$, $(NH_4)_6Mo_7O_{24} \cdot 4H_2O$ at 200 °C. This compound is represented by a blue translucent solid aggregate, soluble in water and alcohol.

The compound is monoclinic, $P2_1/n$, $a$ = 5.1429(3), $b$ = 6.1016(3), $c$ = 19.3065(10) Å, $\beta$ = 90.567(5)°, $V$ = 605.81(6) Å$^3$. The crystal structure was refined to $R_1$ = 0.0351 for 2563 unique observed reflections with $|F_o| \geq 2\sigma F$ .The structure has a layered type, it is composed of $Cu(SO_4)(NO)_3$ complexes with $Rb^+$ and $NH_4^+$cations located in the interlayer space at one mixed-occupied site. Copper atoms are octahedrally coordinated, the $CuO_6$ octahedra are linked *via* corner-sharing with $SO_4$ tetrahedrons by four oxygen atoms, while the other two oxygen atoms are edge-shared with $NO_3$ triangles. The structural type of the compound is similar to bradleyite-group minerals [Krivovichev et al., 2013], although it remains unique since no isotypic minerals and compounds were found. The empirical formula of the compound is $Cu(Rb_{0.65}(NH_4)_{0.35})(NO_3)_{0.95}(SO_4)_{1.05}$, which is in agreement with single-crystal X-ray diffraction data. Raman spectroscopy confirmed the presence of ammonium (3355–3100 cm$^{-1}$), nitrate (1055 cm$^{-1}$) and sulfate groups (982, 610 and 451 cm$^{-1}$) in the compound.

The study by different analytical methods allowed us to describe the new compound, $Cu(Rb,NH_4)(NO_3)(SO_4)$, which may serve as an example of mineral-like phase and extends our knowledge on the crystal chemistry of bradleyite-like phases.

The research was performed at the «Centre for X-ray Diffraction Studies» and the «Center for Geo-Environmental Research and Modeling (GEOMODEL)» of Research park of St.Petersburg State University. This research was supported by the Russian Science Foundation (Grant no. № 19-17-00038 to SVK).

Krivovichev S.V., Chernyatieva A.P., Britvin S.N., Yakovenchuk V.N., Krivovichev V.G. Refinement of the crystal structure of bonshtedtite, $Na_3Fe(PO_4)(CO_3)$. Zapiski RMO, 2013, 1, 46–54.

**Jahn-Teller distortion and cation ordering: the crystal structure of paratooite-(La), a superstructure of carbocernaite**

Sergey V. Krivovichev[1,2,*], Taras L. Panikorovskii[2,3], Andrey A. Zolotarev[2], Vladimir N. Bocharov[4], Anatoly V. Kasatkin[5], Radek Škoda[6]

[1]Kola Science Centre, Russian Academy of Sciences, 184209 Apatity, Russia
[2]Institute of Earth Sciences, St. Petersburg State University, 199034 St. Petersburg, Russia
[3]Laboratory of Nature-Inspired Technologies and Environmental Safety of the Arctic, Kola Science Centre, Russian Academy of Sciences, 184209 Apatity, Russia
[4]Geo Environmental Centre "Geomodel", Saint–Petersburg State University, 198504 St. Petersburg, Russia
[5] Fersman Mineralogical Museum, Russian Academy of Sciences, 119071 Moscow, Russia
[6] Department of Geological Sciences, Faculty of Science, Masaryk University, 61137 Brno, Czech Republic

* s.krivovichev@ksc.ru

The crystal structure of paratooite-(La) [Pring et al., 2006] has been solved using crystals from the type locality, Paratoo copper mine, near Yunta, Olary Province, South Australia, Australia. The mineral is orthorhombic, *Pbam*, $a$ = 7.2250(3), $b$ = 12.7626(5), $c$ = 10.0559(4) Å, $V$ = 927.25(6) Å$^3$, $R_1$ = 0.063 for 1299 unique observed reflections. The crystal structure contains eight symmetrically independent cation sites. The *La* site, which accommodates *REE*s, but also contains Sr and Ca, has a tenfold coordination by seven carbonate groups. The Ca, Na1, and Na2 sites are coordinated by eight, eight, and six O atoms, respectively, forming distorted $CaO_8$ and $Na1O_8$ cubes and $Na2O_6$ octahedra. The Cu site is occupied solely by copper and possess a distorted octahedral coordination with four short (1.941 Å) and two longer (2.676 Å) apical Cu-O bonds. There are three symmetrically independent carbonate groups $(CO_3)^{2-}$ with the average <C-O> bond lengths equal to 1.279, 1.280, and 1.279 Å for the C1, C2, and C3 sites, respectively.

The crystal structure of paratooite-(La) can be described a strongly distorted body-centered lattice formed by metal cations with $(CO_3)^{2-}$ groups filling its interstices.

According to the chemical and crystal-structure data, the crystal-chemical formula of paratooite-(La) can be described as $(La_{0.74}Ca_{0.11}Sr_{0.07})_4CuCa(Na_{0.75}Ca_{0.15})(Na_{0.63})(CO_3)_8$ or $REE_{2.96}Ca_{1.59}Na_{1.38}CuSr_{0.28}(CO_3)_8$. The idealized formula can be written as $(La,Sr,Ca)CuCa(Na,Ca)_2(CO_3)_8$. The structure of paratooite is a 1×2×2 superstructure of carbocernaite, $CaSr(CO_3)_2$. The superstructure arises due to the ordering of the chemically different $Cu^{2+}$ cations, on one hand, and $Na^+$ and $Ca^{2+}$ cations, on the other hand. The formation of superstructure due to the cation ordering in paratooite-(La) compared to carbocernaite results in the multiple increase of structural complexity per unit cell. Therefore, paratooite-(La) versus carbocernaite represents a good example of structural complexity increasing due to the increasing chemical complexity controlled by different electronic properties of mineral-forming chemical elements (transitional versus alkali and alkaline earth metals).

Pring, A., Wallwork, K., Brugger, J., Kolitsch, U. Paratooite-(La), a new lanthanum-dominant rare-earth copper carbonate from Paratoo, South Australia. Mineral. Mag., 2006, 70, 131–138.

## Thermal expansion and hydration/dehydration of euchlorine $KNaCu_3O(SO_4)_3$

Artem S. Borisov[1,*], Oleg I. Siidra[1,2], Natalia V. Platonova[3], Wulf Depmeier[4], Evgeniya A. Lukina[1], Marie Colmont[5], Diana O. Nekrasova[1,5]

[1] Department of Crystallography, St. Petersburg State University, 199034 St. Petersburg, Russia
[2]Kola Science Center, Russian Academy of Sciences, 184200 Apatity, Murmansk Region, Russia
[3] X-ray Diffraction Resource Center, St. Petersburg State University, 199034 St. Petersburg, Russia
[4]InstitutfürGeowissenschaften der Universität Kiel, 24098 Kiel, Germany
[5]Unité de Catalyseet Chimie du Solide (UCCS), UMR 8181 CNRS, Université Lille 1 Sciences et Technologies, 59655 Villeneuve d'ASCQ, France

* as_borisov@inbox.ru

Anhydrous copper sulfate minerals with various alkali metals are the most abundant species in the famous for its mineral diversity fumaroles of Second Scoria Cone of the Great Tolbachik Fissure Eruption (1975–1976), and likewise in the Naboko scoria cone of the 2012–2013 Tolbachik Fissure eruption of the Tolbachik volcano on Kamchatka peninsula, Russia.

Euchlorine, ideally $KNaCu_3O(SO_4)_3$, is the most abundant copper sulfate mineral in the hot sulfate-rich zones of the fumaroles. In this work [Siidra et al., 2019], its thermal expansion and hydration/dehydration behavior have been studied. The results of a structure refinement from new single crystal diffraction data are also reported, and a description of the structure based on anion-centered coordination polyhedra is given.

The strongly anisotropic character of the thermal expansion of euchlorine remains essentially unchanged up to its decomposition. The strongest $\alpha_{11}$ expansion is observed approximately perpendicular to the alkali interlayer of the structure, whereas the minimal $\alpha_{22}$ and $\alpha_{33}$ thermal expansion coefficients are parallel to the plane of $\{Cu_3O(SO_4)_3\}^{2-}$ layers.

Hydration experiments controlled by X-ray powder diffraction reveal a very complex behavior with multicomponent phase formation. Some of the identified mineral phases, have not been found prior to our work in the secondary mineral assemblages of SSC, GTFE.

Unexpectedly, the complex mixture of hydrated sulfates gradually reverses and the minerals recombine and reform the primary euchlorine composition upon heating. Minor anhydrous by-phases dolerophanite and wulffite formed at the final stages of dehydration are structurally related to euchlorine, as their structures are also based on oxocentered $OCu_4$ tetrahedra.

As a side note, the observed multiple transformations of the primary exhalative mineral euchlorine can also be discussed in the light of the "Evolution of minerals" hypothesis developed by Hazen R. M. in the last decade.

This work was financially supported by the Russian Science Foundation through the grant 16-17-10085. Technical support by the SPbSU X-ray Diffraction and Geomodel Resource Centers is gratefully acknowledged.

Siidra O.I., Borisov A.S., Lukina E.A., Depmeier W., Platonova N.V., Colmont M., Nekrasova D.O. Reversible hydration/dehydration and thermal expansion of euchlorine, ideally $KNaCu_3O(SO_4)_3$. Physics and Chemistry of Minerals, 2019, in press.

**Layered copper hydrogen selenites: a family of decorated perovskite derivatives**

D.O. Charkin[1]*, V.Yu. Grishaev[1], M.R. Markovski[2], D.O. Nekrasova[2], O.I. Siidra[2,3]

[1]Moscow State University, 119992 Moscow, Russia
[2] St. Petersburg State University, 199034 St. Petersburg, Russia
[3] Kola Science Center, Russian Acad. Sci., 184200 Apatity, Murmansk Region, Russia

* charkin@inorg.chem.msu.ru

While "normal" and basic selenties and selenite halides of transition metals are in the focus of extensive studies due to natural occurrence and excellent and non-trivial magnetic properties [Verma, 1999], their analogs containing protonated selenite ions received essentially less attention. A small but interesting family involves a set of 2D structures based on neutral $[M(HSeO_3)_2]$ layers ($M$ = commonly $Cu^{II}$, a handful of $Co^{II}$ and $Zn^{II}$ representatives are also known). These layers interleave with sheets of water molecules of various metal-halide or metal-nitrate slabs of varied complexity leading, in most cases, to decorated perovskite-like structures, the decorating ions being $HSeO_3^-$ and $NO_3^-$, respectively [Kovrugin et al., 2015].

Evaporation of strongly acidic aqueous solutions containing $H_2SeO_3$, $CuX_2$, $AX$ ($A$ = univalent cation, $X$ = Cl, Br, or $NO_3$), and $HNO_3$ or $CF_3COOH$ produced single crystals of new copper hydrogen selenite nitrates and halides. The latter contain a series of $(AX)[Cu(HSeO_3)_2]$ compounds demonstrating various distorted versions of decorated $(AX)(BX_2)$ 3D perovskite structures. In all cases, chlorides and bromides are complete analogs and the structural details depend on the relative size of the $A^+$ cation. The smallest $Na^+$ produces a unique monoclinic motif (Kovrugin et al. 2015 and references therein); larger $K^+$ results in a less distorted monoclinic arrangement previously observed for $(RbX)[Zn(HSeO_3)_2]$. The largest $NH_4^+$, $Rb^+$, and $Cs^+$ gives rise to the orthorhombic structure first observed for $(NH_4Cl)[Cu(HSeO_3)_2]$. The dependence of the structure motif vs. the relative size of $A^+$ and $M^{2+}$ suggests that, akin to non-decorated perovskites, an analog of Goldschmidt tolerance factor can be suggested.

On the contrary, related nitrates were found only for the largest $NH_4^+$, $Rb^+$, $Tl^+$, and $Cs^+$. This comes due to the less symmetrical bonding mode of the nitrate ion compared to halide. This family hosts structures exhibiting decorated versions of Ruddlesden – Popper series closely related to cuprate superconductors. While $Cs^+$ and $Tl^+$ contribute to decorated perovskites $(ANO_3)[Cu(HSeO_3)_2]$, intermediate $Rb^+$ gives rise to $(RbNO_3)_2[Cu(HSeO_3)_2]$ (decorated $K_2NiF_4$). The smallest $NH_4^+$, which actively partakes in hydrogen bonding, yields the most complex structure of $(NH_4NO_3)_3[Cu(HSeO_3)_2]$, a decorated version of $TlBa_2CuO_5$. The structure of the ammonium compound was re-determined for more accurate analysis of hydrogen bonding.

Our studies of the halide compounds have also produced some curious side results. While $Li^+$ is too small to contribute to the perovskite-like structure, it serendipitously evokes formation of $Li_2Cu(Se_2O_5)Cl_2 \cdot 2H_2O$ with an unprecedented 2D structure which has no bromide analogue. We have also isolated two isostructural compounds $KX \cdot H_2SeO_3$ ($X$ = Cl and Br) which may be considered as simplest representatives of salt-inclusion structures. We also observed formation of a new 3D compound $CaCl(HSeO_3) \cdot H_2O$, which also has no bromide analogue.

This study was financially supported by the Russian President grant MD-5229.2018.5. Technical support by the X-Ray Diffraction Resource Centre of Saint-Petersburg State University is gratefully acknowledged.

Kovrugin V.M., Krivovichev S.V., Mentré O., Colmont M. $[NaCl][Cu(HSeO_3)_2]$, NaCl-intercalated $Cu(HSeO_3)_2$: synthesis, crystal structure and comparison with related compounds. Z. Kristallogr., 2015, 230, 573–578.

Verma V.P. A review of synthetic, thermoanalytical, IR, Raman, and X-ray studies on metal selenites, Thermochimica Acta, 1999, 327, 63–102

# 4.8. Miscellaneous

### Exotic topochemical alterations of the cationic sub-lattice in oxides

Olivier Mentré*, Houria Kabbour, Angel Arevalo-Lopez, Sylvie Daviero-Minaud, Marielle Huvé

Unité de Catalyse et Chimie du Solide, UMR CNRS 8181, Villeneuve d'Ascq, France

* Olivier.mentre@ensc-lille.fr

The possibility to modify inorganic oxides at moderate temperatures, under kinetic rather than thermodynamic control may lead to metastable structural rearrangements with novel electronic partitions and original properties. In most cases, the abundant literature reports modifications of the anionic sub-array dealing with anionic vacancies, interstitials or anionic exchanges. Here we present recent exotic cases where the observed modification concerns the cationic sub-array. This latter may be drastically re-arranged (sometimes driven by the concomitant alteration of the anionic sublattice). For instance, the controlled oxidation of the 2D-ising ferromagnetic $BaFe^{2+}_2(PO_4)_2$ into Fe-depleted $BaFe^{2/3+}_{2-x}(PO_4)_2$ ($x>$ 0.66) leads to a series of intermediate phases with full vacancy/Fe ordering and to nanometric $Fe_2O_3$ [Blasquez-Alcover, 2015]. Other pertinent examples of metal exsolution will be discussed such NiO exsolution during the reduction of the super-oxidized $BaNi^{4+}O_3$ [Arevalo-Lopez, 2019]. On the opposite, playing redox chemistry in 2D-oxides such as the multiferroic hexagonal $YMn^{3+}O_3$, $YbFe^{2.5+}_2O_4$ and $Yb_2Fe^{2.66+}_3O_7$, the metal content is maintained but re-organized during reduction/oxidation [Nicoud, 2017; Kabbour, 2017]. Generally, all transformed compounds require complex crystal-chemistry features with occurrence of supercells, modulated structures, and/or disordered intergrowths. The possibility to tune in a controlled way various pristine frameworks opens a wide field of investigation for tailor-made crystallographic architectures, within the field of giant anion/cation-labile systems.

Blazquez Alcover. I. et al. Crystal Growth and Design, 2015, 15, 4237–4247.
Arevalo-Lopez A. et al. Chem. Commun., 2019, 55, 3717–3720.
Nicoud S. et al. J. Amer. Chem. Soc., 2017, 139, 17031–17043.
Kabbour H. et al., Inorg. Chem., 2017, 56, 8547–8553.

**The Role of Four-Valent Vanadium in Mineral Structures**

Thomas Armbruster

Institute of Geological Sciences, University of Bern, CH-3012 Bern, Switzerland

armbruster@krist.unibe.ch

$V^{4+}$ has the electron configuration $3s^2 3p^6 3d^1$ and occurs in distorted [5] = [1+4]- (mean V-O bond length 1.90 Å) or [6] = [1+4+1]-oxygen coordination (mean V-O bond length 1.98 Å). The degenerate $t_{2g}$ and $e_g$ orbitals split and the d electron occupies one of the nonbonding orbitals ($3d_{xy}$) leading to one short vanadyl bond (1.5-1.7 Å) with a $\pi$-component from overlap of O($p\pi$) and $V^{4+}$($d\pi$) orbitals [Schindler et al., 2000].

The IMA 2018 mineral list contains 51 $V^{4+}$ -minerals: (1) 4 with $V^{4+}$ and $V^{3+}$, (2) 29 with only $V^{4+}$, and (3) 18 with $V^{4+}$and $V^{5+}$. Members of the latter group belong to the family of vanadium bronzes characterized by $V^{4+}$, $V^{5+}$ disorder and are here disregarded. 28 minerals of the first two groups have refined crystal structures with $V^{4+}$ coordinated by O. However, only 21 display the characteristic vanadyl bond: 8 square pyramids [1+4] and 13 distorted octahedra [1+4+1]. The major reasons for structures lacking a pronounced vanadyl bond are: (1) disorder of $V^{4+}$ with $Ti^{4+}$ and $V^{3+}$ (häggite, oxyvanite, vanadomalayaite, zoltaiite), (2) low crystal structure quality (paramontroseite, doloresite), (3) possible neglect of twinning (watsumiite).

Minerals belonging to $V^{4+}$-oxides and $V^{4+}$-oxyhydroxides have $V^{4+}$ in [6]-coordination, the silicates (suzukiite, haradaite, bavisiite, cavansite and pentagonite) have $V^{4+}$ in [5]-coordination whereas vanadomalayaite, zoltaiite, and watsumiite have $V^{4+}$ in [6]-coordination (without definite vanadyl bond, see above). Vanadates (bassoite, cavosite, and stibivanite) share $V^{4+}$ in [5]-coordination and all (12 examples) $V^{4+}$-sulfates and phosphates display $V^{4+}$ in distorted octahedral coordination.

Unusual$V^{3+}$ and $V^{4+}$-bearing vanadium oxide-minerals were described from the Slyudyanka complex, Lake Baikal, Russia [Döbelin et al., 2006; Reznitsky et al., 2009; Armbruster et al., 2013]. They occur as black xenomorphic grains and are of pseudobinary composition between $TiO_2$ and $(V,Cr)_2O_3$. They were classified according their $TiO_2$ content (wt. %) into 5 groups: (I) 13–15, (II) 18–19, (III) 25–26, (IV) 51–54, (V) 62–70. Single-crystal X-ray structure analysis identified crystals of group (I) as the new mineral oxyvanite $(V^{3+},Cr^{3+})_2(V^{4+}, Ti^{4+})O_5$, of groups (II, III) as berdesinskiite $(V^{3+},Cr^{3+})_2(Ti,V^{4+})O_5$, of group (IV) as schreyerite $V^{3+}{}_2(Ti,V^{4+})_3O_9$ and of group (V) as kyzylkumite $(Ti,V^{4+})_4V^{3+}{}_2O_{10}(OH)_2$. In oxyvanite, berdensikiite, and schreyerite $V^{4+}$ shares strongly distorted face-sharing octahedra with Ti and $V^{3+}$ showing indications of the $V^{4+}$ characteristic [1+4+1]-coordination. Kyzylkumite has a modular structure composed of rutile $TiO_2$ and montroseite $V^{3+}O(OH)$ units, both of which may bear $V^{4+}$, depending on exact composition.

Armbruster T., Lazic B., Reznitsky L. Z., Sklyarov E.V. Kyzylkumite, $Ti_2V^{3+}O_5(OH)$: new structure type, modularity and revised formula. Min. Mag., 2013, 77, 33–44.

Döbelin N., Reznitsky L.Z., Sklyarov E.V., Armbruster T., Medenbach O. Schreyerite, $V_2Ti_3O_9$: New occurrence and crystal structure. Amer. Mineral., 2006, 91, 196–202.

Reznitsky L.Z., Sklyarov E.V., Armbruster T., Ushchpovskaya Z.F., Galuskin E.V., Polekhovsky Y.S, Barash I.G. The new mineraloxyvanite $V_3O_5$ and the oxyvanite-berdisinskiite $V_2TiO_5$ isomorphic join in metamorphic rocks of the Sludyanka complex (South Baikal region). Proc. Russ. Mineralog. Soc., 2009, 138, 70–81.

Schindler M., Hawthorne F.C., Baur W.H. Crystal chemical aspects of vanadium: polyhedral geometries, characteristic bond valences, and polymerization of ($VO_n$) polyhedra. Chem. Mater., 2000, 12, 1248–1259.

**Immersion into the fascinating world of anion-centered units**

Marie Colmont*, Anastasia Zadoia, Marielle Huvé, Angel Arevalo-Lopez, Houria Kabbour, Pascal Roussel, Olivier Mentré

Université Lille, CNRS, Centrale Lille, ENSCL, Université Artois, UMR 8181, Unité de Catalyse et Chimie du Solide, Lille, F-59000, France

* marie.colmont@univ-lille.fr

Several minerals and inorganic compounds are described using ($XM_4$) tetrahedra, where $X$ is an anion ($O^{2-}$, $N^{3-}$ and $F^-$) and $M$ a cation ($Cu^{2+}$, $Zn^{2+}$, $Pb^{2+}$, $Bi^{3+}$, $REE^{3+}$, etc.…) [Krivovichev et al., 2013]. These units are connected together by edge and/or corner sharing, giving a huge variety of compounds with 1D, 2D or 3D structures.

Our lab has a strong experience in the design of new Bi-based materials built on such flexible units. An original predictive approach was established and successfully applied in elaborating novel inorganic compounds with related crystal structures and various dimensionalities [Lü et al., 2014].

Recently, the same procedure was extended to rare earth based compounds as they can act as phosphors [Colmont et al., 2019]. The size and flexibility of the anion-centered units is different and make the task more difficult. Especially, synthesis routes as well as characterization methods needs to be updated. For the first one, the use of high temperature and pressure is particularly powerful in the stabilization of new metastable phases and polymorphs [Colmont et al., 2018]. For the second one, advanced electron crystallography was successfully used to solve complex crystal structures in absence of single crystals.

This presentation will focus on recent results concerning new phases and their structure-properties relation. Particularly, magnetic, magneto caloric and luminescent properties were investigated.

Colmont M., Darie C., Tsirlin A.A., Jesche A., Colin C., Mentré O. Compressibility of $BiCu_2PO_6$: Polymorphism against S = 1/2 Magnetic Spin Ladders. Inorg. Chem., 2018, 57, 6038–6044.

Colmont M., Lemoine K., Roussel P., Kabbour H., Olchowka J., Henry N., Hagemann H., Mentré O. Identification and optical features of the $Pb_4Ln_2O_7$ series (Ln = La, Gd, Sm, Nd); genuine 2D-van der Waals oxides. Chem. Comm., 2019, 55(20), 2944–2947.

Krivovichev S.V., Mentré O., Siidra O.I., Colmont M. and Filatov S.K. Anion-centered tetrahedral in inorganic compounds. Chem. Rev., 2013, 113(8), 6459–6535.

Lü M., Aliev A., Olchowka J., Huvé M., Wickleder C., Mentré O. Multidimensional open-frameworks: combinations of one-dimensional channels and two-dimensional layers in novel Bi/M oxo-chlorides. Inorg. Chem., 2014, 53(1), 528–536.

# Anion-Centered Clusters $(X^{2-}M_{4-12})^{n+}$ in Oxides and Chalcogenides and its Structural Functions

Vladimir V. Bakakin[1,*], Yurii V. Seryotkin[2]

[1]A.V. Nikolaev Institute of Inorganic Chemistry SB RAS, 630090 Novosibirsk, Russia
[2] V.S. Sobolev Institute of Geology and Mineralogy SB RAS, 630090 Novosibirsk, Russia

[*]bakakin@niic.nsc.ru

Structures containing anion-centered tetrahedra $(OM_4)^{n+}$ are widely represented in the crystal chemistry of oxides. They have been comprehensively studied, for example, in the monograph [Krivovichev and Filatov, 2001]. $M^{n+}$ cations are usually $M^{2+}$ or $M^{3+}$. Recently shown [Bakakin, 2019], how in the structures with $M^+$ ($Cu^+$ or $Ag^+$) in an enlarged chalcogenide matrix ($S^{2-}$, $Se^{2-}$, $Te^{2-}$) are formed more capacious, than the tetrahedra, anion-centered clusters (**ACC**s).

Here are typical examples:

Octahedral ACC $\mathbf{(SeAg^{[4]}_6)^{4+}}$ – inside the 12-vertex Se-polyhedron: compound $K_2Ag_{12}Se_7$ [Emirdag et al., 1999]. Note that this structural type includes a very large number of phosphides and arsenides of alkaline, alkaline earth and rare earth metals [Bischoff et al., 2013].

Cubic ACC $\mathbf{(TeCu^{[4]}_8)^{6+}}$ –inside the Te-icosahedron: compound $Ba_3Cu_{20}Te_{13}$ [Yang et al., 2016].

Cuboctahedral ACC $\mathbf{(TeAg^{[4]}_{12})^{10+}}$ – inside the 16-vertex Friauf polyhedron: compound $Tl_4Ag_{18}Te_{11}$ [Moreau et al., 1992].

These ACCs can be thought as highly charged voluminous analogues of large Ba, K, Rb, Tl(I), Cs cations. Together they perform related structural functions (namely as templates).

Anion-centered tetrahedra can also serve as templates. The simplest case is a structure with a tetrahedral framework of sodalith type: for example, borate $\mathbf{(OZn^{[4]}_4)^{6+}}[B_6O_{12}]$ or nitrido-sodalithes$\mathbf{(XZn_4)^{6+}}[P_6N_{12}]$ (X = O, S, Se, Te) [Wester & Schnick, 1996]. But in complex combinations, ACCs can be members of a mixed framework. For example, in [Harrison et al., 1996] described open-framework zincophosphate/arsenate phases $M_3(H_2O)n\cdot[\mathbf{(Zn_4O)}(TO_4)_3]$ *(M* = Rb, K, Na; *n* = 3.5–6.0). Large alkaline cations together with $H_2O$ molecules have typically zeolite characteristics and functions.

This study was partially supported by the RFBR (grant 19-05-00800).

Bakakin V.V. J. Struct. Chem., 2019, 60, 449–456.

Bischoff M., Shlyk L., NiewaR. Solid State Sci., 2013, 21, 100 –105.

Emirdag M., Schimek G.L., Pennington W.T. et al. J. Solid State Chem., 1999, 144, 287–296.

Harrison W.T.A., Broach, R.W., Bedard R.A. et al., Chem. Mater., 1996, 8, 691–700.

Krivovichev S.V., Filatov S.K. Crystal Chemistry of Minerals and Inorganic Compounds with Complexes of Anion-Centered Tetrahedra [in Russian]. Izd. St. Petersburg University, 2001.

Moreau J.M., Allemand J., Brun G., Liautard B., J. Alloys Compd., 1992, 178, 85–90.

Wester F., Schnick W.Z. Anorg. Allgem. Chem., 1996, 622, 1281–1286.

Yang G.,Wu J., Zhang J., Ma D.J. Alloys Compd., 2016, 678, 12–17.

**Crystal structures and comparative crystal chemistry of three new lead oxo-centered compounds**

Anastasiia I. Zadoia[1]*, Oleg I. Siidra[2,3], Marie Colmont[1]

[1] Université de Lille, ENSCL, CNRS, Unité de Catalyse et Chimie du Solide (UCCS), UMR 8181, Villeneuve d'ASCQ, 59650 France
[2] St. Petersburg State University, Department of Crystallography, 199034 St.Petersburg, Russia
[3]Kola Science Center, Russian Academy of Sciences, 184209 Apatity, Murmansk Region, Russia

* zadoia.a@gmail.com

This study is devoted to the synthesis and crystal structures description of three new lead oxo-centered synthetic compounds with silicon, germanium and aluminum. All new phases were grown from the solid-state method using $PbF_2$ and $SiO_2$/$GeO_2$/$Al_2O_3$ as precursors and differently heated.

**$Pb_{6,5}Si_4AlO_{16}$** crystallizes in the *P*-1 space-group with cell parameters $a$ = 10.0029, $b$ = 10.0340, $c$ = 10.4762 Å, $\alpha$ = 80.58, $\beta$ = 70.72 and $\gamma$ = 60.36° where Z = 2 (Figure, a). Its crystal structure is original and among the seven currently known compounds of similar chemical composition, none crystallizes in the same crystal system. Monoclinic **$Pb_6Ge_{3,5}Al_2O_{16}$** crystallizes in the *C*2/*c* space group with cell parameters of $a$ = 10.1055(12), $b$ = 17.825(2), $c$ = 19.436(2) Å and $\beta$ = 95.572(8)° where Z = 8 (Figure, b). Only one compound in Pb/Ge/Al/O chemical system has been described in the literature. Yellow crystals of $Pb_2Al_2O_5$ were obtained on the lid of the crucible exclusively. The new compound **$Pb_2Al_2O_5$** crystallizes in a trigonal unit cell with cell parameters of $a$ = 9.946(6) and $c$ = 18.738(8) Å, *R*-3 (Fig. 1c). This new compound will be the sixth found in Pb/Al/O chemical system.

The structures of the three new compounds have similar crystal chemical features. Particularly, they contain tetrahedrally coordinated atoms of silicon, germanium or aluminum sharing corners and [$OPb_4$] anion-centered tetrahedra. These oxo-centered building units form different 0D blocks using topological and geometrical classification by Krivovichev et al. [2013].

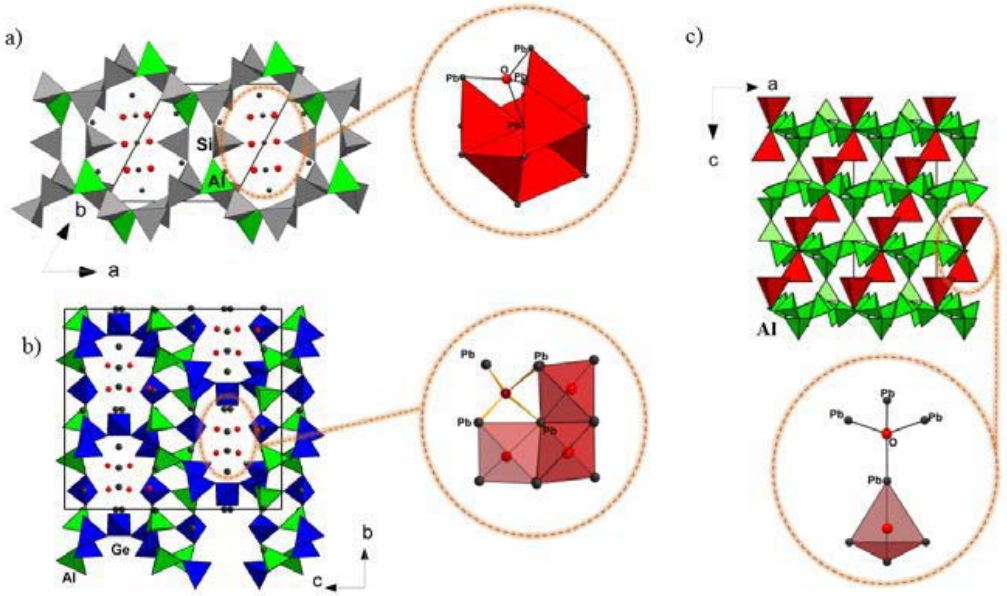

**New structural analogies among layered nitrates and halides: synthesis and structure of a new Sillén-derived fluoride nitrate, $BaPb_2F_5NO_3$**

Dmitri O. Charkin[1], Vadim E. Kireev[1]*, Oleg I. Siidra[2], Aleksandr N. Zaloga[3], Igor V. Plokhikh[4]

[1]Moscow State University, 119992 Moscow, Russia
[2]St. Petersburg University, 199034 St. Petersburg, Russia
[3] Siberian Federal University, 660041 Krasnoyarsk, Russia
[4]University of Regensburg, 93053 Regensburg, Germany

* kvad2000@yandex.ru

The structural analogies between layered nitrates and halides have been extensively investigated, for instance, in the search of materials for trapping of radioactive halide anions from solutions [Kodama et al. 2001], as well as some other toxicants. They have also been put to use in structural design of various nitrate analogs of carbonate minerals [Shenawi-Khalil et al. 2017; Charkin et al. 2018]. In most structures hitherto addressed, anionic sheets formed by nitrate or halide entities interleave with litharge-related $[(Bi,M)_2O_2]$, $[(Pb,Na)_2F_2]$, or $[Pb_2(O,F)_2]$ slabs bearing positive charge. There exists a yet unique example of structural analogy between a bismuth oxychloride compound $[BiTe_2O_5]Cl$ and a lead fluoronitrate $[Pb_3F_5]NO_3$ bearing slabs of different topology [Shenawi-Khalil et al. 2017 and references therein]. This suggests that the structural analogies between layered halides and nitrates may be extended further.

Among other layered halides, a matlockite-based solid solution series $BaPb_2F_5Br_{1-x}I_x$ (Weil et al. 2000) was taken as a candidate for constructing a nitrate analogue. Interaction of $BaF_2$, $PbF_2$, and $Pb(NO_3)_2$ in 2:3:1 ratio at 350°C produced the desired new compound $BaPb_2F_5NO_3$ as an off-white powder with a yield of *ca.* 95% along with traces of $BaF_2$, $PbF_2$, and $Pb_2OFNO_3$. Rietveld refinement (*P*4/*nmm*, $a$ = 5.976(1) Å, $c$ = 10.470(3) Å, $V$ = 373.9(2) Å$^3$, $Z$ = 1, $R_B$ = 0.015) indicated the new compound to be a structural analog of the $BaPb_2F_5Br_{1-x}I_x$. The structure is based on $[BaPb_2F_5]^+$ slabs exhibiting an ordered fcc-derived cation sublattice with $F^-$ filling both tetrahedral and octahedral voids leading to an *anti*-$Li_3Bi$-derived arrangement. The larger $Ba^{2+}$ cations center four-capped $F_{12}$ cubes (truncated cuboctahedra). The coordination of smaller $Pb^{2+}$ is less symmetrical due to positional disorder of nitrate anions and can be averaged to a capped $F_5O_4$ square antiprism. The geometrical centers (nitrogen atoms) of the statistically disordered $NO_3^-$ groups occupy the same site as the halide ions do in the structure of $BaPb_2F_5Br_{1-x}I_x$. Attempts to prepare Sr-based analogs were not successful indicating that the presence of large $Ba^{2+}$ cations is probably essential for the structure formation.

Another example featuring thick fluorite-derived slabs has been found in the system $LiF – PbF_2 – Pb(NO_3)_2$ where a new compound of approximate formula $Pb_4F_7NO_3$ appears to be isostructural to $Pb_4F_7I$ fluorohalide.

Charkin D.O., Plokhikh I.V., Zadoya A.I., Kuznetsova P.L., Kazakov S.M., Siidra O.I. $CdBiO_2NO_3$, a new layered bismuth oxide nitrate. Solid State Sci., 2018, 84, 23–27.

Kodama H., Kabay N. Reactivity of inorganic anion exchanger $BiPbO_2NO_3$ with fluoride ions in solution. Solid State Ionics, 2001, 141/142, 603–607.

Shenawi-Khalil S., Uvarov V.,Charkin D.O., Goaz A., Popov I., Dolgikh V.A., Sasson Y. A new bismuth potassium nitrate oxide, $Bi_{1.7}K_{0.9}O_2(NO_3)_2$: synthesis, structure, thermal behavior, and photocatalytic properties. Solid State Sci., 2012, 14, 159–165.

Weil M., Kubel F. Präparation und Strukturanalyse der Verbindungen $Ba_2Pb_4F_{10}Br_{2-x}I_x$ ($x$=0–2) mit verwandten kristallchemischen Motiven aus der Fluoritund Matlockitstruktur. Z. Anorg. Allg. Chem., 2000, 626, 2481–2486.

**Review of Tl(I) coordination polyhedra in oxysalt minerals and synthetic compounds**

Mishel R. Markovski[1,*], Oleg I. Siidra[1,2]

[1]Department of Crystallography, St. Petersburg State University, 199034 St. Petersburg, Russia
[2]Kola Science Center, Russian Academy of Sciences, 184200 Apatity, Murmansk Region, Russia

* mishelmarkovski@gmail.com

183 unique (i.e. without isostructural duplicates) monovalent thallium oxysalts for which good refinements exist were reviewed. 303 $Tl^{+}$-$O_n$ and 11 $Tl^{+}$-$O_nX_m$ ($X$ = F, Cl, Br) polyhedra containing 2449 $Tl^{+}$-O (≤ 3.55Å) and 74 Tl-$X$ (≤ 3.7 Å) bonds were taken into consideration. Bond-valence calculations and geometrical parameters proposed by [Balic-Žunic, Makovicky, 1996] were employed in order to evaluate the influence of the 'lone pair' (LP) stereoactivity on the distortion of Tl-centered coordination polyhedra. In 2/3 of the described complexes, LP is stereochemically active. LP occupies approximately the volume of O ion and strongly influences on the Tl(I) coordination environments.

5 different types of coordination polyhedra (Figure) were observed:

**I-Hemidirected convex geometry** of the Tl complexes, typical for low CN from 2 to 6, and strong stereoactivity of LP, raised above the surrounding O atoms;

**II-Hemidirected concave geometry**, typical for CN 6-11, and pronounced stereoactivity of LP;

**III-Equatorial geometry** is very rare and observed in $Tl^{+}$-$O_n$polyhedra with CN 5-12;

**IV-Bisdirected geometry** was earlier described for Pb(II) complexes [Severen et al., 2009]. The similar geometry was observed also for $Tl^{+}$-$O_n$.

**V-Holodirected geometry** [Shimoni-Livny et al., 1998] is typical for high CN 8-15 and no indication LP stereoactivity which in turn results in the formation of many relatively weak $Tl^{+}$-O bonds around the central thallium atom.

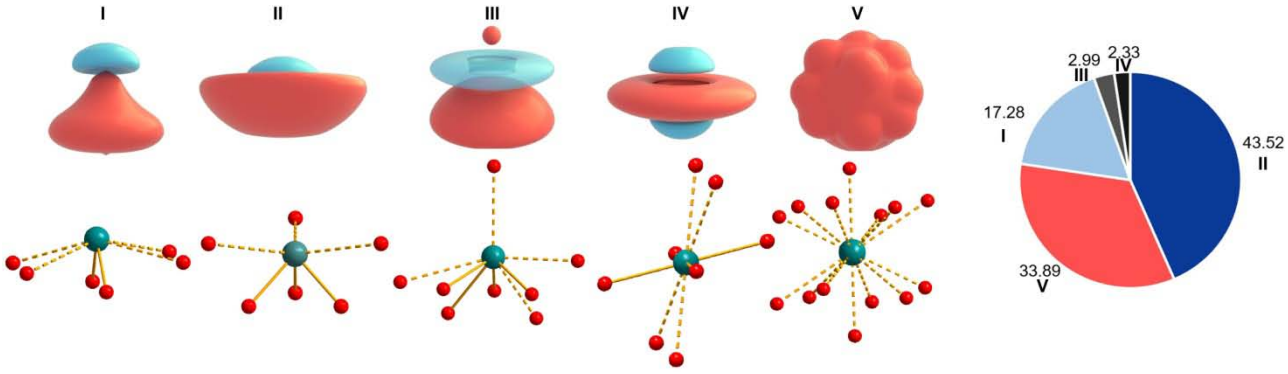


Figure. The 5 different types of Tl(I) coordination polyhedrain oxysalt minerals and synthetic compounds and some examples of Tl-$O_n$ coordination environments (left). Bonds > 3.0 Å are shown by dashed lines. Distribution of Tl(I) coordination polyhedra in reviewed structures (right).

Balic-Žunic T., Makovicky E. New measure of distortion for coordination polyhedra. Acta Crystallogr., 1996, B52, 78–81.

Severen M.-C., Piquemal J.-P., Shimoni-Livny L., Parisel O. Chemistry of lead at a molecular level: The Pb(II) 6s6p lone pair can be bisdirected in proteins. Chem. Phys. Lett., 2009, 478, 17–19.

Shimoni-Livny L., Glusker J.P., Bock C.W. Lone pair functionality in divalent lead compounds. Inorg. Chem. 1998, 37, 1853–1867.

**Matlokite as a structure type of polyhalogenides of lanthanides: crystallography and crystal chemistry of REE dichalcogenides**

Podberezskaya N.V.

Institute of Inorganic Chemistry SB RAS, Novosibirsk

podberez@niic.nsc.ru

There is no unambiguous definition of a structural type. The International Union of Crystallography has discussed this issue more than once, but did not clarify this problem [Urusov, 2009]. The researcher chooses on the basis of similarity of structures. There's more than one choice.

The mineral matlockite, PbFCl, is little known as a structure type of REE polychalcogenides. Features of the structure of matlockite were discussed in [Bannister et al., 1934].

The anions $F^-$ and $Cl^-$ have the same charge, but different ionic radii, 1.15 and 1.81 Å, respectively) [Bergerhoff et al., 1986]. The structure of matlokite is tetragonal (*P*4/*nmm*, $a$ = 4.1062(2), $c$ = 7.2264(9) Å, $V$ = 121.84 $Å^3$, $Z$ = 2, $d_{calc}$ = 7.13 $g \cdot cm^{-3}$). Each sort of atoms (F, Pb, Cl) is located in its own plane. These planes are parallel to each other and perpendicular to the $c$ axis. Atoms are arranged in a square in their sections, forming an infinite grid. The sides of the squares are approximately equal to the values of *a,b*-cell periods in the planes $Pb^{2+}$ and $Cl^-$. The layers $-Pb^{2+}...Cl^- ...Cl^- ...Pb^{2+}$ alternate with the layers of the $F^-$ ions. The F-squares are rotated by 45 degrees relative to the Cl-squares. Single-cap square antiprisms are formed around the metal atoms.

The crystal structures of *REE* polychalcogenides are based upon the sequences of layers $...-(X_2)^{2-}-Ln^{3+}-(X)^{2-} - (X)^{2-} - Ln^{3+} - (X_2)^{2-}-...$ The difference of their structure from that of matlockite is in the change of charges of the ions and the shape of chalcogenides. The layer $(X_2)^{2-}$ consist of dumbbells with covalent X-X bonds [Podberezskaya et al., 1996].

Information about the symmetry and connection of the unit cells of polyhalogenides with the parent cell matlockite (A0, b0, c0) are given in [Doert et al., 2016].

Bannister F.A., Hey V.N. Mineral. Mag., 1934, B23, 587–597

Bergerhoff G., Kilger B., Witthauer C., Hundt R., Sievers R. ICSD CRYSTIN, User's Manual. Bonn: Inst. Anorg. Chem. der Univ., 1986, 60.

Doert T., Müller C.J. Elsevier Inc. Reference in Module Chemistry, Molecule Sciences and Chemical Engineering, 2016.

Podberezskaya N.V., Magarill S.A., Pervukhina N.I., Vasilyeva I.G., Borisov S.V. J. Struct. Chem., 1996, 37, 1137.

Urusov V.S. Crystallography Rep., 2009, 54, 795.

**On the crystal structure of thorium hydrogen arsenate, $Th_2(AsO_4)_2(HAsO_4)(H_2O)$**

D.O. Charkin[1], K.A. Zagidullin[1]*, E.V. Nazarchuk[2], O.I. Siidra[2,3]

[1]Moscow State University, 119992 Moscow Russia
[2] Department of Crystallography, St. Petersburg State University, 199034 St. Petersburg, Russia
[3] Kola Science Center, Russian Academy of Sciences, 184200 Apatity, Murmansk Region, Russia

* zagidullink@yandex.ru

Phosphates and arsenates of thorium are of particular interest as these compounds are closely related to processing of thorium ores and immobilization of radioactive wastes. Thorium hydrogen phosphates, as well as some more complex alkali-containing compounds, have recently received particular attention [Na Yu et al. 2017]. The chemistry of thorium hydrogen arsenates is not so actively studied.

A new compound, $Th_2(AsO_4)_2(HAsO_4)(H_2O)$, was obtained in a small yield in hydrothermal reaction between $Th(NO_3)_4$ and $As_2O_3$ at 200°C. Its structure has been solved from a twinned crystal. The compound crystallizes in space group *Pbca* with cell parameters $a$ = 12.8868(3), $b$ = 7.2379(2), $c$ = 23.9480(7) Å. It is curious no note that the arsenic compound is not isostructural to the corresponding phosphate, $Th_2(PO_4)_2(HPO_4)(H_2O)$ [Salvadó et al. 2005], despite very similar mode of preparation. The structure of $Th_2(AsO_4)_2(HAsO_4)(H_2O)$ contains two unique thorium cations coordinated by eight oxygen atoms one of which belongs to the water molecule. These coordination polyhedra share edges to form chains. They also share edges with the $AsO_4$ tetrahedra, which in their turn share two other vertices with other $ThO_8$ moieties.

This study was financially supported by the Russian President grant MD-5229.2018.5. Technical support by the X-Ray Diffraction Resource Centre of Saint-Petersburg State University is gratefully acknowledged.

Na Yu, Klepov V.V., Schlenz H., Bosbach D., Kowalski P.M., Yan Li, Alekseev E.V. Cation-dependent structural evolution in $A_2Th(T^VO_4)_2$ (A = Li, Na, K, Rb, Cs; T = P and As) series. Cryst. Growth Des., 2017, 17, 1339–1346.

Salvadó M.A., Pertierra P., Bortun A.I., Trobajo C., García J.R. New hydrothermal synthesis and structure of $Th_2(PO_4)_2(HPO_4)\cdot H_2O$: the first structurally characterized thorium hydrogen phosphate. Inorg Chem., 2005, 44, 3512–3517.

## Phase Formation, Structure and Physical Properties of Mg-Containing $Nd_2MoO_6$ Compounds

Valentina I. Voronkova[1,*], Elena P. Kharitonova[1], Ekaterina I. Orlova[1], Egor D. Baldin[1], Nataliya I. Sorokina[2], Alexander M. Antipin[2], Vadim V. Grebenev[2], Timofey A. Sorokin[2]

[1] M.V. Lomonosov Moscow State University, 119991 Moscow, Russia
[2] Shubnikov Institute of Crystallography RAS, 119333 Moscow, Russia

*voronk@polly.phys.msu.ru

The $Ln_2W(Mo)O_6$ compounds, the so-called oxymolybdates and oxytungstates, have a different structural type depending on the ionic radius of the rare-earth cation and the synthesis temperature. The oxymolybdates $Ln_2MoO_6$ with large rare-earth elements Ln = La, Pr, Nd, synthesized at temperatures above 1000°C, have a layered tetragonal structure with space group $I4_1/acd$ [Efremov et al., 1987] or $I\text{-}42m$ [Sillen, Lundborg, 1943] at room temperature. Doping of such compounds with bivalent lead led to a significant improvement in the conductive properties and the appearance of polymorphism [Voronkova et al., 2016]. In the present work, the effect on the phase formation, structure, and physical properties of the $Nd_2MoO_6$ compound upon its doping with bivalent magnesium was studied.

Polycrystalline samples of $(MgO)_x(Nd_2MoO_6)_{(1-x)/2}$ were prepared by solid-phase synthesis in air at a temperature of 1250°C, where $x$ = 0, 0.3, 0.05, 0.10, 0.125, 0.15, 0.20. Single crystals of $Nd_2MoO_6$, pure and doped with magnesium, were grown by the flux method. The resulting mono- and polycrystalline samples were characterized by X-ray phase analysis, EDS microanalysis, X-ray diffraction analysis, differential scanning calorimetry, thermogravimetry, and impedance spectroscopy.

The study of powder X-ray diffraction patterns of polycrystalline samples $(MgO)_x(Nd_2MoO_6)_{(1-x)/2}$ ($x$ = 0, 0.03, 0.05, 0.10, 0.125, 0.15, 0.20) showed that the region of solid solutions with the tetragonal $Nd_2MoO_6$ structure extends to $x$ = 0.20. EDS microanalysis confirmed the entry of magnesium into the $Nd_2MoO_6$ crystal lattice. The study of samples using the DSC method did not reveal any anomalies in the entire temperature range under study. X-ray analysis of the pure and doped monocrystalline samples showed that the model of the structure in which magnesium atoms partially replace molybdenum atoms best fit the observed diffraction pattern.

The study of the electrophysical properties of the synthesized polycrystalline $Nd_2MoO_6$ samples, with different magnesium content, by impedance spectroscopy revealed a significant difference in the magnitude and nature of the conductivity of the samples during cooling and heating. The difference gradually disappears with each new heating-cooling cycle, which may indicate instability of the oxygen sublattice at high temperatures.

This work was supported by Russian Foundation for Basic Research (project No. 18-29-12005).

Efremov V. A., Tyulin A. V., Trunov V.K. Koordinatsionnaya Khimiya, 1987, 13, 1276–1282.

Sillen L.G., Lundborg K.$La_2MoO_6$, ein Lanthanoxymolybdat mit Schichtenstruktur. Z. Anorg. Chem., 1943, 252, 2–8.

Voronkova V.I., Orlova E.I., Kazakov S., Kharitonova E.P., Belov D. Phase relations and physical properties of layered Pb-containing $Nd_2MoO_6$ compounds. Eur. J. Inorg. Chem., 2016, 1022–1029.

**Polymorphs of rare-earth molybdates $Ln_{10}Mo_2O_{21}$ (Ln = Gd, Dy, Ho): structure, conductivity and magnetism**

Anna V. Shlyakhtina[1*], Maxim Avdeev[2], Nikolay V. Lyskov[3], Ksenia S. Denisova[4], Igor V. Kolbanev[1], Sergey A. Chernyak[4], Lidia G. Shcherbakova[1], Olga S. Volkova,[4,5,6] Alexander N. Vasiliev[4,5,6**]

[1]Semenov Institute of Chemical Physics RAS, 119991 Moscow, Russia
[2] Australian Centre for Neutron Scattering, Australian Nuclear Science and Technology Organization, Kirrawee DC, NSW 2232, Australia
[3]Institute of Problems of Chemical Physics RAS, Chernogolovka, Russia
[4]M.V. Lomonosov Moscow State University, 119991 Moscow, Russia
[5]Ural Federal University, 620002 Ekaterinburg, Russia
[6]National Research South Ural State University, 454080 Chelyabinsk, Russia

*annashl@inbox.ru, annash@chph.ras.ru

The polymorphism of $Ln_6MO_{12}$ (*M* = Mo, W) rare-earth molybdates and tungstates has been studied for a rather long time [Bartram, 1966].Nevertheless, many questions related to the structure of *REE* molybdates remain open. The purpose of this work was to find conditions for the synthesis of phase-pure $Ln_{10}Mo_2O_{21}$ (Ln = Gd, Dy, Ho) intermediate rare-earth molybdates; to synthesize high-temperature (fluorite) and low-temperature polymorphs of the $Ln_{10}Mo_2O_{21}$ (Ln = Gd, Dy, Ho) molybdates and study their structure by XRD, to determine the structure of the low-temperature polymorph phase (orthorhombic or tetragonal) by neutron diffraction, using $Ho_{10}Mo_2O_{21}$ as an example, to study the microstructure and conductivity of the synthesized compounds in dry and wet air, and to study the magnetic properties of the $Ln_{10}Mo_2O_{21}$ ( Ln = Gd, Dy, Ho) polymorphs.

Orthorhombic and fluorite $Ln_{10}Mo_2O_{21}$ (Ln = Gd, Dy, Ho) polymorphs have been synthesized by firing mechanically activated $5Ln_2O_3 + 2MoO_3$ (Ln = Gd, Dy, Ho) oxide mixtures at 1200 and 1600 °C, respectively. Stable, phase-pure orthorhombic $Ln_{10}Mo_2O_{21}$ (Ln = Gd, Dy, Ho) molybdates have been obtained for the first time by prolonged (40–160 h) heat treatment at 1200 °C. The preparation of orthorhombic $Gd_{10}Mo_2O_{21}$ requires the shortest time (40 h), the synthesis of orthorhombic $Dy_{10}Mo_2O_{21}$ takes double this time (80 h), and 160 h are needed to obtain orthorhombic $Ho_{10}Mo_2O_{21}$. Higher temperature firing (1600 °C, 3 h) leads to the formation of phase-pure fluorite $Ln_{10}Mo_2O_{21}$ (Ln = Gd, Dy, Ho).

Summarizing the results of the present and earlier works [Bevan et al., 1982; Lashtaberg et al., 2010] it can be stated with all certainty that the structure of the low-temperature $R_{10}Mo_2O_{21}$ (R = Gd-Er, Y) polymorphs is orthorhombic and not tetragonal.

Proton conduction of orthorhombic and fluorite polymorphs $Gd_{10}Mo_2O_{21}$, $Dy_{10}Mo_2O_{21}$, $Ho_{10}Mo_2O_{21}$ has been investigated.

Down to liquid helium temperatures, the title compounds exhibit paramagnetic properties due to weakly interacting localized magnetic moments of rare-earths.

This work was supported by the Russian Foundation for Basic Research (grants no. 16-03-00143, 19-03-00358).

Bartram S.F. Crystal Structure of the Rhombohedral $MO_3 \cdot 3R_2O_3$Compounds (M = U, W, or Mo) and Their Relation to Ordered $R_7O_{12}$Phases.Inorg. Chem., 1966, 5, 749–754.

Bevan D.J.M., Drennan J., Rossell H.J. Structure determination of the fluorite-related superstructure phases $Er_{10}W_2O_{21}$ and $Y_{10}W_2O_{21}$.Acta Cryst., 1982, B38, 2991–2997.

Lashtaberg A., Bradley, J., Dicks A., Auchterlonie G., Drennan J. Structural and conductivity studies of $Y_{10-x}La_xW_2O_{21}$. J. Solid State Chem., 2010, 183, 1095–1101.

**Mixed-valent tellurium oxides$ATe_{1-x}B_xO_6$ (A= Rb, Cs, B=Mo, W) with Pyrochlore-related structure**

D.G. Fukina[1,]*, E.V. Suleimanov[1], Boryakov A.V.[1], G.K. Fukin[2], S.G. Protasova[3], A.M. Ionov[3]

[1]Lobachevsky State University of Nizhny Novgorod, 603950 Nizhny Novgorod, Russia
[2]Razuvaev Institute of Organometallic Chemistry RAS, 603950 Nizhny Novgorod, Russia
[3]Institute of Solid State Physics RAS, Chernogolovka, 142432 Moscow, Russia

* dianafuk@yandex.ru

The ideal α-pyrochlore structure has stoichiometry $AB_2X_6X'$ (where *A* is a large low valence cation, *B* is a small more highly charged cation capable of octahedral coordination, *X* is oxygen ions, as well as ions $OH^-$, $F^-$, or $H_2O$ and *X'* is ions weakly interacting with *B*) and belongs to cubic system with space group $Fd\bar{3}m$ [Darriet et al., 1971]. However, a lot ofpyrochlore-type compounds can deviate from ideal structure. It occurs because atoms with different valence state can occupy the same position *B*. Varying cations in positions *A* and *B* allow to find out new defect pyrochlore-type compounds ($\beta$-pyrochlore$AB_2O_6$).Many investigations are devoted to pyrochlore-related structures where *B* position is occupied by the cations with 5+ ($V^{5+}$, $Nb^{5+}$, $Ta^{5+}$, $Sb^{5+}$) and 6+ ($Mo^{6+}$, $W^{6+}$, $Te^{6+}$) oxidation states. However, there is interest to investigate the possibility of existence the pyrochlore-related structures where *B* position is occupied by the cations with 4+ and 6+ oxidation states. There are investigations of pyrochlores doped with Te ions. The $Te^{4+}$ ion could be located in the position *A* [Subramanian et al., 1983] and $Te^{6+}$ ion could occupy the position *B* [Weber et al., 2000]. However, more perspective pyrochlore structures have the tellurium in both oxidation states at the same time [Siritanon et al., 2011].

We carried out the search for new compounds with the pyrochlore structure in the series $ATe_{1-x}B_xO_6$ (*A*=Na, K, Rb, Cs, *B*=Mo, W) *x* = 0–1, using systematic synthesis based on the phase diagrams of $A_2O$–$TeO_3$–$BO_3$(*A* = Na, K, Rb, Cs, *B* = Mo, W). The pyrochlore-related phases have been obtained for $ATe_{1-x}B_xO_6$ (*A*= Rb, Cs, *B* = Mo, W) compounds. New isostructural mixed-valent tellurium oxides, $CsTeMoO_6$and $RbTe_{1.25}Mo_{0.75}O_6$, have been synthesized by solid-state reactions and characterized by single-crystal X-ray diffraction and thermal analysis. Both compounds have pyrochlore-type structure with cubic space group $Fd\bar{3}m$, *Z* = 8 and the following unit cell parameters: *a* =10.5892(5) Å in $CsTeMoO_6$ and *a* = 10.4421(2) Å in $RbTe_{1.25}Mo_{0.75}O_6$. A small part of the oxygen atoms shifts from the special position 48f to the general crystallographic position 192i, because the $Te^{4+}$ ion is too large for the regular pyrochlore-structure framework and causes local distortions. The thermal instability of the $CsTeMoO_6$ and $RbTe_{1.25}Mo_{0.75}O_6$ phases was found at the 449–521°C and 381–466 °C temperature ranges, respectively. Isostructural $ATe_{1-x}W_xO_6$ (*A*= Rb, Cs) compounds have been investigated by powder X-Ray diffraction. However, it was found that compounds $ATe_{1-x}B_xO_6$ (*A*=Na, K, *B*=Mo, W)*x* = 0–1 with the pyrochlore structure are not formed, but, completely new ternary compounds $Na_{1.5}Te_2Mo_{0.5}O_{6.25}$ and $K_6(Te_9^{4+}Te^{6+})Mo_6O_{42}$ were identified and structurally characterized, and the thermal properties were investigated.

Darriet B., Rat M., Galy J. Sur quelques nouveaux pyrochlores des systemes $MTO_3$ - $WO_3$ et $MTO_3$ - $TeO_3$ (M = K, Rb, Cs, Tl; T = Nb, Ta). Mater. Res. Bull., 1971, 6, 1305–1315.

Siritanon Th., Sleight A.W., Subramanian M.A. Single crystal growth and structure refinements of $CsM_xTe_{2-x}O_6$ (M = Al, Ga, Ge, In) pyrochlores. Mater. Res. Bull., 2011, 46, 820–822.

Subramanian M.A., Aravamudan G., Subba Rao G.V. Oxide pyrochlores. Prog. Solid State Chem., 1983, 15, 55–143.

Weber F.A., Schleid T. $Pr_2Te_2O_7$: A Praseodymium (III) Oxide Oxotellurate (IV) According to $Pr_2O(TeO_3)_2$ with Pyrochlore-Type Crystal Structure. Z. Anorg. Allg. Chem., 2000, 626, 1285 –1287.

**Phase Formation and Polymorphism of $Bi_2O_3$-Based Compounds in $Bi_2O_3$-$Ln_2O_3$-$MeO_3$ (Ln = La, Nd, Pr; Me = Mo, W) Ternary Systems**

Elena P. Kharitonova*, Ekaterina I. Orlova, Valentina I. Voronkova

M.V. Lomonosov Moscow State University, 119991 Moscow, Russia

* harit@polly.phys.msu.ru

$Bi_2O_3$-based solid solutions are interesting as promising oxygen conductors with conductivity reaching 0.1-1 S/cm at 800 °C. The pure $Bi_2O_3$ has a complex polymorphism. Four basic $Bi_2O_3$ phases are well known [Kharton et al., 2001]: 1) α-$Bi_2O_3$ monoclinic phase, stable at room temperature; 2) β-$Bi_2O_3$ tetragonal phase; 3) γ-$Bi_2O_3$ cubic phase; 4) high-temperature δ-$Bi_2O_3$ cubic phase with fluorite structure, which is stable in narrow temperature range 700–780 ºC and demonstrate extremely high oxygen conductivity near 3 S/cm [Takahashi et al., 2001]. The main attention in literature is paid to the stabilization of the oxygen-conducting δ-$Bi_2O_3$ cubic phase at room temperature by doping. The best results were achieved with two different codopants. From this point of view, the ternary systems $Bi_2O_3$-$Dy(Er)_2O_3$-$WO_3$ [Jiang et al., 2002; Watanabe et al., 2005] and $Bi_{14}W_{1-x}La_xO_{24-3x/2}$ solid solutions [Borowska-Centkowska et al., 2011] were investigated. In addition to the δ-$Bi_2O_3$ cubic phase, as a result of doping, less symmetric $Bi_2O_3$-based phases can arise, but little attention is paid to their phase formation and polymorphism. In this work, we investigated the phase formation, polymorphism and conductivity of $Bi_2O_3$-based compounds with different symmetry in ternary $Bi_2O_3$-$Ln_2O_3$-$MeO_3$ systems (Ln = La, Pr, Nd, Me = W, Mo).

Polycrystalline samples were obtained by solid state synthesis in air. Different phases with a cubic, tetragonal, monoclinic, and rhombohedral structure were observed in $Bi_2O_3$-$Ln_2O_3$-$MeO_3$ systems as the composition was changed. In the systems with Me = Mo, phases with a cubic and tetragonal structure prevail. In systems with Me = W, the fields of monoclinic and rhombohedral phases are most pronounced, while cubic and tetragonal compounds form in very narrow regions of compositions. So, for Me = W, the high-temperature cubic δ-$Bi_2O_3$phase is stabilized in a range of 85–90 mol. % $Bi_2O_3$, which is much lower than in similar systems with Me = Mo (55–90 mol.% $Bi_2O_3$). When Ln = Pr, Nd, two fields of cubic compounds with a fluorite structure are formed in $Bi_2O_3$-$Ln_2O_3$-$MeO_3$ ternary systems in regions with high and low bismuth concentrations.

The studies have shown that the concentration of bismuth oxide is the main factor affecting on the magnitude of oxygen conductivity, but for all $Bi_2O_3$-based samples the conductivity remains quite high. At low bismuth concentration (45–50 mol. % $Bi_2O_3$) the conductivity of the samples is close to 0.01 S/cm at 800 °C. At high bismuth concentration (85–90 mol. % $Bi_2O_3$) cubic δ-$Bi_2O_3$ samples demonstrate conductivity, reaching 0.6 S/cm at 800 °C. For most samples, the conductivity obeys the Arrhenius law with activation energy near 0.9–1.2 eV. For cubic samples with high bismuth concentration, 85–90 mol. %, $Bi_2O_3$, above 400 °C, the conductivity can be approximated by the Vogel-Fulcher-Tamman law.

Borowska-Centkowska A., Krok F., Abrahams I., Wrobel W. Solid State Ionics, 2011, 203, 22–28.

Jiang N., Wachsman E.D., Jung S.H. Solid State Ionics, 2002, 150, 347–353.

Kharton V.V., Naumovich E.N., Yaremchenko A.A., Marques F.M.B. J. Solid State Electrochem., 2001, 5, 160–187.

Takahashi T., Iwahara H., Nagai Y. J. Appl. Electrochem., 1972, 2, 97–104.

Watanabe A., Sekita M. Solid State Ionics, 2005, 176, 2429–2433.

**Single Crystal X-Ray Diffraction Studies of [Mn(5′-GMP)terpy] & [Mn(5′-UMP)terpy-$CO_2H$] ternary systems**

Dineshchakravarthy Senthurpandi, M. Nethaji*

Inorganic and Physical Chemistry, Indian Institute of Science, 560 012 Bangalore, India

*mnethaji@iisc.ac.in

Coordination chemistry and supra-molecular chemistry of metal-nucleotide complexes have attracted immense interest in recent decades. Nucleotides are environmentally friendly ligands due to their water solubility, biocompatibility, and chirality, which make them ideal candidates for mimicking biological systems and designing functional materials. Crystallizing metal-nucleotide complexes have greatly been hampered due to the ambivalent properties of nucleotides. We aimed to overcome these difficulties by analyzing the coordination activity of nucleotides to the transition metal atom manganese.

Title compounds were synthesized and structurally characterized using X-ray crystallographic technique. The asymmetric unit consists of [Mń(5′-GMP)terpy]$_2$·18$H_2O$ for complex **1** and [Mn(5′-UMP)terpy-$CO_2H$]$_2$·13$H_2O$ for complex **2** and they were crystallized in the $P2_1$ and $C2$ space groups respectively.The two manganese atoms in complex **1** have the same coordination sphere: Mn1 and Mn2 are bridged by phosphate groups of 5′-GMP ligand and each metal is surrounded by nitrogen atoms from a terpy molecule. Coordination number around both the metals in complex **1** is 5 whereas in complex **2** it is 6 for Mn1 and 7 for Mn2. For complex **2**, the metal centers are surrounded by nitrogen atoms of the terpy ligand, one phosphate oxygen atom, solvent water molecule and carboxylate group in 4′-position of terpy ligand. Around Mn1, one of the oxygen atoms of carboxylate takes part in bonding whereas around Mn2 carboxylate group acts as a chelating ligand. All the ribose rings of 5′-Nucleotide entity shows the usual C2′-endo envelope conformation except, one of the ribose rings in complex 2, which shows C3′-exo envelope conformation. Furthermore, the complexes were stabilized by hydrogen bonding and π-π stacking interactions. Details of the interesting features will be discussed.

Zhou P. et al. Supramolecular self-assembly of nucleotide-metal coordination complexes: From simple molecules to nanomaterials. Coordination Reviews, 2015, 292, 107–143.

Saenger W. Principles of Nucleic Acid Structure. Springer Science & Business Media, 2013.

Abbreviations Used:

- 5′-UMP –5′- Uridine MonoPhosphate
- 5′-GMP – 5′- Guanosine MonoPhosphate
- terpy – 2,2′:6′,2″-Terpyridine
- terpy-$CO_2H$ – 2,2':6',2''-Terpyridine-4'-carboxylic acid

**Preparation of crystals of water-soluble salts of cobalt and nickel**

O.B. Zaimullin*, V.A. Komornikov, I.S.Timakov

Shubnikov Institute of Crystallography of Federal Scientific Research Centre “Crystallography and Photonics” of Russian Academy of Sciences

* evil_hamster@mail.ru

In modern instrumentation, optical filters are an important component. At the Institute of Crystallography methods are developed for growing crystals with a narrow optical transmission band in various regions of the optical spectrum.

Filters with a narrow bandwidth in the UV range are used in devices "solar-blind technology" [Voloshin et al., 2006]. These studies are carried out with the use of double sulfates of transition elements, the so-called Tutton salts [Manomenova et al., 2005]. However, optical filters obtained from the crystals of these substances have an optical transmission region in the visible zone, which negatively affects the technical characteristics of the instruments produced with their use.

This paper is devoted to determining the conditions for obtaining crystals of water-soluble cobalt and nickel salts with the required spectral characteristics. Cobalt and nickel chlorides attract attention with similar optical properties and prospects for increasing the temperature range of operation.

In this work, phase equilibria of $NiCl_2$–$CoCl_2$–$H_2O$, $NiCl_2$–HCl–$H_2O$ water-salt systems are investigated. Based on the experimental data obtained, it was possible to obtain a relatively large crystal of $NiCl_2 \cdot 6H_2O$, the dimensions of which made it possible to study its optical as well as thermal properties. The results of microscopy of the surface of the obtained crystals unambiguously indicate the mechanism of layer-by-layer growth of the face of a crystal with the participation of vicinal mounds. Based on the research results, $NiCl_2 \cdot 4H_2O$ crystalline hydrate is a more promising material due to the wider temperature range of existence compared with $NiCl_2 \cdot 6H_2O$. Next, the conditions for the formation of $NiCl_2 \cdot 4H_2O$ with the minimum necessary concentration of hydrochloric acid at 25°C were determined to further obtain a single-crystal sample of this crystalline hydrate and study its properties.

The fields of crystallization of solid solutions with the general formula $Ni_xCo_{(1-x)}Cl_2 \cdot 6H_2O$ at 25°C were also determined. Under the conditions of the joint presence of $NiCl_2 \cdot 6H_2O$ and $CoCl_2 \cdot 6H_2O$, a series of solid solutions is formed in a wide range of compositions at $0 > x > 1$. The crystallization range of the starting components is very limited and amounts to only a few mole percent.

The optical transmission spectra of solutions of these compounds with a concentration close to saturated solutions, as well as the optical transmission spectra of crystalline samples, were studied. Both the solutions and the resulting crystalline samples have two transmission bands, one of which is located in the ultraviolet region, and the other in the visible part of the spectrum. However, the position of the bands varies and depends on the specific composition of the test substance.

The data obtained as a result of research allow us to develop methods for growing large single crystals from aqueous solutions suitable for practical use in optics.

This work was supported by the Ministry of Science and Higher Education in the framework of the work on the State task of the Federal Research Center “Crystallography and Photonics” of the Russian Academy of Sciences.

Manomenova V.L. et al. Crystallogr. Rep., 2005, 50, 937–942.
Voloshin A.E. et al. Patent RU 2417388, 24.11.2006.

# 5. Materials

**From Minerals to Cathode Materials for Metal-ion batteries**

Evgeny V. Antipov

Lomonosov Moscow State University, 119991 Moscow, Russia

evgeny.antipov@gmail.com

Ninety percent of the energy produced today come from fossil fuels. Rapid consumption of these energy sources makes dramatically negative impact on our future due to ecological damage and climate change. In this sense, the development of the environmentally benign renewable energy sources capable to replace fossil fuels and concurrently efficient large energy storage devices requires no justification.

Li-ion batteries (LIBs) have been originally developed for portable electronic devices, but nowadays new application niches are envisaged in electric vehicles and stationary grid-scale energy storages. However, LIBs may be not fully adopted for these applications. The geographical scarcity and excessive demand for Li resources intensifies the development of alternative sustainable technologies based on vastly accessible materials, namely Na- and K- ion batteries (NIBs and KIBs, respectively).

The battery performance is critically governed by the properties of the electrode materials. The first generation of cathode materials for the Li-ion batteries based on the mixed oxides has already been widely commercialized. However, the potential to further improve the performance of these materials is almost exhausted. The compounds, containing alkali and transition metal cations together with different polyanions $(X_mO_n)^{p-}$ ($X$ = B, P, S, Si) with structures closely related to different minerals, are now considered as the most promising cathode materials for the next generation of the Me-ion batteries. Covalently-bonded structural frameworks in these compounds offer long-term structural stability, which is essential for good cyclability and safety. Further advantages are expected from combining different anions (such as $(XO_4)^{p-}$ and $F^-$) in the anion sublattice, with the hope to enhance the specific energy and power of the batteries.

An overview of the research on phosphates and fluoride-phosphates with the general formula of $LiMPO_4$ and $A_xMPO_4F$ ($A$ = Li, Na, K; $M$ = V, Fe, Co), respectively, adopting various structure types depending on the $A$ and $M$ metals as prospective electrode materials for the Me-ion batteries will be presented with a special emphasis on the interrelation between chemical composition, synthesis conditions, crystal structure peculiarities and electrochemical properties of the materials important for practical applications.

This work was supported by the Russian Science Foundation (grant No. 17-73-30006).

**Nature-inspired synthesis technologies of functional titanosilicates**

Lidia G. Gerasimova, Gregory Yu. Ivanyuk*, Galina O. Kalashnikova, Sergey V. Krivovichev, Anatoly I. Nikolaev, Yakov A. Pakhomovsky, Taras L. Panikorovskii, Gleb O. Samburov, Ekaterina A. Selivanova, Victor N. Yakovenchuk

Kola Science Centre of the Russian Academy of Sciences, 184209 Apatity, Russia

* g.ivanyuk@gmail.com

Alkaline complexes of the Kola Peninsula contain rare titanosilicates that have important functional properties, for example, molecular sieve chivruaiite (Ca-analog of ETS-4), titanosilicate "nanopuzzles" kukisvumite and lintisite (Zn and Li analogues of AM-4, respectively), cation exchangers sitinakite (natural analogue of Ionsiv IE-911) and ivanyukite (natural analogs of SIV), photocatalyst korobitsynite (natural analog of TR01), etc. The alkaline complexes also serve as sources of rich titanium ores, including titanite, loparite, titanomagnetite and murmanite varieties.

All above listed economic minerals can produce secondary rare titanosilicates under the influence of low-temperature hydrothermal solutions, and therefore their synthetic analogues can be produced through the application of similar synthetic protocols. For example, alteration of murmanite by Ca-rich hydrothermal solutions produces selivanovaite by means of a non-trivial re-organization of *HOH*-pockets [Pakhomovsky et al., 2018]. More deep alteration of murmanite (up to its amorphization) leads to the crystallization of framework titanosilicates, in particular, kuzmenkoite and chivruaiite [Men'shikov et al., 2006]. Titanosilicates of the lintisite family may be considered as formed due to the self-assembly of titanosilicate nanosheets $Ti_2Si_4O_{10}(OH)_4$, which can be obtained by the protonation of any members the lintisite family (including synthetic solid AM-4) and used for the manufacturing of new functional titanosilicates [Kalashnikova et al., 2015]. Understanding of structural regularities of cation-exchange in ivanyukite group minerals allowed us to develop new materials to radioactive waste purification [Milutin et al., 2017] and noble metal extraction.

By analogy with natural systems, framework titanosilicates can be obtained by hydrothermal technique from amorphous titanosilicate precipitates resulting from hydrochloric-acidic processing of titanite ores. This method of titanosilicate synthesis is of interest, because it allows to avoid the technically difficult sol-gel method of the Ti-precursor preparation. In particular, this approach has been used to obtain a synthetic analog of korobitsynite for the production of self-cleaning building materials. Sulfuric-acidic processing of titanite ore recovers up to 90% Ti into the liquid phase that is a universal precursor for hydrothermal synthesis of functional titanosilicates, in particular, ETS-4, ETS-10, AM-4, IE-911 and SIV. The last of them has been used for recovering liquid radioactive wastes into Synroc-type titanate ceramics and the production of self-cleaning building materials.

The research is supported by the Kola Science Center of the Russian Academy of Sciences (0226-2019-0009) and the Russian Foundation for Basic Research (18-29-12039).

Kalashnikova G.O., Selivanova E.A., PakhomovskiiYa.A., Zhitova E.S., Yakovenchuk V.N., Ivanyuk G.Y., Nikolaev A.I. Perspekt. Mater., 2015, 10, 64–72 [in Russian].

Men'shikov Y.P., Krivovichev S.V., Pakhomovsky Y.A., Yakovenchuk V.N., Ivanyuk G.Y., Mikhailova J.A., Armbruster T., Selivanova E.A. Chivruaiite, $Ca_4(Ti,Nb)_5[(Si_6O_{17})_2[(OH,O)_5]\cdot 13\text{-}14H_2O$, a new mineral from hydrothermal veins of Khibiny and Lovozero alkaline massifs. Am. Mineral., 2006, 91, 922–928.

Milyutin V.V., Nekrasova N.A., Yanicheva N.Y., Kalashnikova G.O., Ganicheva Y.Y. Sorption of cesium and strontium radionuclides onto crystalline alkali metal titanosilicates. Radiochemistry, 2017, 59, 65–69.

Pakhomovsky Y.A., Panikorovskii T.L., Yakovenchuk V.N., Ivanyuk G.Y., Mikhailova J.A., Krivovichev S.V., Bocharov V.N., Kalashnikov A.O. Selivanovaite, $NaTi_3(Ti,Na,Fe,Mn)_4[(Si_2O_7)_2O_4(OH,H_2O)_4]\cdot nH_2O$, a new rock-forming mineral from the eudialyte-rich malignite of the Lovozero alkaline massif (Kola Peninsula, Russia). Eur. J. Mineral., 2018, 30, 525–535.

**Use of Nature-like Compounds at Synthesis of Proton-conducting Composite Materials**

Vladimir A. Komornikov*, Vadim. V. Grebenev, Ivan. S. Timakov, Oleg. B. Zajnullin

FSRC “Crystallography and Photonics” RAS, 119333 Moscow, Russia

* v.a.kom@mail.ru

Functional proton-conducting composite materials are considered in the report. Their transport properties are studied by impedance spectroscopy. The dependences of the phase composition of the materials on the component ratio are investigated by X-ray diffraction analysis. The spatial phase distribution in the materials is analyzed using scanning electron microscopy. The peculiarity of the materials under consideration is the use of reinforcement component, specific to the modified phase – berlinite.

With the use of a special method of preparative synthesis $x CsH_2PO_4$ – $(1-x)AlPO_4$; $x Cs_4(HSO_4)_3(H_2PO_4)$ – $(1-x)AlPO_4$; $x Cs_6(HSO_4)_3(H_2PO_4)_4$– $(1-x)AlPO_4$ composite materials over a wide range of compositions was obtained. A special feature of the approach used in the synthesis is the formation of a proton-conducting phase and an aluminophosphate component *in one volume*.The application of this technique at the macro level allows obtaining these materials in the form of relatively thin transparent films with the necessary geometry.

At the microlevel, the application of this approach leads to the production of materials with a higher density and a larger interphase boundary area (in comparison with proton-conducting composites on oxide additives of the type $xM_mH_n(XO_4)_{(m+n)/2}$– $(1-x)SiO_2/TiO_2/SnO_2$, ($M$ = K, Rb, Cs, $NH_4$; $XO_4$ = $SO_4$, $SeO_4$, $HPO_4$)). This feature is realized due to the filling of the space between in the first place formed crystallites of the conducting phase to a largely amorphous phase of polyaluminophosphate (conditionally– $AlPO_4$).

A comparative analysis of the temperature dependence of the conductivity for the materials studied revealed increased (in comparison with the single-phase superprotonic crystal) meanings, while the intrinsic conductivity of the polyaluminophosphate component decreases the activation energy of the conductivity.

This study was supported by the Russian Foundation for Basic Research, project No. 18-32-20050. The experiments were performed using the equipment of the Shared Research Center of the Institute of Crystallography, Russian Academy of Sciences.

**Solid acid proton conductors: impact of changes in hydrogen bonds on properties**

Irina P. Makarova

Shubnikov Institute of Crystallography of Federal Scientific Research Centre "Crystallography and Photonics" of Russian Academy of Sciences, 119333 Moscow, Russia

makarova@crys.ras.ru

One of the most rapidly developing fields associated with alternative energy sources is hydrogen energetics. The promising direction is the search for new materials operating at moderate temperatures of 150–400°C at which the highest efficiency and energy saving of fuel cells are achieved. Among available materials, such requirements are satisfied by crystals of the $M_mH_n(AO_4)_{m+n/2}{\cdot}yH_2O$ family ($M$ = K, Rb, Cs, $NH_4$; $AO_4$ = $SO_4$, $SeO_4$, $HPO_4$, $HAsO_4$). In contrast to other hydrogen-containing compounds, changes in the hydrogen bond system occur in superprotonic crystals during phase transitions with increasing temperature, which cause radical changes in physical properties, including the appearance of high proton conductivity at relatively low temperature.

Structural data on these crystals are indicative of the existence of different mechanisms of changes in physical properties: the formation of a dynamically disordered system of hydrogen bonds between the $AO_4$ tetrahedra [Makarova, 2015]; the diffusion of crystallization water that causes a modification of the hydrogen bond system in a partially dynamically disordered, and formation of channels for the possible movement of ions [Makarova et al., 2014], and the formation of a multiphase state. The occurred rearrangement of hydrogen bonds prevents the reverse diffusion of crystallization water, and makes it possible to supercool the high-temperature phases practically to room temperature. The substitution of cations or groups of $AO_4$ even in small quantities changes the system of hydrogen bonds [Makarova et al., 2016], causing a change in physical properties, including the kinetics of the formation of high-temperature phases, and decrease of conductivity by four orders of magnitude or occurrence of conduction already under ambient conditions.

This study was supported by the RFBR (project No. 18-32-20050).

Makarova I. P. Superprotonics – crystals with rearranging hydrogen bonds. Physics of the Solid State, 2015, 57, 442–449.

Makarova I., Grebenev V., Dmitricheva E. et al.$K_9H_7(SO_4)_8{\cdot}H_2O$ crystals – a new representative of the family of solid acid conductors.Acta Cryst. B., 2014, 70(2), 218–226.

Makarova I., Selezneva E., Grebenev V. et al. Structure and properties of new crystals in $CsHSO_4 – CsH_2PO_4 – H_2O$ system. Ferroelectrics, 2016, 500, 54–66.

**Fast ion conductivity and deviations from additivity of empirical electronic polarizability in minerals: Voronoi-Dirichlet method**

Natalya Kabanova[1]*, R.D. Shannon[2], and R. X. Fischer[3]

[1]Samara Center for Theoretical Materials Science, Samara State Technical University, 443100 Samara, Russia
[2]Geological Sciences/ CIRES, University of Colorado, Boulder, Colorado 80309, USA
[3] Universität Bremen, FB 5 Geowissenschaften, Klagenfurter Str. 2, D-28359 Bremen, Germany

*weterrster@gmail.com

Geometrical-topological analysis based on the Voronoi-Dirichlet method is increasingly being used to solve various crystallochemical problems. Earlier, we successfully applied this method for investigation of cation conductive materials [Anurova et al., 2008; Fedotov et al., 2018]. In [Shannon and Fischer, 2016], we have studied infinite migration paths of ions in the minerals that deviate from the additivity of empirical electronic polarizabilities.

Empirical electronic polarizabilities allow one to predict the total mineral polarizabilities and mean refractive indices of a vast majority of minerals and synthetic oxides. Shannon and Fischer [2016] evaluated ~2600 dynamic polarizabilities derived from the refractive indices $n_D$, of ~1200 minerals and 675 synthetic compounds to yield a unique set of the individual electronic polarizabilities of ions which can be used for the interpretation of optical properties. Ion conductivity in minerals and compounds is associated with infinite migration paths and leads to negative total electronic polarizability deviations [$\Delta = (\alpha_{obs} - \alpha_{calc})/\alpha_{obs}$)] up to 13%. Using the Voronoi-Dirichlet method, we have identified the migration paths and the dimensionality of 58 compounds with negative polarizability deviations, 27 of which are confirmed ion conductors. Based on the negative deviations, we predict the remaining 22 compounds to be ion conductors. Among them, 9 are anionic conductors based on the $ZrO_2$,$CeO_2$ and $Gd_2Hf_2O_7$ crystal structures.

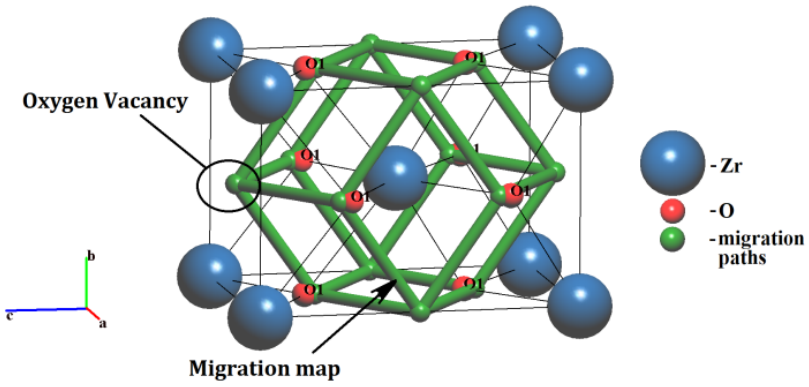


Figure. 3D migration map of $O^{2-}$ ions for the $ZrO_2$ crystal structure

Anurova (*Kabanova*) N.A., Blatov V.A., Ilyushin G.D., Blatova O.A., Ivanov-Schitz A.K, Dem'yanets L.N. Solid State Ion., 2008, 179, 2248.

Fedotov S.S., Kabanova N.A., Kabanov A.A., Blatov V.A., Khasanova N.R., Antipov E.V. Solid State Ion., 2018, 314, 129.

Shannon R. D. and Fischer R. X. Amer. Mineral., 2016, 101, 2288–2300.

**The cation replacements in the systems of superprotonic crystals**

Elena V. Selezneva[1,*], Irina P. Makarova[1], Inna A. Malyshkina[2], Alla L. Tolstikhina[1], Radmir V. Gainutdinov[1], Vladimir A. Komornikov[1]

[1] Shubnikov Institute of Crystallography of Federal Scientific Research Centre "Crystallography and Photonics" of Russian Academy of Sciences, 119333 Moscow, Russia
[2] M.V. Lomonosov Moscow State University, Faculty of Physics, 119991 Moscow, Russia

*msdmitricheva@yandex.ru

A fundamental problem of modern condensed state physics is detection of the relationship between structures and physical properties of the crystals. To elucidate the effect of isomorphic substitution on the kinetics of phase transitions, single crystals of $(K_{1-x}(NH_4)_x)_mH_n(SO_4)_{(m+n)/2}\cdot yH_2O$ solid solutions are grown in the $K_3H(SO_4)_2 - (NH_4)_3H(SO_4)_2 - H_2O$ system which end members are known to undergo superprotonic phase transitions with essentially different kinetics. The crystals of $(K_{1-x}(NH_4)_x)_3H(SO_4)_2$ with 3 – 6% ammonium have the same structure type as $K_3H(SO_4)$[Selezneva et al., 2018]. This amount of ammonium turned out to be sufficient to significantly change the kinetics of structural phase transitions in comparison with $K_3H(SO_4)_2$ crystals, which is related to the formation of additional hydrogen bonds and the change in the anisotropy of the coordination environment of both cations and $SO_4$ tetrahedra.

The crystals of $(K_{1-x}(NH_4)_x)_3H(SO_4)_2$ with 57% ammonium have particular interest. These crystals have the same structure type as the high-temperature phase of $(NH_4)_3H(SO_4)_2$ [Selezneva et al., 2017]. X-ray study showed that crystals have trigonal symmetry, the space group $R\bar{3}$, $Z = 3$, $a = b = 5.7768(3)$, $c = 22.0983(1)$ Å at $T \approx 23$ C. Studies of dielectric properties revealed that the grown samples have high protonic conductivity at the room temperature. This can be related with the appearance of the threefold axis, that leads to the disordering of the O atoms involved in hydrogen bonds and as a result to the formation of a dynamically disordered network of hydrogen bonds, and rise of conductivity. Studies by PFM methods showed that the crystals have a phase transition from paraphase to ferroelectric phase at 9 °C. With further cooling the conductivity decreases.

This study was supported by the RFBR (project No. 18-32-20050).

Selezneva E.V., Makarova I.P., Grebenev V.V. et al. The changes of thermal, dielectric, and optical properties at insertion of small concentration of ammonium to $K_3H(SO_4)_2$ crystals. Cryst. Rep., 2018, 63(4), 553–562

Selezneva E.V., Makarova I.P., Malyshkina I.A. et al. New superprotonic crystals with dynamically disordered hydrogen bonds: cation replacements as the alternative to temperature increase. Acta Cryst., 2017, B73, 1105–1113.

**The Cation Substitution in Superprotonic Crystals**

Ivan S. Timakov*, Vadim V. Grebenev, Vladimir A. Komornikov, Oleg B. Zainullin, Irina P. Makarova, Elena V. Selezneva

Federal Scientific Research Centre “Crystallography and Photonics” of Russian Academy of Sciences, 119333 Moscow, Russia

* selos93@mail.ru

A large number of acidic salts of singly charged cations are promising protonic conductors and attract the attention of researchers along with other ion-conducting compounds. The effect of abnormally high proton conductivity was first discovered at the Institute of Crystallography in the study of proton transport processes in $CsHSO_4$ and $CsHSeO_4$ crystals [Baranov et al., 1982]. This group includes compounds with the general formula $M_mH_n(AO_4)_{(m+n)/2}\cdot xH_2O$ ($M$ = K, Rb, Cs, $NH_4$; $A$ = S, Se, P, As). Their distinctive feature is structural phase transitions at elevated temperatures before melting. During the phase transition, the conductivity values σ in these crystals significantly increase and reach values comparable to the conductivity in the melt, while the compound itself remains solid according to the state of aggregation.

The combination of the properties of high proton conductivity ($\sigma \approx 10^{-3}\Omega^{-1}cm^{-1}$) in a solid state of aggregation at moderate temperatures (140–230 °C) makes these compounds attractive for use, for example, as fuel cell membranes [Norby, 2001; Fitzgerald, 2001].

To obtain new compounds belonging to the $M_mH_n(AO_4)_{(m+n)/2}\cdot xH_2O$ family, we studied the phase equilibria in the quaternary water–salt system $K_2SO_4$–$Rb_2SO_4$–$H_2SO_4$–$H_2O$, which was not investigated previously. The conditions for obtaining large single crystals of complex hydrosulfates are determined.

The results obtained allowed us to present a phase equilibrium diagram for these conditions. Single crystals of solid solutions with the general formulas $(K_xRb_{(1-x)})_9H_7(SO_4)_8\cdot H_2O$, $(K_xRb_{(1-x)})_3H(SO_4)_2$ and $(K_xRb_{(1-x)})_2SO_4$ were obtained. In addition, the obtained single crystals of solid solutions of the $K_3H(SO_4)_2$–$Rb_3H(SO_4)_2$ series were investigated by the methods of differential scanning calorimetry and thermogravimetric analysis.

The work was supported by the Ministry of Science and Higher Education within the State assignment FSRC "Crystallography and Photonics" RAS.

Baranov A.I., Shuvalov L.A., Shchagina N.M. Superionic Conductivity and Phase Transitions in $CsHSO_4$ and $CsHSeO_4$ Crystals. JETP Lett., 1982, 36, 459–462.

Fitzgerald R. Solid acids show potential for fuel cell electrolytes. Physics Today, 2001, 54, 22–24.

Norby T. The Promise of Protonics. Nature, 2001, 410, 877–878.

**Evolution of the structure and ionic conductivity of the solid solutions based on $Nd_2Hf_2O_7$**

Anna V. Shlyakhtina[1]*, Nikolay V. Lyskov,[2] Alexander N. Shchegolikhin,[3]
Galina A. Vorobieva,[1] I.V. Kolbanev,[1] L.G. Shcherbakova[1]

[1]Semenov Institute of Chemical Physics, RAS, 119991 Moscow, Russia
[2]Institute of Problems of Chemical Physics RAS, Chernogolovka, Russia
[3]Emanuel Institute of Biochemical Physics RAS, 119991 Moscow Russia

*annashl@inbox.ru, annash@chph.ras.ru

$(Nd_{2-x}Hf_x)Hf_2O_{7+x/2}$ ($x$ = 0, 0.2, 0.32, 0.39), $Nd_2(Hf_{2-x}Nd_x)O_{7-x/2}$ ($x$ = 0.1) solid solutions were synthesized from mechanically activated mixtures of neodymium and hafnium oxides (ball mill SPEX8000) followed by high-temperature annealing. The homogeneity region of pyrochlore solid solutions in the $Nd_2O_3$–$HfO_2$ system was established in the temperature range 1600–1650°C.

It was shown that annealing at a maximum temperature of 1650 °C, 5 h, allowed us to obtain single-phase $Nd_2(Hf_{2-x}Nd_x)O_{7-x/2}$ ($x$ = 0, 0.1) pyrochlore solid solutions. $(Nd_{2-x}Hf_x)Hf_2O_{7+x/2}$ ($x$ = 0, 0.2, 0.32, 0.39) solid solutions with an excess of hafnium were shown to be non single-phase and contained the original oxides $Nd_2O_3$ and $HfO_2$ as impurities. After annealing at a lower temperature of 1600 °C, 10 h, only nominally stoichiometric $Nd_2Hf_2O_7$ was shown to be single-phase.

$(Nd_{2-x}Hf_x)Hf_2O_{7+x/2}$ ($x$ = 0.2), $Nd_2Hf_2O_7$, $Nd_2(Hf_{2-x}Ln_x)O_{7-x/2}$ ($x$ = 0.1) solid solutions, synthesized at 1650 °C, 5 h, were studied by Raman spectroscopy. For $Nd_2Hf_2O_7$, $Nd_2(Hf_{2-x}Nd_x)O_{7-x/2}$ ($x$ = 0.1), Raman spectra were obtained that characterize them as single-phase pyrochlores. It is shown that the intensity of the Raman lines decreases for $Nd_2(Hf_{2-x}Nd_x)O_{7-x/2}$ ($x$ = 0.1) in comparison with the pyrochlore $Nd_2Hf_2O_7$, which indicates the beginning of the concentration pyrochlore-fluorite transition in the $Nd_2O_3$ – $HfO_2$system at 1650 °C .

The total conductivity of single-phase hafnates $Nd_2Hf_2O_7$ ($T_{sin.}$ = 1600 and 1650 °C), $Nd_2(Hf_{2-x}Nd_x)O_{7-x/2}$ ($x$ = 0.1) ($T_{sin.}$ = 1650 °C) was investigated in dry and wet air. For the first time, proton conductivity was found both in $Nd_2Hf_2O_7$ ($2 \times 10^{-6}$ S/cm at 700 °C) and $Nd_2(Hf_{2-x}Nd_x)O_{7-x/2}$ ($x$ = 0.1) solid solution ($1.2 \times 10^{-5}$ S/cm at 700 °C). The ionic conductivity maximum of $Nd_2Hf_2O_7$ in dry air was $\sim 1 \times 10^{-6}$ S/cm at 700 °C, which is almost an order of magnitude higher than was reported in the literature [Govindan Kutty et al., 1998].

The results of the study of powders and ceramics of the composition $Nd_2O_3$:$2HfO_2$ in the oxidizing ($O_2$) and mild reducing atmosphere (He) by the methods of DTA-TG with mass spectral analysis of the evolved gases and X-ray diffraction analysis, allow us to state that, as the original precursor (mechanically activated mixture of oxides of the appropriate composition), as well as powders and ceramics obtained from it during the subsequent heat treatment, contain carbon-containing compounds (basic carbonates and rare-earth hydroxycarbonates) and/or amorphous (crystalline) carbon in an amount up to 0.5%.

The support of this work by the Russian Science Foundation (Project 18-13-00025) is gratefully acknowledged.

Govindan Kutty K.V., Mathews C.K., VaradarajuU.V.Effect of aliovalent ion substitution on the oxide ion conductivity in rare-earth pyrohafnates $RE_{2-x}Sr_xHf_2O_{7-\delta}$ and $RE_2Hf_{2-x}Al_xO_{7-\delta}$ (RE = Gd and Nd; x = 0, 0.1, and 0.2). Solid State Ionics,1998, 110, 335–340.

**Formation of the cubic modification of LLZ solid electrolyte with garnet structure**

Galina B. Kunshina*, Irina V. Bocharova, Victor J. Kuznetsov

Tananaev Institute of Chemistry, Kola Science Centre of the Russian Academy of Sciences, 184209 Apatity, Russia

*kunshina@chemy.kolasc.net.ru

The newly discovered lithium conductive solid electrolyte with garnet structure and general formula of $Li_7La_3Zr_2O_{12}$ has attracted a lot of attention since its first publication [Muruganet al., 2007]. The ionic conductivity of $Li_7La_3Zr_2O_{12}$ is higher than that of lithium garnet described earlier [Ramakumar et al., 2017]. $Li_7La_3Zr_2O_{12}$ has two crystal modifications: cubic and tetragonal. It is found that the conductivity of cubic $Li_7La_3Zr_2O_{12}$ at room temperature is 2 orders higher than that of its tetragonal modification [Awaka et al., 2009].

For the stabilization of highly conductive cubic modification doping with alumina is used. The samples of $Li_{6.4}Al_{0.2}La_3Zr_2O_{12}$ (LLZ) solid electrolyte was synthesized by solid-phase sintering [Kunshinaet al., 2019]. The LLZ was characterized by X-ray diffraction, DSC/TG, IR-spectroscopy, and impedance spectroscopy methods. The measured powder diffraction pattern of LLZ compared with diffraction pattern of $Li_5La_3Nb_2O_{12}$ with a garnet structure of cubic modification (tetragonal modification of LLZ splitting of (211) reflex is characteristic). The $Li_7La_3Zr_2O_{12}$ diffraction pattern is fully consistent with the $Li_5La_3Nb_2O_{12}$ diffraction pattern, which indicates the ability of the garnet structure to accommodate cations of different valences and sizes without a significant change of symmetry.

According to XRD, as a result of sintering the mixture at 1100 ºC, the formation of a well-crystallized monophase product, which does not contain non-conductive impurity phases occurred ($La_2O_3$, $ZrO_2$, $La_2Zr_2O_7$). All X-ray reflexes of LLZ sintered at 1150 ºC were clearly resolved, and increasing intensity and narrow peaks indicate the growth of ceramic grains as a result of long sintering (Figure). The ionic conductivity of $Li_7La_3Zr_2O_{12}$ at room temperature was $2 \cdot 10^{-4}$ S/cm.

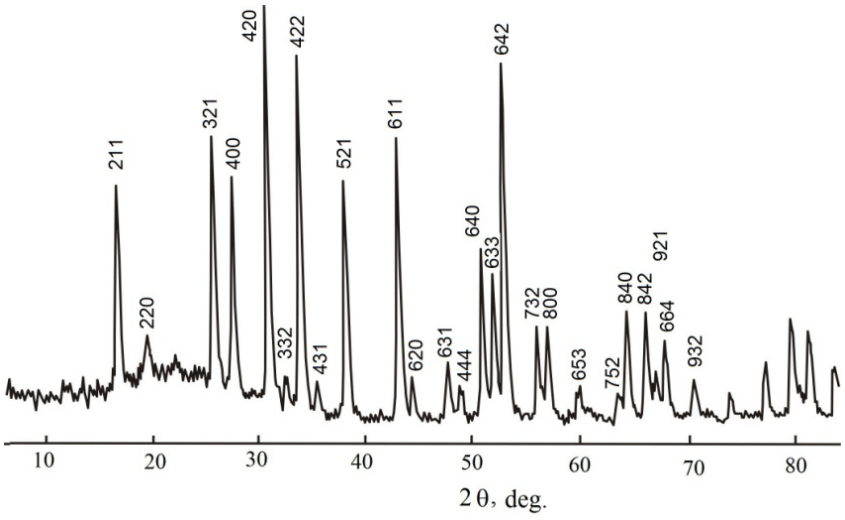


Figure. X-ray diffraction patterns of LLZ sintered at 1150 ºC for 6 h.

Awaka J., Kijima N., Hayakawa H., Akimoto J. Synthesis and structure analysis of tetragonal $Li_7La_3Zr_2O_{12}$ with the garnet-related type structure. J. Solid State Chem., 2009, 182, 2046–2052.

Kunshina G.B., Ivanenko V.I., Bocharova I.V.Synthesis and study of Al-substituted $Li_7La_3Zr_2O_{12}$ conductivity. Russ. J. Electrochem., 2019, 55(6), 558–564.

Murugan R., Thangadurai V., Weppner W. Fast Lithium Ion Conduction in Garnet-Type $Li_7La_3Zr_2O_{12}$. Angew. Chem. Int. Ed., 2007, 46, 7778–7781.

Ramakumar S., Deviannapoorani C., Dhivya L. et al. Lithium garnets: Synthesis, structure, $Li^+$ conductivity, $Li^+$ dynamics and applications. Progr. in Materials Science, 2017, 88, 325–411.

**Magnetocaloric properties of Gd-Al-Me (Me=Ni, Co, Fe) bulk-amorphous alloys**

S. Uporov[1], N. Uporova[2]*

[1]Institute of Metallurgy, Ural Branch of Russian Academy of Sciences, 620016 Ekaterinburg, Russia
[2]Institute of Geology and Geochemistry, Ural Branch of Russian Academy of Sciences, 620016 Ekaterinburg, Russia

* nuporova84@gmail.com

The search for new materials demonstrating a large magnetocaloric effect (MCE) is one of the key problems for modern and environmentally friendly cooling systems. Among rare-earth systems exhibiting a noticeable MCE, amorphous gadolinium-based alloys are of particular interest [Luo et al., 2009]. The increase in glass-forming ability and thermal stability in these materials often leads to a significant increase in MCE [Yu et al., 2018].

In this work, rapidly-quenched $Gd_{60}Al_{25}((NiCo)_{1-x}Fe_x)_{15}$ ($x$ = 0; 1/80; 1/40 and 1/20) alloys were studied. Samples were obtained by arc-melting of appropriate amounts of pure metals under a pure argon atmosphere, followed by quenching via vacuum casting. The quenched specimens in the form of thin rods had different diameters from 1 to 3 mm. The sample structure was analyzed using X-ray diffraction methods. It was found that the structural state of the quenched materials varied significantly depending on the elemental composition.

Analysis of the crystallization processes of the quenched samples was carried out on a NETZSCH STA 409 thermal analyzer using differential scanning calorimetry. The values of temperatures and enthalpies of crystallization processes were determined at various scanning rates. Among the studied alloys, the $Gd_{60}Al_{25}(NiCo)_{15}$ alloy possesses the best glass-forming ability. It was revealed that partial replacement of nickel and cobalt with iron reduced the glass-forming ability, which was reflected in the values of the corresponding thermal parameters.

Studies of magnetic characteristics were carried out by the method of vibration magnetometry (automatic system Cryogenic VSM CFS-9T-CVTI). For magnetic measurements, the quenched specimens with a nominal diameter of 1 mm were selected. As follows from the obtained data, varying the concentration of iron in the alloys leads to strong qualitative and quantitative changes in the behavior of magnetization. At temperatures below 90 K, the alloys exhibit a ferromagnetic behavior. For the first time, the presence of a metamagnetic transition for the studied systems was detected at temperatures below 40 K and magnetic fields less than 3 T. The presence of the revealed anomaly is significantly reflected in the magnetic entropy changes of the materials and largely depends on the concentration of iron in the alloys. From the experimental data, magnetocaloric parameters were calculated in wide ranges of temperatures and magnetic fields. For all alloys, very high values of magnetocaloric parameters are observed. The highest values of the relative cooling power (about 900 J/kg) are obtained in $Gd_{60}Al_{25}(NiCo)_{15}$ glass, which are comparable in magnitude with the best gadolinium-based magnetocaloric materials.

The reported study was financially supported by RFBR according to the research project no. 18-03-00626 and was partly supported by the theme of state assignment of IGG UB RAS No. 0316-2019-0004.

Luo Q., Wang W.H. Rare earth based bulk metallic glasses. J. Non-Cryst. Solids, 2009, 355, 759–777.

Yu P., Chen L.S., Xia L. Phase separation and its effect on the magnetic entropy change profile in an amorphous $Gd_{48}Co_{50}Nb_2$ alloy. J. Non-Cryst. Solids, 2018, 493, 82–85.

**Fragmentary model and atomic structure of metallic and semiconductor glasses**

Kseniya B. Aleynikova*, Elena N. Zinchenko, Alexey A. Zmeykin, and Yuriy N. Perin

Voronezh State University, 394006 Voronezh, Russia

* xenale@mail.ru

All amorphous materials are often called glasses. Along with classical glasses, such as oxide, chalcogenide, borate, etc., amorphous metals are also called glasses. The conditions for obtaining classical and metallic glasses vary greatly. The formers are obtained under relatively mild hardening conditions, the latters – under extremely rigid. In addition, many substances (usually semiconductors) are obtained in the form of thin amorphous films. Conditions for their obtaining them can be called medium hard. Methods for producing glasses are associated with the characteristics of their atomic structure. The atomic structure of amorphous materials has been studied for a long time using a variety of methods [Moroz, 2011]. However, until now, there is no consensus about their atomic structure or unified approach to its study [Zachariazen, 1932; Golubkov, 1998]. Diffraction methods are direct methods for studying the atomic structure. For amorphous substances, the Fourier transformation of the diffraction data allows to obtain the atomic radial distribution function (ARDF). The most successful method for interpreting the experimental ARDF is the pair distribution functions (PDF) method in different versions [Mozzi et al., 1969; Billinge et al., 2004; Aleynikova et al., 2009].

In this work, experimental ARDFs were interpreted using a fragmentary model. The basis of the simulation is an assumption that structure of an amorphous substance is a mosaic of fragments of the structures of crystal analogs, and model ARDFs are constructed based on crystal structural data regardless of the experiment. Analysis of the obtained results showed that all amorphous metallic alloys based on aluminum and some II-V semiconductor thin films consist of crystalline nuclei, which are possible for a given elemental composition of the phases. For metal alloys, a semi-quantitative analysis was conducted. It is shown that the size of nuclei should not exceed 6 nm for metals. In classical glasses, crystal nuclei are absent. Their structure is a complex mosaic of structure fragments of different crystalline phases.

Moroz E.M. X-Ray diffraction structure diagnostics of nanomaterials. Russian Chemical Reviews, 2011, 80, 293–312.

Zachariazen W.H. The atomic arrangement in glass. J. Amer. Chem. Soc., 1932, 54, 3841–3851.

Golubkov V.V. Problema neodnorodnogo stroeniya stekol. Fizika i Khimiya Stekla, 1998, 24, 289–304.

Mozzi R.L., Warren B.E. The structure of vitreous silica. J. Appl. Cryst., 1969, 2, 164–170.

Billinge S.J.L., Kanatzidis M.G. Beyond crystallography: the study of disorder, nanocrystallinity and crystallographically challenged materials with pair distribution functions. Chem. Commun., 2004, 749–760.

Aleynikova K.B., Zinchenko E.N. Fragment model as a phase analysis method for diffraction amorphous materials. Journal of Structural Chemistry, 2009, 50, Supplement, 93–99.

## Chemical composition, IR-spectroscopy and etching behavior of γ-$Si_3N_4$

Thomas Schlothauer[1]*, Gerhard Heide[1], Marcus Schwarz[2], Erica Brendler[3]

[1] Institute of Mineralogy, TU Bergakademie, Freiberg, Germany
[2] Institute ofInorganic Chemistry, TU Bergakademie, Freiberg, Germany
[3] Institute of Analytical Chemistry, TU Bergakademie, Freiberg, Germany

* thomas.schlothauer@mineral.tu-freiberg.de

Spinel-type silicon nitride (γ-$Si_3N_4$), the high-pressure phase of α- and β-$Si_3N_4$, which was discovered in 1999 [Zerr et al., 1999], shows a high hardness and is stable under high temperatures up to 1673 K in air [Jiang et al., 2001]. For a better understanding of its mechanical and physical properties, also a better knowledge about its chemical properties is required. This concerns especially its oxygen values. For this reason, shock-wave synthesized pure γ-$Si_3N_4$ [Schlothauer et al., 2012] with different oxygen values in the precursors was analyzed with infrared spectroscopy, hot-gas extraction and with thermos gravimetry with mass spectrometry. All methods were used before and after etching of the silicon nitride with fluoridic acid. The oxygen value as given for sinoite ($Si_2N_2O$) is not possible for the high-pressure phase also if the precursors contains more oxygen. Also, Sekine et al. [2006] describes the impossibility to form a high-pressure phase from sinoite at pressures up to 64 GPa. He and coworkers found a complete amorphization instead.

Additionally, it was tested if a determination of the oxygen value in γ-$Si_3N_4$ is possible with its infrared spectra as shown already for α- and β-$Si_3N_4$(e.g. after Antsiferov et al., 2003). In principle this calculation is possible with the first tetrahedral vibration ($\nu_3$-vibration, Si-N-Si-stretching), but here more investigations are still required.

Antsiferov V.N., Gilev V.G., Karmanov V.I. Infrared spectra and structure of $Si_3N_4$, $Si_2ON_2$, and sialons, Refractories and Industrial Ceramics, 2003, 44(2), 108–114.

Jiang J.Z., Kragh F., Frost D.J., Stahl K., Lindelov H. Hardness and thermal stability of cubic silicon nitride. Journal of Physics: Condensed Matter, 2001, 13(22), L515.

Schlothauer T., Schwarz M.R., Ovidiu M., Brendler E., Moeckel R., Kroke E., Heide G. "Shock Wave" Synthesis of Oxygen-Bearing Spinel-Type Silicon Nitride γ-$Si_3(O,N)_4$ in the Pressure Range from 30 to 72 GPa with High Purity. In: Minerals as Advanced Materials II, edited by S. V. Krivovichev, Springer Berlin Heidelberg, Berlin, Heidelberg, 2012, 375–388.

Sekine T., He H.L., Kobayashi T., Shibata K. Sinoite ($Si_2N_2O$) shocked at pressures of 28 to 64 GPa, Am. Mineral., 2006, 91, 463–466.

Zerr A., Riedel R., Miehe G., Serghiou G., Schwarz M., Kroke E., Fueß H., Kroll P., Boehler, R. Synthesis of cubic silicon nitride. Nature, 1999, 400, 6742, 340–342.

# 6. Diamond and Carbon Compounds

**Effect of crystallization conditions on the formation of defect-impurity centers in diamond**

Yury N. Palyanov*, Igor N. Kupriyanov, Yury M. Borzdov

Sobolev Institute of Geology and Mineralogy, Siberian Branch of the Russian Academy of Sciences, 630090Novosibirsk, Russia

* palyanov@igm.nsc.ru

Modern concepts and models of diamond genesis are based on quite different viewpoints suggesting a wide range of conditions for diamond formation in the Earth's mantle, including crystallization environment composition, *P-T* parameter and oxygen fugacity. The type and concentration of defect-impurity centers in diamonds is a potential source of information about the conditions of diamond formation. In the last decade, diamond crystallization processes in model systems corresponding in composition to natural diamond-forming media have been actively studied. In this work, we present the results of the study of defect-impurity centers in diamonds crystallized in the model media with different composition and describe the established regularities caused by the crystallization conditions. Investigations into the processes of diamond nucleation and growth are performed using multi-anvil BARS equipment at pressures 5–7.5 GPa and temperatures from 1100 to 1900°C. Systems of various compositions are used in the experiments, including carbonate, silicate, sulfide, chloride, metallic and fluid-containing media. The results obtained in this study allow us to substantiate the indicator properties of the silicon-containing and oxygen-containing centers in diamond. It is found that the SiV centers can serve as an indicator of reducing and ultra-reducing conditions ($fO_2 \leq IW$). Oxygen-containing centers (1065 $cm^{-1}$) are characteristic of diamonds synthesized in the $Na_2CO_3$-$CO_2$-C system in a narrow range of oxidizing conditions at $fO_2$ between CCO and CCO-0.5 log. unit [Palyanov, 2016].

Traditional solvent-catalysts based transition metals (Fe, Ni, Co) and their alloys allow producing large high-quality diamond single crystals of types Ib, IaA, IIa and IIb. The search for the new diamond crystallization media makes it possible to produce crystals with defect-impurity centers that are not found in natural diamonds, but currently, represent particular interest for high-tech applications. Semiconductor diamond crystals doped with phosphorus were synthesized in the P-C system. Diamond crystals with the SiV, GeV and SnV color centers, which are promising for quantum physics research and applications, were synthesized in the ultra-reduced Mg-based melts [Palyanov, 2015; 2016; 2019].

Thus, the investigation of diamond crystallization processes over a wide range of conditions and the study of the diamond properties enables both gathering new information necessary for building up diamond genesis models and producing diamond crystals with new properties.

This work was supported by the Russian Science Foundation, Grant No. 19-17-00075.

Palyanov Yu.N., Kupriyanov I.N., Sokol A.G.,Borzdov Yu.M., Khokhryakov A.F. Effect of $CO_2$on crystallization and properties of diamond from ultra-alkaline carbonate melt. Lithos, 2016, 265, 339–350.

Palyanov Yu.N., Kupriyanov I.N., Borzdov Y.M. High-pressure synthesis and characterization of Sn-doped single crystal diamond. Carbon., 2019, 143, 769–775.

Palyanov Yu.N., Kupriyanov I.N., Borzdov Yu.M., Khokhryakov A.F., Surovtsev N.V. High-pressure synthesis and characterization of Ge-doped single crystal diamond. Crystal Growth & Design, 2016, 16, 6, 3510–3518.

Palyanov Yu.N., Kupriyanov I.N., Borzdov Yu.M., Surovtsev N.V. Germanium: a new catalyst for diamond synthesis and a new optically active impurity in diamond. Sci. Rep., 2015, 5, 14789.

**Effect of REE oxides on diamond crystallization in Mg-based systems**

Alexander F. Khokhryakov*,Yuri N. Palyanov, YuriM. Borzdov, IgorN. Kupriyanov

Sobolev Institute of Geology and Mineralogy, Siberian Branch of the Russian Academy of Sciences, 630090Novosibirsk, Russian Federation

* khokhr@igm.nsc.ru

The combination of the unique properties of the diamond determines the significant prospects of its application in various fields of science and technology, including a new direction associated with quantum technologies.In recent years, the subject of obtaining diamonds containing ions of rare earth elements (*REE*) is of heightened interest.It is well known, that *REE* ions have unique optical and magnetic properties and are widely used in various areas of modern technology, including laser technology and telecommunication systems.Experimental studies aimed at obtaining diamonds doped with *REE* are just beginning.As potentially promising media for the crystallization of diamonds doped with large-cation impurities, we experimentally tested Mg-based systems.This choice is based on previous studies in which it was shown that in ultra-reduced Mg melt at HPHT, doping of diamond with silicon, germanium and tin is possible[Palyanovetal., 2015, 2016, 2019].

Diamond synthesis experiments were carried out at pressure 7.8 GPa and temperature 1800–2000° using a split-sphere multi-anvil high-pressure apparatus. The duration of all experiments was 1 hour. The starting materials were a graphite rod, metallic magnesium and oxides of rare-earth elements $R_2O_3$ (where *R* = Nd, Sm, Eu, Gd, Tb, Dy, Ho, Er, Tm and Yb).A mixture of Mg and *REE* oxides together with seed diamond crystals were placed in thick-walled graphite capsules.The first series of experiments was carried out with the $R_2O_3$content of 10%. In the second series of experiments, the effect of the content of one of the oxides, namely $Sm_2O_3$, on diamond crystallization in the Mg-$Sm_2O_3$-C system was studied. Methodical features of the high-pressure cell assembly and the *P*, *T*, *t* parameters were constant.Only the content of $Sm_2O_3$ was changed from 0 to 50 wt%.The degree of transformation of graphite into diamond, the morphology and internal structure of diamond crystals were studied. The defect-impurity composition of the synthesized diamond was studied by the methods of IR Fourier spectroscopy, luminescence and electron paramagnetic resonance.

The reported study was funded by RFBR according to the research project № 18-29-12041.

Palyanov Y.N., Kupriyanov I.N., Borzdov Y.M. High-pressure synthesis and characterization of Sn-doped singlecrystal diamond. Carbon, 2019, 143, 769–775.

PalyanovY.N., KupriyanovI.N., Borzdov Y.M., BatalevaY.V. High-pressure synthesis and characterization ofdiamond from an Mg–Si–C system. Cryst. Eng. Comm., 2015, 17, 7323–7331.

PalyanovY.N., KupriyanovI.N., BorzdovY.M., KhokhryakovA.F., Surovtsev N.V. High-Pressure synthesis and characterization of Ge-doped single crystal diamond. Cryst. Growth Des., 2016, 16, 3510−3518.

**Transformation of nitrogen centers in natural diamonds under plastic deformation**

S.V.Titkov

Institute of Geology of Ore Deposits, Petrography, Mineralogy and Geochemistry, Russian Academy of Sciences, 119017Moscow, Russia

titkov@igem.ru

Isomorphic impurities of nitrogen form in the structure of natural diamonds several dozens of various centers. When considering the ontogenicsignificance of nitrogen centers, the main attention of researchers for many years was paid to the process of their transformation under high-temperature annealing, which diamonds underwent in the Earth's mantle. Such annealing was studied in detail experimentally. This report describes the results of the study of nitrogen centers transformation under the plastic deformation,suffered by diamonds in the process of transportation from the mantle to the surface of the Earth by kimberlite and lamproite magmas (references in [Titkov, 2018]). Plastically deformed diamond crystals are common in all deposits world-wide.

The study of diamonds from various Russian deposits using EPR-, IR-, UV-Vis- spectroscopy and photoluminescence has shown that the character of nitrogen centers transformation under plastic deformation is noticeably different in diamonds of varieties I and II according to the classification byYu.L. Orlov, as well as in crystals deformed by dislocation slipping and by mechanical twinning mechanisms.

Under plastical deformation, in diamonds of variety I, formed by octahedral growth sectors, common nitrogen A-centers [N-N] destroyed to form a series of various paramagnetic N1, N4, W7, M2, M3centers, in which two nitrogen atoms are separated from each other at different distances in the structure. In addition, nitrogen impurities attached to deformation dislocations formingparamagnetic N2 centers and to deformation vacancies giving rise to the H3, H4 and 575 nm centers.

In plastically deformed diamonds of variety II, composed of cubic growth sectors, deformationnitrogen-dislocation N2 centerwere not found. The N1, N4, W7, M2, M3 centers were not detected as well, despite the high concentrations of the A centers.At the same time, in these diamonds, new unusual paramagnetic M4, M5 and M6 centers were revealed, in which two nitrogen atoms are separated from each other by 8-10 interatomic distances in the structure. Deformation nitrogen-vacancy H3, 575 nm and 637 nmcenters were also observed.

As it was established, plastic deformation of diamonds in nature can occur not only by the mechanism of dislocation slipping, as was previously suggested, but also by the mechanisms of rotational plasticity and mechanical twinning. According to experimental data, deformation by twinning develops at relatively low temperatures and shock loading, and, obviously, occurred in the last stages of diamonds transportation to the Earth's surface. In crystals plastically deformed by dislocation slipping, nitrogen-dislocation N2 centers substantially dominate over other deformation centers. The features of crystals deformed bymechanical twinning arehigh concentration of the M2 centers and their unusual twin orientation relative to the main volume of the crystal. That orientation is due to localization of these centers within deformation microtwins, which clearly observed in EPR-spectra.The N2 centers causeundesirable brown coloration of natural diamond and the M2 centers, valuable purple-pink coloration.

Titkov S.V. Isomorphic impurities in natural diamonds and their genetic significance.Doct.geol.-min. sci. Thesis.IGEM RAS, Moscow, 2018

# Preliminary Experimental Data on Isotope and Impurity' Fractionation at Diamond Crystallization by Dodecahedron and Trapezohedron Faces

Vadim N. Reutsky*,Yury N. Palyanov

V.S.Sobolev Institute of geology and mineralogy SB RAS, 630090Novosibirsk, Russia

* reutsky@igm.nsc.ru

Despite wide interest and intensive studies, internal compositional heterogeneity of diamond crystals, which results from growth on non-equivalent crystallographic faces, remains poorly understood. Limited data on carbon and nitrogen isotope compositionsalong with nitrogen content were collected from literature [Burns et al., 1997, Watt et al., 2001, Reutsky et al., 2008] and preliminary tested together with some our measurements of minor growth sectors of dodecahedra and trapezohedra in synthetic HTHP diamond crystals from metal carbon model system. Like sectors of octahedra and of cube, diamond material of named growth sectors appears to have significant compositional contrast.

All the datashown that the sector of trapezohedra is equal in carbon isotope composition to sectors of octahedra but strongly depleted with nitrogen impurity. At the same time, opposite to case of sector of cube, where the nitrogen depletion is accompanied by significant enrichment with nitrogen heavy isotope, the sector of trapezohedra shows $\delta^{15}N$ value equal to the sector of octahedra. So, the face of trapezohedrashows some intermediate features of faces of octahedra and faces of cube.

Even less representative dataexists ondiamond material of growth sector of dodecahedra. Together with published data [Burns et al., 1997, Watt et al., 2001] our results also reveal complicated behavior of carbon and nitrogen in dodecahedral surface of diamond. No significant equilibrium carbon isotope fractionation is expected on the face of dodecahedra [Reutsky et al., 2016]. However, strong nitrogen depletion with unknown nitrogen isotope effect is documented by now.

The work is supported by the Russian Science Foundation under Grant No. 19-17-00075.

Burns R.C., Cvetkovic V., Dodge C.N., Evans D.J.F., Rooney M.-L.T., Spear P.M., Welbourn C.M., Growth-sectordependence of optical features in large synthetic diamonds. J. Crys.Growth,1990, 104, 257–279.

Watt G.A., Newton M.E., Baker J.M., EPR and optical imaging of the growth-sector dependence of radiation-damage defect production in synthetic diamond. Diam. Relat. Mater., 2001, 10, 1681–1683.

Reutsky V.N., Harte B., EIMF, Borzdov Y.M., Palyanov Y.N. Monitoring diamond crystal growth, a combined experimental and SIMS study. European J. Mineral., 2008, 20, 365–374.

Reutsky V., Kowalski P., Palyanov Y., EIMF,Wiedenbeck M. Experimental and theoretical evidence for surface-induced carbon and nitrogen fractionation during diamond crystallization at high temperatures and high pressures. Crystals, 2017,7(7), 190

**Main Hosts of Carbon and Nitrogen in Reduced Mantle:Implications for Deep Cycles of Volatiles**

Alexander G. Sokol*, Alexey N. Kruk, Yury N. Palyanov, Ivan A. Sokol

V.S. Sobolev Institute of Geology and Mineralogy,Siberian Branch of the Russian Academy of Sciences, 630090Novosibirsk, Russia

*sokola@igm.nsc.ru

Most of carbon and nitrogen in the reduced mantle at the oxygen fugacity about the iron-wüstite (IW) equilibrium reside in metallic iron, fluids, and diamond/graphite. C- and N-rich metal melts in the Fe–$Fe_3C$–$Fe_3N$ system have quite a large stability field at 7.8 GPa and 1350 °C, i.e., at the *P-T* parameters corresponding to precipitation of the metal phase in the asthenosphere. Iron nitride ε-$Fe_3N$ can contain up to 2.0-2.5 wt.% C and 6.0–7.3 wt.% N equilibrated with the melt but only 1.0 wt.% C and 3.2 wt.% N in equilibrium with γ–Fe. Nitrogen solubility in cementite ($Fe_3C$) is within 0.5 wt.%. Thus, the metal melt and austenite (γ-Fe) can be stable in the precipitating metal when all carbon and nitrogen from the mantle depleted in volatiles have been dissolved, while the metal melt and iron carbide ($Fe_3C$) become stable upon C and N extraction from the mantle enriched in volatiles. N-poor C-O-H-N fluids at IW-buffered $fH_2$ contain abundant $C_1$-$C_4$ alkanes, at trace amounts of all other carbon species, and metaneimine ($CH_3N$) as the main N host. Light alkanes are likewise main carbon species in N-rich fluids, at the same redox conditions, but most of N occurs as $NH_3$ and $N_2$. Thus, the nitrogen cycle must be controlled mostly by $CH_3N$ in reduced fluids in N-poor peridotitic mantle and by $NH_3$ in N-rich eclogitic mantle. Carbon in HC-rich fluids which rise from the reduced asthenosphere to the relatively oxidized lithosphere decreases from 15 to 5 mol.%, and the elemental carbon released upon HC oxidation can maintain diamond crystallization.

The γ-Fe and metal melt phases are stable in the C- and N-depleted Fe-C-O-H-N system at 6.3 GPa, 1300 °C and IW- or MMO-buffered $fH_2$, in equilibrium with a fluid consisting of $NH_3$, $H_2O$, alkanes, and oxygenated HCs (mainly alcohols and esters). In an C-saturated system, at 6.3 GPa and 1200–1300 °C, iron carbide reacts with an N-rich fluid to form iron nitride: $Fe_3C + N_{Fl} = Fe_3N + C_{Gr,Dm}$, while N-rich melt appears at 1400 °C. The equilibrium fluid compositions vary from high $NH_3$ to high $H_2O$ contents (in all cases $NH_3/N_2>1$), with quite high concentrations of alkanes. The N-rich metal melt is stable in equilibrium with a fluid consisting of alkanes, oxygenated HCs (mainly carboxylic acids) and $N_2$ synthesized in N-depleted but C-saturated conditions at 7.8 GPa, 1400 °C, and unbuffered$fH_2$. Therefore, the fluid with relatively high C and N enrichment is stable in equilibrium with the metal phase at the upper mantle *P-T* parameters. Estimates show that $D_N^{Met/Fl}>D_C^{Met/Fl}$, i.e., nitrogen has greater affinity to the metal phase than carbon. In this case, reduced fluids can be efficient carriers of volatiles from the metal-saturated mantle to the oxidized lithosphere. However, the greater iron affinity is expected to provide selective accumulation of N in the metal phase and high C mobility in the fluid phase. These patterns should control deep carbon and nitrogen cycles in the $Fe^0$-saturated mantle.

The study was supported by the Russian Foundation for Basic Research (Project 16-17-10041).

**Experimental modeling of decarbonation reactions resulting in the formation of Mg,Fe,Ca,Mn garnets and $CO_2$-fluid under lithospheric mantle *P,T*-parameters**

Yuliya V. Bataleva[1,*], Ivan D. Novoselov[1,2], Aleksey N. Kruk[1,2], Yuri N. Palyanov[1,2]

[1] Sobolev Institute of Geology and Mineralogy, Siberian Branch of Russian Academy of Sciences, 630090 Novosibirsk, Russia
[2] Novosibirsk State University, 630090 Novosibirsk, Russia

* bataleva@igm.nsc.ru

Studies of the conditions for the stability of natural carbonates and $CO_2$-fluid generation during the mantle-crust interaction are crucial for the reconstruction of the global carbon cycle processes, including the mantle metasomatism, natural diamond formation, as well as the formation and evolution of carbonated eclogites and peridotites. One of the most common fluid-generating processes that occur during the interaction of a subducted slab material with mantle oxides or silicates, determining the stability of carbonates in carbonate-oxide or carbonate-silicate media, is decarbonation. Depending on the composition of carbonates, as well as host rocks, the *P,T*-parameters of decarbonation can vary over a very wide range. For example, subducted $MgCO_3$ and $CaCO_3$ can be thermodynamically stable to the depths of the lower mantle, while the introduction to iron and manganese impurities can reduce the temperature of the onset of decarbonation reactions by several hundred degrees and 1-2 GPa [e.g. Berman, 1991]. Implementation of decarbonation reactions in the zones of mantle-slab interaction leads to the formation of various mantle silicates – olivine, pyroxenes and garnet, whose composition depends on the composition of subducted carbonates and host rocks. Most of the published experimental studies have simulated decarbonation reactions in carbonate-oxide and carbonate-silicate systems to form olivine and pyroxenes [e.g. Newton, Sharp, 1975; Luth, 1995], while experimental data on the formation of a garnet + $CO_2$ fluid assemblage are still rare [Knoche et al., 1999; Pal'yanov et al., 2005]. Thus, it seems very relevant to determine the *P* and *T* regions of the stability of various natural carbonates in association with oxides, to carry out experimental modeling of decarbonation reactions associated with the formation of garnets characteristic of the mantle assemblages and $CO_2$ fluid, and also to determine the position of the corresponding decarbonation curves under mantle *P* and *T*.

Initial stage of experimental studies aimed at the modeling of decarbonation reactions was carried out using the high-pressure multi-anvil apparatus of a split-sphere type (BARS) at 6.3 GPa, in the temperature range of 1100–1400 °C and duration of 20–40 h. Experiments were performed using outer hematite buffer, to control oxygen fugacity in the reaction volume. As a result of experimental modeling of decarbonation reactions, there were estimated the *T*-regions of stability of natural carbonates (magnesite, Mg-siderite, rhodochrosite, ankerite and dolomite) in assemblage with oxides, as well as corresponding parameters for the formation of pure garnets (pyrope, almandine, spessartine, and pyrope-almandine) from carbonated eclogites. The regularities of fluid generation in the initially solid-phase matrix are determined.

This work was supported by the Russian Foundation for Basic Research (project No. 18-35-20016) and a state assignment of IGM SB RAS.

Berman R.G. Thermobarometry using multi-equilibrium calculations: a new technique with petrologic applications. Can. Mineral., 1991, 29, 833–855.

Knoche R., Sweeney R.J., Luth R.W. Carbonation and decarbonation of eclogites: the role of garnet. Contrib. Mineral. Petrol., 1999, 135, 332–339.

Newton R.C., Sharp W.E. Stability of forsterite+$CO_2$ and its bearing on the role of $CO_2$ in the mantle. Earth Planet. Sci. Lett., 1975, 26, 239–244.

Pal'yanov Yu.N., Sokol A.G., Tomilenko A.A., Sobolev N.V. Conditions of diamond formation through carbonate-silicate interaction. Eur. J. Miner., 2005, 17, 207–214.

**Formation of phlogopite and magnesite in kimberlite-like systems at 5.5–7.5 GPa**

Aleksey N. Kruk*, Alexander G. Sokol, Yuri N. Palyanov

Sobolev Institute of Geology and Mineralogy, Siberian Branch, Russian Academy of Sciences, 630090 Novosibirsk, Russia
Novosibirsk State University, 630090 Novosibirsk, Russia

*krukan@igm.nsc.ru

The study of metasomatic alterations of peridotites of the upper mantle by kimberlite-like melts is of great interest, since such processes create conditions for the accumulation of volatiles in the lithosphere and the subsequent generation of kimberlite magmas.

Hydrous kimberlite-like systems were experimentally studied at 5.5–7.5 GPa and 1200–1350 °Cin terms of phase relations and conditions for the phlogopite and magnesite formation. The initial samples were phlogopite–carbonatite–phlogopite, harzburgite–carbonatite sandwiches and harzburgite–K-rich carbonatite mixtures.It was established that in experiments with harzburgite–carbonatite sandwiches, olivine–orthopyroxene–garnet–magnesite–melt assemblage was stable within the entire range of the studied parameters. As temperature increased in the system, Ca# of the melt and the olivine fraction in the peridotite matrix were significantly decreased. The composition of silicate phases in the run products was close to those of high-temperature mantle peridotite.

Experiments with phlogopite–carbonatite–phlogopite sandwiches and harzburgite–K-rich carbonatite mixtures showed, that in the presence of carbonatitic melt, phlogopite can partly melt in a peritectic reaction at 5.5 GPa and 1200–1350 °C, as well as at 6.3– 7.0 GPa and 1200 °C: 2Phl + $CaCO_3$ (L)↔Cpx + Ol + Grt + $K_2CO_3$ (L) + $2H_2O$ (L). Synthesis of phlogopite at 5.5 GPa and 1200–1350 °C, with an initial mixture of $H_2O$-bearing harzburgite and carbonatite, demonstrated that equilibrium in this reaction can be shifted from right to left. Therefore, phlogopite can equilibrate with ultrapotassic carbonate–silicate melts in a ≥ 150 °C region between 1200 and 1350 °C at 5.5 GPa. On the other hand, it can exist but cannot nucleate spontaneously and crystallize in the presence of such melts in quite a large pressure range in experiments at 6.3–7.0 GPa and 1200 °C.

Analysis of resulted data let us suggest that magnesite at the base of subcontinental lithosphere could be derived by metasomatic alteration of peridotite by asthenospheric hydrous carbonate meltsat depths of 180–225 km. The process is possible in the temperature range typical of heat flux of 40–45 mW/$m^2$, which corresponds to the conditions of formation of the deepest seated peridotite xenoliths. Crystallization of magnesite during interaction with peridotite matrix can be considered as experimentallysubstantiated mechanism of $CO_2$ accumulation in subcratonic lithosphere.

Phlogopite can result from metasomatism of peridotite by ultrapotassic carbonatite agents at the base of continental lithospheric mantle at depths shallower than 180–195 km. The possibility of phlogopite crystallization during such metasomatism creates the mechanism of water retaining in lithosphere.

Work is done on state assignment of IGM SB RAS.All analytical studies were performed at the Analytical Center for Multi-Elemental and Isotope Research SB RAS.

## New $CaCO_3$ polymorphs and polytypes stable at ambient conditions

Pavel N. Gavryushkin[1,2]*, Nursultan Sagatov[1,2], Anatoly Belonoshko[3], Aleksander Rečnik[4], Nina Daneau[4], Elena Zhitova[5], Dinara Sagatova[1,2], Konstantin D. Litasov[1,2]

[1] Institute of Geology and Mineralogy SB RAS, 630090Novosibirsk, Russia
[2]Novosibirsk State University, 630090 Novosibirsk, Russia
[3] Royal Institute of Technology (KTH), 10691 Stockholm, Sweden
[4]Jožef Stefan Institute, 1000 Ljubljana, Slovenia
[5] Institute of volcanology and seismology, 683006Petropavlovsk-Kamchatsky, Russia

* gavryushkin@igm.nsc.ru, p.gavryushkin@g.nsu.ru

Calcium carbonate shows reach both ambient and *HP-HT* polymorphism. It was experimentally observed eleven different polymorphs: calcite, aragonite, vaterite, recently found monoclinic aragonite, $CaCO_3$-II, III, IIIb, IV, V, VI, VII, aragonite-II, $P2_1/c$. In the present work, we perform theoretical search of $CaCO_3$ polymorphs, which can be stable at ambient pressure, and verify their existence with transmission electron microscopy and powder X-ray diffraction experiments.

The enthalpies of found new phases relative to the enthalpy of aragonite at 1 bar and K (in eV/f.u.) are the following: aragonite-$P6_3$ -0.02, hexarag -0.05, hexagonal calcite -0.09,calcite -0.12.

The first new structure we found with*ab initio* molecular dynamic simulation (VASP package), it is formed on heating of aragonite to 800 K and has$P6_322$ symmetry, based on which we will call it hexarag. During transition to hexarag, $CO_3$ triangles are rotated on $30^o$ and shifted to the plane middle between close-packed Ca-layers.Thus, hexarag is the intermediate structure between calcite and aragonite and can be considered as 2-layered polytype of calcite.Performed topological analysis (ToposPro package) reveals only on analogue of hexarag in ICSD database – the oxygen- andlead-deficit borate $Pb_{0.75}[BO_{2.25}]$, which under heating transforms from aragonite to hexarag structure. $CaCO_3$-hexarag have not been found in nature or experiment.Our *in situ*TEM experiments do not reveal it too. We observed direct decomposition of aragonite, without formation of calcite or hexarag. However, during TEM investigation of aragonite from different localities, we found new polytypes of aragonite, which are produced by ordered twining of aragonite by each $n^{th}$ {110} plane. Twinning by {110} has the strong effect on aragonite to calcite transformation. Changes of aragonite electron diffraction patternson heatingindicate on movement and ordering of twin boundaries.Results of performed X-ray powder diffraction experiments are under processing and will be presented on conference.

By consequent compressing of hexarag to 3 GPa, heating to 1000 K and quenching in molecular dynamic simulation, we obtain another aragonite-like structure with $P6_3$ symmetry, which we will call aragonite–$P6_3$.The coordination number (CN) of Ca by O in this structure equal to 8, which is intermediate between that of calcite (CN=6) and aragonite (CN=8). At ambient pressure and 0 K, enthalpy of aragonite–$P6_3$ is lower than that of aragonite and higher than that of calcite.

Another new structure, which we will call hexagonal calcite, was revealed in evolutionary metadynamic calculation (USPEX package). This structure has $P6_322$ symmetry and characterized by the 6-layered close packing of Ca-atoms. Hexagonal calcitecan be considered as interlayering of calcite and hexarag structures. Enthalpy of hexagonal calcite is lowest among all found structures, but it is slightlyhigher than that of calcite.The formation of hexagonal calcite is possible during mechanochemical transformation of calcite to aragonite. In our TEM experiments, we have observed superstructures of aragonite with periodicity perpendicular to close packed layer increased 6 times in comparison to aragonite.

The research was supported by the Russian Foundation for Basic Research through Grant № 18-35-20047.

**Influence of high-pressure on $Na_4Ca(CO_3)_3$structure: single-crystal X-ray diffraction and Raman spectroscopy study**

Romanenko A.V.[1, 2]*, Anastasia Brazhnikova[1,2], Anton Shatskiy[1], Sergey Rashchenko[1,2]

[1]Sobolev Institute of Geology and Mineralogy of the Siberian Branch of the RAS, 630090Novosibirsk, Russia
[2]Novosibirsk State University, 630090Novosibirsk, Russia

* romanenko@igm.nsc.ru

Petrological experiments with carbonated pelites and eclogites showed a possibility of Na-Ca carbonate formation at transition zone conditions [Grassi and Schmidt, 2011; Thomson et al., 2016]. Recently, a number of high-pressure Na-Ca carbonates has been discovered [Podborodnikov et al., 2018; Shatskiy et al., 2013]. One of such carbonates is $Na_4Ca(CO_3)_3$with atypical for this class of compounds cubic symmetry (*Ia*3*d*, *a* = 14.5770(5) Å), which was synthesized from the Na–Ca carbonate melt in a system containing 60 mol% $Na_2CO_3$ and 40 mol% $CaCO_3$ in a Kawai-type multi-anvil apparatus. [Rashchenko et al., 2018; Shatskiy et al., 2013]. As carbonates are carbon-concentrating minerals in the mantle domains, so information about the *P–T* region of their stability and phase transformations is necessary to create models of the global carbon cycle of our planet. We carried out a series of Raman spectroscopy and single-crystal X-ray diffraction experiments using diamond anvil cell technique in order to establish high-pressure behavior of the $Na_4Ca(CO_3)_3$.

High-pressure Raman measurements were performed using a Horiba Jobin-YvonLabRAM HR800 Raman microspectrometer, with a 488 nm solid state laser, at Novosibirsk State University. Silicone oil was used as a pressure-transmitting medium. $\nu_1$ ($CO_3^{2-}$)band of $Na_4Ca(CO_3)_3$demonstrates abrupt change of d$\nu$/d$P$ at pressure near 10GPa.

A series of single-crystal X-ray diffraction high-pressure experiments was carried out up to 20 GPaat European Synchrotron Radiation Facility (ESRF) on ID15B beamline using helium as hydrostatic pressure-transmitting medium. The obtained data showed that $Na_4Ca(CO_3)_3$ changes symmetry from cubic (*Ia*3*d*) to rhombohedral (*R*32) at pressure of about 10 GPa without volume anomaly. Asecond-degree Birch – Murnaghan state equation was calculated. The coefficients of the state equation are$V_0$ = 3101.4, $K_0$ = 54.76(22).

Grassi D., Schmidt M.W. et al.The Melting of Carbonated Pelites from 70 to 700 km Depth. J. Petrol.,2011, 52, 765–789.

Podborodnikov I.V., ShatskiyA. et al. The system $Na_2CO_3$–$CaCO_3$ at 3 GPa. Phys. Chem. Miner., 2018, 45, 773–787.

Rashchenko S.V., Shatskiy A., et al.$Na_4Ca(CO_3)_3$: a novel carbonate analog of borate optical materials. Cryst. Eng. Comm., 2018, 20, 5228–5232.

Shatskiy A., Sharygin et al. New experimental data on phase relations for the system $Na_2CO_3$-$CaCO_3$ at 6 GPa and 900–1400 C. Am. Mineral., 2013, 98, 2164–2171.

Thomson A.R., Walter et al. Slab melting as a barrier to deep carbon subduction. Nature, 2016, 529, 76–79.

## Crystal Chemistry of Cl-dominant Hydrotalcite-Supergroup Members

Elena S. Zhitova[1,2]*, Sergey V. Krivovichev[1,3], Igor V. Pekov[4], Nikita V. Chukanov[5]

[1]St. Petersburg State University, 199034 St. Petersburg, Russia
[2]Istitute of Volcanology and Seismology, RAS, 683006 Petropavlovsk-Kamchatsky, Russia
[3]Russian Academy of Sciences, Kola Science Centre, 184209 Apatity, Russia
[4]Moscow State University, 119991 Moscow, Russia
[5]Institute of Problems of Chemical Physics, RAS, 142432 Chernogolovka, Moscow Region, Russia

* zhitova_es@mail.ru

Hydrotalcite-supergroup consists of more than 40 minerals, with at least 4 members that are Cl-dominant specie [Mills et al., 2017]. Hydrotalcite-supergroup minerals and their synthetic analogs are known as layered double hydroxides (LDHs), which found many applications in the modern industry. However, their structural characterization commonly appears as unfulfilled or incomplete. The aim of the present study was to provide a detailed crystal chemical study of Cl-dominant LDHs in order to develop their diagnostic features and peculiarities of Cl distribution at the interlayer level.

The study has been carried out for chlormagaluminite, $Mg_4Al_2(OH)_{12}Cl_2(H_2O)_2$,and iowaite, $Mg_6Fe^{3+}{}_2(OH)_{16}Cl_2(H_2O)_4$,that are different by $M^{2+}$:$M^{3+}$ ratios that are 2:1 and 3:1, respectively. The samples have been studied using single-crystal and powder X-ray diffraction, electron-microprobe analyses and infrared or Raman spectroscopy.

The empirical formula of chlormagaluminite is close to the ideal stoichiometry. For iowaite, the Mg/Fe ratio may vary slightly from the ideal of 3:1. The $Cl^-$ is dominant interlayer anion in all studied samples. The $Cl^-$ substitution is by $OH^-$ groups, whereas $CO_3^{2-}$ groups have not been detected by vibrational spectroscopy. The characteristic feature of the infrared and Raman spectra of chloride LDHs in comparison to carbonate ones is an additional band in the OH stretching region (3700 –3400 $cm^{-1}$). Single-crystal study shows that the localization of interlayer specie is different for chloride and carbonate LDHs. The Cl-dominant members have some ordering in localization of $Cl^-$ ions and $H_2O$ molecules, whereas for $CO_3$-dominant LDHs, the position of $H_2O$ molecules cannot be distinguished from the O atoms of $CO_3$ groups [Zhitova et al., 2019]. The study suggests that characteristic *d*-values of Cl-dominant LDHs having $M^{2+}$:$M^{3+}$ = 2:1 and 3:1 are around 7.65 and 8.00 Å, which is higher than those for $CO_3$-dominant specie having the following characteristic *d*-values 7.56 and 7.80 Å for $M^{2+}$:$M^{3+}$ = 2:1 and 3:1, respectively [Zhitova et al., 2016]. The difference in the *d*-value between carbonate and chloride LDHs is not due to the size of the interlayer ion as commonly suggested by the literature but in the strengths of bonding between layer and interlayer which is mainly affected by the charge of interlayer ion and its geometry.

The study has been carried out using facilities of XRD and Geomodel Centers of St. Petersburg State University.

Mills S.J., Christy A.G., Génin J.-M.R., Kameda T., Colombo F. Nomenclature of the hydrotalcite supergroup: Natural layered double hydroxides. Mineral. Mag, 2012, 76, 1289–1336.

Zhitova E.S., Krivovichev S.V., Pekov I.V., Yakovenchuk V.N., Pakhomovsky Y.A. Correlation between the *d*-value and the $M^{2+}$:$M^{3+}$ cation ratio in Mg–Al–$CO_3$ layered double hydroxides. Applied Clay Science, 2016, 130, 2–11.

Zhitova E.S., Krivovichev S.V., Pekov I.V., Yapaskurt V.O. Crystal Chemistry of Chlormagaluminite, $Mg_4Al_2(OH)_{12}Cl_2(H_2O)_2$, a Natural Layered Double Hydroxide. Minerals, 2019, 9, 221; doi:10.3390/min9040221.

**Ion substitutions and nonstoichiometry of oxalic acid salts formedwith participation of the litobiont microbial community**

Olga V. Frank-Kamenetskaya*, Alina R. Izatulina, Vlad V. Gurzhiy, Marina S. Zelenskaya
Aleksey V. Rusakov, Mariya A. Kuz'mina, Dmitry Yu. Vlasov

Saint Petersburg State University, 199034Saint Petersburg, Russia

* o.frank-kamenetskaia@spbu.ru

Metabolism of litobiont microbial community (microscopic fungi, lichens and other) is an important factor of secondary mineral formation on the surface of different rocks and minerals. By the participation of microscopic fungi and lichens oxalic acid salts **(**oxalates) are most often formed [Gadd et al. 2017]. Among microbial oxalic acid salts calcium oxalates are most common: the tetragonal dihydrateweddelite $CaC_2O_4 \cdot (2 + x)H_2O$ (sp. gr. *I*4/*m*) and monoclinic monohydrate whewellite $CaC_2O_4 \cdot H_2O$ (sp. gr. $P2_1/c$). The results of the structure refinement for four biomimetic weddellites produced by the microscopic fungus Aspergillus niger showed that the zeolitic water content in the structures under study (*x*) varies from 0.10 to 0.24 *mpfu*. The increase in *x* is accompanied by an increase in the number of octahedral groups formed by water molecules (4OW1 + 2OW3) and (4OW1 + 2OW31). The number of groups with the oxygen atoms OW3, weakly bound to the structure increases with increasing *x*, resulting in a decrease in structural stability. An increase in the water content is accompanied by a substantial increase in the parameter *a*and the OW1–OW1 distance, the OW1–OW2 distance being decreased.The synthesized weddellites are similar to weddellites from biofilms and kidney stones in regards to water content and structural parameters.

The possibility of incorporation of $Sr^{2+}$ ions in calcium oxalates was detected by EDX spectra of weddellite in the thallus of the Lecanorapolytropa lichen on the Sr-containing fluorapatite from the Kukisvumchorr deposit (Kola Peninsula), and oxalates obtained in syntheses with the participation of the fungus Aspergillus niger on the surface of complex oxide Ca and Mn (todorokite). Refinement of a series of crystal structures of synthetic (Ca, Sr)-weddelite confirmed the presence of the complete isomorphic series of Ca-weddelite – Sr-weddelite. As the larger strontium cation enters the calcium site (Sr/(Ca + Sr)= = 0, 15, 30, 42, 68 and 100% in solution), the interatomic distance (Ca, Sr)-O increased from 2.452 to 2.584 Å. At the same time, the parameters and volume of the tetragonal unit cell increased: *a* from 12.313 to 12.799 Å, *c* from 7.354 to 7.534 Å, *V* from 1114.9 to 1234.2 $Å^3$. Until the content of strontium ~0.40 *apfu*, the increase in the parameters and volume of the unit cell occurs not only due to a change in the occupancy of the calcium position, but also due to an increase in the content of zeolite water (~ to 0.30 *mpfu*). With further increase in the content of strontium, the amount of zeolite water practically does not change, and further changes in the unit cell occur only due to the strontium incorporation.

The crystal structure of the humboltin group minerals (sp. gr. *C*2/*c*) consists of parallel [010] chains formed by octahedra, in the center of which are $Me^{2+}$ ions, alternating with oxalate ions. The results of the study of biomimetic analogs of the humboldtine group of minerals (humboldtine, *glushenskite* and lindbergite), which were produced by the microscopic fungus Aspergillus niger participation on the surface of various minerals (biotite, pyrrhotite, siderite, todorokite, kutnogorite, magnesite), have demonstrated that there are solid solutions with the general formula (Fe, Mg, Mn) $C_2O_4 \cdot 2H_2O$. Using the example of synthetic Mn-containing gluschenskites and Mg-containing linbergites, it was shown that an increase in the Mn/Mg ratio leads to chain compression and, consequently, to a decrease in the parameter *b*.

The research was supported by the RSF project no 19-17-00141 and performed using the equipment of the SPBU resource centers «X-Ray Diffraction Methods», «Geomodel» and «Microscopy and Microanalysis».

Gadd G. M. Fungi, Rocks, and Minerals. Elements, 2017, 13, 171

**Binary systems of organic substances with chiral molecules: enantiomers of the same substance, enantiomers of different substances, and diastereomers**

Elena N. Kotelnikova,[1]* Anton I. Isakov,[1] Heike Lorenz[2]

[1] Saint Petersburg State University, 199034 Saint Petersburg, Russia
[2] Max Planck Institute for Dynamics of Complex Technical Systems, 39106Magdeburg, Germany

* kotelnikova.45@mail.ru

The results of experimental investigations (by means of PXRD, SCXRD, TRPXRD, HPLC, DSC, IR, and other techniques) of discrete homomolecular and heteromolecular compounds and limits of solid solutions formed in binary systems of organic substances with chiral molecules are reviewed [Isakov et al., 2015, 2016; Kotelnikova et al., 2017, 2019; et al.].

Systems of enantiomers of the same substance. Known physical and chemical properties of enantiomers are identical except for the direction of rotation of a plane-polarized light. Therefore, phase diagrams of such systems are symmetrical and, consequently, it is enough to study any half of the diagram. Systems of three types were studied. A representative system with eutectic point is the system composed of *S* and *R* enantiomers of ethanolamine salt of 3-chloromandelic acid, the system formed by L and D enantiomers of phenylglycine is a system containing equimolar (binary) compound LD (true racemate), the system of malic acid *S* and *R* enantiomers is a system containing equimolar *SR* (1:1) and non-equimolar $SR_3$ (1:3) and $S_3R$ (3:1) discrete compounds. Discrete compounds formed in the systems of this type are homomolecular compounds.

Systems of enantiomers of different substances. Components of such systems have different chemical and physical properties. One type of such systems is composed of enantiomers having opposite signs of optical activity. Some systems of this type are described in published literature. Systems of the other type consist of enantiomers having the same sign of optical activity. The only known examples are amino acids studied by the present authors. The enantiomeric systems L-valine – L-isoleucine, L-valine – L-leucine, and L-isoleucine – L-leucine are found to include non-equimolar discrete compounds $V_2I$, $V_3L$, and $I_3L$, respectively. The discrete compounds formed in the systems of this type are heteromolecular compounds.

Systems of diastereomers. Diastereomers have identical chemical properties, but differ in their physical properties, since their molecules are stereoisomers of different configurations. The system of L-threonine – L-*allo*-threonine (the components have the same sign of optical activity) is a eutectic system, while the system of D-threonine – L-*allo*-threonine (the components have the opposite signs of optical activity) is a system containing continuous solid solutions.

The investigations were performed using equipment of the Centre for X-ray diffraction studies (SPSU Research Park) with the financial support of the RFBR (Project 18-35-00183 mol_a).

Isakov A., Kotelnikova E., Lorenz H. Non-Equimolar Discrete Phases Formed in the System of Malic Acid Enantiomers. Chem. Eng. Technol., 2015, 38(6), 1047–1052.

Isakov A., Kotelnikova E., Muenzberg S., Bocharov S., Lorenz H. Solid Phases in the System L-Valine – L-Isoleucine. Cryst. Growth & Des., 2016, 16, 2653–2661.

Kotelnikova E., Isakov I., Kryuchkova L., Zolotarev A. Jr, Bocharov S., Lorenz H. Acids with chiral molecules as essential organic compounds of biogenic–abiogenic systems. In the book: Processes and phenomena on the boundary between biogenic and abiogenic nature. Springer, 2019 (in press).

Kotelnikova E., Isakov I., Lorenz H. Non-equimolar discrete compounds in binary chiral systems of organic substances (Highlight). Cryst. Eng. Comm., 2017, 19(14), 1851–1869.

**Hydrated calcium oxalates: crystal structures, thermal stability and phase evolution**

Alina R. Izatulina*, Vladislav V. Gurzhiy, Maria G. Krzhizhanovskaya, Mariya A. Kuz'mina, Olga V. Frank-Kamenetskaya

Department of Crystallography, St. Petersburg State University, 199034 St. Petersburg, Russia

* alina.izatulina@mail.ru

Calcium oxalates are represented in nature by three hydrated forms: whewellite ($CaC_2O_4 \cdot H_2O$; COM), weddellite ($CaC_2O_4 \cdot (2+x)H_2O$; COD) and caoxite ($CaC_2O_4 \cdot 3H_2O$; COT). Calcium oxalates are also found among the pathogenic mineral precipitates in human bone marrow, myocardium, joints, lungs, liver, thyroid gland, intestinal mucosa, eyes, and urinary system. Oxalates span therefore several fields (medicine, biology, mineralogy, materials science, etc.), which is reflected in a large number of publications. Nevertheless, many questions remain unresolved. For instance, the role of water in the formation of calcium oxalate crystal structures as well as the mechanisms of phase transition is still unclear. Thermal stability, structural evolution pathways and phase transition mechanisms of the calcium oxalates whewellite, weddellite and caoxite have been analyzed using single crystal and powder X-ray diffraction (XRD) [Izatulina et al., 2018]. The reduction of $H_2O$ content in the structures increases dimensionality from dimers and chains to the layered structural units and from rarefied to denser sheets within the compounds whose structures are based on the 2D units. While studying the phase transitions pathways within the calcium oxalate family, two crystalline compounds have been structurally characterized for the first time ($\alpha$-$CaC_2O_4$ and $CaC_2O_4 \cdot H_2O$), among which the novel COM modification has been obtained for the first time as well.

The highest thermal expansion of these compounds is observed along the direction of the hydrogen bonds, whereas the lowest expansion and even contraction of the structures occur due to the displacement of neighbor layered complexes towards each other and to an orthogonalization of the monoclinic angles. Within the calcium oxalate family, whewellite should be regarded as the most stable crystalline phase at ambient conditions. Weddellite and caoxite transform to whewellite during dehydration-driven phase transition promoted by time and/or heating. Finally, we'd like to emphasize the particular importance of the structural and chemical evolution studies of calcium oxalates, as their phase transitions occur at temperatures typical of the human body and can therefore have a significant effect on health.

This work was supported by the Russian Science Foundation (no. 18-77-00026). The XRD measurements have been performed at the X-ray Diffraction Centre of St. Petersburg State University.

Izatulina A.R., Gurzhiy V.V., Krzhizhanovskaya M.G., Kuz'mina M.A., Leoni M., Frank-Kamenetskaya O.V. Hydrated Calcium Oxalates: Crystal Structures, Thermal Stability and Phase Evolution. Cryst. Growth Des.,2018, 18, 5465−5478.

**Structural and morphological of carbonate hydroxyapatite prepared in the presence of glycine**

O.A. Golovanova*, S.A. Gerk

Dostoevsky State University, 644077 Omsk, Russia

* golovanoa2000@mail.ru

The mechanism underlying the interaction between the organic and inorganic bone components has not yet been studied in sufficient detail. The deposition of CHA crystals is thought to begin in zones between collagen fibrils when these are shifted by a quarter of their length, and the first forming crystals act as nucleation centers for further formation of the inorganic component of the bone tissue.

As know, polypeptide collagen chains contain crystalline segments in the form of –Gly–X– Y– triplets consisting largely of neutral amino acids (Gly = glycine, 33 wt %; X = proline or hydroxyproline, 22 wt %; Y = hydroxylysine), and amorphous segments consisting of polar amino acids (lysine, histidine, and others). However, the role played by individual amino acids and collagen regions in binding with the solid phase is essentially unexplored.

This problem can be partially resolved in experiments aimed at investigating calcium phosphate (brushite, hydroxyapatite (HA), octacalcium phosphate, etc.) biomineralization processes in artificial systems (urine, saliva, and others), as well as by computer simulation. As know, amino acids and proteins may inhibit or stimulate crystallization of calcium phosphates through adsorption interactions with their surface and complexation with calcium ions, thus influencing the crystallinity, morphology, and particle size of the solid phase. However, since data available in the literature are limited mainly to the proposed models, gaining insight into the role of organic substances on CHA formation processes is of great current interest.

The purpose of this work was to assess the effect of glycine on the morphology, degree of crystallinity, and resorption properties of CHA synthesized from model solutions of human joint synovial fluid (synovia). Glycine was chosen as a reference because its molecule has small dimensions without lateral radicals and active centers with opposite (acidic and basic) properties and enters into the composition of various proteins, including collagen.

The HA precipitation process in the solution under investigation can be represented by the following reaction scheme:

$$10\ CaCl_2 + 6\ M_2HPO_4 + 8MOH \Rightarrow Ca_{10}(PO_4)_6(OH)_2\downarrow + 20MCl + 6H_2O, \qquad \text{where } M = Na^+, K^+.$$

We have synthesized CHA from prototype human synovial fluid in the presence of glycine. The resultant powders contain 75 to 80 wt % the amino acid. It has been shown that, if the model solution contains less than 0.08 mol/L of glycine, the latter has no effect on the size of the forming CHA crystals, but leads to changes in the degree of their crystallinity and their specific surface area. At glycine concentrations in the model solution above 0.08 mol/L, we observe the formation of poorly crystallized CHA–Gly composites having a large specific surface area and consisting of smaller nanocrystallites. Such samples contain larger amounts of the amino acid (≈80%), adsorbed and chemically bound water, highly volatile impurities (including adsorbed carbon dioxide), and carbonate ions substituting for phosphate tetrahedra in the structure of HA.

The dissolution of the samples in a 0.9% NaCl solution, modeling a “passive” resorption stage, has been shown to be a two-step process.

The samples synthesized from a medium containing more than 0.08mol/L of glycine dissolve at a higher rate and in a shorter time. The CHA–Gly powders were found to dissolve at a slower rate in an acetate buffer solution.

The highest solubility under weakly acidic conditions has been demonstrated by the precipitates containing the largest amount of the amino acid.

**The Raman spectroscopy of meta-anthracite and coal graphite of contact metamorphism**

Natalia S. Biske

Institute of Geology, Karelian Research Centre, RAS, 185910 Petrozavodsk, Russia

nataliabiske@yandex.ru

The goal of the present report was studying of change of the Raman spectrum and the Raman parameters of coal material at the stage meta-anthracite – graphite of contact metamorphism. Samples were selected from the graphite deposits in the Tungus and Taimyr coal Basins (Russia, Eastern Siberia). The composition, optical parameters and X-ray diffraction data of graphite and meta-anthracite are brought in the work [Vyalov, 1995]. Meta-anthracite has a lower reflection power ($R_{max} \leq 7.4\%$) than coal graphite. Some macroscopic types of coal graphite: columnar, platy and concretion-like are described [Vyalov, 1995].

The Raman spectra were obtained using the 532 nm excitation laser wavelength. On the first-order region the main bands: the G at ~ 1598 $cm^{-1}$ (FWMH=50–54 $cm^{-1}$) and the D1 at ~ 1355 $cm^{-1}$ (FWMH=52–60 $cm^{-1}$) and some disorder bands with the intensity ratio (mean value): D2/G=0.42; D3/G=0.17 and D4/G=0.07 are recorded after deconvolution of the meta-anthracite spectra. The D1/G intensity ratio is more than 2.0. On the second order region four weak lines are detected. The band at 2695 $cm^{-1}$ intensity usually slightly exceeds the band at ~ 2945 $cm^{-1}$ one.

The columnar and platygraphites consist of the homogeneous microcrystalline mass with the "shadow" relics of coal macerals. The close values of the Raman parameters are received for sites with the different structure: half-width of G (1588–1589 $cm^{-1}$) varies from 27 to 28 $cm^{-1}$, half-width of D1 (1356 $cm^{-1}$) respectively – from 37 to 39 $cm^{-1}$; the intensity ratio D1/G=0.76–0.87; D2/G=0.18–0.20. There is a very intensive 2D band at 2703–2705 $cm^{-1}$ (2D/G=0.6–0.9) and a weak band at ~2900 $cm^{-1}$ on the second order region. But according to lack of the 2D band doublets and presence of weak defect bands D3 and D4, the final stage of graphitization was not reached.

Concretion-like graphite with the relict microstructures of coal is localized within the columnar graphite layers. This type is similar to meta-anthracite, according to spectroscopy. The aggregates of graphite-like microcrystalline particles have been distinguished among the ground mass in the concretion-like graphite and meta-anthracite. Raman parameters of these particles are similar to ones of the columnar and platygraphite. Flaky graphite of different degree of crystallinity is defined in contact with the intrusion.

Vyalov V.I. Solid Fuel Chemistry, 1995, 1, 15–24.

**Study of the effect of “free” carbon content in the initial micron powder of WC – Co and sintering temperature on the phase composition of hard alloys obtained by the SPS method**

Ksenia E. Smetanina*, Pavel V. Andreev, Evgeny A. Lantsev, Maksim S. Boldin

Lobachevsky State University, 603950 Nizhny Novgorod, Russia

* smetanina-ksenia@mail.ru

The unique combination of physical and mechanical properties of hard alloys based on the WC – Co system allows their use in the production of tool materials.

Adding cobalt to the initial tungsten carbide powder increases the variety of possible crystalline phases in the composition of the sintered ceramics. In the case of the stoichiometric composition of tungsten monocarbide, the amount of carbon is ~ 6.1 wt. %, with the addition of 10% cobalt, it decreases, while falling into the non-stoichiometric region of the phase diagram, which leads to the formation of the η-phase in the ceramic sample. It is known that the presence in the ceramic sample of the η-phase adversely affects its physical and mechanical properties [Kurlov, Gusev, 2014]. Attempts are being made to eliminate the appearance of the η-phase by adding graphite, the so-called “free” carbon, to the initial composition.

The objects of study were 12 ceramic samples sintered from micron α-WC powder with β-Co and “free” carbon, the amount of which ranged from 0 to 0.5 wt. % in increment of 0.1 wt. %. The samples were compacted with a diameter of 12 mm and a thickness of 3 mm by the method of spark plasma sintering (SPS) at $T$ = 1100°C and $T$ = 1400°C. Conventionally, these temperatures can be considered “liquid phase” and “solid phase” sintering, because the aggregate state of cobalt is the reason for the launch of various diffusion mechanisms that ensure the sintering of ceramics. Then the surface was mechanically polished with a diamond paste and finished with the paste with dispersion of 1/0 μm. X-ray diffraction experiments was carried out on a Shimadzu XRD-700 powder diffractometer (CuKα, λ = 1.54 Å).As a result, it was found that the content of η-phase in the sample sintered at a lower temperature (1100°C) with 0.2 wt. % C is at the detection limit, when as at a higher temperature η-phase is suppressed at 0.3 wt. % C.Thus, in the case where the cobalt is in the “liquid phase”, more “free” carbon is required to “suppress” the η-phase.

The cobalt peaks are displaced on experimental diffractograms. We can conclude the change of the unit cell parameters in accord with the Bragg equation. So, if the parameters of the cell of the α-WC phase do not change within the limits of error with an increase in the content of “free” carbon in the initial powder, then the cobalt peaks are shifted toward larger angles. This suggests a decrease in the cubic cobalt cell parameter $a$. Qualitatively, this can be explained by the fact that the introduction of carbon atoms into the cell of cobalt occupying interstices reduces the diffusion of tungsten atoms, the atomic radius of which is larger than the carbon atomic radius.

It was also found that the intensity of the cobalt peaks decreases with increasing content of “free” carbon. This may be due to the fact that the embedded carbon atoms reduce the average atomic factor of the structure, which leads to a decrease in intensity.

To study the dissolution of tungsten and carbon atoms in cobalt, another series of samples of the composition WC + 10% Co + 0.5% C, sintered in the temperature range from 750°C to 1000°C with a step of 50°C with isothermal exposure for 70 minutes at each temperature, was considered. It turned out that, starting from 900°C, the parameters of α-WC and β-Co do not change within the limits of the calculated errors. Therefore, at these temperatures, the solubility limit of carbon and tungsten in solid-phase cobalt can be reached.

Kurlov A.S., Gusev A.I. Physics and chemistry of tungsten carbides, 2014, 272.

# 7. Descriptive Mineralogy

**Mineralogical Diversity of the Hatrurim Combustion Metamorphic Rocks (Dead Sea Region)**

Ella V. Sokol*, Victoria A. Danilovsky, Svetlana N. Kokh, Victor V. Sharygin

Sobolev Institute of Geology and Mineralogy SB RAS, 630090 Novosibirsk, Russia

* sokol@igm.nsc.ru

By December 2018, there had been 140 IMA-approved primary mineral species described in high- and ultrahigh-temperature and low-pressure (UHT-LP) combustion metamorphic (CM) rocks of the so-called Hatrurim Fm. (Mottled Zone) complexes adjacent to the Dead Sea Transform. Their mineralogical productivity was estimated as ($K=M_{minerals}/N_{elements}= 140/30 = 4.67$). The Hatrurim $Ca_2SiO_4$-bearing and melt (paralava) decarbonated UHT-LP rocks found on the western side of the Dead Sea result from subsurface burning of high-calorific gas jets (*T* up to 1500 °C). The lower-temperature marbles widespread on the eastern side were heated by gases released by smoldering of S-rich disseminated organic matter. The mineralogy of the UHT-LP rocks varies from predominant oxygen-bearing compounds (99 species; 77.3%) to sulfides + selenides (17; 13%), phosphides (7; 5.5%), and native elements (4; 3.1%). The minerals mainly consist of elements that are abundant in the upper crust but their descending order of species numbers is unusual and records the chemical features of the sedimentary precursors: 99 O, 77 Ca, 53 Si, 42 Fe, 28 Al, 28 S, 19 P, 16 K, 13 Mg, 10 Ti, and 5 Na species. Apart from mayenite supergroup minerals containing $H_2O$ or (OH)-groups, the primary CM mineral assemblages are totally anhydrous. Chemically complex solid solutions are typical only of "omnivorous" perovskite, antiperovskite, and NaCl structural types, such as pseudobinary perovskite-brownmillerite series, nabimusaite supergroup minerals, and periclase (Mg,Fe,Ni,Zn)O. Other compounds show relatively low chemical flexibility and are close to the end-member composition of solid solutions. The diversity of the Hatrurim UHT mineral world is additionally supported by trace and minor elements which become mineral-forming species for the lack of the appropriate hosts in the Ca-rich UHT-LP environment: 15 Ba, 12 Cu, 12 F, 7 Ni, and 5 Zn species, as well as Se, U, Zr, V that form three species each, Mo and Sr (two species each) and Sn, Cr, Ce, and Ag (one species each). Trace elements in the CM rocks are commonly within tens to hundreds ppm, but local anomalies of Ba, Sr, Zn, Cu, Ni, Cd, U, Cr, Mo, Ag, Se, V, and Ce are sufficient for forming minerals; additionally, six polymorphic compounds totally form 13 minerals.

Most of compounds are chemically simple and consist of 3 or 4 elements (35 and 34 species): double oxides (Ca-Ti-O; Ca-Zr-O; Ca-U-O; Ca-Fe-O; Ca-Al-O; Fe-Ni-O; Fe-Ti-O; Fe-Mn-O; Fe-Mg-O; Fe-Ba-O; Al-Fe-O; Mg-Al-O) and simple Ca and Zr silicates. The compounds of 4 elements include silicates (Si-O) with two cations (Ca-Mg; Ca-Fe; Ca-Al; K-Al; Ba-Al); poly-anion Ca compounds (Ca-Si-O-F; Ca-Si-S-O; Ca-Si-P-O; Ca-Si-C-O; Ca-P-O-F; Ca-Fe-S-O; Ca-Al-O-Cl; Ca-Al-O-F); sulfates (Ca-Al-S-O; Ca-K-S-O; K-Sr-S-O); oxides (Ca-Al-Fe; Ca-Ti-Fe), and one sulfide (murunskite, $K_2Cu_3FeS_4$). Minerals in metacarbonate CM rocks are mainly of cubic (22.6 %) or orthorhombic (22.6 %) symmetry; medium symmetric phases are less frequent (36.3 % totally), while monoclinic (12 %) and triclinic (8.1 %) symmetry are rare. This distribution differs from that for lithospheric minerals (38 % monoclinic) but is similar to that for synthetic anhydrous inorganic compounds [Chesnokov, 2001]. The reason is in very young age (4.2-0.1 Ma) and an anhydrous composition of the mineral-forming system. Many large-cation minerals are endemic to the Hatrurim Fm. (Ca silicates with high Ca/Si ratios, Ca aluminates and zincate-aluminates, Ca-Al sulfates, Ca-Fe oxysulfides, Ca uranates, Ba-Ca and K-Ca polyanion minerals of the nabimusaite supergroup, and polycation sulfides with Ca, Ba, K) [Vapnik et al., 2004].

The study was supported by grant 17-17-01056 from the Russian Science Foundation

Chesnokov B.V. The groups of syngonies and respective distribution of crystals. The Ural Mineralogical Collected Papers, 2001, No. 11.

Vapnik Y., Galuskina I., Murashko M., Britvin S., Galuskin E. The Hatrurim complex - the new unique locality on world mineral map: the review of mineral discoveries. Israel Geological Society, 2014, 143–144.

# Siwaqaite, $Ca_6Al_2(CrO_4)_3(OH)_{12}\cdot 26H_2O$,a New Mineral Belonging to the Ettringite Group Minerals from Daba-Siwaqa Complex, Jordan

Rafał Juroszek[1]*,Biljana Krüger[2],Irina Galuskina[1],Hannes Krüger[2],Yevgeny Vapnik[3], Evgeny Galuskin[1]

[1] University of Silesia, 41-200 Sosnowiec, Poland
[2] University of Innsbruck, 6020 Innsbruck, Austria
[3] Ben-Gurion University of the Negev, 84105Beer-Sheva, Israel

* rjuroszek@us.edu.pl

A new mineral siwaqaite, ideally $Ca_6Al_2(CrO_4)_3(OH)_{12}\cdot 26H_2O$, a member of the ettringite group minerals, was discovered in thin veins and small cavity within spurrite marble at North Siwaqa complex, Jordan. In spurrite marble, composed mainly by calcite, fluorapatite and brownmillerite, siwaqaite occurs with calcite, minerals of the baryte-hashemite series, and highly hydrated Ca-silicate. The new mineral forms hexagonal prismatic crystals up to 250 μm in size but most common are aggregates which filled veins and occurred together with calcite on the border of cavities.

The empirical formula of holotype siwaqaite calculated on the basis of 8 framework cations is as follow$Ca_{6.01}(Al_{1.87}Si_{0.12})_{\Sigma 1.99}[(CrO_4)_{1.71}(SO_4)_{1.13}(SeO_4)_{0.40}]_{\Sigma 3.24}(OH)_{11.63}\cdot 26H_2O$.

The structural investigation, as well as, Raman and FTIR spectroscopy analyses confirm the presence of $(CrO_4)^{2-}$, $(SO_4)^{2-}$and $(SeO_4)^{2-}$ groups, which occupy tetrahedral sites in inter-column space (channels) of siwaqaite structure. The synchrotron radiation SC-XRD analysis yielded the trigonal symmetry: $a = b = 11.3640(2)$ Å, $c = 21.4485(2)$ Å, $V = 2398.78(9)$ Å$^3$, $Z = 2$. The structure was solved and refined to R = 0.0454 in the non-centrosymmetric *P*31*c* space group bythe analogy to ettringite [Moore and Taylor, 1970; Berliner, 1998].

Siwaqaite is a low-temperature, hydrothermal mineral. The temperature of its formation is not higher than ~70-80°C as indicated by mineral association and also by the formation conditions of the natural and synthetic analogues, which are stable at the restricted conditions [Wieczorek-Ciurowa et al., 2001; Jiménez and Prieto, 2015].

Minerals of the ettringite group are very important compounds in the cement industry. The siwaqaite structure byanalogy to ettringite has the ability to immobilization and storage various contaminants and toxic ions in both cationic and anionic positions through substitution, sorption and phase mixing, and for that reason, this phase may be used, for example, as a material for $Cr^{6+}$ removal from liquid industrial waste.

This project was partly supported by the National Science Centre (NCN) of Poland, grant no. 2016/23/N/ST10/00142 (J.R) and by OeAD, CEEPUS CIII-RO-0038, ICM-2018-12254 (R.J.)

Berliner R. The structure of ettringite in M. Cohen, S. Mindess, J. Skalny, Material Science of Concrete, American Ceramic Society, 1998, 127–141.

Jiménez A., and Prieto M. Thermal stability of ettringite exposed to atmosphere: implications for the uptake and harmful ions by cement. Envir. Science & Technology, 2015, 49, 7957–7964.

Moore A., and Taylor H.F.W. Crystal structure of ettringite. ActaCrystallographica, 1970, B26, 386–393.

Wieczorek-Ciurowa K., Fela K., and Kozak A.J. Chromium(III)-ettringite formation and its thermal stability. Journal of Thermal Analysis and Calorimetry, 2001, 65, 655–660.

**Zadovite with Anomalously High Si Content fromNegev Desert, Israel**

Arkadiusz Krzątała[1,*], Biljana Krüger[2], Irina O. Galuskina[1], Hannes Krüger[2], Yevgeny Vapnik[3], Evgeny V. Galuskin[1]

[1] University of Silesia, Będzińska 60, 41-200 Sosnowiec, Poland
[2]University of Innsbruck, 6020 Innsbruck, Austria
[3]Ben-Gurion University of the Negev, 84105 Beer-Sheva, Israel

* arkadiusz.krzatala@gmail.com

Minerals of the zadovite, $BaCa_6[(SiO_4)(PO_4)](PO_4)_2F$, – aradite, $BaCa_6[(SiO_4)(VO_4)](VO_4)_2F$, series have been described from paralava of the pyrometamorphic Hatrurim Complex from Gurim Anticline, Negev Desert, Israel [Galuskin et al., 2015]. Zadovite with anomalously high Si-content was found in coarse-grained paralavafrom Zuk Tamrur, Negev Desert. Rock-forming minerals of the ZukTamrurparalava are rankinite, melilite, garnets of the andradite-schorlomiteseries, fluorapatite, wollastonite and cuspidine.Accessory minerals are aradite, zadovite, barioferrite, magnesioferrite, khesinite, gurimite, delafossite, walstromite andferrian perovskite.Minerals of the zadovite group exhibita modular structure with intercalatedantiperovskite layers $\{[FCa_6](TO_4)_2\}^{X+}$and $Ba(TO_4)_2^{X-}$ layers, where *T* = $Si^{4+}$, $P^{5+}$, $V^{5+}$and $S^{6+}$.In the case of stracherite, $BaCa_6(SiO_4)_2[(PO_4)(CO_3)]F$, one of the $PO_4$tetrahedra is replaced by a$CO_3$ group[Galuskin et al., 2018].

In zadovite from ZukTamrur,Si-content reaches up to15.5 wt.% $SiO_2$or 2 Si *pfu*in the crystal chemical formula. High Si-content in zadovite can be connected with anisomorphicheterovalent substitutionaccording to the scheme:$(PO_4)^{3-}{}_2 \rightarrow (SiO_4)^{4-}+[(SO_4)^{2-}/(CO_3)^{2-}]$, leading to the following end-member formulas: $BaCa_6(SiO_4)_2[(PO_4)(SO_4)]F$ or $BaCa_6(SiO_4)_2[(PO_4)(CO_3)]F$.Apart from the high Si-content, the same crystals yield minor S and C too. Consequently, resulting chemical formula calculated for analyzed crystals in the form of $BaCa_6(SiO_4)_2(PO_4)_2F$was not charge balanced.

The structural studies of high-Si zadovitereveal vacancies at the*O*3site in $Ba(TO_4)_2^{X-}$and presence of $(PO_3)^-$triangulargroups. This suggests the heterovalent substitution $(PO_4)_2^{3-} \rightarrow (SiO_4)^{4-}+[(PO_4)_{0.5}^{3-}+(PO_3)_{0.5}^-]$and the following chemical formula $BaCa_6(SiO_4)_2[(PO_4)_{1.5}(PO_3)_{0.5}]F$. The empirical chemical formula of high-Si zadovite will look as follow$(Ba_{0.97}Sr_{0.02}Na_{0.01})_{\Sigma1}(Ca_{5.92}Fe^{2+}_{0.04}Na_{0.03}Mg_{0.01})_{\Sigma6}[(SiO_4)_{1.94}(PO_4)_{0.06}]_{\Sigma2}[(PO_4)_{1.20}(PO_3)_{0.43}(VO_4)_{0.22}(SO_4)_{0.13}(TiO_4)_{0.01}(AlO_4)_{0.01}]_{\Sigma4}F$.This is, probably, the first known inorganic phase with $P^{5+}$ in triangular $PO_3$coordination.

The investigations were partially supported by the National Science Centre of Poland, Preludium no. 2016/21/N/ST10/00463 and OPUS no. 2016/23/B/ST10/00869

Galuskin E.V., Gfeller F., Galuskina I.O., Pakhomova A., Armbruster T., Vapnik Y., Włodyka R., Dzierżanowski P., Murashko M. New minerals with modular structure derived from hatrurite from the pyrometamorphic Hatrurim Complex, Part II: Zadovite, $BaCa_6[(SiO_4)(PO_4)](PO_4)_2F$, and aradite, $BaCa_6[(SiO_4)(VO_4)](VO_4)_2F$, from paralavas of the Hatrurim Basin, Negev Desert, Israel. Min. Mag., 2015, 79, 1073–1087.

Galuskin E.V., Krüger B., Galuskina I.O., Krüger H., Vapnik Ye., Pauluhn A., Olieric V. Stracherite, $BaCa_6(SiO_4)_2[(PO_4)(CO_3)]F$, the first $CO_3$-bearing intercalated hexagonal antiperovskite from Negev Desert, Israel. Am. Mineral.,2018, *103* (10), 1699–1706.

**$CO_3$-free and P-bearing Latiumitefrom EsseneiteParalava of the HatrurimComplex, Negev Desert, Israel**

Katarzyna Nowak[1]*, Rafał Juroszek[1], Biljana Krüger[2], Irina O. Galuskina[1], Evgeny V. Galuskin[1]

[1]University of Silesia, 41-200 Sosnowiec, Poland
[2]University of Innsbruck, 6020 Innsbruck,Austria

*knowak12@us.edu.pl

Minerals of the $KCa_3(Al,Si)_5O_{11}[(PO_4),(SO_4)]$ solid-solution were found in coarse-grained esseneite-wollastonite paralava of the pyrometamorphic Hatrurim Complex in the Negev Desert, Israel. Minerals with $(SO_4)>(PO_4)$ are classified as latiumite, which was known before,just only from a few localities in Italy [Tilley and Henry, 1952; Orlandi et al., 1977]. Minerals with $(PO_4)>(SO_4)$ fall within the composition field of a new mineral – levantite [Galuskin et al. 2017]. Minerals of the latiumite–levantite series from paralava are associate with gehlenite, garnet of the andradite-schorlomite series and fluorapatite.

The latiumite group combines, except levantite $KCa_3(Al_2Si_3)O_{11}(PO_4)$ and latiumite $(Ca,K)_4(Si,Al)_5O_{11}(SO_4,CO_3)$, also tuscanite $KCa_6(Si,Al)_{10}O_{22}(SO_4,CO_3)_2(OH)\cdot H_2O$ and queitite $Zn_2Pb_4(Si_2O_7)(SiO_4)(SO_4)$.

Members of the levantite–latiumite series from the Negev Desert differ from Italian minerals by the absence of $CO_3$-group in composition. This was confirmed by Raman spectroscopy and X-ray diffraction analysis. An empirical formula of $CO_3$-free and $PO_4$-bearing latiumite obtained on the basis of mean 20 microprobe analyses and calculated on 15O looks as follows: $(K_{0.77}Sr_{0.02}Ba_{0.02}\square_{0.19})_{\Sigma1}(Ca_{2.92}Na_{0.05}Mg_{0.03})_{\Sigma3}(Si_{2.56}Al_{2.23}Fe^{3+}_{0.10}P_{0.07})_{\Sigma4.96}O_{11}[(SO_4)_{0.63}(PO_4)_{0.37}]_{\Sigma1}$.Its empirical formula is close to the structural formula obtained as a result of the single-crystal XRD study: $(K_{0.85}\square_{0.15})_{\Sigma1}Ca_3(Si,Al)_5O_{11}[(SO_4)_{0.6}(PO_4)_{0.4}]_{\Sigma1}$.

Latiumite from Israel ($P2_1$, $a$ = 11.992 Å, $b$ = 5.08Å; $c$ = 10.813Å, $\beta$ = 106.92°) has unit cell parameters close to the holotype latiumite from Italy ($P2_1$, $a$ = 12.06, $b$ = 5.08, $c$ = 10.81 Å, $\beta$ = 106°; [Cannillo et al., 1973]). The difference is observed in $a$-direction, due tohigher Al content in double tetrahedral layers in latiumites from Italy.

Tetrahedral hybrid *zweier* double layers, $[(Si,Al)_{10}O_{22}]$, are the main structural elements of latiumite as well as of levantite and tuscanite. Potassium occurs in the cavities of these layers, whereas Ca-atoms and $(PO_4)/(SO_4)$ groups are located between them. Transition from levantite to latiumite takes place due to realisation of the two main mechanisms of isomorphic substitution of $P^{5+}\rightarrow S^{6+}$: 1) $(PO_4)^{3-} + (SiO_4)^{4-}\rightarrow (SO_4)^{2-} + (AlO_4)^{5-}$ and 2) $K^+ + (PO_4)^{3-}\rightarrow\square + (SO_4)^{2-}$, which respectively lead to the two end-member formulas: $KCa_3(Al_3Si_2)O_{11}(SO_4)$ and $\square Ca_3(Al_2Si_3)O_{11}(SO_4)$. The empirical formula of the holotype latiumite, $(K_{0.85}\square_{0.15})Ca_3(Al_{2.85}Si_{2.15})O_{11}(SO_4)_{0.7}(CO_3)_{0.3}$ [Cannillo et al., 1973], can be simplified to $KCa_3(Al_3Si_2)O_{11}(SO_4)$.Latiumite from Israel has a higher content of Si than Al, as it can be seen from the empirical formula above. This is supported by high P content in the composition.

The investigations were partially supported by NCN of Poland, grant no. 2016/23/B/ST10/00869, and CEPUS, CIII-RO-0038

Cannillo E., Dal Negro A. and Rossi G. The crystal structure of latiumite, a new type of sheet silicate. Am. Min., 1973, 58, 466–470.

Galuskin E.V., Krüger B., Galuskina I.O., Krüger H., Vapnik Ye., Pauluhn A., Olieric V. Levantite, IMA2017-010, CNMNC Newsletter No. 37. Min. Mag., 2017, 81, 737–742.

Orlandi P., Leoni L., Mellini M. and Merlino S. Tuscanite, a new mineral related to latiumite. Am. Min., 1977, 62, 1110-1113. Tilley C.E., Henry N.F.M Latiumite (sulphatic potassium-calcium-aluminum silicate), a new mineral from Albano, Latium, Italy. Min. Mag.,1953, 30, 39–45.

**Minerals of schreibersite-nickelphosphide series, $Fe_3P$–$Ni_3P$, in different meteorite groups**

Sergey N. Britvin[1,2]*, Maria G. Krzhizhanovskaya[1], Andrey A. Zolotarev[1], Liudmila A. Gorelova[1]

[1] Dept. Crystallography, St. Petersburg State University, 199034St. Petersburg, Russia
[2] Kola Science Centre, 184209 Apatity, Murmansk Region, Russia

* sergei.britvin@spbu.ru

Natural phosphides – the minerals containing phosphorus in the oxidation state lower than zero – are typical constituents of space matter though rarely found on Earth [Britvin et al., 2015]. Iron-nickel phosphides comprise substantial part of this mineral group and considered sensitive indicators of crystallization pathways in the metal-rich meteorites and their parent bodies. The most common phosphide, schreibersite, $(Fe,Ni)_3P$, belongs to the earliest known meteoritic minerals [Berzelius, 1832] whereas its nickel-dominant analogue, nickelphosphide, $(Ni,Fe)_3P$, was recognized as a distinct species for almost 170 years later [Britvin et al., 1999]. In spite of compositional simplicity, the minerals related to schreibersite-nickelphosphide join exhibit complex crystal chemistry, due to presence of three independent metal sites in their crystal structure. Doenitz (1970) first demonstrated the non-random distribution of Fe and Ni among *M*1, *M*2 and *M*3 sites of schreibersite structure. Further studies of these minerals were mainly devoted to schreibersite halve of $Fe_3P$–$Ni_3P$ join, whereas studies of nickelphosphide were performed only on a single synthetic sample – a counterpart of natural nickelphosphide [Skála and Drábek, 2003].

In the course of ongoing research of natural phosphides, we conducted a structural study of representative sampling of the minerals related to schreibersite–nickelphosphide series originated from more than 40 meteorites of different chemical and structural groups. It was found that distribution of Fe and Ni among *M*1, *M*2 and *M*3 sites is more complex than it was supposed in the earlier studies. In particular, nickelphosphide halfof the join had showed substantial sensitivity of Fe/Ni distribution depending on the origin of the mineral. The results of the present study could provide interesting genetic implications related to crystallization histories of meteorites and their parent bodies.

This work was supported by St. Petersburg State University and Russian Science Foundation (grant № 18-17-00079).

Berzelius J.J. Undersökning af en vid Bohumiliz I Böhmen funnen jernmassa. Kongelige Svenska Vetenskaps-Academiens Handlingar, 1832, 106–119.

Britvin S.N., Kolomensky V.D., Boldyreva M.M., Bogdanova A.N., Kretser Yu.L., Boldyreva O.N., Rudashevsky N.S. Nickelphosphide $(Ni,Fe)_3P$ – the nickel analog of schreibersite. Zapiski VMO 1999, 128, 64–72 (Russian).

Britvin S.N., Murashko M.N., Vapnik Ye., Polekhovsky Yu.S., Krivovichev S.V. Earth's phosphides in Levant and insights into the source of Archaean prebiotic phosphorus. Sci. Rep. 2015, 5, 8355.

Doenitz F.D. Die Kristallstruktur des meteoritischen Rhabdits $(Fe,Ni)_3P$. Z. Kristall. 1970, 131, 222–236.

Skála R., Drábek M. Nickelphosphide from the Vicenice octahedrite: Rietveld crystal structure refinement of a synthetic analogue. Mineral. Mag. 2003, 67, 783–792.

# Detailed Mineralogy and Trace Element Composition of Silicate-Bearing IAB Iron Meteorite NWA11104

D. S. Ponomarev[1]*, K. D. Litasov[1], A. Ishikawa

[1]Sobolev Institute of Geology and Mineralogy SB RAS, 630090Novosibirsk, Russia

*denis_ponomarevs@mail.ru

**Introduction:**IAB iron meteorites often contain silicate-bearing clasts, which, based on mineralogy, trace element and oxygen isotope evidences, are indicative for close genetical relations with winonaites. Here we report first detailed results on NWA 11104 iron meteorite, which was found in 2016 and preliminary classified to IAB irons on the basis of metal composition.

**Methods:** Few thin 2-4 cm plates of meteorite were investigated by scanning electron microscopy with energy-dispersive system X-Max-80 (Oxford Instr.). Trace element composition was obtained by LA-ICP-MS. We used homogenous Campo del Cielo iron and synthetic FeNi-metal [Litasov et al., 2018] as standards.

**Results and discussion:** Metal part consists of kamacite and taenite forming *Widmanstätten* patterns and abundant irregular schreibersite grains. Silicate inclusions have variable forms including separate silicate grains in metal matrix. Large troilite aggregates are associated with silicate inclusions and usually form rounded aggregates along boundaries of silicate clasts. Silicate (+phosphate) inclusions contain olivine ($Fa_{5–6}$), orthopyroxene ($En_{90–93}Fs_{5–7}Wo_{1–2}$), clinopyroxene ($En_{51–53}Fs_{3–4}Wo_{43–45}$), plagioclase ($Ab_{70-81}$ $An_{16–27}Or_{2–3}$), apatite (F = 2.3(3) wt.%, Cl = 0.5-1.7(3) wt.%), merrillite, and chromite; we also found quartz and rutile in this sample. Average metal composition was calculated from the mean kamacite: taenite ratio of 75:25 in 12 analyses. Important concentrations include Ni = 10.17 wt.% and (in ppm): Cr = 2.21, Co = 5740, Cu = 338.2, Ga = 70.1, Ge = 218.2, As = 15.9, Mo = 4.1, Sb = 2.36, W = 0.82, Re = 0.32, Os = 4.4, Ir = 3.59, Pt = 5.44, Au = 1.96. Accordingly, NWA 11104 meteorite is located at the edges of IAB and IIF fields at the Ni-Ga and Ni-Ge classification plots, however it falls certainly into IAB group in Ni-Ir diagram. In the Au-Ni based classification inside IAB group [Wasson, Kallemeyn, 2002] NWA 11104 falls into the region between the sLH and Pitts subgroups and corresponds well to Ungrouped (Anomal). Trace elements in silicates revealed that orthopyroxene has *LREE* depleted chondrite-normalized spectra with minor Eu anomaly. Clinopyroxene has M-shaped *REE* pattern and is depleted by Nb and Sr. Plagioclase has positive Eu anomaly and enriched in *LREE* and Sr relative to other IAB irons. Apatite and merrillite are strong concentrators of *REE* and Sr, have pronounced Eu anomaly and are depleted by Zr and Nb.

The results obtained for NWA11104 meteorite are consistent with basic model of IAB iron-winonaite formation [Benedix et al., 2000] resulting from a catastrophic impact event, which caused removal of outer chondrite-winonaite shell. The minor impacts on the rest of parent body formed IAB irons (including those with silicate inclusions) and winonaites.

Benedix G.K., McCoy T.J., Keil K., Love G. A petrologic study of the IAB iron meteorites: Constraints on the formation of the IAB-Winonaite parent body. Meteoritics & Planetary Science, 2000, 35, 1127–1141.

Litasov K.D., Ponomarev D.S., Bazhan I.S., Ishikava A., Podgornykh N.M. Altaite (PbTe) in the Maslyanino Iron Meteorite with silicates inclusions. Doklady Earth Sciences, 2018, 478, 62–66,

Wasson J., Kallemeyn G. The IAB iron-meteorite complex: A group, five subgroup, numerous grouplets, closely related, mainly formed by crystal segregation in rapidly cooling melts. Geochimica et Cosmochimica Acta, 2002,66,2445–2473.

**X-Ray Diffraction Study of Ordinary Chondrites**

Svetlana S. Hontsova*, Elena M. Maksimova, Igor A. Nauhatsky

Crimean Federal University, 295007Simferopol, Russia

* sgoncova@gmail.com

The study of structure, properties and variations of chemical composition of meteorites formed under space conditions with extreme changes in pressure and temperature is of great interest among specialists from the fields of geology, cosmochemistry and condensed matter physics and materials science.Ordinary chondrite meteorites are silicate-rich meteorites composed mostly of olivine and low calcium pyroxene, with inclusions of the Fe-Ni-alloy and sulfide phases. Based on the iron amount as total as metallic iron and mineralogical composition, the ordinary chondrites have been subdivided into three distinct groups that are designated as H, L, and LL chondrites [Dodd, 1981].

This paper presents the results of studies of iron-containing inclusions from ordinary chondrites of different types by X-ray diffraction.The phase composition of meteorite samples: Chelyabinsk (LL5), North-West Africa 869 (L4-6) and GandomBeryan (H5) was investigated by X-ray diffraction (XRD) using powder diffractometer.

The following phases were detected in all samples examined: olivine $(Fe,Mg)_2SiO_4$, chlorapatite $Ca_5(PO_4)Cl$, plagioclase $(Na,Ca,K,Al)_{2.5}[Si_{2,5}O_8]$, kamacite α-Fe(Ni,Co), taenite γ-Fe(Ni,Co), troilite FeS, chromite $FeCr_2O_4$. In the sample of the Chelyabinsk meteorite, there also were found following minerals: pentlandite $(Fe,Ni)_9S_8$; NWA 869 – pigeonite $(Mg,Fe,Ca)SiO_3$, ilmenite $Fe(Ti,Mg)O_3$, merrillite $Ca_9Na(Mg,Fe)[PO_4]_7$; GandomBeryan – orthopyroxene $(Fe,Mg)SiO_3$, clinopyroxene $(Fe,Mg,Ca)SiO_3$, hercynite $(FeAl_2O_4)$. In ordinary chondrites, there were also found ferric oxides and oxyhydroxides such as goethite α-FeOOH and hematite $\alpha$-$Fe_2O_3$ (GandomBeryan), magnetite $Fe_3O_4$ (NWA 869).

The structural parameters were determined for iron-containing inclusions, such as kamacite, taenite, troilite. The results obtained are different from the table values. This may be due either to the Ni, Co and Cu impurity presence or to the deficiency of iron cation’s in the crystal structure of troilite. This fact can be explained by thermodynamic and kinetic conditions of the formation of their crystal structures.

DoddR.T.Meteorites: a Petrologic-chemical Synthesis. Cambridge University press, NY, 1981.

**Fluorellestadite from Chelyabinsk coal basin: crystal structure refinement, chemical analysis, vibration spectroscopy data and thermal behavior**

Margarita S. Avdontceva[1]*, Andrey A. Zolotarev[1], Maria G. Krzhizhanovskaya[1], Mikhail A. Rassomakhin[2,3], Sergey V. Krivovichev[4]

[1]St. Petersburg State University, 199034St. Petersburg, Russia
[2]Ilmensky State Reserve SU FRC MG UB RAS, 456317Miass, Russia
[3]Institute of Mineralogy SU FRC MG UB RAS, 456317Miass, Russia
[4] Kola Science Center, RAS, 184209Apatity, Russia

* m.avdontceva@spbu.ru

Burned dump formations of Chelyabinsk coal basin continue to attract significant attention due to the large variety of mineral species and theirimmediate connection tothe processes of technogenesis. Fluorellestadite, $Ca_5(SiO_4)_{1.5}(SO_4)_{1.5}F$, is a sulphato-silicate mineral, which belongs to the ellestadite group of the apatite supergroup, and have the general chemical formula $^{IX}M1_2{}^{VII}M2^3(^{IV}TO_4)_3X$, where $M$ = $Ca^{2+}$, $Pb^{2+}$, $Mn^{2+}$, $Ba^{2+}$, $Sr^{2+}$, $Na^{+}$, $Ce^{3+}$, $La^{3+}$, $Y^{3+}$, $Bi^{3+}$; $T$ = $P^{5+}$, $As^{5+}$, $V^{5+}$, $Si^{4+}$, $S^{6+}$, $B^{3+}$; $X$ = $F^{-}$, $Cl^{-}$, $OH^{-}$ [Pasero et al., 2010].

Seven different samples of fluorellestadite from Natural Science Museum of the IlmenskyNatural Reserve (personal collection of B.V.Chesnokov) were studied by single-crystal X-ray diffraction analysis, thermal X-ray diffraction (25–800 °C) and Raman spectroscopy.

Fluorellestadite is hexagonal, space group $P6_3/m$, the unit cell parameters for seven samples studied vary in a small range:$a$ = 9.415(5)–9.4808(7) Å, $c$ = 6.906(2)–6.931(8) Å, $V$= 530.3(4)–538.41(9) $Å^3$.Mineral is isotypic with apatite, the structure is based upon isolated $TO_4$ tetrahedra, where $T$ position is occupied by $Si^{4+}$ and $S^{6+}$(the ideal ratio Si:S is 1:1).The fluorine atoms are located in channels of the $Ca_4[(S,Si)O_4]_6$ framework oriented parallel to the $c$ axis.Raman spectra of seven samples studied show that the more intensive bands are related to the symmetric vibrations of tetrahedral sites (1003 $cm^{-1}$, 857 $cm^{-1}$ for $SiO_4^{4-}$, and $SO_4^{2-}$ groups, respectively) [Środek et al., 2018]. The band at 958 $cm^{-1}$corresponds to the vibration of the$PO_4^{5-}$groups; its intensity varies from sample to sample. It is almost absent for the samples 7 and 1, but has a high intensity for the samples 5 and 6. This fact is in good correlation with the results of the chemical analyses that indicate that the P content (in atoms per formula unit, *apfu*) varies in the range from 0.02 to 0.94. The bands at 1084 $cm^{-1}$, 1073 $cm^{-1}$and 1066 $cm^{-1}$for the samples 2, 3 and 4, respectively, indicate the presence of $CO_3^{2-}$ groups. The spectra of the samples 1, 2 and 5 show an insignificant $H_2O$ content (OH-stretching bands at 3540 $cm^{-1}$, 3530 $cm^{-1}$ and 3532 $cm^{-1}$ respectively). The thermal expansion of fluorellestadite is almost isotropic in the temperature range 25–800 °C (for room temperature: $\alpha_a = 11.9\times10^{-6}$ °$C^{-1}$, $\alpha_c = 11.8\times10^{-6}$ °$C^{-1}$; for 800 °C:$\alpha_a = 18.2\times10^{-6}$ °$C^{-1}$, $\alpha_c = 18.6\times10^{-6}$ °$C^{-1}$). Thesimilar thermal behavior had been observed for fluorapatite [Chernorukov et al., 2011].

Thus, seven different samples of fluorellestadite (various color: from light-blue to blue-green) were studied. In general, they show a similar structural motif, but at the same time are different in the S/Si/P ($T$-position) and F/Cl/OH ($X$-position) ratios, which was confirmed by the chemical analysis, single-crystal X-ray diffraction and Raman spectroscopy.

The study was supported by the Russian Foundation for Basic Research (grant № 19-05-00628).

Chernorukov N.G, Knyazev A.V., Bulanov E.N. Phase transition and thermal expansion of apatite-structured compounds. Inorganic materials, 2011, 47, 172–177.

Pasero M., Kampf A., Ferraris C., Pekov I., Rakovan J., White T. Nomenclature of the apatite supergroup minerals. Eur.J.Mineral., 2010, 22, 163–179.

Środek D., Galuskina I., Dulski M., Książek M., Kusz J., Gazeev V. ChlorellestaditeCa$_5$(SiO$_4$)$_{1.5}$(SO$_4$)$_{1.5}$Cl, a new-ellestadite groupmineral from the Shadil-Khokh volcano, South Ossetia. Mineralogy and Petrology, 2018, 112, 743–752.

**Crystal chemistry of ammonium phases from burned dumps of the Chelyabinsk coal basin**

Andrey A. Zolotarev[1,*], Elena S. Zhitova[1,2], Maria G. Krzhizhanovskaya[1], Mikhail A. Rassomakhin[3,4], Vladimir V. Shilovskikh[1], Sergey V. Krivovichev[1,5]

[1]St. Petersburg State University, 199034Saint-Petersburg, Russia
[2]Institute of Volcanology and Seismology FEB RAS, 683006Petropavlovsk-Kamchatsky, Russia
[3]Ilmensky State Reserve SU FRC MG UB RAS, 456317Miass, Russia
[4] Institute of Mineralogy SU FRC MG UB RAS, 456317Miass, Russia
[5]Russian Academy of Sciences, Kola Science Center, 184209Apatity, Russia

* a.zolotarev@spbu.ru

The ammonium minerals originate either as fumarolic or mofettic, i.e. as `volcanic` minerals or as secondary phases formed due to the contact with organic matter including environments at the burned coal dumps. The burned dumps of the Chelyabinsk coal basin appeared to be an important locality of ammonium species [Chesnokov et al., 2008]. Here we report on the crystal chemical features of $NH_4$-bearingphases from the burned dumps of the Chelyabinsk coal basin and detailed crystal chemical description of $NH_4MgCl_3 \cdot 6H_2O$ and $(NH_4)_2Fe^{3+}Cl_5 \cdot H_2O$ including determination of their stability underincreasing temperature. $NH_4MgCl_3 \cdot 6H_2O$ is monoclinic, *C*2/*c*, *a* = 9.3091(9), *b* = 9.5353(7), *c* = 13.2941(12) Å, $\beta$ = 90.089(8)°, *V* = 1180.05(18) Å$^3$, $R_1$ = 0.076. The crystal structure of $NH_4MgCl_3 \cdot 6H_2O$ [Solans et al., 1983; Okrugin et al., 2019] is based upon $Mg(H_2O)_6$ octahedra that are connected with $Cl^-$ and indirectly with $NH_4^+$ through the system of hydrogen bonds into a three-dimensional framework. The $(NH_4)_2Fe^{3+}Cl_5 \cdot H_2O$ phase is orthorhombic, *Pnma*, *a* = 13.725(2), *b* = 9.9365(16), *c* = 7.0370(11) Å, *V* = 959.7(3) Å$^3$, $R_1$= 0.020. The crystal structure of $(NH_4)_2Fe^{3+}Cl_5 \cdot H_2O$ [Figgis et al., 1978] is based upon isolated $FeCl_5(H_2O)$ octahedra that are connected with $NH_4^+$ions through the system of hydrogen bonds.

$NH_4MgCl_3 \cdot 6H_2O$ is stable up to 90 °C and then (at *T*~95 °C) transforms to the dihydrate$NH_4MgCl_3 \cdot 2H_2O$, which is stable up to 150 °C. The $(NH_4)_2Fe^{3+}Cl_5 \cdot H_2O$ is stable up to 120 °C and then transforms to an X-ray amorphous phase. Hydrogen bonds provide an important linkage between the main structural unitsand play the key role in structural stability and physical properties of the studied phases. The twotechnogenic ammoniumphases are complete analogues of novograblenovite [Okrugin et al., 2019] and kremersite [Kremers, 1851], respectively.

The study was supported by the Russian Foundation for Basic Research (grant No. 19-05-00628).ESZ is grateful to President Federation Grant for Young Candidates of Sciences (MK-3246.2019.5).

Chesnokov B.V., Shcherbakova E.P., Nishanbaev T.P. Minerals of burnt dumps of the Chelyabinsk coal basin. Miass, Ural branch of RAS, 2008, 1–139 (in Russian).

Figgis B.N., Raston C.L., Sharma R.P. and White A.H. Crystal structure of diammonium aquapentachloroferrate (III). Australian Journal of Chemistry, 1978, 31, 2717–2720.

Kremers P. Ueber die Aschenbestandtheile und die Producte der Trocknendestillationbeibraun- und Steinkohlen. Ueber das natürlichevorkommen des Doppelsaizes von Eisenchloridmit den Chloralkalien. Annalen der Physik und Chemie, 1851, 84, 67–80 (in German).

Okrugin V.M., Kudaeva S.S., Karimova O.V., Yakubovich O.V., Belakovskiy D.I., Chukanov N.V., Zolotarev A.A., Gurzhiy V.V., Zinovieva N.G., Shiryaev A., Kartashov P.M. The new mineral novograblenovite, $(NH_4,K)MgCl_3 \cdot 6H_2O$ from the Tolbachik volcano, Kamchatka, Russia: mineral information and crystal structure. Mineralogical Magazine, 2019 (in press).

Solans X., Font-Altaba M., Aguiló M., Solans J. and Domenech V. Crystal form and structure of ammonium hexaaquamagnesium trichloride, $NH_4[Mg(H_2O)_6]Cl_3$. Acta Crystallographica, 1983, C39, 1488–1490.

**Sb, W and U in Perovskite from Pyrometamorphic Rocks**

Evgeny V. Galuskin*, Irina O. Galuskina

University of Silesia, 41-200 Sosnowiec, Poland

* evgeny.galuskin@us.edu.pl

In large altered carbonate-silicate xenolith within ignimbrites of the Upper ChegemCaldera (Northern Caucasus, Kabardino-Balkaria), perovskite with anomalous high content of $Sb_2O_5$ ~ 6.2 wt.% was found. This perovskite with the simplified crystal chemical formula $Ca(Ti_{0.86}Sb^{5+}_{0.07}Fe^{3+}_{0.07})_{\sum 1}O_3$forms later zone about 10 μm in thickness on perovskite crystal with the composition $CaTi_{0.9}Fe^{3+}_{0.1}O_{2.95}$. The core of perovskite crystal is represented by lakargiite with the $Ca(Zr_{0.65}Ti_{0.15}Sn_{0.1}Nb^{5+}_{0.05}Fe^{3+}_{0.05})_{\sum 1}O_3$ composition. Sb-bearing perovskite is confined to cuspidine zone with widespread development of Sb-garnets of the bitikleite group.

Perovskite with anomalous high content of $WO_3$~ 6.8wt.%was detected in high-temperature rustumite-monticellite zone of skarns at the contact of the Birkhingabbroid complex (Baikal area, Eastern Siberia, Russia). W-bearing perovskite with the simplified formula $Ca(Ti_{0.85}Fe^{3+}_{0.10}W^{6+}_{0.05})_{\sum 1}O_3$forms thin later zones about 5 μm on perovskite crystals with the $Ca(Ti_{0.96}Fe^{3+}_{0.03}Zr_{0.01})O_{2.99}$composition. This perovskite forms intergrowths with garnet of the andradite–schorlomite–kerimasite series.

In gehlenite-merwinite zone of Birkhinskarns, perovskite crystal cores about 20 μm in sizewith stoichiometric composition are enriched with $UO_2$ up to 4.2 wt.%. The empirical crystal chemical formula of that perovskite looks as follows: $(Ca_{0.98}U^{4+}_{0.02})(Ti_{0.96}Fe^{3+}_{0.04})O_3$. A uranium content in the associated kerimasite is lower than EPMA limit detection.

$Sb^{5+}$incorporatesto perovskite ($CaTiO_3$ – $ABO_3$)as the end-member $CaFe^{3+}_{0.5}Sb^{5+}_{0.5}O_3$ that isresponded to the double perovskite of the $A_2BB'O_6$type. Only the one double perovskite – vapnikite, $Ca_2CaU^{6+}O_6$, is known in nature, while a status of „latrappite" with the formula $Ca_2Fe^{3+}Nb^{5+}O_6$has been questioned [Mitchell et al., 2017]. The double perovskite $Ca_2FeSbO_3$is known as a synthetic phase [Faik et al., 2010].$W^{6+}$enters in perovskite as the end-member $CaFe_{0.66}W_{0.33}O_3$, i.e. as a triple perovskite of the $A_3B_2B'O_9$type. Minerals belonging to the structural type of the triple perovskite are not known in nature [Mitchell et al., 2017]. Triple perovskite with the composition $Ca_3Fe_2WO_9$was synthesized before [Ivanov et al., 2005]. $U^{4+}$substitutes for Ca in perovskiteat *A* site and enters as the end-member $(Ca_{0.5}U^{4+}_{0.5})Fe^{3+}O_3$answering to the double perovskite of the $AA'B_2O_6$type – $CaU^{4+}Fe^{3+}_2O_6$. Interestingly, that in zirconian perovskite – lakargiite, from spurritepyrometamorphic rocks of the Negev Desert, Israel, uranium content reaches 17 wt.% $UO_3$: $Ca(Zr_{0.62}Ti_{0.12}U^{5+}_{0.10}U^{6+}_{0.02}Fe^{3+}_{0.11}Cr^{3+}_{0.03})O_3$. Uranium enters in octahedral *B*site of lakargiite,replacing for Zr,as the double perovskite end-member,$Ca_2Fe^{3+}U^{5+}O_6$and/or triple perovskite end-member,$Ca_3Fe_2U^{6+}O_9$. It is not excluded, that part of iron can be as $Fe^{2+}$, that determines uranium incorporation in lakargiite as the double perovskite $Ca_2Fe^{2+}U^{6+}O_6$end-member.

The investigations were partially supported by the National Science Centre (NCN) of Poland, grant no. 2016/23/B/ST10/00869.

Faik A., Igartua J.M., Iturbe-Zabalo E., Cuello G.J. A study of the crystal structures and the phase transitions of $Sr_2FeSbO_6$, $SrCaFeSbO_6$ and $Ca_2FeSbO_6$ double perovskite oxides. J. Molec. Struc., 2010, 963, 145–152.

Ivanov S.A., Eriksson S.G., Tellgren R., Rundlöf H. Structural and magnetic properties of perovskite $Ca_3Fe_2WO_9$. J. Solid State Chem., 2005, 178, 3605–3614.

Mitchell R.H., Welch M.D., Chakhmouradian A.R. Mineral. Mag., 2017, 81, 411–461.

# Ordering of As and Sb in the crystal structures of arsenopalladinite $Pd_8As_{2.5}Sb_{0.5}$ andmertieite-II $Pd_8Sb_{2.5}As_{0.5}$

Oxana V. Karimova[1]*, Andrey A. Zolotarev[2]

[1] Institute of Geology of Ore Deposits RAS, 119017Moscow, Russia
[2] Saint-Petersburg State University, 199034 Saint-Petersburg, Russia

* oxana.karimova@gmail.com

The crystal structures of arsenopalladinite, $Pd_8As_{2.5}Sb_{0.5}$, and mertieite-II, $Pd_8Sb_{2.5}As_{0.5}$ [Karimova et al., 2018], from the Kaarreoja River, Inari commune, Finnish Lapland, were studied. Arsenopalladinite is triclinic, sp. gr. *P-1*, the unit cell parameters are $a$ = 7. 329(2) Å, $b$ = 7.383(2) Å, $c$ = 14.137(3) Å, $\alpha$ = 95.983(4), $\beta$ = 92.027(4), $\gamma$ = 119.053(4)°, $V$ = 661.8(2) Å$^3$, $Z$= 2, $R$ = 0.0533. Mertieite-II is trigonal, sp. gr. *R-3c*,$a$ = 7.5172(3) Å, $c$ = 43.037(2) Å, $V$ =2106.1(2) Å$^3$, $Z$ = 12, $R$ = 0.0222.The minerals belong to one mineral group with common formula $Pd_8X_3$ ($X$=As, Sb). Despite similar composition, they are not isostructural. But their crystal structures are closely related together. The $a$ and $b$ parameters of the unit cells are very close. They differ in the value of the $c$ parameter. The constitution of the structure explains this regularity.

As and Sb occupy separate sites in the structure. Compositions of the named minerals are characterize by the ratio of components equal to 5:1 (As:Sb in the arsenopalladinite and Sb:As in the mertieite-II). Amount of minor component is exactly equal for the full occupation of one structure site.

A net-like monoatomic layers of atoms parallel to the (110) plane constitute the structures. As and Sb atoms are located in triangular nets, $3^6$ type, in accordance with Pearson [1972] (Figure 1A and 1D). Pd atoms are separated in another nets (distorted triangular $3^6$ and pentagon-triangular $3.5^3$, Figure 1B and 1C). The atomic nets of different orientation stack along the $c$ axis (Figure 2). Alternation of the nets caused the elongation of the $c$ axis. The unit cell of mertieite-II contains total 36 layers, the unit cellof asrenopalladinite – 12.

The block, containing 6 layers (two (As,Sb)-nets and fourPd-nets) is the main building units (BU) of the structures.The arsenopalladiniteunit cell contains 2 such layeredBUs, the mertieite-II unit cell contains 6 BUs.This fact is also confirmed by the difference in the value of the $c$parameter.The thickness of the layered module is nearly 7 Å. The $c$ parameters of the unit cells are a multiple 7Åin both minerals: 2·7 Å for arsenopalladinite and 6·7 Å for mertieite-II.

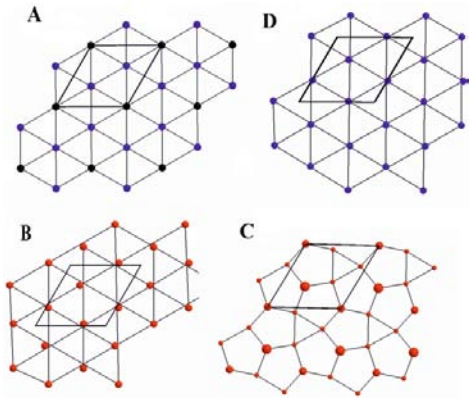


Figure 1. Atomic nets in the mertieite-II and asrenopalladinite structures

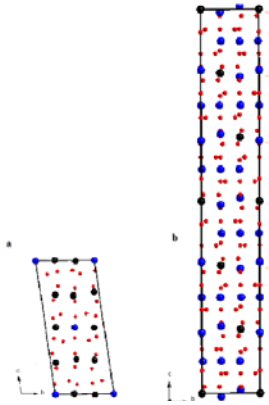

Figure 2. Projection of the arsenopalladinite (a) and mertieite-II (b) structures along $x$ axis

Karimova O.V., Zolotarev A.A., Evstegneeva T.L., Johanson B.S. Mertieite-II, $Pd_8Sb_{2.5}As_{0.5}$, crystal-structure refinement and formula revision. Min. Mag., 2018, 82(S1), S247–S257.

Pearson W.B. The crystal chemistry and physics of metals and alloys. Wiley–Interscience, NY, 1972.

# 8. Experimental Mineralogy and Petrology

**Mineral indicators of modal potassic metasomatism in the upper-mantle: a review of natural, experimental and crystal chemical data**

Oleg G. Safonov[1, 2]*, Valentina G. Butvina[1], Eugenii V. Limanov[1]

[1] Korzhinskii Institute of Experimental Mineralogy, Russian Academy of Science, 142432Chernogolovka, Moscow Region, Russia
[2]Department of Petrology, Geological Faculty, Moscow State University, 119991Moscow, Russia

* oleg@iem.ac.ru

The term "modal mantle metasomatism» combines processes of modifications ofmantle peridotites and eclogitesvia external fluids and/or meltsproducing phases, which arenon-characteristic of the mantle rocks.Along with $H_2O$ and $CO_2$ activities and oxygen fugacity, activity of alkalis, predominantly of potassium, is a leading factor of thisprocess. The presentation reviews data on major mineral indicatorsof K activity during the upper-mantle metasomatism.

Phlogopite, which is stable to pressures above 6 GPa in common peridotites and to 10-12 GPa in highly metasomatized peralkaline assemblages, is a major indicator of K activity in the upper mantle. According to experimental data, phlogopite is formed almost independently on water activity in a wide range of $H_2O$/salt ratios, from aqueous-salt fluids to hydrous salt melts, via reactions of Al-bearing phases (garnet, spinel, amphibole) with orthopyroxene.The Si/Al ratio of phlogopite serves a monitor of both pressure and degree of metasomatic transformations of rocks. Compositions of minerals coexisting with phlogopite regularly change with K activity.In reactions of the phlogopite formation, Ca becomes fixed in Al-poor clinopyroxene, while Cr and Ti are accommodated mostly in Cr-rich spinel, ilmenite and rutile.

As K activity increases, potassium starts to be bound in Ca-bearing phases, specifically in Al-poor amphibole – K-richterite.This phase is stable up to pressure about 14GPa, its maximum thermal stability is approximately 1450 °C at 10 GPa.Pressureincrease results in substitution of Nafor K in *M*4 site in addition to the *A* site and formation of the $K_2CaMg_5Si_8O_{22}(OH)_2$end-member, which stabilizes K-richterite solid solution up to 15 GPa.Extreme rarity of K-richterite in common peridotite assemblages is explicableby instabilityof its assemblageswith garnet and olivine at pressure below 6-7 GPawith respect to the assemblageclinopyroxene+phlogopite. K-richterite easily crystallizes in the peralkaline systems oversaturated with potassium.

Further increase of potassium activity results in affinity of K to Cr and Ti forming exoticCr-bearing K-(Ba)-titanates of the yimengite-hawthorneite, lindsleyite-mathiasite and prideritegroups, which are stable with wide mantle *P-T* conditions. Their association with phlogopite and K-richterite manifests the most advanced or multi-stage metasomatism of peridotites corresponding tothe highestK activityin the mineral-forming medium. Experiments on formation of K-end-members duringreactions of chromite, chromite+rutile and chromite+ilmenite assemblages in the presence of silicate material with $H_2O$-$CO_2$-$K_2CO_3$ fluids at 3.5 and 5 GPa demonstratethat the relationship between thetitanates is a function of the activity of the potassium component in the fluid/melt. Priderite is an indicator of the highest potassium activity in the mineral-forming medium.

Potassium-bearing clinopyroxene is a specific indicator of K activity in the upper-mantle up to pressures 9-10 GPa, which forms exclusively in equilibrium with potassium-rich silicate and carbonate-silicate melts. However, this mineral is extremely rare in the assemblages related to the upper-mantle metasomatism.Available experimental and crystal-chemicaldataon K-bearing clinopyroxenes, as well as predictions of thermodynamic properties ofmineral equilibriainvolving the $KAlSi_2O_6$pyroxene end-membershow that the reason for the limited concentrations of $K_2O$ in clinopyroxene from upper-mantle rocksis likely instability of this end-member withrespect to other common K-bearing phases forming during upper-mantle metasomatism.

**Fe(II) and Fe(III) complexation and the oxidation state of Fe in chloridic hydrothermal fluids**

Christian Schmidt[1,*],Lea Scholten[1,2],Pilar Lecumberri-Sanchez[3], Matthew Newville[4], Antonio Lanzirotti[4], Mona-Liza C. Sirbescu[5],Matthew Steele-MacInnis[3]

[1] GFZ German Research Centre for Geosciences, 14473 Potsdam, Germany
[2] Kiel University, Institute of Geosciences, 24118 Kiel, Germany
[3] University of Alberta, Edmonton, Alberta, T6G 2E3 Canada
[4] Center for Advanced Radiation Sources, University of Chicago, Chicago, Illinois 60637, U.S.A.
[5] Central Michigan University, Mt. Pleasant, Michigan 48859, U.S.A.

* Christian.Schmidt@gfz-potsdam.de

Iron is a major aqueous solute in crustal fluids, up to tens of %(m/m) $FeCl_2$in magmatic-hydrothermal fluids [Bodnar et al., 2014]. Knowledge of the predominant species and the oxidation state in such fluids is required to identify the important reactions resulting e.g. in ore deposit formation.Using hydrothermal diamond-anvil cell experiments and Raman andsynchrotron-radiation XANES and XRF spectroscopy, in situ at temperatures to 600 °C, westudied the behavior of iron in aqueous fluids with or without buffering by the mineral assemblages hematite-magnetite (HM), ferrosilite-magnetite-quartz (FsMQ), and magnetite-pyrite-pyrrhotite.

The pre-edge in XANES spectraof HM indicates preponderance of Fe(II)possibly a smallFe(III) content, which was not detectable in spectra of a 3.2 molal NaCl fluid equilibrated with FsMQ. Based on the calculated XANES spectra from [Testemale et al., 2009],octahedral $FeCl_x(H_2O)_{6-x}^{2-x}$($x$=0–3) are the predominant Fe(II) species at lower Cl-Fe ratios, and tetrahedral $FeCl_4^{2-}$and/or $FeCl_3(H_2O)^-$are present at higherCl-Fe ratios.

Raman spectra of Fe(III) solutions showeda band at about 315 $cm^{-1}$from $FeCl_2(H_2O)_4^+$[Sharma, 1974]at temperatures less than 100 °C. Between 100 and 200 °C, $FeCl_4^-$forms at the expense of $FeCl_2(H_2O)_4^+$. An intense Raman band at about 330 $cm^{-1}$is characteristic for $FeCl_4^-$[Sharma, 1974], which remained the most abundant Fe(III) species to at least 600 °C. Some spectra of $H_2O$+HCl fluid,reacted with hematite at temperatures >300 °C, displayed an additional band at about 350 $cm^{-1}$, which weinterpret to stem from Fe(III)–Cl stretching vibrations of $FeCl_3(H_2O)_x$($x$=0–3) species[Sitze et al. 2001] from the reaction $Fe_2O_3$ + 6HCl = $2FeCl_3(H_2O)_x^0$ + (3-$x$)$H_2O$. All aqueouschloridicFe(II) solutions showed a Raman band at about 280 $cm^{-1}$, which we assign to$FeCl_x(H_2O)_{6-x}^{2-x}$($x$=0–3) species at Cl-Fe ratios of about two or less, or to $FeCl_3(H_2O)_x^-$ ($x$=0–3) (point group $D_{3h}$) species.

The incongruent dissolution reaction$2Fe_3O_4$(s) + 4HCl + $7H_2O$ = $2Fe_2O_3$(s) + $FeCl_2(H_2O)_4^0$ + $FeCl(H_2O)_5^+$ + $Cl^-$occurred in the HM + 0.32 molal HClruns as concluded from the Cl-Fe ratio of about 1.5 in the fluid determined by in situ XRF spectroscopy and from the complete consumption of magnetite in one experiment. Raman spectra of more concentrated HCl solutions reacted with hematite±magnetite show either Fe(III) or Fe(II). In summary, Fe(II) is the only oxidation state of significance of iron in hydrothermal fluids at oxygen fugacities below the HM buffer.

Bodnar R.J., Lecumberri-Sanchez P., Moncada D., Steele-MacInnis M. Fluid inclusions hydrothermal ore deposits. In: Treatise on Geochemistry, 2nd ed., Elsevier, 2014, 13, 119–142.

Sharma S. K. Raman study of ferric chloride solutions and hydrated melts. J. Chem. Phys., 1974, 60, 1368–1375.

Sitze M. S., Schreiter E. R., Patterson E. V., Freeman R. G. Ionic liquids based on $FeCl_3$ and $FeCl_2$. Raman scattering and ab initio calculations. Inorg. Chem., 2001, 40, 2298–2304.

Testemale D., Brugger J., Liu W., Etschmann B., Hazemann J.-L. In-situ X-ray absorption study of iron(II) speciation in brines up to supercritical conditions. Chem. Geol., 2009, 264, 295–310.

**The complexity behind the simple Ti oxide structure:**
**Can rutile be used as an elastic geobarometer?**

Kira A. Musiyachenko[1,2]*, Mara Murri[1], Mauro Prencipe[1], Matteo Alvaro[1]

[1] Dipartimento di Scienze della Terra e dell'Ambiente, Università degli Studi di Pavia, Pavia, Italy
[2]V.S. Sobolev Institute of Geology and Mineralogy of the Siberian Branch of the RAS, 630090Novosibirsk, Russia

* kira.musiiachenko01@universitadipavia.it

Rutile stability and abundance in several geological environments under a variety of physical and chemical conditions makes it a unique tool for reconstructing rock histories from their crystallization at depth toexhumation to the Earth's surface. As a consequence, rutile is often trapped as inclusions in garnets. Beside chemical barometric methods, Raman elastic geobarometry for host-inclusion systems can be used to determine their entrapment conditions [Murri et al. 2018]. This approach is based on the concept of phonon-mode Grüneisen tensor [Ziman 1960] to interpret Raman band shifts as measured on inclusions in terms of their strain state and in turn their stress state. However, rutile inclusions trapped in garnet hosts from ultra-high-pressure metamorphic rocks show Raman shifts that are the same as from crystals in air (Campomenosipers.commun.) This is consistent with thermodynamic calculations using the EoS of rutile [Zaffiro et al., 2019].

In the present study, we investigated the elastic and vibrational properties of rutile.We performed *ab initio* hybrid HF/DFT simulations on rutile under different strain conditions in order to determine its phonon-mode Grüneisen tensor following the protocol adopted by [Murri et al. 2018].Recent experimental studies revealed a complexity of the phonon behavior in the rutile structure. A softening of the TA $A_{2u}$ acoustic mode around q= ½ ½ ¼ that also decreases to zero under specific strain conditions has been observed by Mitev et al. [2010]. Whereas Lan et al. [2015] found that this acoustic mode increases in frequency as a function of temperature stabilizing the rutile structure.To resolve this ambiguity, we therefore adopted a supercell approach using HF/DFT to study the behavior of this acoustic mode beyond the center of the Brillion zone.

This project has received funding from the European Research Council under the H2020 research and innovation program (N. 714936 TRUE DEPTHS to M. Alvaro)

LanT., Li C.W., HellmanO., Kim D.S., Muñoz J.A., Smith H., Abernathy D.L., Fultz B. Phonon Quarticity Induced by Changes in Phonon-Tracked Hybridization during Lattice Expansion and Its Stabilization of Rutile $TiO_2$. Physical Review B, 2015, 92(5), 054304.

Mitev P.D., Hermansson K., Montanari B., Refson K. Soft Modes in Strained and Unstrained Rutile $TiO_2$. Physical Review B, 2010, 81(13), 134303.

Murri M., Mazzucchelli M.L., Campomenosi N., Korsakov A.V., Prencipe M., Mihailova B.D., Scambelluri M., Angel R.J., Alvaro M. Raman Elastic Geobarometry for Anisotropic Mineral Inclusions. American Mineralogist, 2018, 103(11), 1869–1872.

Zaffiro G., Angel R.J., Alvaro M. Constraints on the Equations of State of stiff anisotropic minerals: rutile, and the implications for rutile elastic barometry. Mineralogical Magazine, 2019 (in press).

Ziman J. M. Electrons and Phonons.The International Series of Monographs on Physics,

**Effect of chloride components in water fluid onto serpentine dehydration: in situ HP-HT Raman spectroscopic study**

Anna Yu. Likhacheva[1,*], Sergey V. Goryainov[1], Sergey V. Rashchenko[1,2], Oleg G. Safonov[3,4]

[1]V.S. Sobolev Institute of Geology and Mineralogy SibB RAS, 630090 Novosibirsk, Russia
[2] Novosibirsk State University, 630090 Novosibirsk, Russia
[3] Institute of Experimental Mineralogy RAS, 142432 Chernogolovka, Moscow Region, Russia
[4] Moscow State University, 119991 Moscow, Russia

* alih@igm.nsc.ru

The serpentine dehydration is regarded as the key step in metamorphic transformation of serpentinized peridotites in subduction zone, leading to the melting of the mantle wedge rocks and arc volcanism [Schmidt, Poli, 1998]. Though the *PT*-conditions and kinetics of serpentine dehydration were extensively studied [Perrillat et al., 2005], no attention was given to the effect of alkali chlorides which effectively lower the $H_2O$ activity in supercritical fluid, thereby decreasing the dehydration temperature by hundreds of degrees [Aranovich, Newton, 1997]. The abundance of alkaline-chloride brines inclusions in ultramafic rocks of the mantle wedge [Kendrick et al., 2017] makes important the correction of the (*P*)-*T* conditions of principal reactions involving water fluid, which control the evolution of subducting lithosphere.

The behavior of serpentine (chrysotile) in the presence of NaCl-$H_2O$ fluid was studied at 100–400 ºC and 10–40 kbar by Raman spectroscopy combined with resistively heated diamond anvil cell. Irreversible amorphisation, which can be regarded as the onset of chrysotile breakdown, is observed within 150–300 ºC, depending on the NaCl/$H_2O$ ratio. The temperature gap between amorphisation and crystallization of new phases (dehydration products) decreases at higher $H_2O$ content in the fluid. At that the lowest temperature at which new phases crystallize is about 370 ºC. In the presence of water-rich (NaCl-saturated without excess salt) fluid, we observe quick formation of 10 Å phase at 35 kbar and talc at $P<$ 10 kbar. Under ultra-dry conditions of almost 100% NaCl "brine", only anhydrous and highly non-equilibrium assemblage "forsterite + enstatite + $SiO_2$" appears at 10 kbar. This is obviously a consequence of extremely low $H_2O$ activity (much less than that of dry serpentine system) created by the presence of NaCl.

The obtained data allow to preliminarily estimate the temperature shift of chrysotile dehydration to be no less than 200 ºC compared to that established for salt-free system [Ulmer, Trommsdorff, 1995]. A similar effect can be assumed for the stability of antigorite, a high-pressure serpentine polymorph relevant to the *P*,*T*-conditions of subduction zone. Such a large effect can prompt to reconsider the thermal structure of subducting slab and its relations with seismic zones.

This study is supported by RFBR grant 18-05-00312.

Aranovich L.Y., Newton R.C. H2O activity in concentrated KCl and KCl-NaCl solutions at high temperatures and pressures measured by the brucite-periclase equilibrium. Contrib. Mineral. Petrol., 1997, 127, 261–271.

Kendrick M.A., Hémond C., Kamenetsky V.S., et al. Seawater cycled throughout Earth's mantle in partially serpentinized lithosphere. Nature Geoscience., 2017, 10, 222–228.

Perrillat J.-P., Daniel I., Koga K.T., et al. Kinetics of antigorite dehydration: A real-time X-ray diffraction study. Earth. Planet. Sci. Lett., 2005, 236, 899– 913.

Schmidt M.W., Poli S. Experimentally based water budgets for dehydrating slabs and consequences for arc magma generation. Earth. Planet. Sci. Lett., 1998, 163, 361–379.

Ulmer P., Trommsdorff V. Serpentine stability to mantle depths and subduction-related magmatism. Science, 1995, 268, 858–858.

**Geochemical and mineralogical studies of amphiboles from garnet amphibolites in the Xigaze ophiolite, southern Tibet**

Xu-Ping Li

College of Earth Science & Engineering, Shandong University of Science and Technology, 266590Qingdao, China

lixuping@sdust.edu.cn

The amphiboles from the garnet amphibolites of the Xigaze ophiolite, southernTibet, were investigated for their geochemical characteristics and pressure-temperature conditions. The garnet amphibolites, which experienced four metamorphic stages, and their mineral assemblages are distinguished as $Amp_1$+ $Pl_1$ + $Cpx_1$ + Ttn (M1); Grt-c + $Cpx_2$ + $Amp_2$ + $Pl_2$ + Rt + Ttn (M2); Grt-r + $Cpx_3$ + $Amp_3$ + $Pl_3$+ Rt + Ttn (M3), and final subgreenschistfaciesPrh + Ab + Act + Chl + Cal respectively. *P-T* calculation estimate: the peak stage metamorphism (M2) is defined at ~720–820°C / 13–8 Kbar; the third stage metamorphism (M3) at ~550–650°C / 6–10.1 Kbar and at ~800–900°C / 6–11.3 Kbar respectively, when they occur as massive block and as foliated gneiss; and final stage subgreenschist metamorphism at low *P-T* conditions.

Major mineral elements of amphiboles were classified as magnesio-hornblende, pargasite and tschermakite and they follow a trend between tremolite and pargasite of high-*T* trend, and tremolite and tschermakite of more high-*T* trend respectively, corresponding to type A and type B Grtamphibolites. Trace mineral elements of amphiboles were also showed distinguishable *REE* and multi-elements patterns. The abundances of major elements, trace elements as well as *REE* and multi-trace element patterns of amphibole are all similar to that of suprasubduction amphiboles. Most amphiboles have low concentration of Ba, Rb (alkaline and alkali earth large ion lithophile element), but with Sr being enriched. Several high field strength elements (HFSE: Ti, Zr, Hf, Nb, Ta) shows Ti-poor, Zr-rich, Hf-rich with Nb depletion. Using discrimination of Ti and Zr vs Nb diagrams and further discrimination of the plots of Zr/Nb versus Ti/Nb and Zr/Nb versus Ti/Zr, we conclude that amphiboles in this study formed in suprasubduction tectonic environments with HFSE and Nb depletion.

**Crystal-Chemical Element Fractionation Under HT-LP Metamorphic Conditions: Case Study from Kochumdek Contact Aureole (Podkamennaya Tunguska Basin)**

Anna S. Deviatiiarova[1,2]

[1] Sobolev Institute of Geology and Mineralogy SB RAS, 630090 Novosibirsk, Russia
[2] Novosibirsk State University, 630090 Novosibirsk, Russia

devyatiyarova@igm.nsc.ru

Spurrite- and merwinite-bearing marbles on the Kochumdek River formed along the top margin of a flood basalt intrusion ($T_1$) from a marly limestone ($S_1$kč), at a pressure of ~200 bar.The aureole comprises three HT zones marked by the mineral assemblages: $T \geq$ 900 °C (merwinite, spurrite, gehlenite, ±rankinite, ±bredigite); $T \geq$ 750 °C (spurrite); $T \geq$ 700 °C (tilleyite, wollastonite, and melilite (Gehl<50)). Very high temperatures at the contact ($T_{cont} > 2/3\ T_{melt}$) result from magma flow along a conduit [Sokol et al., 2019]. Mineral compositions and zonality were studied by EDS SEM and microprobe methods to reveal main and trace elements fractionation under the conditions of *HT-LP* metamorphism. Calcite contains impurities of MgO, $Na_2O$ and SrO up to 0.3 wt.%. The Ca silicates and silicate-carbonates such as tilleyite ($Ca_5Si_2O_7(CO_3)_2$, Tly), wollastonite and parawollastonite ($Ca_3Si_3O_9$ , Wol), and rankinite ($Ca_3Si_2O_7$, Rnk) are not prone to any isomorphic substitutions, but spurrite (Spu) is exclusive host for P ($Ca_{4.9–5}Na_{0–0.1}[Si_{1.9-2}P_{0–0.1}O_8](CO_3)$ with the average incorporation ratios $K_P \sim 3$ and $K_{Na} \sim 2.5$ ($K_{El} = El_{mineral}/El_{rock}$).

All Ca-Mg silicates: bredigite (Brd), merwinite (Mw), and montichellite (Mtc) – show restrictedisomorphic substitution Mg for Fe and Mn. The range of solid solutions depends on the Mg/Ca ratio and is minimal for Brd ($Ca_7(Mg_{0.82-0.85}Fe_{0.09-0.11}Mn_{0.02-0.04})[SiO_4]_4$), maximal for Mtc ($Ca(Mg_{0.59-0.82}Fe_{0.12-0.26}Mn_{0.03-0.07})[SiO_4]$), and intermediate for Mw ($Ca_3(Mg_{0.77-0.95}Fe_{0.05-0.21}Mn_{0-0.04})[Si_2O_8]$). Thus, among silicates Mtc stores most of Mn and Fe ($K_{Mn} \sim 18$ and $K_{Fe} \sim 4$). The only Mw shows progressive zonality with the core enriched in Fe relative to rims. The composition of melilite (Mll), which is a common mineral in all assemblages, changes markedly, being a sensitive temperature indicator. It should be attributed to the wide range of complex solid solution (in mol%): gehlenite ($Ca_2Al_2SiO_7$, $Gehl_{7–77}$), akermanite ($Ca_2MgSi_2O_7$, $Ak_{13–68}$), soda-melilite ($CaNaAlSi_2O_7$, $Na\text{-}Mll_{0–21}$), ferro-akermanite ($Ca_2Fe^{2+}Si_2O_7$, $Fe\text{-}Ak_{0–17}$), and ferri-gehlenite ($Ca_2Fe^{3+}Si_2O_7$, $Fe\text{-}Gehl_{0–13}$). The atomic Mg/(Mg+Fe) in melilite varies from 0.70 to 0.82. Thus, in the marbles Mll is an exclusive host for Al, Na, and K ($K_{Al} \sim 5.3$, $K_{Na} \sim 5.9$, $K_K \sim 1.8$) besides of Mg, Mn, Fe ($K_{Mg} \sim 2.8$, $K_{Mn} \sim 1.9$, $K_{Fe} \sim 1.7$).

Melilite from Tly-Wol zone is enriched in Na-Mll (up to 16 mol%) and shows progressive zonality, whereas, the composition of melilite from Mw zone approaches to refractory Gehl (up to 80 mol%). In spite of low bulk $TiO_2$ content in the rock (0.25 wt%), negligible Ti content in rock-forming minerals ($K_{Ti} \leq 0.1$) leads to crystallization of abundant perovskite ($CaTiO_3$) with high Nb, Ta, REE, U, Th, Zr contents. Its large grain sizes and high $UO_2$ and $ThO_2$ contents (up 0.4 and 0.6 wt%, correspondingly) allows one to carried out U-Th-Pb dating of the metamorphic event by LA ICP-MS technique. Opaque phases are dominated by sulfides of Fe, K, Zn, and Mn: rasvumite ($KFe_2S_3$), djerfisherite ($K_6(Fe,Cu,Ni)_{25}S_{26}Cl$), (Zn,Fe,Mn)S and alabandite besides of relatively abundant pyrrhotite. Generally divers mineral assemblages of the Kochumdek marbles and wide range of chemical composition of the minerals seems to be favorable for detailed constrains of *PT* conditions of both prograde and retrograde metamorphic events.

The study was carried out as part of a government assignment to IGM SB RAS.

Sokol E.V., Polyansky O.P., Semenov A.N., Reverdatto V.V., Kokh S.N., Deviatiiarova A.S., Kolobov V.Yu., Babichev A.V. High-grade contact metamorphism in the Kochumdek river valley: evidence for magma flow (Podkamennaya Tunguska basin, East Siberia). Russian Geology and Geophysics, 2019,60(4).

**Compositions and properties of gold chalcogenides synthesized in the Au-S-Se-Te system**

Galina A. Palyanova[1,2,*], Nadezda D. Tolstykh[1], Veronika Yu. Zinina,[1,2], Konstantin A. Kokh[1,2], Yurii V. Seryotkin[1,2]

[1] Sobolev Institute of Geology and Mineralogy, Siberian Branch of the RAS, 630090 Novosibirsk, Russia
[2]Novosibirsk State University, 630090 Novosibirsk, Russia

*palyan@igm.nsc.ru

Some quaternary gold chalcogenides in the Au-S-Se-Te system were synthesized for the first time. We have carried out experiments by the dry method using the evacuated silica ampoules at temperatures from 700 to 25ºC with annealing at 400ºC. The initial compositions of the system were $AuTe_{0.667}Se_{0.167}S_{0.167}$ (X/Au=1), $AuTeSe_{0.5}S_{0.5}$ (X/Au=2), $AuTe_2Se_{1.125}S_{0.375}$, $AuTe_2Se_{0.75}S_{0.75}$ (X/Au=3.5) and $AuTe_{2.5}SeS_{0.5}$ (X/Au=4), where the ratios X=Σ(Te+Se+S)/ Au ranged from 1 to 4.

Optical microscopy, scanning electron microscopy (SEM), electron-microprobe analysis (EPMA), Raman spectroscopy and X-ray powder diffraction methods (XRD) were applied to study the samples. According to the EPMA results, three gold chalcogenides of compositions – $AuX_2$ ($AuTe_{1,8}Se_{0,2}$– $AuTe_{1,8}Se_{0,1}S_{0,1}$), $Au_3X_{10}$ ($Au_3Te_6Se_3S$ – $Au_3Te_6Se_{2.5}S_{1.5}$) and$AuX$ ($AuTe_{0,7}Se_{0,2}S_{0,1}$) – were identified in thesolid phase synthesis products. In the experiment with the initial composition $AuTe_2Se_{0.75}S_{0.75}$, two chalcogenides of the composition $Au_3X_{10}$ and $AuX_2$were found. There were also metallic gold, the amount of which decreases as the chalcogens increase in the initial compositions, and native chalcogens, represented by a mixture of Te, Se and S.

According to XRD, the synthesized gold chalcogenide $AuTe_{1.8}Se_{0.1}S_{0.1}$ corresponds to calaverite$AuTe_2$ (PDF card 01-074-7043). According to the EPMA, the amount of S and Se impurities in that phase reaches 0.7 and 2.9 wt.%, respectively, which indicates their isomorphic substitution for Te. On the diffractograms, there are additional unidentified peaks, which, obviously, belong to two or one of the new phases – $AuTe_{0.7}S_{0.1}Se_{0.2}$ and $Au_3Te_6Se_3S$. These new phases can be natural counterparts of new unnamed phases found in the Gaching ore occurrence (Kamchatka, Russia) [Tolstykh et al., 2018]. According to preliminary data, their compositions are 1) $Au_{0.99\text{-}1.00}Te_{0.70\text{-}0.71}Se_{0.25\text{-}0.27}S_{0.03\text{-}0.06}$; 2) $Au_{2.91\text{-}3.08}Te_{5.85\text{-}6.06}Se_{1.57\text{-}3.66}S_{2.63\text{-}0.44}$. Raman spectra of synthesized and natural compounds with close compositions are quite similar.

The obtained results are in good agreement with the results of experimental studies in the ternary system Au-Se-Te, for which the phases $Au_2SeTe$, $Au_3Te_6Se_4$, $Au_2Se_3Te_4$ - $Au_4Se_5Te_8$ solid solution were established [Cranton, Heyding, 1968; Tuhý et al., 2018; Wang, 2000]. Our data confirm the existence of stable compounds of the composition $AuTe_3$ and AuTe, predicted in the recent work [Streltsov et al., 2018].

Cranton G., Heyding R. The gold/selenium system and some gold seleno-tellurides. Canadian Journal of Chemistry, 1968, 46, 2637–2640.

Streltsov S.V., Roizenc V.V., Ushakova A.V., Oganov A.R., Khomskiie D.I. Old and new puzzles of gold tellurides: incommensurate crystal structure of calaverite $AuTe_2$ and predicted stability of AuTe. PNAS, 2018, 115, 9945–9950.

Tolstykh N., Vymazalova A., Tuhy M., Shapovalova M. Conditions of formation of Au-Se-Te mineralization in the Gaching ore occurrence (Maletoivayam ore field), Kamchatka, Russia. Mineralogical Magazine, 2018, 83, 649–674.

Tuhý M., Vymazalová A. Tolstykh N.D., Plášil J., Laufek F., Drábek M. Precious metals chalcogenides, experimental study and their comparison to natural analogues. Abstract of 13 Pt Simposium, Polokwane, 2018.

Wang N.D. New synthetic ternary chalcogenides. Neues Jahrbuchfür Mineralogie, 2000, 8, 348–356.

# 9. Applied Mineralogy

**Structure of synthetic silicate-rich corium – model for Chernobyl lava**

Polina S. Mikhailowa[1], Alexei A. Averin[2], Boris E. Burakov[3], Vasily O. Yapaskurt[1], Andrey A. Shiryaev[2,*]

[1] Geology Dept., Moscow State University, 119234 Moscow, Russia
[2]Frumkin Institute of physical chemistry and electrochemistry RAS, 119071Moscow, Russia
[3]V.G. Khlopin Radium Institute, 194021St. Petersburg, Russia

*shiryaev@phyche.ac.ru

In case of severe accident at a nuclear reactor hot fuel (usually $UO_2$) interacts with Zr-based cladding and subsequently may react with silicate construction materials forming highly radioactive glass-ceramics termed corium. During accident at Chernobyl nuclear power plant in 1986 several thousand tons of the lava-like fuel-containing materials (LFCM) were formed and spread in reactor building. Results of detailed investigation of the glassy matrix and mineral inclusions in real Chernobyl LFCM and extensive literature summary could be found in [Shiryaev et al., 2016, 2018]. In particular, numerous mineral-like phases such as U-rich zircon, various types of zirconia etc. are crucial components of the corium. Detailed understanding of the corium structure and properties are important for reconstruction of historic nuclear accidents and for development of corium traps in novel types of nuclear power plants.

Despite numerous studies and experiments, some important features of the LFCM structure remain poorly constrained. Here we present results of characterization of materials, obtained during at various stages of experiments aimed at synthesis of corium-like materials. At the first stage of the experiment $UO_2$ fuel pellet was reacted with a zircaloy cladding. Subsequently, the obtained material was reacted with K-Al silicates. Samples were characterized by Raman spectroscopy, micro-XRF, optical and Scanning Electron Microscopy.

Maps obtained with micro-XRF and SEM allowed to address spatial distribution of comprising elements and morphological features of the precipitates. Using Raman spectroscopy, we were able to distinguish several mineral phases in the samples.The main phases dispersed in the glass matrix are zirconium oxide ($ZrO_2$) and uranium oxide ($UO_2$). Raman spectra reveal presence of several zirconia modifications – dominating monoclinic (baddeleyite) and tetragonal; sometimes these varieties are intermixed on a micron-scale. Spectra of urania are characterized by an intense peak at approx. 450 $cm^{-1}$ and a band at ~1155 $cm^{-1}$ indicating that the inclusions are close to stoichiometric $UO_2$.

Qualitatively experimental samples are fairly close to the real Chernobyl LFCMs; however, some important differences exist. Namely, up to now we were unable to find U-rich zircons (“chernobylite”) and Zr-U-O phase in our experiments. Possible reasons for the discrepancies with the LFCMs will be discussed in detail.

Shiryaev A.A., Vlasova I.E., Yapaskurt V.O., Burakov B.E., Averin A.A., Elantyev I. Forensic study of early stages of the Chernobyl accident: Story of three hot particles. Journal of Nuclear Materials, 2018, 511, 83–90.

ShiryaevA.A., Vlasova I.E., Burakov B.E., Ogorodnikov B.I., Yapaskurt V.O., Averin A.A., Pakhnevich A.V., Zubavichus Y.V. Physico-chemical properties of Chernobyl lava and their destruction products. Progress in Nuclear Energy, 2016, 92, 104–118

**Thermal annealing of heterogeneous zircon with high concentration of impurity elements**

Dmitry A. Zamyatin[1,*], Sergey L. Votyakov[1], Yuiya V. Shchapova[1]

[1]Zavaritsky Institute of Geology and Geochemistry UB RAS, 620016Ekaterinburg, Russia

*zamyatin@igg.uran.ru

Petrogenetic and geochronological issues require to study the mechanisms of the redistribution of impurity elements at elevated temperatures in the important geochronometer zircon. This paper is devoted to the study of the influence of lab annealing ($T$ = 1400˚C, 96 h) on the internal texture, structural state, chemical composition, luminescent and vibrational properties of zircon from metamorphic rocks (K1098, Taldyk block Mugodzhary Hills, South Urals) [Krasnobaev, Davydov, 1999]. Zircon grains consist of crystalline bulks and metamict cores (Figure, a,c,d,f). The cores contain significant amounts of Y, Yb, heavy *REE*, Hf, U, and also minor impurities of Fe, Ca, Al, F (electron microprobe Cameca SX100) and $H_2O$, which are signs of alterations of the zircon under the influencer of aqueous fluid [Geisler et al., 2007]. According to Raman spectroscopy (Horiba LabRam HR800 Evolution spectrometer), the degree of metamictization varies from mildly (in bulks) to strongly (in cores).

Thermal annealing significantly affects the properties of zircon: the color of the cores changes from brown to dull white (Figure, b,e), cores retain many mineral inclusions, the CL brightness increases, the bands in the Raman and photoluminescence spectra narrow and vary in width and position (Figure, g); full width at half maximum of $\nu_3(SiO_4)$ are 5–9 $cm^{-1}$. In the annealed zircons, regions with high O content and pores are preserved, zones with extremely high concentrations of *REE* appear (Dy-Lu up to 3 wt% and Y up to 9 wt%), in which, according to EBSD (Jeol JSM-6390LV electron microscope with the Nordlys Nano attachment) a non-typical zircon phase with a monoclinic structure is observed.

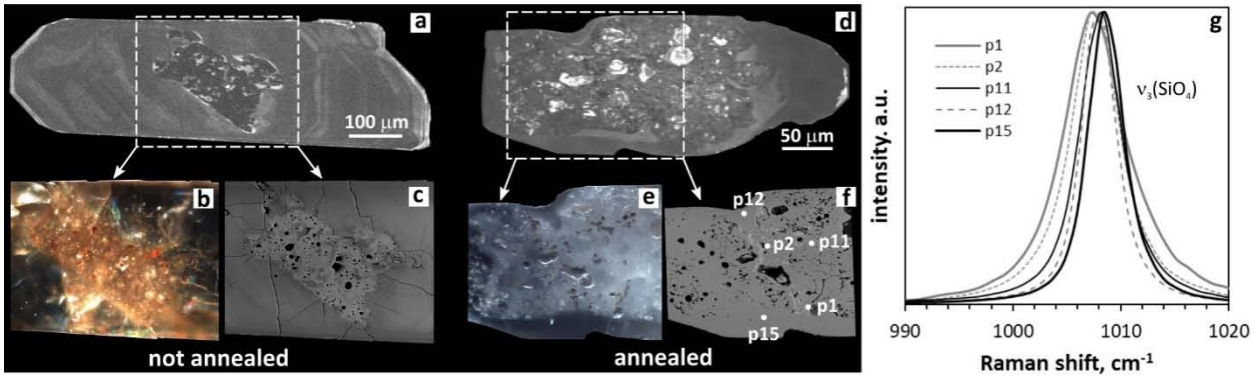


Figure. BSE (c, f), CL (a, d) and optic (b,e) imagesofnot annealed (a-c) and annealed (d-f) zircons; Raman band $\nu_3(SiO_4)$ in points (white spots) in annealed zircon(g).

The work was carried out at the Common Use Center “Geoanalyst” with the financial support by the Russian Science Foundation (grant No. 16-17-10283).

Geisler T., Schaltegger U., Tomaschek F. Re-equilibration of Zircon in Aqueous Fluids and Melts. Elements, 2007, 3 (1), 43–50.

Krasnobaev A.A., Davydov V.A. A zircon geochronology of Taldykblock in Mugodzoir. Dokl.Akad.Nauk, 1999, 366 (1), 95–99.

**X-Ray Diffraction Study of Natural Sulfide Minerals for Technetium immobilization**

Yulia V. Konevnik, Alexey V. Makarov, Yana Yu. Karaseva, Alexey V. Safonov, Elena V. Zakharova

A.N. Frumkin Institute of Physical Chemistry and Electrochemistry, Russian Academy of Science, 119071Moscow, Russia

leonenko@gmail.com

Radioactive wastes management is one of the major challenges facing the nuclear energyindustry in countries where radioactive wastes have been accumulated due to operation of nuclear power plant and reprocessing SNF. According to the IAEA guidelines and Russian nationalregulations radioactive wastes repository should be designed as multibarrier safety system, which prevents radionuclides migration.

Technetium is assumed to be one of the most mobile radionuclides releasedfrom radioactive wastes to environment. There is a very restricted number of materials applicable for Tc retention.Natural sulfide minerals are considered to be the prospective component of the multibarrier safety systemowing to their ability to provide proper fixation of pertechnetate ion by incorporating it in crystal structure or in some cases to reduceTc(VII) to low soluble Tc (IV) species.

About 20 different sulfide minerals were studied in aerobic and anaerobic conditions to estimate theirsuitability as appropriate clay barrier components for Tc (VII) fixation. The highest sorption activity wasmeasured for antimonite, biogenic pyrite, stibnite and orpiment.

The work is supported by Russian Foundation for Basic Research (RFBR) project №19-03-00617.

**Features of structure and phase formation of basalt containing glazes for porcelain tiles**

Ivan A. Levitskii*, Hanna N. Shymanskaya, Victoria S. Krasnova

Belarusian State Technological University, 220006 Minsk, Republic of Belarus

*levitskii@belstu.by

In the Republic of Belarus, imported glazes are used in the production of ceramic granite tiles. Dependent of producers on imports puts a premium on the developing of glaze compositions using existing local raw materials. This will ensure import substitution and reduction in the cost of production. In this connection, the aim of this study is to evaluate the possibility of using basalt (Republic of Belarus) as a pigment to obtain colored glazes for porcelain stoneware tiles.

As shown by X-ray fluorescence analysis, the main minerals of basalt are plagioclase, clinopyroxene, ore minerals,hlorofeit andolivine.

Raw composition for producing glazes included the following (weight content, %):

- the glazes of the series 1 – basalt – 41–47; frit OR [Levitskii, 2011] – 19–23; dolomite – 12–18, with constant content of technical alumina, kaolin, zinc oxide and refractory clay, total amount 20;
- the glazes of the series 2: basalt – 34–44; copper (II) oxide – 8–14; frit OR – 18–24, with constant content of technical alumina, kaolin, refractory clay and dolomite, total amount 30.

The study of physical-chemical properties founded that synthesized glaze coatings conformed to requirements of technical standards documents, as well as had high decorative effect (Table). In addition, all glaze coatings were chemically stable.

Table. Physical-chemical properties and decorative-aesthetic characteristics of the glazes

| Description | The glazes of the series | |
|---|---|---|
| | 1 | 2 |
| Color | Brown | Dark grey, metallic effect |
| Surface texture | Matte | Matte, semi-matte |
| Luster, % | 9–21 | 34–43 |
| Microhardness, MPa | 7620–10750 | 5550–7000 |
| The linear thermal expansion coefficient, $\alpha \cdot 10^7, K^{-1}$ | 56.4–68.6 | 59.0–73.1 |
| Heat resistance, °C | 150 | 150 |
| Class of surface abrasionresistance | 2–3 | 1–2 |

The following crystalline phases were identified in the glazes of the series 2: ($CaO \cdot Al_2O_3 \cdot 2SiO_2$), maghemite ($\gamma$-$Fe_2O_3$) and corundum ($Al_2O_3$). The XRD patterns of the glazes of the series 2 showed tenorite (CuO), cuprite ($Cu_2O$) and anorthite. The data obtained in the investigation of the structure of glazes by means of electronic microscopy correlated with x-ray phase analysis. Glazes had a solid glass-ceramic structure (Figure).

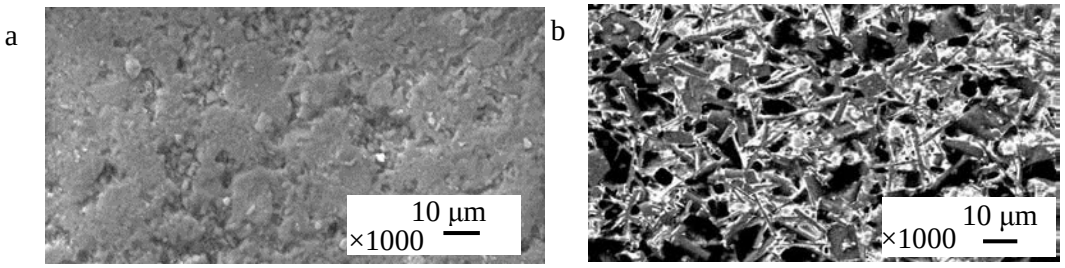


Figure. Electronic photographs of a composition-optimized glaze coatings of the series 1 (a), 2 (b)

The tests performed under production plant conditions at Keramin JSC (Minsk, Republic of Belarus) showed that the newly developed coatings can be used in industrial manufacturing.

Levitskii I.A., Barantseva S.E., Lugin V.G., Poznyak A.I. Optimization of the composition of the fritted component of the raw material mix of durable coatings. Glass and ceramics, 2011, 67, 291–294.

**Textural and structural characteristics and composition of Russian tiles**

RaisabV.Lobzova[1]*, Oxana V. Karimova[2]

[1] State Research Institute for Restoration, Moscow,
[2] Institute of Geology of Ore Deposits RAS (IGEM RAS), Moscow

*lobzovarv@mail.ru

Ceramic is one of the oldest finishing materials. Its peculiarity lies in the episodic flowering or decline, improvement or re-opening of production technology. This is especially true of its "white-clay" variety and blue glazes. The first Russian tiles, dated to the XV century, are represented by relief terracotta and ant products with a red shard, their peculiarity lies in the presence of tiller. The flowering of polychrome tiles fell on the XVII century. Under the imitation of white stone – the main building material – the red shard was covered with white engobe, white clay was used as a substrate for glaze watering. At the beginning of the XVIII century the imported Dutch tiles were widely developed, by the middle of the century domestic production was established. Findings of two-component tiles of white-clay face plate and red-clay tiller indicate the first experiments of technological search in the manufacture of domestic white-blue painted and embossed tiles.

Optical (stereomicroscope Leica EZ4 D, Germany, polarizing microscope Olympus BX-51,USA) X-ray diffraction and analytical electron microscopy (raster electron microscope JSM 5300, link ISIS program) were used to study samples of ceramic architectural decor with a light shard of the mid-XVI – early XX century.

Revealed visual differences, tiles of blue and white painted were: the thickness of the faceplate; the presence or absence of rumpy; structural features, porosity, and stratification of the ceramic body; the presence of small inclusions of red clay; additional surface treatment before applying the white enamel; the presence of tiny inclusions in blue glaze, etc. The presence of gas bubbles, their size and distribution in the glaze of impurity chromophores, the residual inclusions of crystals of the components of raw materials, neoplasms, etc. color, light effects and the stability of the paste and glaze to external impact.Particular attention was paid to the intermediate layer, the nature of which affects the degree of preservation of the object, which is important for solving restoration tasks. So, on the red shard there was a contact discoloration of the glaze coating, an increase in the number and dimension of pores. On a white shard, the absence of an intermediate layer leads to the detachment of the coating, while the presence of microcrystals oriented perpendicular to the contact of the coating and the shard contributes to the preservation of the surface layer. Conducted study of the material composition of the ceramic body by methods of petrography and analytical electron microscopy allowed to carry these products in porcelain with tin-lead decoration.

Lobzova R. V., Karimova O. V. Blue glazes and technogenic glass. Materials of the anniversary Congress of the Russian mineralogical society “200 years of RMO”,II, 102–103.

Lobzova R. V., Yarosh V. N. Technological research of early tiles of the architectural decor of the Church of the Intercession on the Moat (St. Basil's Cathedral). Questions of museology. 2013, 1(7), 116–124.

**Mineral features of raw materials in the Early Iron Age pottery techniques from Northern Pontic Region**

K.Nedaivoda*, M.Vetrova, A.Kulkov

[1]St.Petersburg State University, 199034 St. Petersburg, Russia

* ksenia-nedayvoda@mail.ru

In Northern Pontic, cultural changes had happened in the end of 10th – the first half of 7th centuries BC. This was connected with a mass migration of tribes from East Europe to the West region. All these migrations had an influence on both morphology and pottery techniques.

The goal of our research is correlation between the mineralogical compound of clays and their physic-mechanical properties.Samples were selected from outcrops located near the archaeological sites of Saharna, Sholdaneshti, Glijeni (Northern Moldavia).

The following methods were used for the investigation: optical mineralogy, X-ray diffraction, granulometric analysis, Atterberg's limits (plasticity index), thermogravimetry differential thermal analysis (TG/DTA), pores analysis and X-ray micro-Computed Tomography (μ-CT). Cylinders shapes were formed from ceramic pastes. Later experimental ceramics were dried and fired in the range from 400 to 900°C [Ricci, 2017].

It was revealed that various clays have different physical and mechanical properties. Carbonate component has an important role for the firing of pottery. The amount of fracture and porosity of cylinders were increased as a result of using high temperatures of firing ceramic.

We can suppose these problems were reasons for using different methods of polishing with iron oxide pastes.

Ricci G. Archaeomethric studies of historical ceramic materials. Venetia, 2017, 203, 48–54.

**X-Ray Study of Deposits from the Emine-Bayir-Khosarcave**

Gleb S. Maksimov, Igor A. Nauhatsky, Elena M. Maksimova*

V.I. Vernadsky Crimean Federal University, 295007 Simferopol, Russia

* maksimovaem@cfuv.ru

The karst represents about 84% of the territory of the Crimea. The study of the mineral and chemical composition of karst makes it possible to identify the features of the thermal and water regimes of mineralization processes, which is especially important for the Crimea, since more than 80% of groundwater reserves are concentrated in karst collectors. Modern scientific equipment allows for high accuracy and localization of such research [Tischenko, 2008].

In this study, we investigated four samples of karst deposits from the Emine-Bair-Khosar(EBK) cave and, for comparison, three samples from the calcite veins found around of this cave. The Emine-Bair-Khosar cave is located on the Chatyr-Dag massif in the middle of the Main ridge of the Mountain Crimea. The karst on Chatyr-Dag are represented by Upper Jurassic limestones of Kimeridzh-Luzitansky and Tithonian age (160–145 million years), occupying the upper structural floor (up to depths of 250–1250 m) of the geological section of the massif. In Emine-Bair-Khosar, there are various genetic types of cave deposits: landslide, organogenic, chemogenic, etc.

Elemental and phase analysis of samples was investigated by the X-ray analysis on Supermini200 and by X-ray diffraction analysis on SmartLab, Rigaku. The main phase of all the samples is calcite. Exception – pebbles from clayon the lower part of the Idols hall (EBK).This sample contains a large amount of iron and its main crystalline phases are cohenite and quartz.The chemical composition of the vein calcite from the vicinity of the Emine-Bair-Khosar cave corresponds to the classical composition of calcite. Different colors of these samples are due to chemical impurities. So, in the composition of “honey” calcite, there is manganese, which is not present in the two other calcites (white and clear); higher iron content, no chlorine. In calcites from the vicinity of the cave, there is no, for example, titanium, in contrast to the samples of cave deposits, which include it.

Tischenko A.I. Mineralogical study ofkarst cavities of Crimea. Speleology and Karstology, 2008, 1, 81–84.

# Structure of aged $^{238}$Pu-doped Eu-monazite

Andrey A. Shiryaev[1,*], Maximilian S. Nickolsky[1, 2], Vasily O. Yapaskurt[3], Polina S. Mihaylowa[3], Nikolai N. Eremin[3], Boris E. Burakov[4]

[1]Frumkin Institute of physical chemistry and electrochemistry RAS, 119071 Moscow, Russia
[2]Institute of geology of ore deposits, petrography, mineralogy and geochemistry RAS, 119017 Moscow, Russia
[3]Geology Dept., Moscow State University, 119234 Moscow, Russia
[4]V.G. Khlopin Radium Institute, 194021 St. Petersburg, Russia

* shiryaev@phyche.ac.ru

Monazites are promising forms for long-term immobilization of high-level radioactive waste due to ability to retain high amounts of actinides in the lattice. An important property of *REE*-monazites is low critical temperature of amorphization, leading to preservation of crystallinity under reasonable levels of ion irradiation even at room temperature. Though ion irradiation studies of monazites show promising results, experimental data on self-irradiation of actinide-doped monazites are scarce. It was shown that pure Pu-monazite ($PuPO_4$) readily amorphises due to self-irradiation, but Pu-doped *REE*-monazites appear to be more resistant [Burakov et al., 2011]. The maximal concentration of actinides such as Pu at which the material remains stable on long time scales are still unknown.

We report results of investigation of behavior of single crystalEu-monazite doped with several wt% of $^{238}$Pu –an isotope with very high specific activity – on scale of up to 20 years. Despite significant doses of accumulated damage, the sample remains a single crystal as testified by X-ray diffraction. However, during storage in air at ambient conditions unusual whitish secondary phases were formed on surfaces of the Pu-doped monazites; intense cracking of the crystals was also observed. Remarkably, the amount of the secondary phases appears to depend on crystallography of the studied monazite specimen. The secondary phases are easily detached from the crystals, possess unusual spheroid morphology; their structure and behavior of the secondary phases are of significant scientific and applied interest.

Spectroscopic data indicates that the white phase represents distorted, but still crystalline monazite. However, electron diffraction of the surface layer shows close resemblance with rhabdophane. Presumably, damage of the monazite lattice due to self-irradiation promotes interaction with moisture with formation of rhabdophane-like phases. Radiation and chemical stability of rhabdophane differ considerably from that of monazite. In addition, radiation stability of nanoparticles materials may be inferior to that of bulk materials.

BurakovB.E.,Ojovan M., Lee W.E., Crystalline materials for actinide immobilization, 2011, Imperial college press, London.

# Crystal Structure of $La_2W_{1+x}O_{6+3x}$

Nataliya E. Novikova*,[1], Timofey A. Sorokin[1], Alexander M. Antipin[1], Nadejda B.Bolotina[1], Olga A. Alekseeva[1], Nataliya I. Sorokina[1], and Valentina I. Voronkova[2]

[1] Shubnikov Institute of Crystallography of Federal Scientific Research Centre "Crystallography and Photonics" of Russian Academy of Sciences, LeninskiyProspekt 59, 119333 Moscow, Russia
[2]Department of Physics, Lomonosov Moscow State University, GSP-1, Leninskiye Gory1-2, 119991 Moscow, Russia

*natnov@ns.crys.ras.ru

The $La_2O_3$–$WO_3$ systemwas studied repeatedly.It was found [Yanovskiiet al., 1975] that a compound appeared near $La_2WO_6$ with a slight increase in the tungsten oxide content (~2.5 mol. %), which had a hexagonal structure and chemical composition $La_2W_{1+x}O_{6+3x}$ with the maximum tungsten content at $x$ = 0.25. It was believed that in most cases these crystals were intergrowths of two or more different polytypes, among which polytypes with hexagonal unit cell parameters $a \approx 9.0$, $c \approx 32.6$ Å and $c \approx 27.3$ Å prevailed whereas others polytypes were present only as impurities. Recently, the structure of polycrystal sample with the composition $La_{18}W_{10}O_{57}$ which was obtained by solid state synthesis in the $La_2O_3$–$WO_3$ system at $WO_3$ concentration of 52.65 mol. %,was studied [Chambrieret al., 2009]. The structure was hexagonal with the unit cell parameters $a$ = 9.0448(1), $c$ = 32.6846(3) Å, space group $P\bar{6}2c$, $Z$ = 2. All attempts to obtain single crystals of $La_{18}W_{10}O_{57}$ were unsuccessful.It was of particular interest to obtain single crystals of lanthanum tungstate with an excess of tungsten oxide near $La_2WO_6$, to study their composition and structural features.

Crystals of $La_2W_{1+x}O_{6+3x}$ ($x \leq 0.25$) were obtained by a self-flux method from high temperature solutionsin the $Li_2O$–$La_2O_3$–$WO_3$ system. Some crystal samples were studied by the single crystal X-ray structure analysis. Careful study of the complicated diffraction patterns revealed in each sample two equally orientedlattices with the common period $a \approx 9.0$ Å and non-equal in length but equally oriented superstructure periods 6$c$ (phase I) and 5$c$ (phase II), $c \approx 5.4$ Å. This indicated the coexistence of phases I and II in one crystal, different in the character of superstructure ordering. The structures I and II are solved in the space groups $P\bar{6}2c$ and $P321$, respectively, based on the X-ray data from crystals I and II with predominant content of the first and second phase. Both structures contain unbound trigonal $WO_6$ prisms on the cell edges.$WO_6$ octahedra, both isolated and joined by faces, are distributed along the $c$ axis within unit cells. Phase I contains extra layers of isolated $WO_6$ octahedra as compared to phase II. Tungsten sites in joined octahedra are disordered and partly occupied. Disordering is more expressed in phase II, which contains rather more W and O per one La atomas compared to phase I. Refined chemical compositions are $La_2W_{1.11}O_{6.33}$ (I) and $La_2W_{1.13}O_{6.40}$ (II).It has been first discovered that chemical composition can vary within one crystal but not only from one crystal to other because of growth under different conditions as stated earlier.

This workwas supported by the Ministry of Science and Higher Education within the State assignmentFSRC "Crystallography and Photonics" RAS in part of X-ray data collection, by the Russian Foundation for Basic Research (project no.18-29-12005) in part of synthesis of single crystals, study of their properties, and structure analysis.

Yanoskii V. K.,Voronkova V. I. Crystallography and properties of lanthanum oxytungstate, $La_2WO_6$. Sov. Phys. Crystallogr. 1975, 20, 354−355.
Chambrier M.-H., Le Bail A.,Kodjikian S.,Suard E.,Goutenoire F. Structure determination of $La_{18}W_{10}O_{57}$. Inorg. Chem. 2009, 48, 6566−6572.

**Structure of new mixed samarium aluminum-iron borates $SmFe_{3-x}Al_x(BO_3)_4$**

Ekaterina S. Smirnova[1,*], Olga A. Alekseeva[1], Vladimir V. Artemov[1], Irina A. Gudim[2]

[1] FSRC «Crystallography and Photonics» RAS, Leninskiy Prospekt 59, Moscow, 119333 Russia
[2] Kirensky Institute of Physics of the Siberian Branch of the RAS, Akademgorodok 50, Krasnoyarsk, 660036 Russia

* esmi@ns.crys.ras.ru

The rare-earth iron borates $RFe_3(BO_3)_4$ and rare-earth aluminum borates $RAl_3(BO_3)_4$ are being studied recently due to a range of promising advanced magnetoelectric properties, understanding the nature of which could significantly contribute to the general knowledge of multiferroics, which are the material promising for applications in electronics. Crystal structure of $RFe_3(BO_3)_4$ at high temperatures belongs to a huntite structure type with sp. gr. $R32$ and there is a structural phase transition to the low-temperature sp. gr. $P3_121$ for iron borates with smaller $R$ ionic radius [Kadomtseva et al. 2010]. Aluminum borates at room temperature also belong to $R32$ huntite type, but there are monoclinic modifications for several of them [Cavalli and Leonyuk, 2019]. Both families of compounds become magnetically ordered at low temperatures. Since rare-earth iron borates have two magnetically ordered sublattices, that are iron and rare-earth, while the alumoborates have only one strong magnetic sublattice, that is rare-earth, it is of interest to trace their properties and structure in comparison.

In the present work the structure of a new family of mixed samarium iron-aluminum borates $SmFe_{3-x}Al_x(BO_3)_4$ has been studied by means of single crystal X-ray structure analysis (XRD). The single crystals were grown by the standard technique [Bezmaternykh L. N., 2004] from a solution in melt with $Bi_2Mo_3O_{12}$ in the system. The chemical composition of the crystals was verified by X-ray energy-dispersive elemental analysis. It was found that Bi atoms entered the composition during the growth process, similarly to that in case of $RFe_3(BO_3)_4$ crystals studied by us earlier. Final chemical formulas were stated using XRD data. Bi atoms partly substitute Sm atoms, and both Fe and Al share one mixed site. Bi atoms entered the structure with an occupancy factor about 7-10 %. XRD occupancy of Fe-Al site is in agreement with values expected on the base of growing conditions. One of the samples does not contain Al in the composition, the content of Al for three other samples is $x$ = 0.04, 0.22, 0.28.

The unit cell parameters $a$, $b$, $c$ decrease with the growth of Al content from $a = b$ = 9.565(2) Å and $c$ = 7.587(1) Å with $x$=0 to $a = b$ = 9.534(1) Å and $c$ = 7.555(1) Å with $x$ = 0.28. The structure of all four crystals was refined in trigonal sp. gr. $R32$ with $R$-factors less than 1.5 %. The average distance (Sm,Bi)–O in $(Sm,Bi)O_6$ prisms slightly decreases by 0.004 Å with the addition of Al ($x$=0.28) into composition, and (Fe, Al)–O average distance in $(Fe,Al)O_6$ octahedra decreases by 0.011 Å, whereas B–O average distances in $B1O_3$ and $B2O_3$ triangles almost do not change. At the same time, there is a noticeable distortion of $(Fe,Al)O_6$ octahedra and $B2O_3$ triangles with the addition of Al atoms.

The study was partly supported by the RFBR (pr.no. 18-29-12005).

Kadomtseva A.M., Popov Yu. F., Vorob'ev G.P., et al. Magnetoelectric and magnetoelastic properties of rare-earth ferroborates. Low Temperature Physics, 2010, 36, 511-521.

Cavalli E. and Leonyuk N.I. Comparative Investigation on the Emission Properties of RAl3(BO3)4 (R = Pr, Eu, Tb, Dy, Tm, Yb) Crystals with the Huntite Structure. Crystals, 2019, 9, 44.

Bezmaternykh L. N., Kharlamova S. A., Temerov V. L. Flux crystallization of trigonal $GdFe_3(BO_3)_4$ competing with the crystallization of α-$Fe_2O_3$. Crystallography Reports, 2004, 49(5), 855-857.

# X-RAY DIFFRACTION STUDY OF QUATERNARY SULPHIDES OF RARE EARTH ELEMENTS

Anna V. Ruseikina[1,] *, Leonid A. Solovyov[2], Maxim V. Grigoriev[1], Anna E. Pinigina[1] and Oleg V. Andreev[1]

[1]University of Tyumen, Cemakova 10, Tyumen, 625003 Russia
[2]Federal Research Center KSC SB RAS, Academgorodok 50/24, Krasnoyarsk, 660049 Russia
* adeschina@mail.ru

In the series of $ALnCuS_3$ compounds (A = Sr, Eu, Ln = La-Lu) four types of crystal structures of orthorhombic symmetry were detected in the temperature range of 970-1170 K (table.1., fig.1.) by means of powder X-ray diffraction. The structure type changing consecutively in the order $BaLaCuS_3 \rightarrow Eu_2CuS_3 \rightarrow KZrCuS_3$ as the $Ln^{3+}$ ionic radius decreases in the order La, Pr→ Sm, Gd → Er, Lu. The similarity of the crystal structures of compounds $ALnCuS_3$ (A = Sr or Eu) is due to the proximity of ionic radii: = 1.21 Å and = 1.20 Å (CN = 7). Compound $SrLnCuS_3$ has a greater bond iconicity as compared to $EuLnCuS_3$. For ionic compound $SrLnCuS_3$, the low-symmetry coordination (CN = 7) is less characteristic. In the series of REE compounds with strontium, changes in the structural type (ST) proceed more rapidly ($SrErCuS_3$ has space group Cmcm, ST is $KZrCuS_3$) as compared to compounds $EuLnCuS_3$, which are characterized by slow changes in ST. The regularity of changes in the structural parameters of compounds $ALnCuS_3$ were established. The change of the structure type causes an abrupt change in the parameters of u.c also change in the type of coordination polyhedral with $LnS_7$, $AS_7$ (one-capped trigonal prisms) to $LnS_6$ (octahedron) and $AS_6$.( trigonal prism). The intermittence morphotropic changes in Nd – Sm correlates with the manifestation of the tetrad effect. It was found that $ALnCuS_3$ (Ln = La, Ce, Pr, Nd) have polymorphic transitions. The temperatures of polymorphic transitions are determined by means of dilatometric method.

Table.1. Structural types of $ALnCuS_3$ (A = Sr, Eu; Ln = La-Lu)

| T, K | $EuLnCuS_3$ structural type | | | | | | | | | | | | |
|---|---|---|---|---|---|---|---|---|---|---|---|---|---|
| | La | Ce | Pr | Nd | Sm | Gd | Tb | Dy | Ho | Er | Tm | Yb | Lu |
| 1170 | | | | | | | | | | | | | |
| 970 | | | | | | | | | | | | | |
| $SrLnCuS_3$ structural type | | | | | | | | | | | | | |
| 1170 | | | | | | | | | | | | | |
| 970 | | | | - | | | | - | - | | | | |

The background cell coloring denotes the structural type (ST) in which the compound crystallizes: vertical stripes – $BaLaCuS_3$ ST, crosshatched cells – $Eu_2CuS_3$ ST, dark gray cells – $Ba_2MnS_3$ ST, horizontal-striped cells – $KZrCuS_3$ ST and hyphenated white cells –van undetermined ST

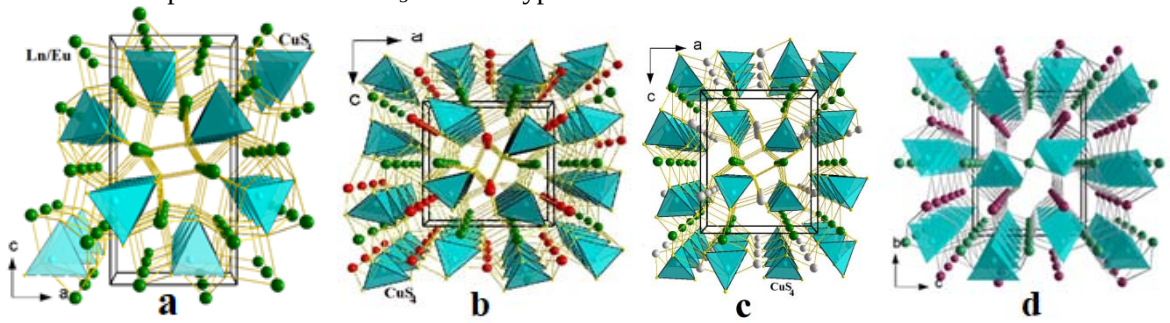


**Fig.1.** [010] perspective projections of $ALnCuS_3$ (A = Sr, Eu; Ln = La-Lu) $Ba_2MnS_3$ (a), $BaLaCuS_3$ (b), $Eu_2CuS_3$ (c) and $KZrCuS_3$ (d).

# INCLUSIONS OF MOISSANITE IN GRAPHITE FROM PYROXENITE (KIMBERLITE PIPE UDACHNAYA, SIBERIAN CRATON)

Romanenko A.V.[1, 2], Alifirova T.A.[1], Mikhailenko D.S.[1], Golovin A.V.[1], Korsakov A.V.[1], Ohfuji H.[3]

[1]Sobolev Institute of Geology and Mineralogy of the Siberian Branch of the RAS,3, Akademica Koptyuga prospect, Novosibirsk 630090, Russian Federation
[2] Novosibirsk State University, Novosibirsk, Pirogova str.2, 630090, Russia
[3]Geodynamics Research Center, Ehime University, Matsuyama, Ehime 790-8577, Japan
romanenko@igm.nsc.ru

Oxygen fugacity is fundamental thermodynamic parameter, together with pressure and temperature, which influences on the onset and evolution of major geological processes such as magma genesis, metasomatism, diffusion and stability of carbon polymorphs (i.e. graphite and diamond) in Earth's upper mantle [1]. The determining of the upper mantle oxidation state allows reconstruction the evolution of the global carbon cycle and graphite-diamond stability in the upper mantle through geological time.

Here we present the findings of moissanite inclusions in graphite from garnet pyroxenite xenolith from kimberlite pipe "Udachnaya". According to the transmission electron microscopy (TEM) data, the crystallization of the moissanite preceded the formation of the graphite. The isotope composition of the graphite (-7.94 ‰) indicates a mantle source of carbon.

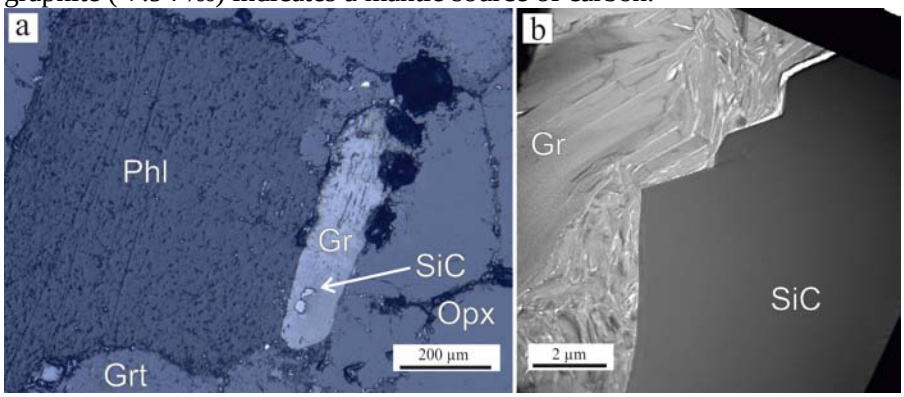


Fig.1. (a) - Photo of intergrowth of phlogopite grain with graphite crystal in pyroxenite Uv-506; (b) - TEM image showing the boundary between moissanite and graphite.

Formation of moissanite in upper mantle serves as an evidence of ultra-reduced conditions ($\log f_{O_2}$ = -20.1 or IW =-8.3) [2]. Moissanite in the mantle rocks can result fromlocal conditions or infiltration of a reduced fluid/melt in the rocks [3]. Moreover, ultra-reduced conditions can occur during serpentinization of ophiocarbonates and peridotite during subduction [4]. We suppose formation of moissanite in pyroxeniteto take place due to infiltration of C-fluid from subducted oceanic crust into the surrounding mantle.

The study was supported by grant of RFBR (№18-35-00219 and 18-35-20072).

[1] Frost D. J., McCammon C. A. The redox state of Earth's mantle. Annu. Rev. Earth Planet. Sci., 2008, 36, 389-420.
[2] Mathez E. A., Fogel R. A., Hutcheon I. D., Marshintsev V. K. Carbon isotopic composition and origin of SiC from kimberlites of Yakutia, Russia. GeochimicaetCosmochimicaActa, 1995, 59, 4, 781-791.
[3] Schmidt M. W., Gao C., Golubkova A., Rohrbach A., Connolly J. A. Natural moissanite (SiC)–a low temperature mineral formed from highly fractionated ultra-reducing COH-fluids. Progress in Earth and Planetary Science, 2014, 1(1), 27.
[4] Brovarone A. V., Martinez I., Elmaleh A., Compagnoni R., Chaduteau C., Ferraris C., Esteve I. Massive production of abiotic methane during subduction evidenced in metamorphosed ophicarbonates from the Italian Alps. Nature communications, 2017, 8, 14134.

# Index

PHOSAGRO®

## Кировский филиал АО «Апатит»

Кировский филиал АО «Апатит» - предприятие горно-химической отрасли с 90-летней историей. Входит в Группу компаний «ФосАгро» - одного из мировых лидеров по производству экологически чистых минеральных удобрений, востребованных в России и ста зарубежных странах.

КФ АО «Апатит» осуществляет добычу апатит-нефелиновой руды и её переработку в апатитовый, нефелиновый и сиенитовый концентраты. Апатитовый концентрат характеризуется исключительно высоким содержанием $P_2O_5$ и практически не содержит опасных примесей (например, кадмий, мышьяк), что выгодно отличает его от фосфатного сырья других производителей.

В структуру КФ АО «Апатит» входят три рудника: на Кировском и Расвумчоррском добыча ведётся подземным способом, на Восточном – в открытых карьерах. Переработка сырья организована на апатит-нефелиновых фабриках № 2 и № 3, которые за последний год прошли полное техперевооружение.

За всё время работы предприятием добыто 2 млрд тонн руды и произведено 700 млн тонн апатитового концентрата. На производственных площадках КФ АО «Апатит» внедряются передовые технологии, отвечающие мировым стандартам эффективности и безопасности труда. Одна из последних новинок – уникальная для России система дистанционного бурения, дающая возможность управлять подземными буровыми машинами с поверхности.

Компания «ФосАгро» ставит перед собой высокую планку социальной ответственности. Социальный пакет работников КФ АО «Апатит» - один из лучших в регионе. В Кировске и Апатитах, как и во всех городах присутствия компании, созданы «ФосАгро-школы» с многоступенчатой системой профориентации, внутри них - профильные «ФосАгро-классы».

Отдельный проект – организация «Детям России – образование, здоровье, духовность» (ДРОЗД). «ДРОЗД – Хибины» в Кировско-Апатитском районе организует работу 31 секции по 16 видам спорта, в которых занимаются более двух тысяч детей.

Компания возрождает дореволюционную традицию строительства заводских храмов. В 2017 году на Кировском руднике был открыт храм святой великомученицы Варвары – покровительницы горняков, в 2019 – храм святого целителя Пантелеимона на АНОФ-3, завершается строительство храма в честь Апостола Андрея Первозванного на Расвумчоррском руднике и в честь Николая Чудотворца - на Восточном руднике.

КФ АО «Апатит» - стабильное, передовое производство, выступающее гарантом социально-экономического развития Кировско-Апатитского района и Мурманской области в целом.

# Монокристальные дифрактометры D8 QUEST и D8 VENTURE

D8 QUEST и D8 VENTURE — современные инструменты рентгеновской кристаллографии. Все компоненты дифрактометров, включая детектор, гониометр, источники излучений и программное обеспечение основаны на самых современных достижениях.

## CMOS детектор — прорывная технология

Детекторы PHOTON II/III состоят из единой большой матрицы с применением технологий, используемых в XFEL. Благодаря современным разработкам детектор обладает исключительно низким уровнем шума, большим динамическим диапазоном и позволяет снимать в режиме Shutterless (без заслонки).

## Правильный источник излучения

Наши источники излучения METALJET, TXS, IuS и керамические трубки выдают самую высокую интенсивность и работают с разными материалами анода: Cu, Mo, Ag, Ga


## KAPPA или трехкружный гониометр — ваш выбор

Самая точная механика среди лабораторных дифрактометров. Диаметр сферы несовпадения осей менее 7 микрон. Вы можете доверить нам работу с самыми сложными и маленькими кристаллами.


## Низкотемпературные приставки

Наши дифрактометры позволяют установить самые разные типы систем охлаждения. Это позволяет работать в разных условиях и значительно улучшить качество экспериментальных данных.



## Качественное железо + удобный софт = эксперимент высочайшего качества

Программное обеспечение APEX3 просто и интуитивно понятно проводит через все этапы проведения эксперимента, обработки экспериментальных данных и подготовки результатов к печати. Новички почувствуют всю мощность и высокий интеллект автоматических процедур съемки и обработки. Для опытных пользователей есть возможность индивидуально настраивать каждый параметр и полностью контролировать все этапы съемки и обработки.

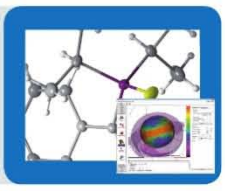

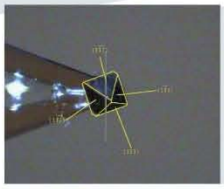

## Современная наука заслуживает современных инструментов

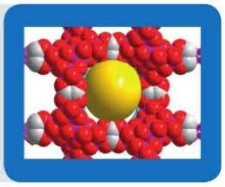

Rigaku

E-Globaledge Corporation
イーグローバレッジ株式会社

# SmartLab SE

## *Automated Multipurpose XRD for Mineral Analysis*


- Low-maintenance 3 kW sealed X-ray tube
- Choice of detectors
  - D/teX Ultra 250 (0/1D) – ultrafast silicon strip
  - HyPix-400 (0D /1D/2D) – 2D hybrid pixel array
- Choice of optics
  - CBO-*f* for micro area and mapping
  - CBO-E/Gandolfi for small samples or single crystals
- SmartLab Studio II measurement and analysis software

***www.Rigaku.com***

**E-Globaledge Corporation**
12, Krasnopresnenskaya emb., Moscow, Russia 123610, WTC, M-2, 15th floor, office 1512
+7 (495) 967 0959 | info@e-globaledge.ru | www.e-globaledge.ru

TechnoInfo

sales@technoinfo.ru
www.technoinfo.ru
+7 (499) 270 66 26


Компания «Техноинфо» предлагает широкий спектр уникального оборудования для решения задач во многих областях науки. Будучи официальным представителем ведущих мировых производителей, «Техноинфо» также обеспечивает гарантийное и постгарантийное обслуживание установленных систем, обучение персонала и методическую поддержку пользователей.

Все сотрудники компании имеют профильное образование в своей области, поэтому мы подбираем наиболее подходящее решение в зависимости от потребностей пользователя. Большинство систем производится по индивидуальному заказу с учётом пожеланий клиента.

К нашим ключевым партнёрам относятся компании: Thermo Fisher Scientific (former FEI Company), Rigaku Oxford Diffraction, Applied Photophysics, Molecular Devices, IonTOF, Kratos, Keyence, Olympus, Xenocs, и другие.

TECHNOINFO

MOLECULAR DEVICES · Xenocs · Rigaku oxford diffraction · ThermoFisher SCIENTIFIC · Xenemetrix · KRATOS ANALYTICAL A SHIMADZU GROUP COMPANY · IONTOF

Официальный представитель
Thermo Fisher Scientific в России
компания Technoinfo

ThermoFisher
SCIENTIFIC

## Сканирующие электронные микроскопы

- Prisma
- Quattro
- Apreo
- Verios

## Двулучевые системы и системы фокусированного ионного пучка

- Aquilos Cryo-FIB
- Scios
- Helios
- Helios PFIB

## Просвечивающие электронные микроскопы

- Talos
- Titan
- Glacios

## Основные преимущества систем TFS

- Сверхвысокое разрешение на всех инструментах
- Уникальные запатентованные технологии
- Полностью автоматизированное управление
- Полный и современный набор программ и утилит для последующей работы с изображениями

TechnoInfo

sales@technoinfo.ru
www.technoinfo.ru